Oregon Health & Science University

School of Medicine

# Developing Optically-Cleavable Targeted (OCT)-Ligands: A chemigenetic approach for studying endocannabinoid signaling in pancreatic islets.

By

Janelle Marie Tobias

Thesis Dissertation

Presented to

The Department of Chemical Physiology and Biochemistry

&

The Oregon Health & Science University School of Medicine

In partial fulfilment of

The requirements for the degree of

Doctor of Philosophy

January 2024

**TABLE OF CONTENTS**

**Acknowledgments** ..... **9**

**Abstract**..... **11**

**Chapter 1. Introduction** ..... **13**

**1.1. The role of the endocannabinoid system in islet biology.** ..... **13**

**1.2. Current chemical biology tools to study the endocannabinoid system** ..... **17**

**1.3. Design of Optically-Cleavable Targeted (OCT)-Ligands** ..... **22**

**Chapter 2. Genetically-targeted photorelease of endocannabinoids enables optical control of GPR55 in pancreatic β-cells** ..... **24**

**2.1. Introduction** ..... **25**

**2.2. Results** ..... **28**

2.2.1. Synthesis of an OCT-ligand for GPR55. ..... 28

2.2.2. GPR55 and PEA mediate $Ca^{2+}$ signaling in INS-1 β-cells. ..... 31

2.2.3. Expression and labeling of cell surface SNAP-tags in INS-1 β-cells. ..... 34

2.2.4. Plasma membrane PEA uncaging mediates INS-1 $Ca^{2+}$ levels via GPR55. ..... 39

**2.3. Discussion** ..... **45**

**2.4. Methods** ..... **47**

2.4.1. General synthetic methods ..... 47

2.4.2. UV-Vis spectroscopy ..... 47

2.4.3. Cell culture media and solutions ..... 48

2.4.4. Cell culture ..... 49

2.4.5. cDNA constructs and site-directed mutagenesis ..... 50

2.4.6. Cell viability assay - MTT ..... 50

2.4.7. Immunofluorescence microscopy ..... 51

2.4.8. Live-cell confocal fluorescence microscopy ..... 53

2.4.9. Data analysis and code availability .....53

**2.5. Detailed Synthetic Methods .....55**

2.5.1. Synthesis of Ethyl 2-(3-formyl-4-nitrophenoxy) acetate (1). .....56

2.5.2. Synthesis of (2-*tert*-butoxyethyl)-(5-ethoxycarbonylmethoxy-2-nitrobenzyl)amine (2). …….. .....57

2.5.3. Synthesis of *N*-(*2-tert*-butoxyethyl)-*N*-(5-ethoxycarbonylmethoxy-2-nitrobenzyl) palmitoylamide (3). .....58

2.5.4. Synthesis of *N*-(2-*tert*-butoxyethyl)-*N*-(5-carboxymethoxy-2-nitrobenzyl) palmitoylamide (4)…… .....63

2.5.5. Synthesis of *N*-(2-*tert*-butoxyethyl)-*N*-(5-methoxy-6-((4-(aminomethyl)benzyl)oxy)-*9H*-purin-2-carbamoyl-2-nitrobenzyl)palmitoylamide (5). .....64

2.5.6. Synthesis of *N*-(ethyl-2-ol)-*N*-(5-methoxy-6-((4-(aminomethyl)benzyl)oxy)-*9H*-purin-2-carbamoyl-2-nitrobenzyl)palmitoylamide (OCT-PEA).....69

**Chapter 3. Optical control of endocannabinoid signaling in human pancreatic islets with tethered photopharmacology. .....74**

**3.1. Introduction .....75**

**3.2. Results .....77**

3.2.1. Design and synthesis of hOCT-PEA derivatives.....77

3.2.2. Comparing hOCT-PEA derivatives' labeling efficiency and toxicity in INS-1 cells……. .....81

3.2.3. Plasma membrane uncaging of hOCT-PEA4 in INS-1 cells .....85

3.2.4. Endocannabinoids mediate $Ca^{2+}$ and insulin release in intact human islets .....87

3.2.5. HaloTag AAV virus and targeted hOCT-PEA4 uncaging in islets .....90

**3.3. Discussion .....94**

**3.4. Methods.....97**

3.4.1. General synthetic methods ....97
3.4.2. UV-Vis spectroscopy ....97
3.4.3. Cell Culture media and solutions ....98
3.4.4. Cell Culture ....99
3.4.5. INS-1 Competition Labeling Assay ....100
3.4.6. rAAV production and purification ....101
3.4.7. Immunofluorescence staining in cultured β-cells and islets ....102
3.4.8. Live-cell confocal microscopy ....103
3.4.9. Fixed cell microscopy ....104
3.4.10. MTT assay ....105
3.4.11. Insulin ELISA assay ....105
3.4.12. Data analysis and code availability ....106

**3.5. Detailed synthetic methods ....107**

3.5.1. Synthesis of *N*-(2-(*tert*-butoxy)ethyl)-*N*-(5-(2-((2-(2-((6-chlorohexyl)oxy) ethoxy)ethyl) amino)-2-oxoethoxy)-2-nitrobenzyl)palmitamide (4) ....108
3.5.2. Synthesis of *N*-(5-(2-((2-(2-((6-chlorohexyl)oxy)ethoxy)ethyl)amino)-2-oxoethoxy)-2-nitrobenzyl)-*N*-(2-hydroxyethyl)palmitamide (hOCT-PEA1) ....113
3.5.3. Synthesis of methyl 2-(4-((3-(((2-(*tert*-butoxy)ethyl)amino)methyl)-4-nitrophenoxy) methyl) phenyl)acetate (6) ....119
3.5.4. Synthesis of methyl 2-(4-((3-((*N*-(2-(*tert*-butoxy)ethyl)palmitamido)methyl)-4-nitrophenoxy)methyl)phenyl)acetate (7) ....124
3.5.5. Synthesis of *N*-(2-(*tert*-butoxy)ethyl)-*N*-(5-((4-(2-((2-(2-((6-chlorohexyl) oxy)ethoxy)ethyl) amino)-2-oxoethyl)benzyl)oxy)-2-nitrobenzyl)palmitamide (8) ....129
3.5.6. Synthesis of *N*-(5-((4-(2-((2-(2-((6-chlorohexyl)oxy)ethoxy)ethyl)amino)-2-oxoethyl)benzyl)oxy)-2-nitrobenzyl)-*N*-(2-hydroxyethyl)palmitamide (hOCT-PEA2) ....134

3.5.7. Synthesis of 2-(*tert*-butoxy)-*N*-(2-nitro-5-(prop-2-yn-1-yloxy)benzyl)ethan-1-amine (10)……. .....140
3.5.8. Synthesis of *N*-(2-(*tert*-butoxy)ethyl)-*N*-(2-nitro-5-(prop-2-yn-1-yloxy) benzyl)palmitamide (11)…….. .....144
3.5.9. Synthesis of 2-(2-(2-(2-azidoethoxy)ethoxy)ethoxy)-*N*-(2-(2-((6-chlorohexyl)oxy)ethoxy) ethyl)acetamide ($N_3$-$PEG_3$-CA).....149
3.5.10. Synthesis of *N*-(2-(*tert*-butoxy)ethyl)-*N*-(5-((1-(24-chloro-11-oxo-3,6,9,15,18-pentaoxa-12-azatetracosyl)-1*H*-1,2,3-triazol-4-yl)methoxy)-2-nitrobenzyl)palmitamide (12) …… .....153
3.5.11. Synthesis of *N*-(5-((1-(24-chloro-11-oxo-3,6,9,15,18-pentaoxa-12-azatetracosyl)-1*H*-1,2,3-triazol-4-yl)methoxy)-2-nitrobenzyl)-*N*-(2-hydroxyethyl) palmitamide (hOCT-PEA3) …….....158
3.5.12. Synthesis of 1-azido-*N*-(2-(2-((6-chlorohexyl)oxy)ethoxy)ethyl)-3,6,9,12,15,18,21,24-octaoxaheptacosan-27-amide ($N_3$-$PEG_8$-CA).....164
3.5.13. Synthesis of 1-(4-((3-((*N*-(2-(*tert*-butoxy)ethyl)palmitamido)methyl)-4-nitrophenoxy) methyl)-1*H*-1,2,3-triazol-1-yl)-*N*-(2-(2-((6-chlorohexyl)oxy)ethoxy)ethyl)-3,6,9,12,15,18,21,24-octaoxaheptacosan-27-amide (13).....168
3.5.14. Synthesis of *N*-(2-(2-((6-chlorohexyl)oxy)ethoxy)ethyl)-1-(4-((3-((*N*-(2-hydroxyethyl) palmitamido)methyl)-4-nitrophenoxy)methyl)-1*H*-1,2,3-triazol-1-yl)-3,6,9,12,15,18,21,24-octaoxaheptacosan-27-amide (hOCT-PEA4).....173
**Chapter 4. Expanding the OCT-ligand platform to other ligands: hOCT-Anandamide 178**
**4.1. Introduction .....179**
**4.2. Results .....181**
4.2.1. Design and synthesis of hOCT-AEA.....181
4.2.2. INS-1 cells express FAAH.....183

4.2.3. Labeling of cell surface HaloTags in INS-1 cells ..... 184

4.2.4. Plasma membrane uncaging of hOCT-AEA affects $Ca^{2+}$ but not cAMP in INS-1 cells ..... 185

4.2.5. AEA stimulates $Ca^{2+}$ and insulin in human islets, preliminary data ..... 188

**4.3. Discussion ..... 190**

**4.4. Methods ..... 192**

4.4.1. General synthetic methods ..... 192

4.4.2. UV-Vis spectroscopy ..... 192

4.4.3. Cell Culture media and solutions ..... 193

4.4.4. Cell Culture ..... 194

4.4.5. INS-1 Competition Labeling Assay ..... 195

4.4.6. rAAV production and purification ..... 196

4.4.7. Immunofluorescence staining in cultured β-cells ..... 197

4.4.8. Live-cell confocal microscopy ..... 198

4.4.9. Fixed cell microscopy ..... 199

4.4.10. Western Blot ..... 199

4.4.11. Insulin ELISA assay ..... 200

4.4.12. Data analysis and code availability ..... 200

**4.5. Detailed synthetic methods ..... 202**

4.5.1. Synthesis of (5Z,8Z,11Z,14Z)-*N*-(2-(tert-butoxy)ethyl)-*N*-(2-nitro-5-(prop-2-yn-1-yloxy)benzyl)icosa-5,8,11,14-tetraenamide (3). ..... 203

4.5.2. Synthesis of 1-(4-((3-(((5*Z*,8*Z*,11*Z*,14*Z*)-*N*-(2-(*tert*-butoxy)ethyl)icosa-5,8,11,14-tetraenamido)methyl)-4-nitrophenoxy)methyl)-1*H*-1,2,3-triazol-1-yl)-*N*-(2-(2-((6-chlorohexyl)oxy)ethoxy)ethyl)-3,6,9,12,15,18,21,24-octaoxaheptacosan-27-amide. (4) ..208

4.5.3. Synthesis of *N*-(2-(2-((6-chlorohexyl)oxy)ethoxy)ethyl)-1-(4-((3-(((5*Z*,8*Z*,11*Z*,14*Z*)-*N*-(2-hydroxyethyl)icosa-5,8,11,14-tetraenamido)methyl)-4-nitrophenoxy)methyl)-1*H*-1,2,3-triazol-1-yl)-3,6,9,12,15,18,21,24-octaoxaheptacosan-27-amide (hOCT-AEA). .....213

**Chapter 5. Outlook .....218**

**Chapter 6. Appendix .....221**

**6.1. Abbreviations.....221**

**6.2. Synthesis of OCT-stearoylethanolamine (SEA) .....223**

6.2.1. Synthesis of ethyl 2-(3-((*N*-(2-(*tert*-butoxy)ethyl)stearamido)methyl)-4-nitrophenoxy)acetate (3).....224

6.2.2. Synthesis of *N*-(5-(2-((4-(((2-amino-9*H*-purin-6-yl)oxy)methyl)benzyl)amino)-2-oxoethoxy)-2-nitrobenzyl)-*N*-(2-(*tert*-butoxy)ethyl)stearamide (4). .....229

6.2.3. Synthesis of *N*-(5-(2-((4-(((2-amino-9*H*-purin-6-yl)oxy)methyl)benzyl)amino)-2-oxoethoxy)-2-nitrobenzyl)-*N*-(2-hydroxyethyl)stearamide (OCT-SEA).....232

**References…... .....234**

**TABLE OF FIGURES**

*Figure 1.1. N-acylethanolamines (NAEs) vary in acyl chain length and degree of unsaturation.14*

*Figure 1.2. GSIS relies on signaling input from many pathways, including the ECS.....17*

*Figure 1.3. Common photochemical tools: photoswitches and photocages.....19*

*Figure 1.4. Chemical biology approaches to study receptor signaling. .....21*

*Figure 1.5 The OCT-ligand approach allows for genetic targeting of photocaged ligands.....23*

*Figure 2.1. OCT- palmitoylethanolamide (PEA) targets SNAP-tags and activates GPR55. .....27*

*Figure 2.2. Chemical synthesis of **OCT-PEA**, which was prepared in 6 steps with a 26% yield.28*

*Figure 2.3. UV-Vis characterization of uncaging **OCT-PEA**. .....30*

*Figure 2.4. INS-1 $\beta$-cells express GPR55 and insulin.....32*

*Figure 2.5. PEA activates GPR55 in INS-1 cells.....33*

*Figure 2.6. **OCT-PEA** labels SNAP-tags in a time and concentration dependent manner.....35*

*Figure 2.7. **OCT-PEA** is not cell permeable.....36*

*Figure 2.8. SNAP-tag internalization over prolonged labeling.....37*

*Figure 2.9. SNAP-tag mutant maintains surface localization but does not recognize BG motif..38*

*Figure 2.10. **OCT-PEA** was not toxic to INS-1 cells.....39*

*Figure 2.11. Targeted uncaging of **OCT-PEA** on the INS-1 cell surface.....40*

*Figure 2.12. Targeted uncaging of **OCT-PEA** on the INS-1 cell surface with GPR55 KD.....43*

*Figure 2.13. Targeted uncaging of **OCT-PEA** on half of the field of view. .....44*

*Figure 2.14. Numbering system utilized in the NMR assignments for **OCT-PEA**. .....55*

*Figure 3.1. OCT-palmitoylethanolamide (PEA) labels HaloTags and activates GPR55.....76*

*Figure 3.2. Synthetic scheme for hOCT-PEA derivatives.....78*

*Figure 3.3. Photophysical characterization of hOCT-PEA derivatives by UV-Vis spectroscopy..80*

*Figure 3.4. Comparing uncaging across LEDs. .....81*

*Figure 3.5. Expression of pDisplayHalo-EGFP and pDisplayHalo$^{D107A}$-EGFP in INS-1 cells.....82*

*Figure 3.6. Evaluating **hOCT-PEA** labeling in INS-1 β-cells. ....84*

*Figure 3.7. Evaluating prolonged **hOCT-PEA4** treatment on INS-1 cell viability. ....85*

*Figure 3.8. Uncaging **hOCT-PEA4** on the INS-1 cell surface. ....86*

*Figure 3.9. $Ca^{2+}$ imaging to evaluate glucose sensitivity across donors....88*

*Figure 3.10. Evaluating ECS tone in human islets....90*

*Figure 3.11. Expression of AAV-Halo and AAV-$Halo^{D107A}$ in human islets. ....91*

*Figure 3.12. Targeting β-cells in intact human islets. ....92*

*Figure 3.13. Uncaging hOCT-PEA4 on β-cells in human islets. ....93*

*Figure 3.14. Synthetic scheme of **hOCT-PEA1**. ....107*

*Figure 3.15. Synthetic scheme of **hOCT-PEA2**. ....118*

*Figure 3.16. Synthetic scheme of **hOCT-PEA3**. ....139*

*Figure 3.17. Synthetic scheme of **hOCT-PEA4**. ....163*

*Figure 4.1. hOCT-Anandamide (AEA) labels HaloTags and activates CB1....180*

*Figure 4.2. Chemical synthesis of **hOCT-AEA**, which was prepared in 5 steps with 12% yield. ....181*

*Figure 4.3. Photophysical properties of uncagingg **hOCT-AEA** with 365 nm. ....182*

*Figure 4.4. FAAH characterization in model β-cells lines INS-1 and MIN6....184*

*Figure 4.5. hOCT-AEA labels surface expressing HaloTags in INS-1 cells. ....185*

*Figure 4.6. Surface targeted uncaging of **hOCT-AEA** does not affect cAMP in INS-1 cells. ....186*

*Figure 4.7. Surface targeted uncaging of **hOCT-AEA** stimulates $Ca^{2+}$ in INS-1 cells....187*

*Figure 4.8. AEA stimulates $Ca^{2+}$ and insulin in human islets....189*

*Figure 4.9. Numbering system utilized in the NMR assignments for **hOCT-AEA**. ....202*

*Figure 6.1. Chemical synthesis of **OCT-SEA**, which was prepared in 6 steps with 5% yield....223*

*Figure 6.2. Numbering system utilized in the NMR assignments for **OCT-SEA**. ....223*

# Acknowledgments

I am grateful for many people who allowed me to achieve this academic milestone. I appreciate my DAC members –Show-Ling Shyng, Carsten Schultz, Marc Freeman, and Paul Kievit—for their critical feedback, access to resources, career advice and words of encouragement. I am grateful for my mentor, James Frank. I appreciate the intellectual freedom I had to explore β-cell and islet biology, his support for me to attend conferences, and how his mentorship style allowed me to grow into a confident scientist. We both gambled on each other, and together we established a successful Team Pancreas. Each member of the Frank lab was instrumental for my growth as a scientist. From day one Xander has been my pal and confidant, Gabi was an excellent partner, and Sarahi and Carmel have been like sisters. I will cherish my time in the Frank lab, and the life-long friendships I created in this environment.

My family taught me the power of dedication and determination. My Abuelita and Grandma are two incredibly strong women who had to leave their home countries to give their children opportunities for a more stable life. They poured their love into every homecooked meal and served as positive role models to show me the strength of independent women. Their sacrifices allowed my parents to have successful careers, which provided my siblings and I with an incredible childhood. I know I can always count on my Dad to share words of wisdom over a beer. From a young age he taught me to have self-respect and to be ambitious, traits that have been crucial for my success as a Latina in STEM. My Mom pours her heart into everything she does. She is my pillar of support who is always there when I need, and I cannot think of a life problem for which she doesn't have a solution. I am grateful for my siblings Justine and Jake, who made time to visit me in Portland, gave me two cute nieces, and equally share my love for Taylor Swift. I am who I am because of my family's love and support.

I have incredible friends who have helped me throughout my PhD. From my childhood friends, SAJI, rommies Moni and Ana, Kesem alumni and fellow Swifties, I have a wonderful

network of people who I love and who have supported me. I am grateful to my dear friend Homma, who always matches my energy and shared her home with me as a defended my thesis. And finally, I am beyond grateful for my fiancé Daniel, who supported me through every high and low point of my PhD. His kindness, generosity and cooking fixed every tough moment, and I am looking forward to our next chapter together.

# Abstract

Marijuana legalization in the United States, both recreationally or medicinally, has increased its use in adults, yet the full impact of cannabinoid molecules found in marijuana on endogenous signaling pathways is unknown. Cannabinoid signaling has been tied to metabolism and pancreatic islet function, which is responsible for maintaining euglycemia. Diabetes is the resulting disease state when blood glucose levels are not properly regulated. In the islet, pancreatic β-cell excitability and insulin secretion are regulated by a plethora of cannabinoid receptors (CBRs), which respond to lipids called *N*-acylethanolamines (NAEs). NAEs contain an ethanolamine headgroup attached to a lipid chain that varies in length and unsaturation, and they can target both stimulatory and inhibitory CBRs expressed on several cell populations within the islet, including β-cells. However, NAEs' complex pharmacology and hydrophobicity make them difficult to control in time and space after application to cells. This complicates our understanding of NAE signaling in β-cells and prevents us from developing therapies for metabolic disorders that target CBR pathways. To address these challenges, we developed Optically-Cleavable Targeted (OCT)-ligands, which combine the spatial resolution of self-labeling protein tags (i.e. SNAP- and HaloTags) with the temporal control of photocaged ligands. By linking a photocaged NAE to a bioconjugation motif, we can enrich NAEs on a genetically-defined targets, and then activate them with light. Using OCT-ligands, we showed that uncaging palmitoylethanolamide (PEA) on the surface of INS-1 β-cells increased $Ca^{2+}$ oscillations through a stimulatory cannabinoid receptor, GPR55. Development of a second generation of OCT-ligands tethers to HaloTags (**hOCT-PEA**) and have improved solubility and labeling efficiency relative to the original probe. We then developed an adeno-associated virus (AAV) to express protein tags on the surface of β-cells in intact human islets, and showed that photorelease of PEA selectively on β-cells stimulated $Ca^{2+}$ oscillations in islets. Finally, we

expanded the OCT-ligand approach to release other NAEs, including anandamide (AEA), a classic endocannabinoid. Preliminary results suggest that releasing AEA on the surface of β-cells in model β-cells and primary islets stimulates $Ca^{2+}$. Moving forward, the OCT-ligand approach can be expanded to other ligands and receptors and will allow for new experimental possibilities in targeted photopharmacology.

# Chapter 1. Introduction

## 1.1. The role of the endocannabinoid system in islet biology.

In the United States, the legalization of cannabis (recreational and medicinal) has increased cannabis use in adults[1]. Washington DC and 18 states have fully legalized marijuana (cannabis) use, while another 18 states have legalized medical cannabis use[1]. The active components in marijuana, including $\Delta^9$-tetrahydrocannabinol (THC) and cannabidiol (CBD), hijack endogenous signaling pathways (coined *endocannabinoid* signaling) to carry out their effects, yet much of the basic biology behind these pathways are poorly understood[2]. Endocannabinoid signaling is mediated by cannabinoid receptors (CBRs), lipid-derived ligands, and the metabolic enzymes that control their synthesis and degradation. The canonical receptors of the endocannabinoid system (ECS) include cannabinoid receptor 1 (CB1), which is highly expressed in the central nervous system, and CB2, which is primarily expressed in immune cells[3]. Besides CB1 and CB2, recent studies have revealed an "extended endocannabinoid system" that also responds to cannabinoid ligands—including other G protein-coupled receptors (GPCRs), ion channels, and nuclear receptors[4].

*N*-acylethanolamines (NAEs) are a family of endocannabinoid ligands that are characterized by a polar ethanolamine headgroup attached to a lipid chain that can vary in length and degree of saturation. More than 70 NAE species have been identified[5], but a majority of NAEs still have unknown function(s). However, a general trend has emerged, where polyunsaturated NAEs tend to activate inhibitory CBRs[6,7] and saturated NAEs tend to target stimulatory CBRs[8–11] (**Figure 1.1**). Key examples include anandamide (AEA), a 20 carbon / 4 *cis*-double bond NAE which activates CB1 and CB2 ($G_i$ coupled)[12], and palmitoylethanolamide (PEA), a 16 carbon / no double bond NAE which activates the atypical CBR GPR55 and GPR119 ($G_q$ coupled)[10,13]. NAEs are abundant in plasma, and global changes to their

abundance is tied to metabolic stressors[14–16]. For example, polymorphisms in fatty acid amide hydrolase (FAAH)—an enzyme which degrades NAEs—are associated with obesity in humans[17,18].

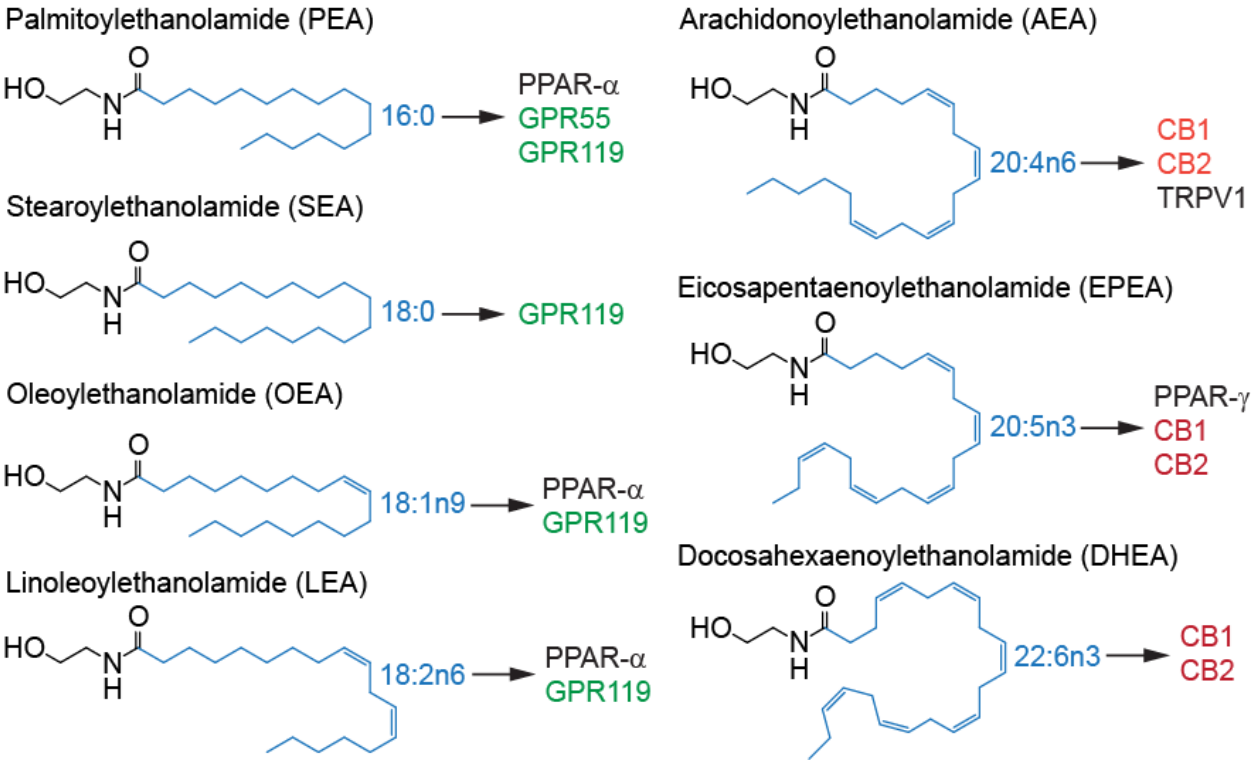


*Figure 1.1. N-acylethanolamines (NAEs) vary in acyl chain length and degree of unsaturation. Shorter, saturated NAEs tend to target stimulatory CBRs, including GPR55 and GPR119 (green). In contrast, longer polyunsaturated NAEs tend to target inhibitory CBRs, including CB1 and CB2 (red). The length and number of double bonds is denoted in blue, as (length:degree of unsaturation).*

According to the Centers for Disease Control and Prevention, 38.4 million people have diabetes mellitus in the United States (11.6% of the US population), while an additional 97.6 million adults over age 18 have prediabetes[19]. Diabetes mellitus results from a dysregulation of blood glucose levels caused by the abnormal function or autoimmune destruction of β-cells. Pancreatic β-cells are found in the islets of Langerhans, a multicellular endocrine hub that

releases hormones to regulate global blood glucose levels[20]. In the islets β-cells release insulin to lower blood glucose, and α-cells secrete glucagon to raise blood glucose. Insulin facilitates cellular glucose uptake for metabolism and serves as a critical regulator of energy homeostasis.

Cannabinoid signaling has been tied to metabolism and pancreatic islet function, yet its specific role is unclear[21,22]. In 1986, researchers found that primary rat islets treated with pure THC had enhanced insulin release under basal and glucose-stimulated conditions[23]. Epidemiological studies have shown chronic cannabis use to be protective against diabetes and associated with leanness and lower insulin resistance[24–27]. In contrast, Qi M et al. found that when human islets from chronic marijuana users were transplanted into diabetic mice, diabetes was reversed at a lower rate (35%) compared to transplantation with islets from non-users (77%)[28]. Of note, the chronic marijuana donors did not have any clinical signs of islet malfunction. Together, these studies suggest that the ECS has an active role in islets, while chronic activation of the ECS changes islet function. Organ transplantation is not a viable cure for diabetes due to limited donor availability and the need to be on life-long immunosuppressants. Thus, a more promising therapeutic strategy is the use of small molecules to restore β-cell and islet function[3]. Rimonabant is a CB1 inverse agonist that was used in multiple clinical trials for treating obesity[22,29]. In the SERENADE trial, rimonabant-treated participants with type 2 diabetes showed decreased bodyweight and improved lipid profile and glycemic control[30]. However, rimonabant was removed from the clinic following multiple negative side effect reports, including increased risk of adverse psychiatric effects and two deaths by suicide[29]. While rimonabant was not a perfect therapy, the clinical trials showed the therapeutic potential of targeting the ECS with small molecules for treating diabetes and obesity and warrants further study.

In the β-cell, glucose-stimulated insulin secretion (GSIS) is initiated when GLUT transporters uptake glucose, which is metabolized via glycolysis. An increase in the intracellular

ATP:ADP ratio closes the ATP-sensitive $K^+$ channel, triggering cell depolarization. Upon cell depolarization, $Ca^{2+}$ enters through voltage-dependent $Ca^{2+}$ channels, which induces insulin secretion. The cell is repolarized through inwardly rectifying and voltage-gated $K^+$ channels, which allows GSIS to repeat in an oscillatory behavior. The frequency and amplitude of these oscillations correlate tightly to insulin secretion[31]. Notably, β-cells express multiple cannabinoid-sensitive receptors and channels that affect β-cell excitability and GSIS[32,33], including CB1, CB2, transient receptor potential cation channel subfamily V member 1 (TRPV1)[34], peroxisome proliferator-activated receptors[35], GPR119[36] and the atypical cannabinoid receptor GPR55[32,37,38], which is a stimulatory GPCR (**Figure 1.2**). While CB1 inhibits cAMP via coupling to $G\alpha_i$, GPR55 increases $[Ca^{2+}]_i$ via coupling to $G\alpha_{q/11}$ and phospholipase C (PLC)[39]. While NAE signaling can modulate β-cell activity through CBR activation, our understanding of these pathways is limited by our ability to control these molecules in time and space. Due to the presence of multiple cell types in the islet with overlapping CBR expression[3,40,41], external ligand perfusion fails to distinguish NAE signaling on specific CBR pathways in β-cells within an intact islet. Further, the lipophilicity of NAEs makes their application to cells and tissue technically problematic, due to their highly variable diffusion in physiological solution and ability to permeate cellular membranes. As such, there is a critical need for tools that can acutely manipulate NAEs with high spatiotemporal precision to assess the impact of endocannabinoid signaling on specific CBR pathways in pancreatic β-cells and islets.

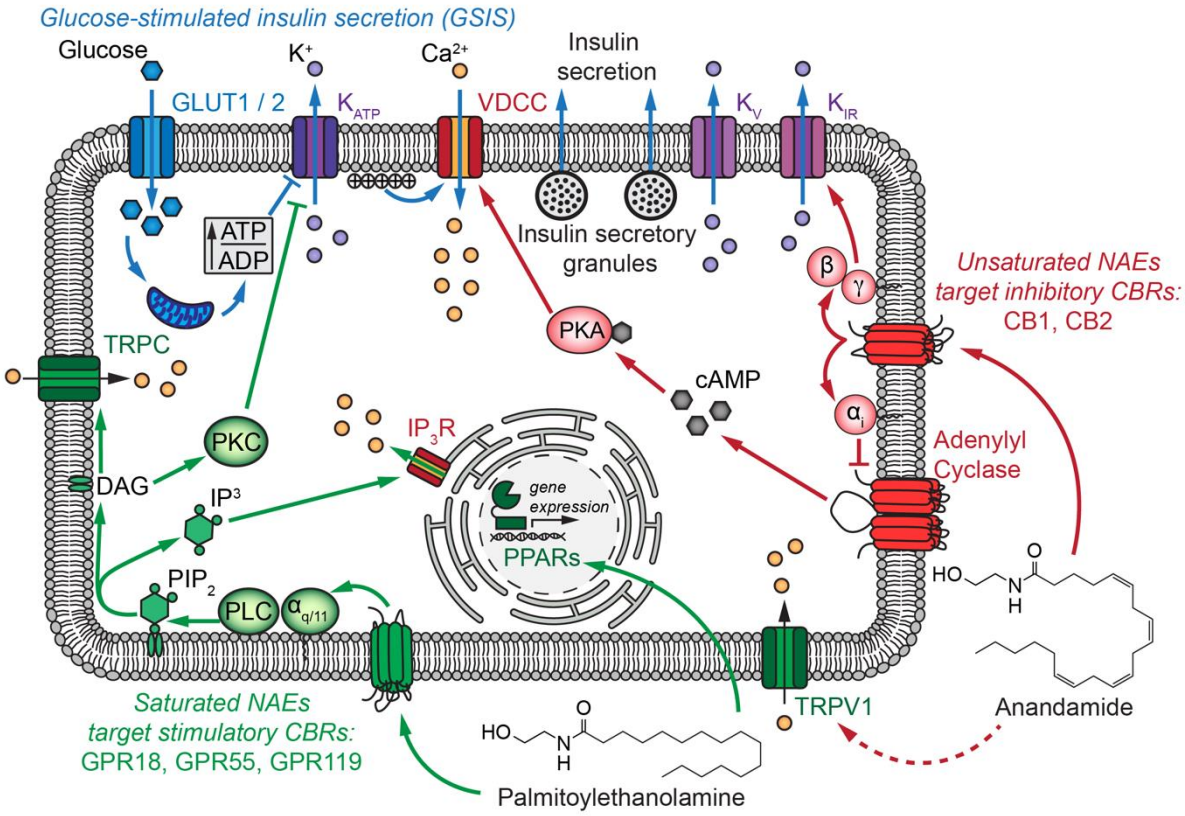


*Figure 1.2. GSIS relies on signaling input from many pathways, including the ECS. β-cells secrete insulin in response to elevated blood glucose in a process known as GSIS (blue arrows). Unsaturated NAEs tend to target CBRs coupled to inhibitory $G\alpha_{i/o}$ proteins (red). Saturated NAEs tend to target CBRs coupled to stimulatory $G\alpha_{q/11}$ proteins (green). CBR pathways can manipulate $[Ca^{2+}]_i$ and membrane polarity, which can impact β-cell excitability GSIS.*

## 1.2. Current chemical biology tools to study the endocannabinoid system

Chemical biology involves using chemical tools to investigate biological systems. An advantage of chemical biology is that once a tool is developed, it can be applied to different systems to investigate a variety of biological questions. Each technique has a set of advantages and

disadvantages that should be considered before applying a strategy to address a biological question.

Photopharmacology is an approach that makes small molecules respond to light[42]. The key advantage to this technique is that light can be applied with unmatched speed, and a degree of spatial control. Two examples of photopharmacological tools include photoswitches and photocages (**Figure 1.3**). A photoswitch is a small chemical motif that can be reversibly isomerized with light into an 'active' and 'inactive' state. For example, the classic photoswitch azobenzene can be reversibly switched to the *cis* isomer under UV-A light and to the *trans* isomer under blue light. Azobenzenes have been used to put cannabinoid signaling under reversible control[43–45]. *azo*-THC was the first photoswitch to put CBR signaling under optical control, with a bias towards CB1 agonism[43]. A benzimidazole-based photoswitch was the first selective CB2 photoswitch with nanomolar potency[44]. In contrast, photocages consist of a ligand whose activity is masked by a photolabile protecting group, which irreversibly releases the active molecule. Common photocages include the nitrobenzyl and coumarin photocages[46]. Photocages have also been used to probe cannabinoid receptor signaling, including caged AEA and 2-arachidonoylglycerol (2-AG). Caged AEA was first used to evaluate the dynamics of retrograde endocannabinoid signaling in rat hippocampus slices[47], while caged 2-AG was used to characterize the impact of 2-AG on the MIN6 β-cell signaling network[48].

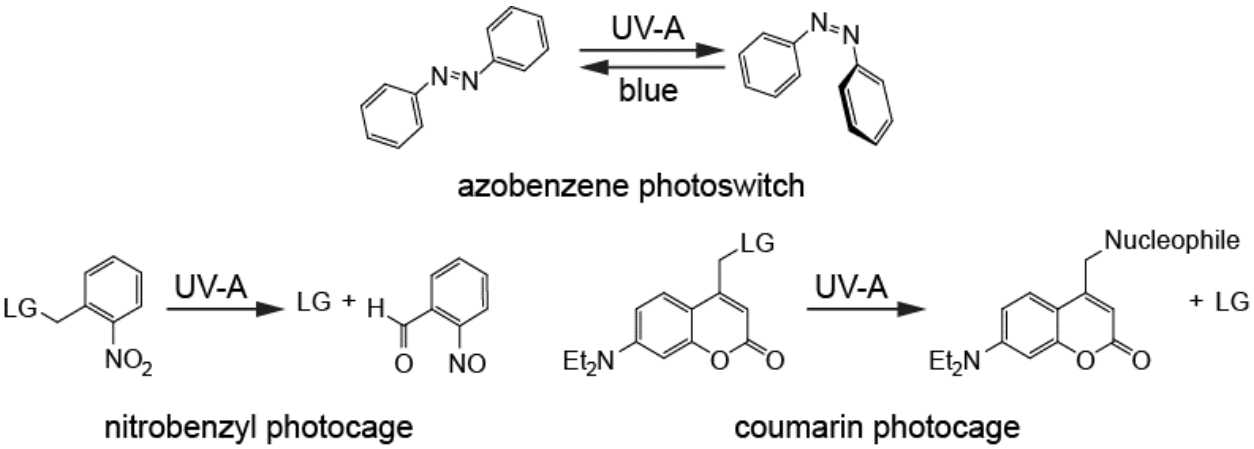


*Figure 1.3. Common photochemical tools: photoswitches and photocages.*
*An azobenzene (top) can be photoswitched to the cis isomer with UV-A light and to the trans isomer with blue light. A nitrobenzyl cage (bottom left) can be released with UV-A (365 nm) light. A diethylamino coumarin cage (bottom right) can be released with UV-A (405 nm) light. LG = leaving group.*

While photopharmacology has expanded the toolset to study cannabinoid signaling, there are a few limitations. UV light is toxic to cells and has limited tissue penetration, limiting the use of some tools *in vivo*. Red-shifting optical tools to uncage or photoswitch with longer wavelengths of light will improve the applicability of photopharmalogical tools in complex systems[49–51]. While photoswitches allow for optical control over a system, the photoswitch remains permanently incorporated into the ligand of interest and cannot investigate endogenous ligand signaling. Further, the physical properties of the photocage largely determines their localization in cells[52,53]. For example, a cationic triphenylphosphonium group on a coumarin photocage can allow for mitochondria targeting, while sulfonated coumarin can allow for plasma membrane targeting of the photocage[53]. However, since both tools are freely diffusible, when transitioning to 3D structures such as a pancreatic islet, these tools cannot selectively activate cannabinoid signaling pathways on specific cell types.

Genetic approaches can offer cell specificity that traditional pharmacology cannot afford. For example, genetic knockout (KO) or knockdown (KD) experiments can selectively reduce a

protein of interest's expression in a specific cell type. However, KO and KD are slow, requiring a days time scale to take effect, and are prone to compensation artefacts. Thus, a chemigenetic approach is a promising alternative, which combines the speed and specificity granted by pharmacology with the spatial precision offered by genetics to allow for precise control over signaling pathways (**Figure 1.4**). A few strategies for chemigenetic targeting include designer receptors and self-labeling proteins (SLPs). Designer receptors exclusively activated by designer drugs (DREADDS) use synthetic ligands that specifically activate engineered designer GPCRs[54]. There are DREADDS that are $G\alpha_i$, $G\alpha_s$, or $G\alpha_q$-coupled, and have been broadly used to modulate neuronal activity in a cell-specific manner. Similarly, SLPs such as SNAP-tags and HaloTags are biologically inert proteins that specifically and covalently recognize a small chemical group. For example, a benzylguanine motif labels SNAP-tags[55], while a chloroalkane motif labels HaloTags[56]. These biorthogonal motifs can be synthetically appended to other groups, such as a fluorescent dye for microscopy or a biotin for protein enrichment, and the ligand will be directed toward the site of SLP expression.

SLPs are a useful tool for achieving cell type specificity. For example, photoswitchable orthogonal remotely tethered ligand (PORTL) combines a photoswitchable ligand to a benzylguanine via a flexible linker to label SNAP-tags and reversibly control receptors with light[57]. The first PORTL ligands were benzylguanine-azoglutamate (BGAG), which labelled a SNAP-tagged metabotropic glutamate receptor (mGluR2) and enabled reversible optical control of mGluR2 function in cultured hippocampal neurons[57]. Drugs acutely restricted by tethering (DART) uses a similar strategy as PORTL, where a standard drug is directed towards HaloTags via a chloroalkane motif. The DART approach was used to target $\alpha$-amino-3-hydroxy-5-methylisoxazole-4-propionic acid receptors (AMPAR) with a DART equipped with YM90K, an AMPAR antagonist, and was applied to a mouse model of Parkinson's disease[58].

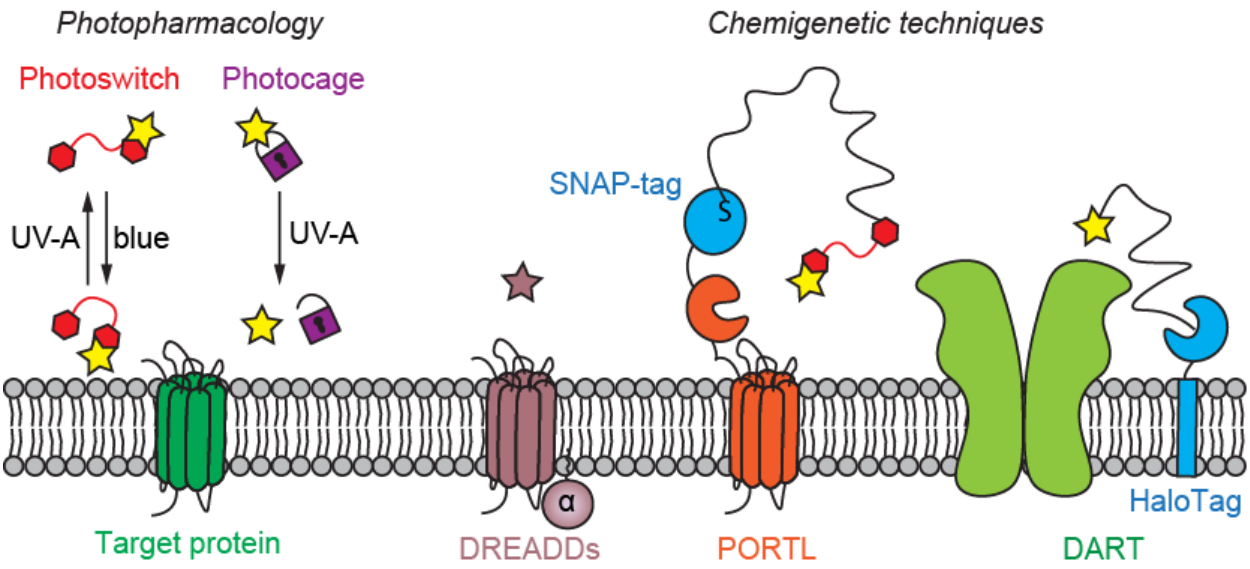


*Figure 1.4. Chemical biology approaches to study receptor signaling. Photopharmacology puts a ligand of interest (yellow star) under optical control. A photoswitch (red) reversible controls the activity of a ligand with different wavelengths of light, while a photocage (purple) irreversibly releases a ligand of interest in response to a flash of light. DREADDS (mauve) are designer receptors that are activated by designer synthetic ligands (mauve star). PORLT (orange) combines the genetic targetability of SLPs (blue, SNAP-tag) with the optical control of photoswitches. DART (green) anchors a drug of interest to a genetically defined membrane-bound SLP (blue, HaloTag).*

While these chemigenetic strategies are promising, they fail to target *endogenous* signaling pathways using *unmodified endogenous* ligands. DREADDs utilize a synthetic ligand with an engineered receptor, and can interrogate the activity of specific cell types, but not endogenous signaling pathways. PORTL has the same limitations of photoswitches, in that the ligand of interest is permanently modified with the photoswitch, which can affect its pharmacology in cells. In the original PORTL publication, the SNAP-tag was fused to the mGluR2, thus endogenous receptors were not targeted. However, membrane-anchored SNAP-tags are available to overcome this limitation. DART targets endogenous receptor pools but uses synthetic ligands which are permanently modified *via* linker attachment to biorthogonal

motif. As a result, a new tool is needed to target receptors with unmodified ligands to study endogenous signaling pathways.

## 1.3. Design of Optically-Cleavable Targeted (OCT)-Ligands

This work introduces a novel chemigenetic technique to place cannabinoid signaling under genetically-targeted optical control. Coined Optically-Cleavable Targeted (OCT)-ligands, our approach tethers photocaged NAEs to genetically-encoded SLPs to permit photorelease of endocannabinoid ligands on genetically-defined membranes (**Figure 1.5**). OCT-ligands are small molecules composed of four units; the NAE ligand (red), photocage (purple), linker (black), and bioorthogonal motif (blue). As a proof of concept, I synthesized OCT-Palmitoylethanolamide (**OCT-PEA**), which was capable of targeting GPR55 to investigate the downstream mechanisms by which this cannabinoid receptor affects β-cell excitability (**Chapter 2**). To improve the labeling efficiency of **OCT-PEA**, I generated four derivatives that covalently labelled HaloTags over SNAP-tags, coined **hOCT-PEA**. We also generated an AAV-Halo virus, which selectively expresses HaloTags on the surface of human β-cells. Together, these tools allowed us to achieve cell targeted photopharmacology in intact human islets (**Chapter 3**). To expand the OCT-ligand approach to other protein targets, I synthesized OCT-Anandamide (**OCT-AEA**) (**Chapter 4**). Unlike PEA which is fully saturated, AEA has a longer acyl chain with 4 double bonds and targets the $G\alpha_i$-coupled CB1. Collectively, this work serves as a proof-of-principle for a platform that will advance our understanding of endocannabinoid signaling with subcellular resolution.

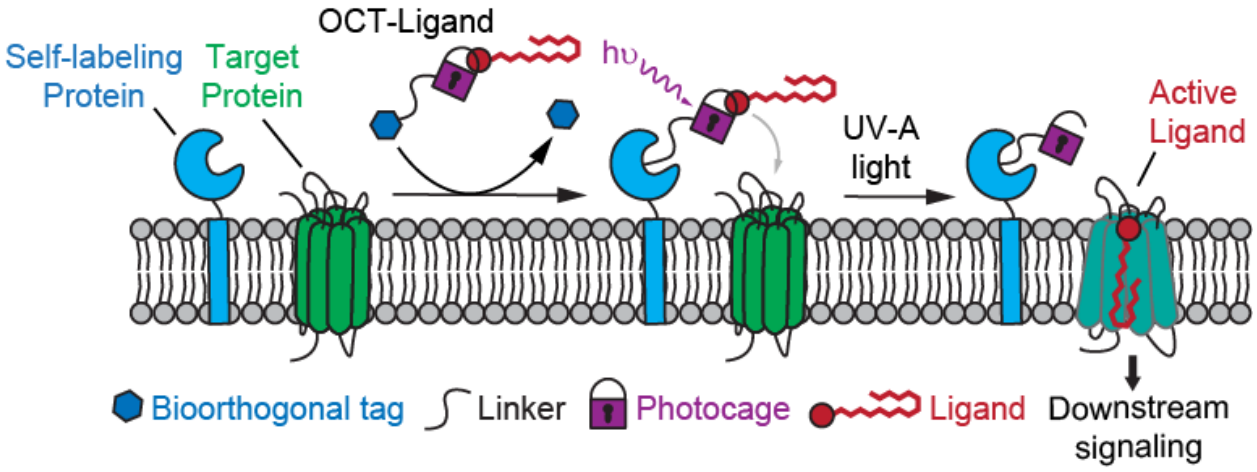


*Figure 1.5 The OCT-ligand approach allows for genetic targeting of photocaged ligands. OCT-ligands can be spatially directed to the site of SLP expression, then with light the photocage is released to expose an unmodified ligand of interest to activate nearby endogenous receptors.*

# Chapter 2. Genetically-targeted photorelease of endocannabinoids enables optical control of GPR55 in pancreatic β-cells

Janelle M. Tobias[1,2], Gabriela Rajic[1], Alexander E.G. Viray[1,2], David Icka-Araki[1,2] and James A. Frank[1,2]

[1] Vollum Institute, Oregon Health & Science University, Portland, OR, USA.

[2] Department of Chemical Physiology & Biochemistry, Oregon Health & Science University, Portland, OR, USA.

Chapter 2 has been adapted from *Tobias et al.*, published in Chemical Science in 2021[59].

Author contribution:

J.A.F. conceived and coordinated the study. **J.M.T.** synthesized and characterized the compounds. **J.M.T.**, G.R., and A.E.G.V. carried out imaging experiments in cultured cells. A.E.G.V. carried out the cytotoxicity assay. **J.M.T.**, J.F., and D.I.A. performed UV-Vis and HPLC-MS experiments. **J.M.T.** wrote MATLAB codes for $Ca^{2+}$ and UV-Vis data analysis. **J.M.T.** and J.A.F. wrote the manuscript with contributions from all other co-authors.

## 2.1. Introduction

Palmitoylethanolamide (PEA) is a NAE that is part of the extended ECS[4] and has been shown to have therapeutic benefits in pain, inflammation, and diabetic neuropathy[60,61]. PEA is composed of an ethanolamine head group attached via an amide linkage to a palmitate (16:0) lipid chain[62,63], and activates GPR55 selectively over CB1 and CB2. GPR55 signals through $G\alpha_{q/11}$, which activates phospholipase C and downstream leads to an increase in $[Ca^{2+}]_i$ from the endoplasmic reticulum stores[39]. GPR55 potentiates β-cell excitability and GSIS both *in vitro* and *in vivo*[60]. Treatment of isolated pancreatic islets with O-1602, a specific GPR55 agonist, significantly increased insulin secretion from both rat and mouse islets, but not in GPR55-KO mouse islets[32,64]. Further, chronic IP injections of PEA in a diabetic mouse model led to increased serum insulin levels compared to vehicle due to preserved islet morphology[60]. Taken together this data suggests that PEA signaling could play an important role in pancreatic islet function. Yet, our knowledge of GPR55's precise function in β-cells is hindered by a lack of tools that enable its precise manipulation.

Advances in chemical biology have provided a collection of tools to interface with endocannabinoid signaling, including ligands that are activated on an optical stimulus[43–45]. As light can be applied with unmatched spatiotemporal precision, optical tools like photocaged endocannabinoids have illuminated the function of CB1 and CB2 receptors in excitable cells[47,48]. These probes contain a photolabile protecting group (cage) which masks the endocannabinoids' activity until exposed to irradiation, triggering the release of endogenous ligands within milliseconds. However, a limitation of this approach is that the cage's structure impacts the probe's subcellular localization before irradiation, making the signal difficult to control within the cell. Although this spatial restriction has been exploited to release ligands on specific organelles by modifying the cage charge or aromaticity[52,53], this approach is quite restricted in its

application. Adding an element of genetic control, such as a genetically-encoded SNAP-tag[55], would allow us to direct caged signaling molecules toward any membrane or protein of interest.

To this end, we developed Optically-Cleavable Targeted (OCT-) ligands to combine a photocaged NAE with a bioorthogonal handle, which can be recognized by genetically-encoded SNAP-tags (**Figure 2.1**). As a proof-of-concept, I synthesized OCT-Palmitoylethanolamide (**OCT-PEA**), which has a PEA ligand whose activity is masked by an ortho-nitrobenzyl photocage[47], and the distal end of the cage is linked to an $O^6$-(4-aminomethyl-benzyl)guanine (BG) motif for covalent tethering to SNAP-tags. The tethered probe can then be quickly uncaged (activated) by a flash of light, generating bursts of the active molecule at the site of SNAP-tag expression. When applied to β-cells, **OCT-PEA** revealed that plasma membrane GPR55 stimulates β-cell $Ca^{2+}$ activity *via* phospholipase C. Moving forward, the OCT-ligand approach can be translated to other ligands and receptors, and will open up new experimental possibilities in targeted pharmacology.

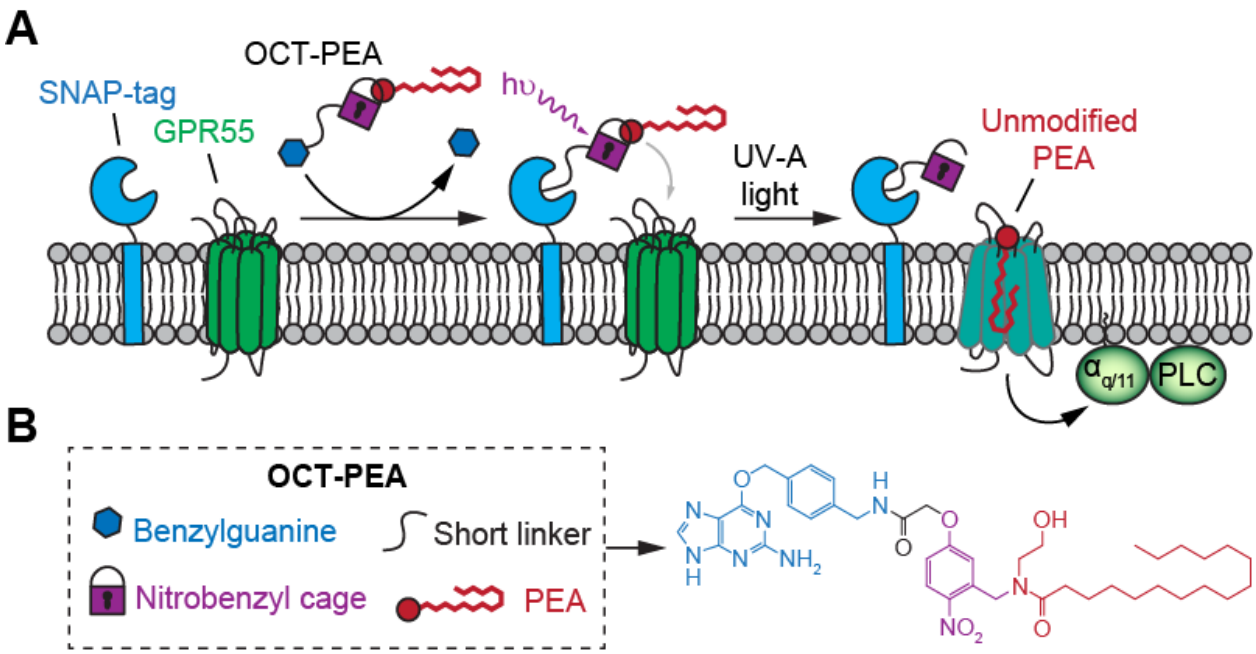


*Figure 2.1. OCT- palmitoylethanolamide (PEA) targets SNAP-tags and activates GPR55. (**A**) Schematic depiction of **OCT-PEA**, which activates GPR55 through $G\alpha_{q/11}$ and PLC. (**B**) Chemical structure of **OCT-PEA** which contains: a benzylguanine tag, short linker, nitrobenzyl cage, and PEA ligand.*

## 2.2. Results

### 2.2.1. Synthesis of an OCT-ligand for GPR55.

The synthesis of **OCT-PEA** (**Figure 2.2**) commenced with the reaction of 5 hydroxy-2-nitrobenzaldehyde and ethyl bromoacetate to form the phenolic ether **1**. A reductive amination with 2-(t-butyloxy)-ethanamine formed the amine **2**, and then acylation with palmitoyl chloride led to the tertiary amide **3**. Ester hydrolysis under basic conditions afforded carboxylic acid **4**, which was then coupled to 6-((4-(aminomethyl)benzyl)oxy)-*9H*-purin-2-amine (BG-$NH_2$)18 to produce **5**. Finally, tBu-ether deprotection using $BBr_3$ at −78 °C afforded **OCT-PEA** in six steps and 26% overall yield.

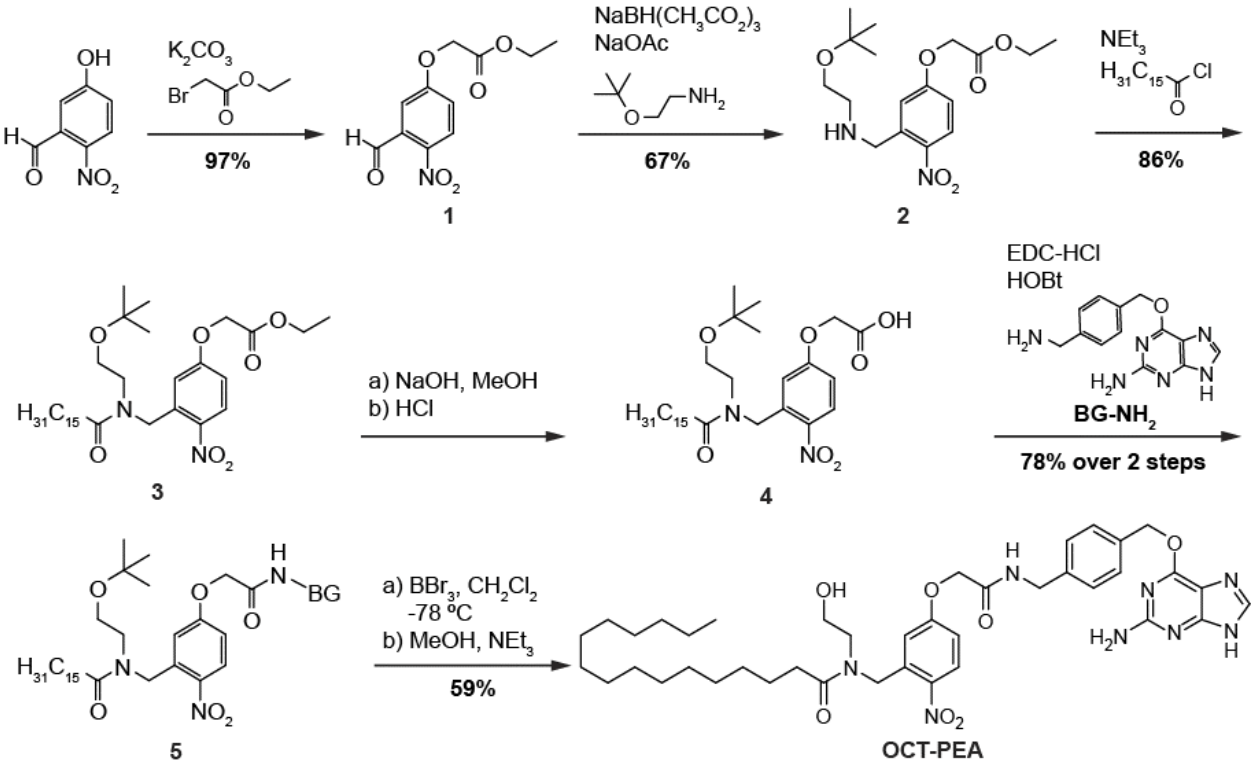


*Figure 2.2. Chemical synthesis of **OCT-PEA**, which was prepared in 6 steps with a 26% yield.*

UV-Vis spectroscopy was used to characterize the photochemical properties of uncaging **OCT-PEA** (**Figure 2.3 A**). In the dark, OCT-PEA (in DMSO) possessed a $\lambda_{max}$ at 287 nm and an

extinction coefficient of 15,345 ($mol^{-1}$•$cm^{-1}$) (**Figure 2.3 B**). LED irradiation at 365 nm resulted in a bathochromic wavelength shift to 354 nm, consistent with the expanded electron $\pi$-network present in the uncaged product. Longer wavelengths—such as 415 nm (navy), 470 nm (blue), and 565 nm (green)—did not uncage **OCT-PEA** as efficiently (**Figure 2.3 B,C**). This feature is advantageous for applications in fluorescence microscopy, since the ligand will not be released during imaging of blue and green fluorescent reporters. We also conjugated **OCT-PEA** to purified SNAP-tags *in vitro*, which allowed the probe to be uncaged in aqueous buffer. In this case, 365 nm irradiation induced uncaging with a $\tau$ ~ 46 s (**Figure 2.3 D,E**), demonstrating **OCT-PEA**'s ability to be released from SNAP-tags in a physiological environment.

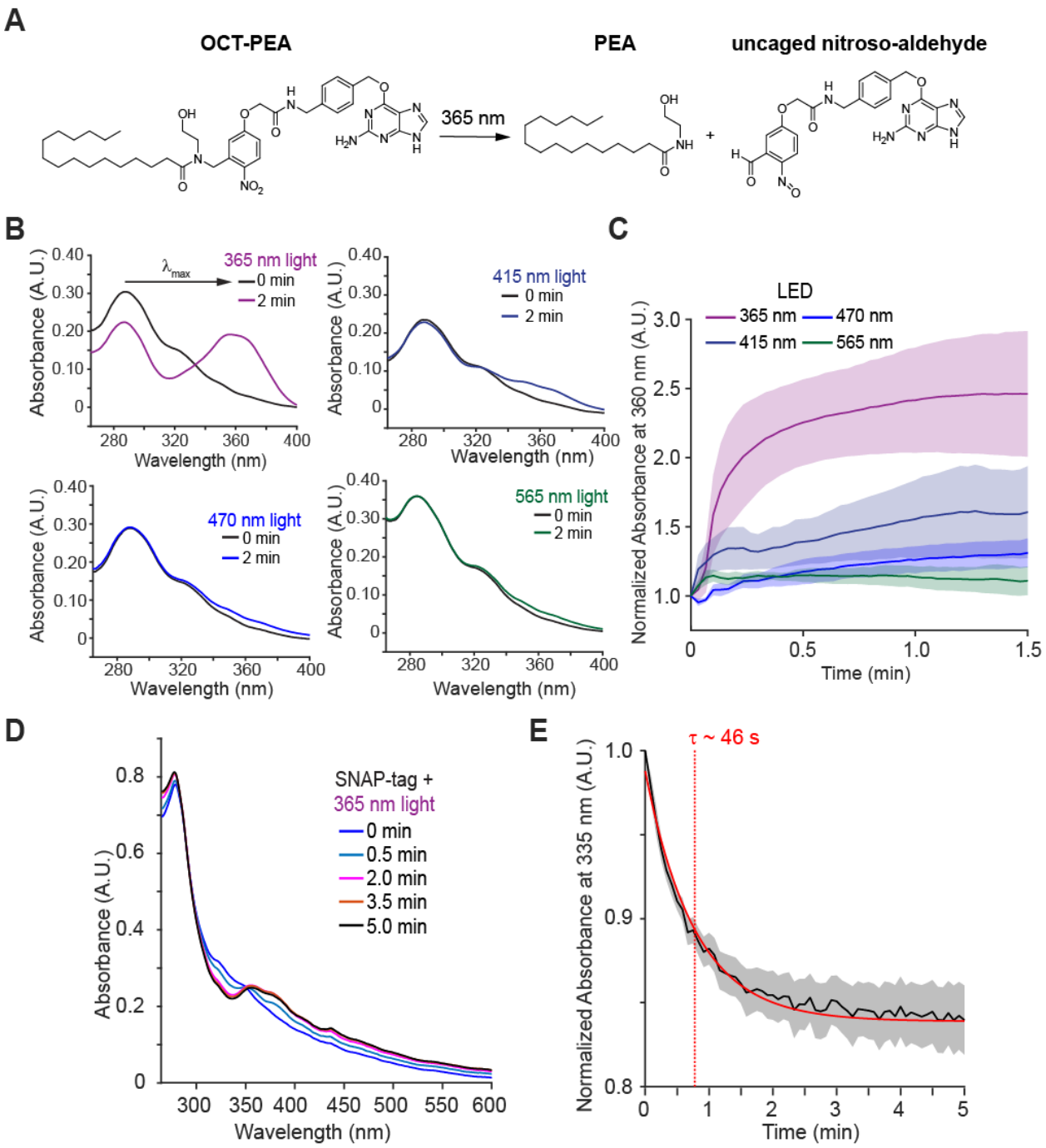


*Figure 2.3. UV-Vis characterization of uncaging **OCT-PEA**.*

*(**A**) Chemical structures showing the uncaging reaction of OCT-PEA, which releases PEA and the nitroso-aldehyde attached to the BG. (**B**) Absorbance vs. Wavelength scan of OCT PEA (20 μM, in DMSO) before LED exposure (black), and after 2 min uncaging using 365 nm (top left, magenta, ~35 mW), 415 nm (top right, navy, ~31 mW), 470 nm (bottom left, blue, ~35 mW), or 565 nm (bottom right, green, ~31 mW) LED. (**C**) Absorbance at 360 nm over time of **OCT-PEA***

*(20 $\mu$M in DMSO) uncaging with 365 nm LED (magenta), 405 nm (navy), 470 nm (blue), and 565 nm (green) LEDs. N = 3 trials. (**D**) Absorbance vs wavelength of scan of **OCT-PEA** after it had been conjugated to purified SNAP-tag protein (10 $\mu$M in PBS). (**E**) Absorbance over time at $\lambda = 335$ nm of **OCT-PEA** in the presence of SNAP-tag purified protein. Red dotted line indicates $\tau \sim 46$ s for **OCT-PEA** uncaging under 365 nm LED irradiation. The exponential best-fit is displayed as a solid red line. N = 3 trials. Shaded error bars = mean ± S.E.M.*

### 2.2.2. GPR55 and PEA mediate $Ca^{2+}$ signaling in INS-1 β-cells.

We used the rat insulinoma INS-1 cell line[65,66] to evaluate the effect of **OCT-PEA** on β-cell excitability. Although other β-cell lines (MIN6, BRIN-D11) and primary islets (human, mouse, rat) are known to express GPR55[32,37,64], its expression and function in INS-1 cells remain unresolved[34,67]. Therefore, we used immunofluorescence microscopy to confirm the expression and localization of GPR55. INS-1 cells were co-stained with anti-GPR55 and anti-insulin antibodies (**Figure 2.4 A**). GPR55 immunoreactivity was observed on the INS-1 plasma membrane, while insulin was observed throughout the cell. In control experiments, removal of the primary antibody abolished GPR55 immunofluorescence, ruling out the possibility of nonspecific secondary antibody binding (**Figure 2.4 B**).

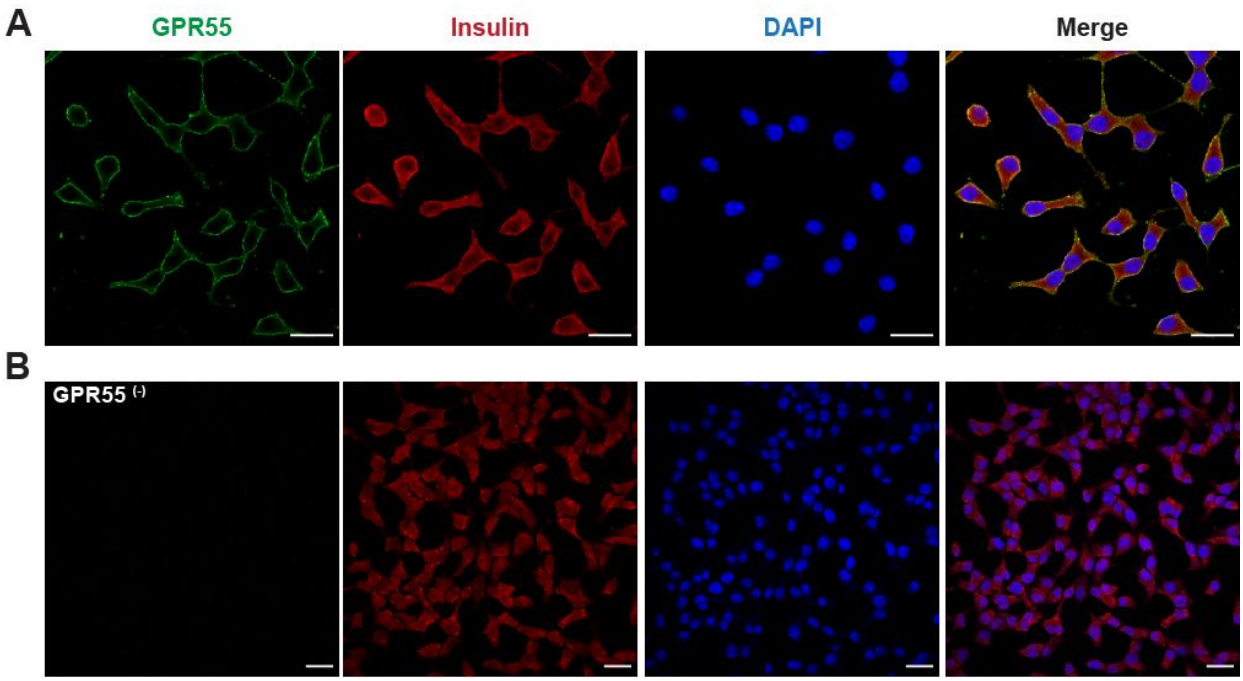


*Figure 2.4. INS-1 β-cells express GPR55 and insulin.*
*(**A**) Double immunofluorescence staining of GPR55 (green) and insulin (red). DAPI (blue) was used as a nuclear marker. Displayed are individual channels and the merged image. (**B**) Control experiment without the GPR55 primary antibody. No GPR55 immunofluorescence is observed, demonstrating that the effect is not caused by non-specific secondary antibody binding. Scale bars = 20 μm.*

To determine the effect of freely diffusible PEA application on the β-cell $[Ca^{2+}]_i$, INS-1 cells were transfected with the fluorescent biosensor R-GECO[68], which allows for visualization of $[Ca^{2+}]_i$ in real-time. Under high glucose conditions (20 mM), PEA increased both the overall $[Ca^{2+}]_i$ level (**Figure 2.5 A**) and oscillation frequency (**Figure 2.5 B**) in a dose-dependent manner. Further, at lower glucose concentrations (11 mM and 3 mM), PEA's effect on the $[Ca^{2+}]_i$ was reduced (**Figure 2.5 C**), while at high glucose (20 mM) PEA best stimulated $[Ca^{2+}]_i$ (**Figure 2.5 C, blue**, **Figure 2.5 D**). Under high glucose, pretreatment with either the GPR55 antagonist CID16020046 (**Figure 2.5 E,F**, blue) or PLC inhibitor U73122 (**Figure 2.5 E,F**, red) abolished PEA's action[69,70]. In control experiments, the effect of PEA remained in the presence of an

inactive PLC inhibitor analogue (U73343) (**Figure 2.5 E,F**, green)[70]. $Ca^{2+}$ levels were not sensitive to 375 nm irradiation alone, nor vehicle addition (**Figure 2.5 E,F**, grey). Combined with the results above, our experiments confirm that GPR55 is expressed on the surface of INS-1 β-cells and that it responds to PEA to mediate glucose-stimulated $Ca^{2+}$ oscillations via PLC.

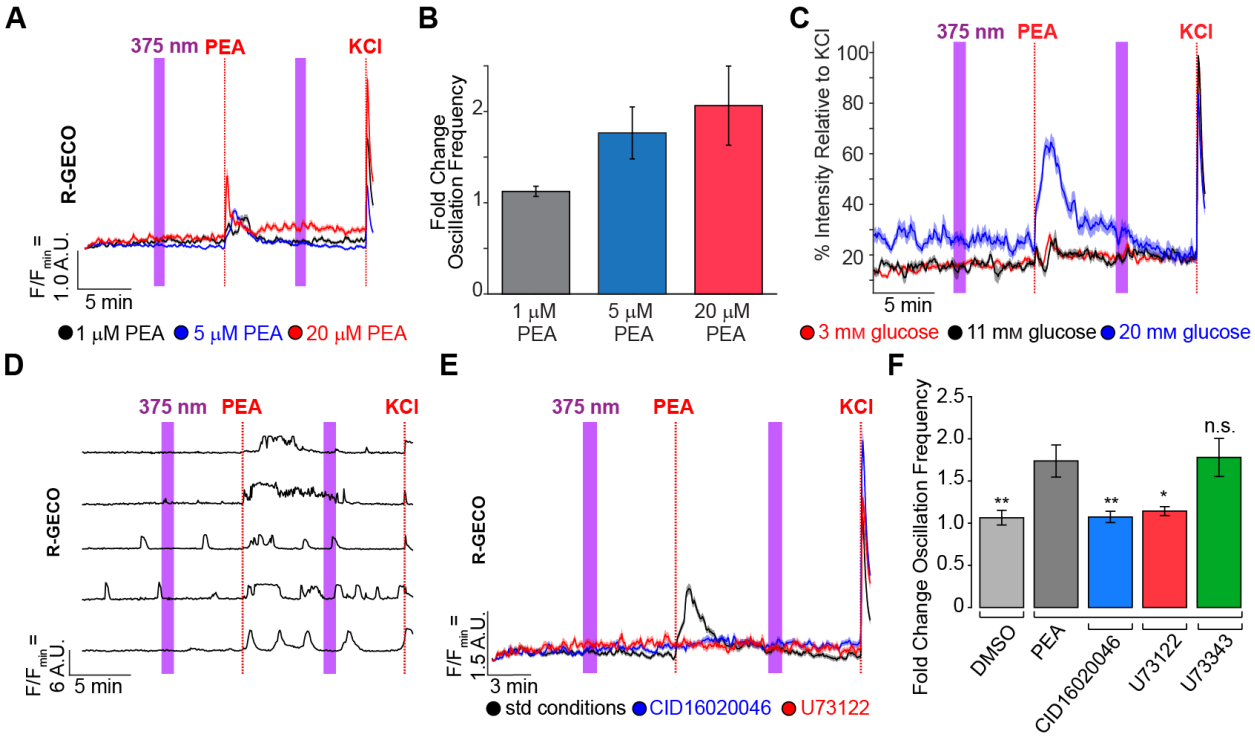


*Figure 2.5. PEA activates GPR55 in INS-1 cells.*

*(**A**) Average $[Ca^{2+}]_i$ traces for R-GECO-transfected INS-1 cells in response to 1 μM PEA (black, N = 165, T = 3), 5 μM PEA (blue, N = 494, T = 7), and 20 μM PEA (red, N = 224, T = 4). (**B**) Bar graph displaying the fold change in $Ca^{2+}$ oscillation frequency after PEA addition relative to baseline for data in panel **A**. (**C**) R-GECO-transfected INS-1 cells showed that PEA addition caused an increase in $Ca^{2+}$ in a glucose-dependent manner. Shown is the response to a 5 μM PEA addition at a glucose concentration of 3 mM (red, N = 485, T = 6), 11 mM (black, N = 307, T = 4), and 20 mM (blue, N = 494, T = 7). (**D**) Five representative R-GECO-transfected INS-1 cells showing that PEA addition (5 μM) increased $[Ca^{2+}]_i$. (**E**) Average $[Ca^{2+}]_i$ traces for PEA addition under standard conditions (black, 5 μM, N = 612, T = 10), overlaid with average $[Ca^{2+}]_i$ traces for PEA addition following pre-incubation with a GPR55 antagonist (CID16020046, 5 μM, blue, N =*

*449, T = 6) or PLC inhibitor (U73122, 5 μM, red, N = 296, T = 4), which blocked PEA's effect. KCl (25 mM) was applied at the end of each experiment. (**F**) Bar graph displaying the fold change in $Ca^{2+}$ oscillation frequency induced by compound stimulation. Vehicle addition (DMSO, 0.1% v/v, grey, N = 418, T = 6) did not stimulate $[Ca^{2+}]_i$. The inactive PLC inhibitor analogue (U73343, 5 μM, green, N = 511, T = 7) did not block the effect of PEA. Error bars = mean ± S.E.M. **P<0.01, *P<0.05, ns = P>0.05, see Table 2.1.*

*Table 2.1. Statistical significance calculations for fold change in oscillation frequency for PEA. **P<0.01 (dark red), *P<0.05 (pink), ns = P>0.05 (white)*

| | DMSO | PEA |
|---|---|---|
| DMSO | - | 0.0072 |
| PEA | 0.0072 | - |
| CID16020046 | 0.9361 | 0.0071 |
| U73122 | 0.4640 | 0.0127 |
| U73343 | 0.0190 | 0.8904 |

### 2.2.3. Expression and labeling of cell surface SNAP-tags in INS-1 β-cells.

To localize **OCT-PEA** nearby GPR55 receptors, we transfected INS-1 cells with a plasmid encoding pDisplay™-SNAP, a plasma membrane-anchored SNAP-tag. We then performed a competition labeling assay between **OCT-PEA** and a non-permeable SNAP-Surface® Alexa Fluor® 488 (A488) dye to optimize the conditions for **OCT-PEA** tethering. Transfected cells were labelled with either a vehicle or increasing concentrations and duration of **OCT-PEA**. They were then thoroughly washed and exposed to A488 to detect any un-reacted SNAP-tags. When preceded with the vehicle, A488 fluorescence was observed on the perimeter of transfected cells (**Figure 2.6**, top). Pre-treatment with **OCT-PEA** blocked A488 labeling in a dose- and time-

dependent manner (**Figure 2.6**). SNAP-tag labeling was abolished most consistently when cells were labelled with 5 μM **OCT-PEA** for 2 h.

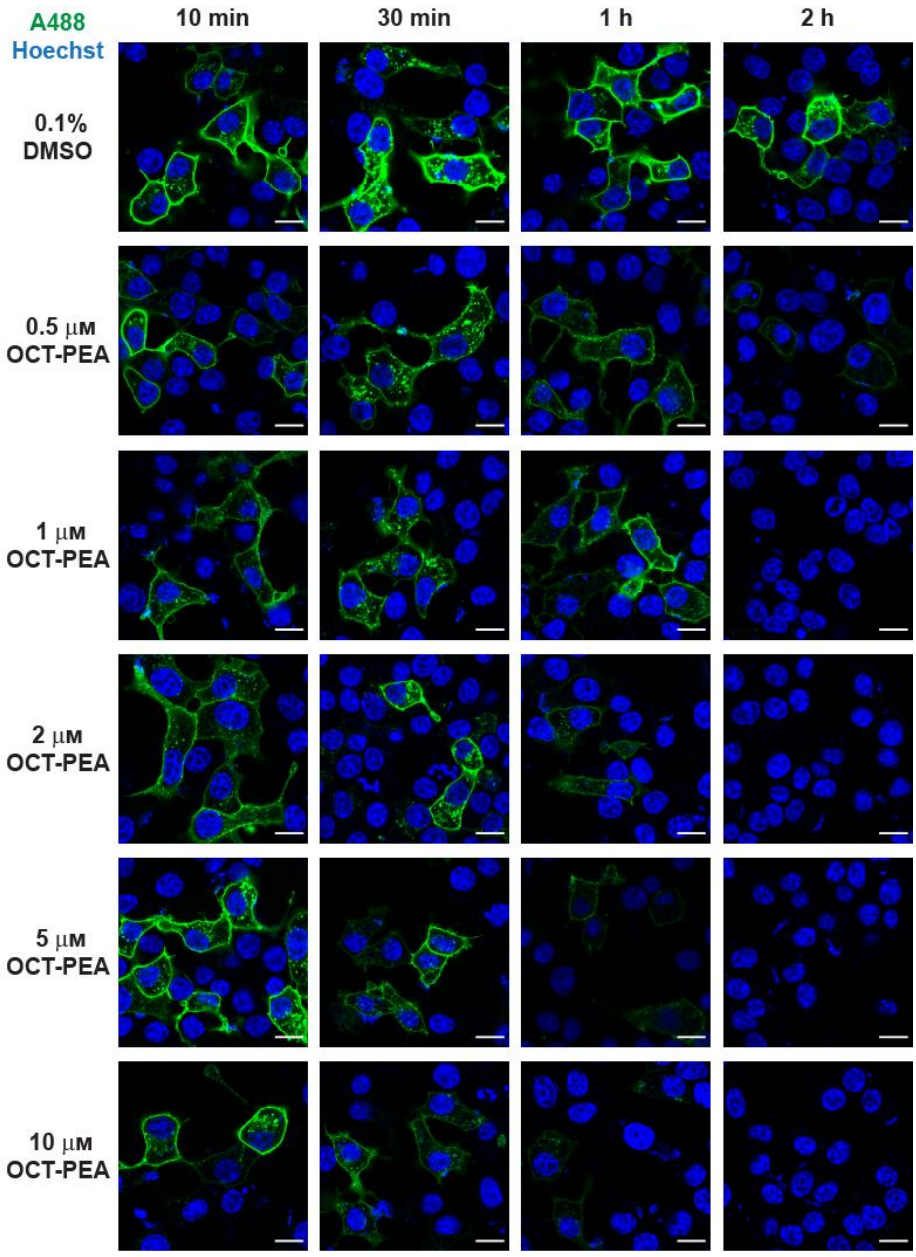


*Figure 2.6.* ***OCT-PEA*** *labels SNAP-tags in a time and concentration dependent manner. INS-1 cells transfected with pDisplay™-SNAP were treated with probe first, washed, then stained with SNAP-Surface® Alexa Fluor® 488 (A488, green). SNAP-tags that were not completely labelled with* ***OCT-PEA*** *are thus shown in green. Hoechst-33342 (blue) was used as a nuclear marker. Scale bars = 10 μm.*

To assess **OCT-PEA**'s ability to label intracellular SNAP-tags, a similar competition labeling was performed using the above-optimized labeling conditions, except using the cell-permeable dye, SNAP-Cell® Oregon Green®. When pre-treated with vehicle, we observed Oregon Green fluorescence on intracellular compartments, presumably representing pDisplay™-SNAP in the secretory pathway (**Figure 2.7 A**). When pretreated with **OCT-PEA** (5 μM, 2 h), dye labeling of intracellular SNAP-tags was still observed (**Figure 2.7 B**). This indicates that **OCT-PEA** is not cell permeable under these conditions, and primarily labels surface-expressed SNAP-tags.

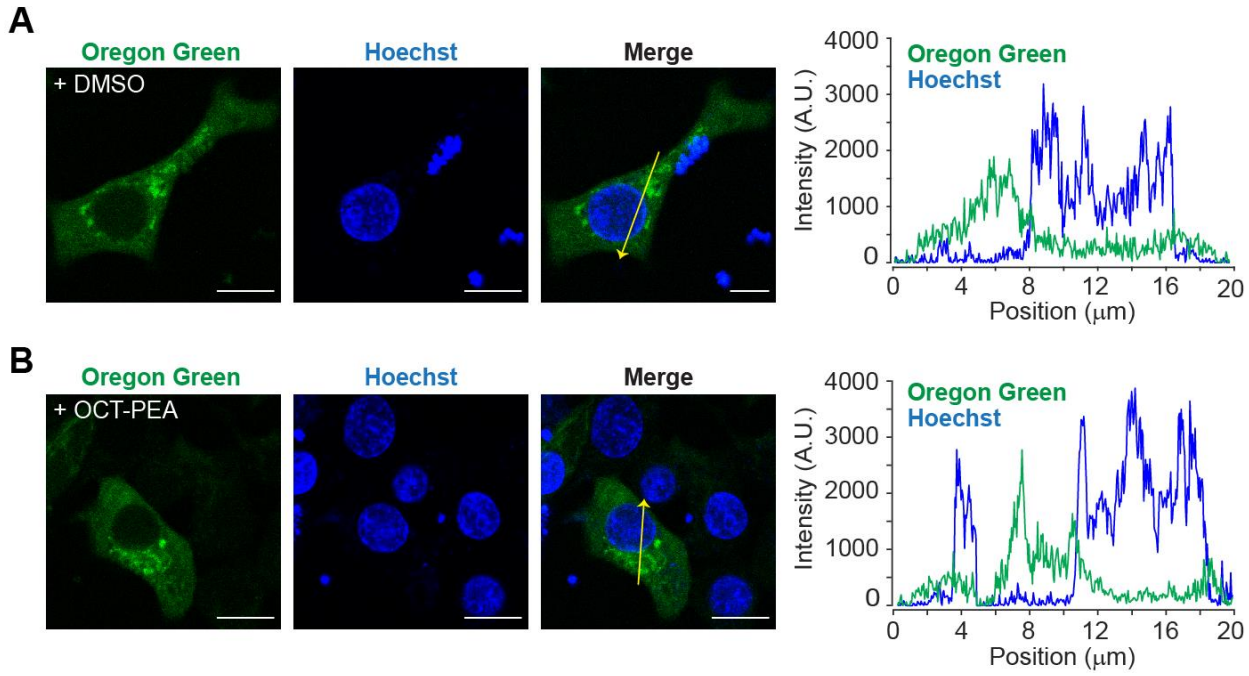


*Figure 2.7.* ***OCT-PEA*** *is not cell permeable.*
*INS-1 cells transfected with pDisplay™-SNAP were treated with DMSO (0.1% v/v,* ***A****) or* ***OCT-PEA*** *(5 μM,* ***B****) for 2 h, followed by incubation with cell-permeable SNAP-Cell® Oregon Green® (1 μM, 30 min). Hoechst-33342 (blue) serves as a nuclear marker. Intensity values of green and blue channels plotted along the yellow line shown in the merge image. Scale bars = 10 μm.*

To assess the extent of SNAP-tag internalization during this labeling time, pDisplay™-SNAP-expressing cells were incubated with the non-permeable A488 for 2 h (**Figure 2.8 A**).

Although most of the fluorescence remained enriched at the plasma membrane, small puncta appeared inside the cells slowly over time (**Figure 2.8 B**). This finding confirms that the labelled SNAP-tags remain enriched on the plasma membrane, with a fraction of internalized SNAP-tags present.

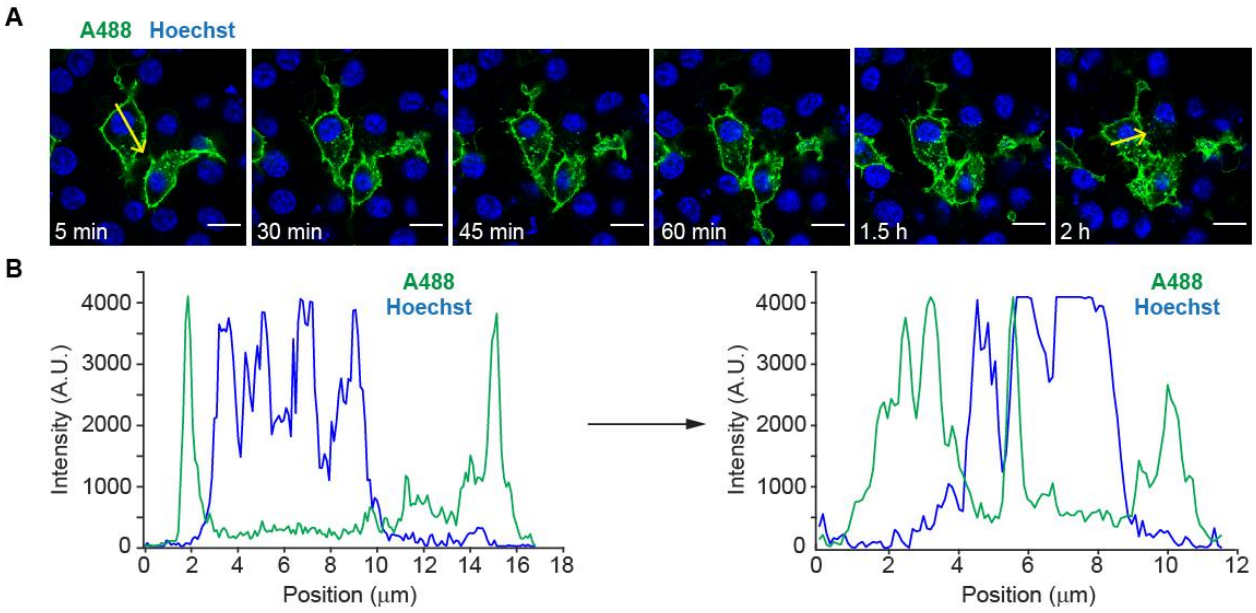


*Figure 2.8. SNAP-tag internalization over prolonged labeling.*
*(**A**) INS-1 cells transfected with pDisplay™-SNAP were labeled with non-permeable dye SNAP-Surface® Alexa Fluor® 488 (A488, 1 μm, 30 min, green), washed, and imaged over time. Hoechst-33342 (blue) serves as a nuclear marker. Displayed are representative images of the same cells over time. (**B**) Intensity values of green and blue channels along the yellow line shown in panel **A**, at 5 min (left) and 2 h (right) post wash. While some SNAP-tags are internalized over time, a majority remains enriched at the plasma membrane. Scale bars = 10 μm.*

We performed site-directed mutagenesis to our standard pDisplay™-SNAP construct to remove the reactive cysteine. Using immunohistochemistry we confirmed that the C145A mutation prevents the SNAP-tag from labeling the BG, but did not affect its trafficking or localization (**Figure 2.9**).

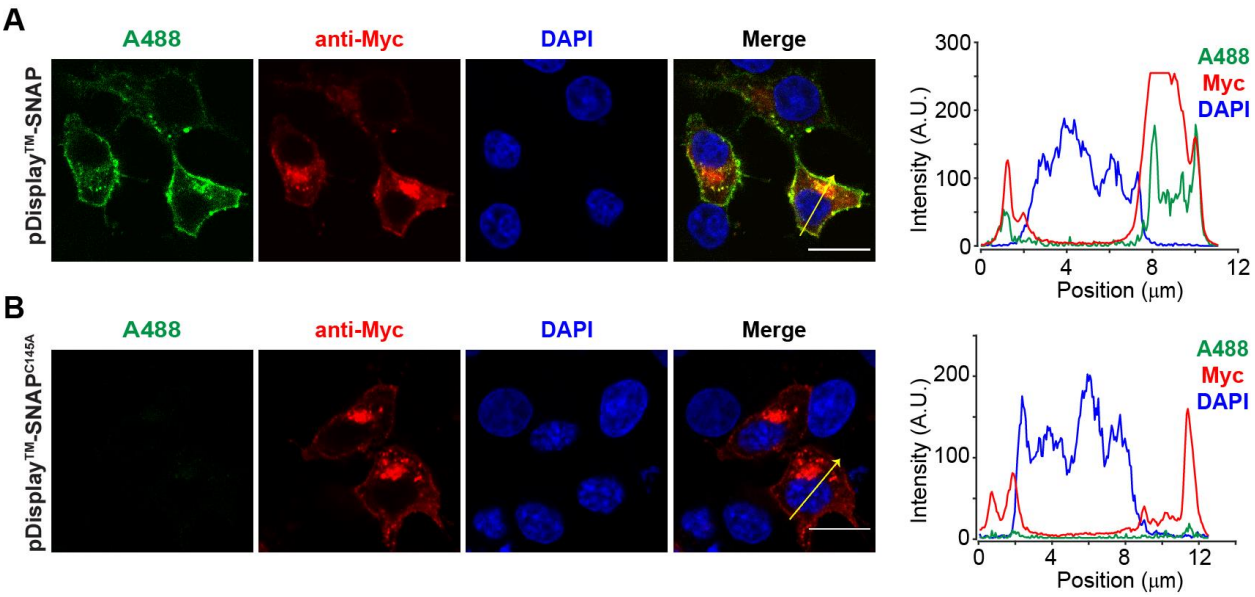


*Figure 2.9. SNAP-tag mutant maintains surface localization but does not recognize BG motif. Both pDisplay™-SNAP and pDisplay™-SNAP$^{C145A}$ constructs contain a Myc-tag. (**A**) Images showing pDisplay™-SNAP labeling with SNAP-Surface® Alexa Fluor® 488 (green), immunofluorescent staining of anti-MYC tag (red), and DAPI (blue). Intensity plot along the position of the yellow line shown in the merged image. (**B**) Images showing pDisplay™-SNAP$^{C145A}$ labeling with SNAP Surface-Alexa488 (green), immunofluorescent staining of anti-MYC tag (red), and DAPI (blue). Intensity plot along the position of the yellow line shown in the merged image. Scale bars = 10 μm.*

To evaluate the cytotoxicity of our probe, INS-1 cells were incubated with caged or uncaged **OCT-PEA** for 24 h and then subjected to a cell viability assay. We did not observe any effect on cell viability induced by the caged or uncaged **OCT-PEA** up to its solubility limit in the physiological buffer (**Figure 2.10**). PEA also did not affect cell viability[37,71], confirming that our probes are not cytotoxic to INS-1 cells.

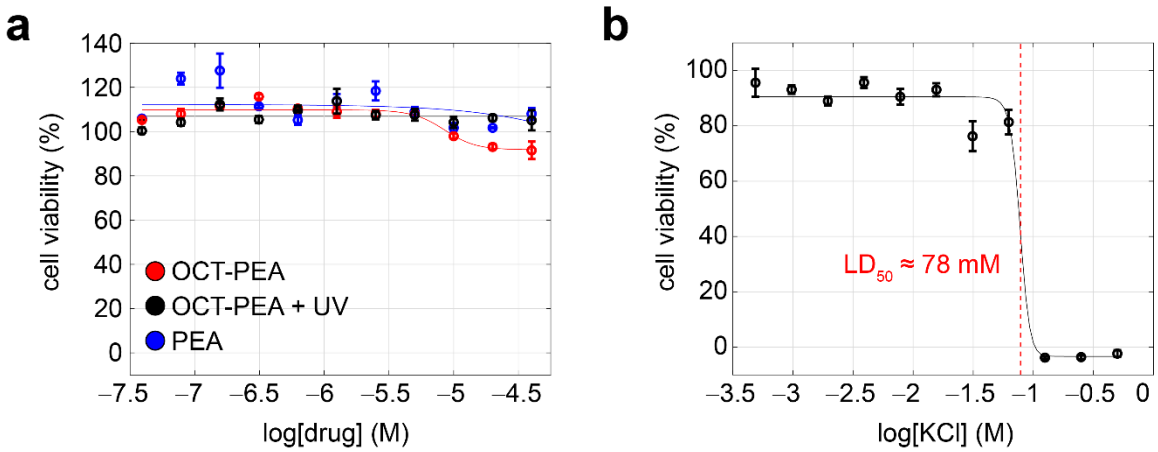


*Figure 2.10.* ***OCT-PEA*** *was not toxic to INS-1 cells.*
*INS-1 cells were incubated with compound for 24 h, then evaluated by the 3-(4,5-dimethylthiazol-2-yl)-2,5-diphenyltetrazolium bromide (MTT) assay. (**A**) INS-1 cell viability remained stable when the cells were incubated with* ***OCT-PEA*** *(caged, red), UV-A irradiated* ***OCT-PEA*** *(uncaged, black) or PEA (blue) up to 40 μM, near its solubility limit in physiological buffer. (**B**) As a positive control for the assay, INS-1 cells were incubated with KCl for 24 h, which had an $LD_{50}$ of ~78 mM. Four biological replicates were performed for each condition. Error bars = mean ± S.E.M.*

### 2.2.4. Plasma membrane PEA uncaging mediates INS-1 $Ca^{2+}$ levels via GPR55.

Finally, we evaluated how uncaging **OCT-PEA** on the cell surface influenced $[Ca^{2+}]_i$ dynamics in β-cells under high-glucose conditions (20 mM). INS-1 cells expressing R-GECO and pDisplay™-SNAP were labelled with **OCT-PEA**, followed by a washing step to remove any untethered probe. In contrast to the large $Ca^{2+}$ spike observed from bath-applied PEA, **OCT-PEA** uncaging on the cell surface caused a more subtle increase in $[Ca^{2+}]_i$ (**Figure 2.11 A**,**B**). However, we observed that **OCT-PEA** stimulation strongly increased the $Ca^{2+}$ oscillation frequency (**Figure 2.11 C**). Following probe labeling, treatment with the GPR55 antagonist CID16020046 or PLC inhibitor U73122 blocked the effect of **OCT-PEA** uncaging (**Figure 2.11 A**,**C**), confirming the involvement of GPR55 and PLC. In control experiments, the inactive PLC inhibitor analogue (U73343) did not significantly block the effect of **OCT-PEA** uncaging (**Figure 2.11 C**). Again,

INS-1 cells that were exposed to a vehicle did not respond to 375 nm irradiation (**Figure 2.11 C**).

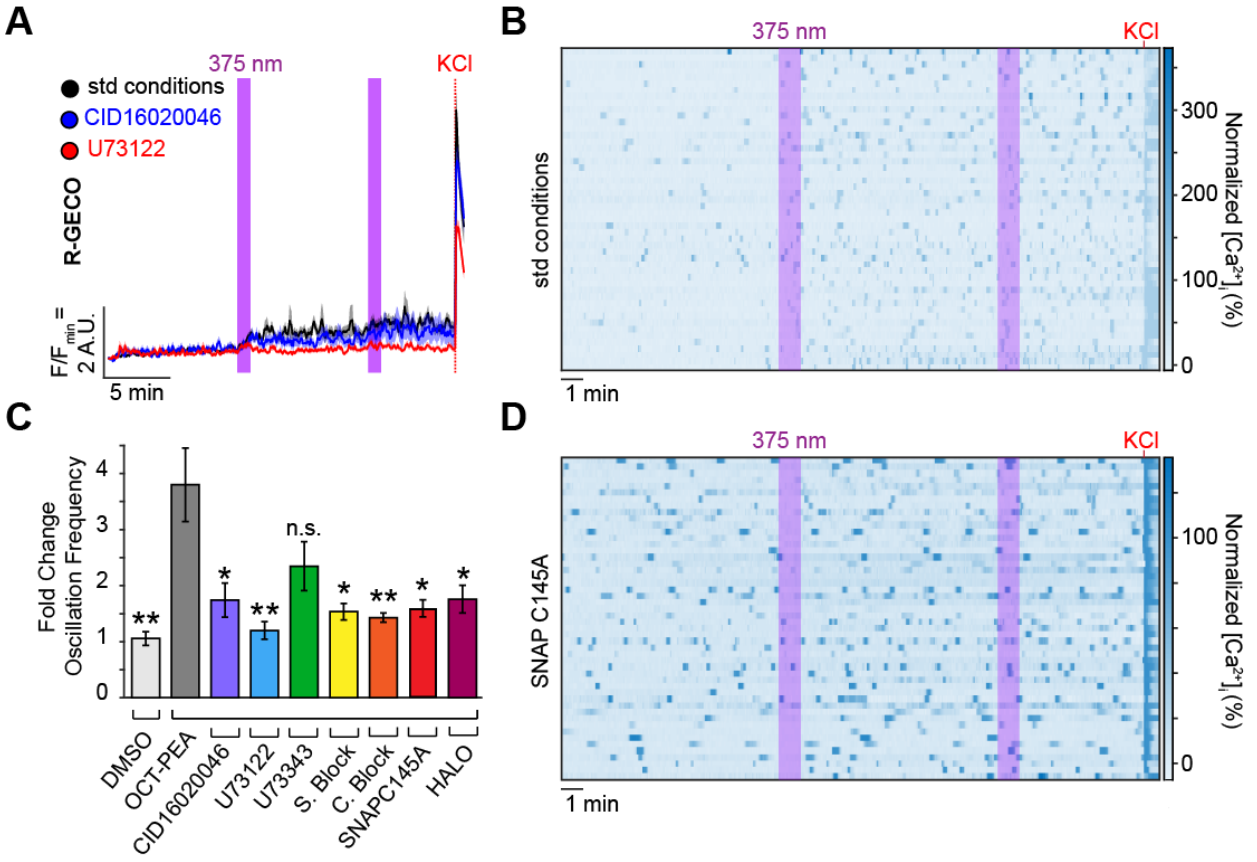


*Figure 2.11. Targeted uncaging of **OCT-PEA** on the INS-1 cell surface.*
*(**A**) Fluorescent $Ca^{2+}$ imaging using R-GECO showed that **OCT-PEA** (5 $\mu$M, 2 h, black, N = 352, T = 8) increased the average $[Ca^{2+}]_i$ in INS-1 cells. Overlaid with averages in the presence of a GPR55 antagonist (CID16020046, 5 $\mu$M, blue, N = 212, T = 4) or PLC inhibitor (U73122, 5 $\mu$M, red, N = 173, T = 4), which reduced the effect of **OCT-PEA**. KCl (25 mM) was applied at the end of each experiment. (**B**) Heat map showing individual $Ca^{2+}$ traces from fifty representative cells which were pre-incubated with **OCT-PEA** (5 $\mu$M, 2 h). Cells normalized to the KCl response. (**C**) Comparison bar graph of fold change in oscillation frequency in response to **OCT-PEA** uncaging across different conditions. Pre-incubation with vehicle (0.1% v/v DMSO 2 h, white, N = 247, T = 4) did not sensitize the cells to UV-irradiation. Uncaging **OCT-PEA** in the presence of GPR55 antagonist (CID16020046, 5 $\mu$M, purple, N = 212, T = 4), PLC inhibitor (U73122, 5 $\mu$M, blue, N = 173, T = 4), SNAP-Surface® Block (20 $\mu$M, yellow, N = 278, T = 5), SNAP-Cell® Block (10 $\mu$M, orange, N = 248, T = 4), pDisplay™-$SNAP^{C145A}$ (red, N = 244, T = 5) or pDisplay™-HALO*

*(magenta, N = 330, T = 4) reduced the probe's effect on oscillation frequency. The inactive PLC inhibitor analogue (U73343, 5 μM, green, N = 357, T = 6) did not block the effect of* ***OCT-PEA****. (****D****) Uncaging* ***OCT-PEA*** *in INS-1 cells transfected with pDisplay$^{TM}$-SNAP$^{C145A}$ reduced the effect of the probe, displayed as heat map of representative traces from fifty cells, normalized to the KCl response. Error bars = mean ± S.E.M. **P<0.01, *P<0.05, see Table 2.2.*

*Table 2.2. Statistical significance calculations for fold change in oscillation frequency for OCT-PEA $Ca^{2+}$ data. **P<0.01 (dark red), *P<0.05 (pink), ns = P>0.05 (white)*

| | **DMSO** | **OCT-PEA** |
|---|---|---|
| DMSO | - | 0.0039 |
| OCT-PEA | 0.0039 | - |
| CID16020046 | 0.1045 | 0.0184 |
| U73122 | 0.4944 | 0.0051 |
| U73343 | 0.0310 | 0.0911 |
| S. Block | 0.0400 | 0.0104 |
| C. Block | 0.0490 | 0.0084 |
| SNAP$^{C145A}$ | 0.0238 | 0.0118 |
| Halo | 0.0583 | 0.0178 |

To confirm that covalent attachment of **OCT-PEA** to the SNAP-tags on the cell surface is necessary for the probes' mechanism of action, we applied **OCT-PEA** under conditions in which

the tethering reaction could not occur. First, cells were pretreated with SNAP-Cell® Block to prevent subsequent **OCT-PEA** labeling. This pharmacological approach greatly diminished the impact of **OCT-PEA** uncaging on $[Ca^{2+}]_i$ (**Figure 2.11 C**). We performed similar experiments with SNAP-Surface® Block, which is non-permeable and only blocks SNAP-tags on the cell surface, and not intracellular pools. Again, this blocked the effect of **OCT-PEA** uncaging, confirming that cell-surface uncaging is the main driver of our observed effect (**Figure 2.11 C**). Alternatively, we transfected INS-1 cells with pDisplay™- Halo, which does not react with the BG moiety on **OCT-PEA**. This biorthogonal tag exchange also reduced **OCT-PEA**'s effect (**Figure 2.11 C**). Using our pDisplay™-SNAP$^{C15A}$ mutant, we observed a reduced effect of **OCT-PEA** uncaging on INS-1 $Ca^{2+}$ oscillations (**Figure 2.11 C**,**D**). Further, GPR55 knockdown (KD) using two independent siRNAs blocked the effect of **OCT-PEA** uncaging on oscillation frequency, further supporting GPR55 involvement for mediating the probe's response (**Figure 2.12**). Combined, these results confirm that background activity from untethered **OCT-PEA** was not driving our observed response to uncaging, and that SNAP-tags effectively deliver **OCT-PEA** to the INS-1 cell surface to activate GPR55. Targeted compound uncaging activates GPR55 receptors and PLC near the plasma membrane to stimulate β-cell $Ca^{2+}$ activity.

A

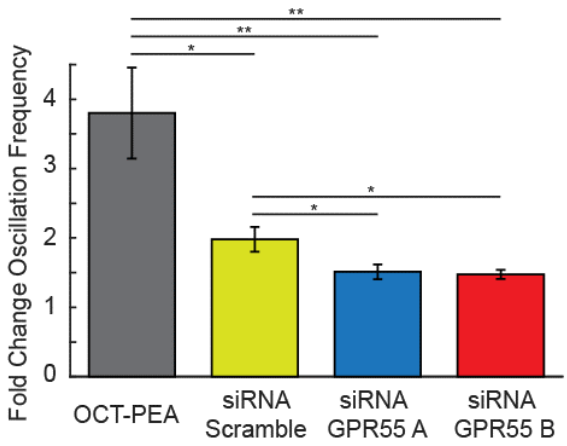


B

| | OCT-PEA | Scramble |
|---|---|---|
| Scramble | 0.0278 | - |
| siRNA GPR55 A | 0.0099 | 0.0483 |
| siRNA GPR55 B | 0.0093 | 0.0273 |

*Figure 2.12. Targeted uncaging of **OCT-PEA** on the INS-1 cell surface with GPR55 KD. (**A**) Comparison bar graph of fold change in oscillation frequency in response to **OCT-PEA** uncaging in INS-1 cells transfected with siRNA scramble (yellow, N = 300, T = 8), siRNA GPR55 A (blue, N = 160, T = 4), or siRNA GPR55 B (red, N = 177, T = 4), and expressing R-GECO and pDisplayTM-SNAP. Standard conditions without siRNA transfection (**OCT-PEA**, grey, N = 398, T = 8) shown for comparison. Error bars = mean ± S.E.M. (**B**) p-values for data in panel **A**. **P<0.01 (dark red), *P<0.05 (pink).*

Finally, we sought to demonstrate the spatial utility of our OCT-ligand approach. SNAP-tag expressing INS-1 cells were labelled with **OCT-PEA**, and this time only half the field of view was exposed to 375 nm irradiation. As expected, we observed that only the irradiated cells increased in their $Ca^{2+}$ oscillation frequency, while those that were not irradiated remained at a constant oscillation frequency (**Figure 2.13**). This provides a mechanism for researchers to directly compare cells in which GPR55 was activated to those which were not, under the exact same experimental conditions.

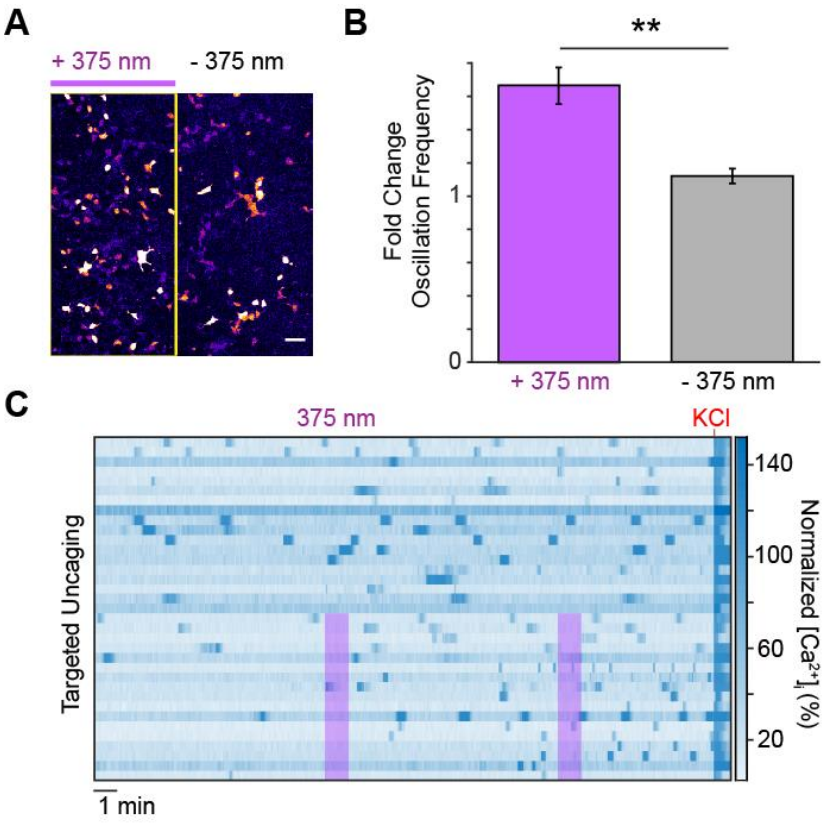


*Figure 2.13. Targeted uncaging of **OCT-PEA** on half of the field of view.*

*(**A**) Field of view, where the left half was exposed to 375 nm (purple) and the right half was not. (**B**) Bar graph comparing fold change in oscillation frequency between irradiated (N = 145, T = 5) and nonirradiated regions (N = 132, T = 5). (**C**) Heat map of representative traces from one trial, normalized to KCl response. Error bars = mean ± S.E.M, **P<0.01.*

## 2.3. Discussion

This study presents a new chemical technology for manipulating cannabinoid signaling on a genetically-defined cellular target. We introduce **OCT-PEA**, the first photochemical tool that has been shown to target GPR55 in living cells. A photocaged PEA was tethered to the plasma membrane of INS-1 β-cells using membrane-anchored SNAP-tags, and uncaging **OCT-PEA** on the cell surface stimulated $[Ca^{2+}]_i$ oscillations. These results confirm that INS-1 cells express functional GPR55 on their plasma membrane, which is activated by PEA to increase $[Ca^{2+}]_i$ oscillations through PLC activation. Similar to other approaches which utilize membrane-anchored SNAP-tags to localize pharmacologically-active ligands[58,72], this approach does not require the overexpression of signaling proteins and enables the targeting of endogenous receptors. Because SNAP-tags are inactive until conjugated with a pharmacophore, OCT-ligands allow us to acutely manipulate receptor function while avoiding compensatory artefacts. Because **OCT-PEA** is only uncaged with UV-A irradiation, we can combine **OCT-PEA** with other blue/green fluorescent biosensors (i.e. $Ca^{2+}$, cAMP, kinase activity). Reflected by the more subtle effect of **OCT-PEA** stimulation on the overall $Ca^{2+}$ level when compared to the application of freely diffusible PEA, we hypothesize that our approach releases PEA similar to how endogenous NAE are typically generated transiently during periods of cell stimulation[73].

Because we observed that GPR55 is expressed on the INS-1 plasma membrane, **OCT-PEA** was targeted to the cell surface. While similar results could also be achieved using other specialized photocages[52,53], future applications of our approach with alternative SNAP-tag targeting sequences will allow us to direct NAE signaling to a variety of subcellular locations without requiring the synthesis of new compounds. Moreover, an increasing body of work indicates that CBRs can be found on internal membranes, even in β-cells[33,74,75]. Thus applying OCT-ligands to target organelles such as mitochondria or the endoplasmic reticulum will allow us to investigate the function of intracellular receptor pools. Our probes will also be useful to

study cannabinoid signaling in intact tissues. Leveraging genetic techniques for cell-type selective SNAP-tag expression, OCT-ligands will allow us to focus ligand release on β- or α-cells in the intact pancreatic islet.

Our future efforts will aim to develop OCT-ligands with alternate pharmacological or photophysical properties. For example, probes capable of releasing different NAEs will help us dissect the contributions of specific CBR subtypes. Red-shifting the photocage toward longer visible wavelengths will also help translate our strategy *in vivo*, as lower-energy photons are less phototoxic and penetrate deeper into tissue. Combined with the expansion of our approach to utilize alternative bio-conjugation tags (i.e. HaloTags[56]), OCT-ligands will allow us to generate sophisticated patterns of NAE signaling orthogonally, with unprecedented precision.
Beyond applying OCT-ligands to study CBR signaling in β-cells, this approach will be generalizable to other cell types, ligands, and signaling pathways. These advances will enhance the acuity with which we can manipulate signaling in time and space, setting the stage for the next generation of targeted pharmacology.

## 2.4. Methods

### 2.4.1. General synthetic methods

Unless otherwise noted, all chemicals were purchased from TCI Chemicals, Fisher Scientific, Sigma-Aldrich, or Acros Organics, and were used without further purification. Dry solvents were purchased as “extra dry” or “anhydrous” and used without further purification. Reactions and chromatography were monitored by analytical thin layer chromatography (TLC) on Merck silica gel 60 $F_{254}$ plates. The plates were first visualized under 254 nm UV light, followed by staining with $KMnO_4$ solution or cerium (IV) molybdate solution (Hanessian’s stain) and gentle heating with a heat gun. Flash column chromatography was performed using silica gel (ACROS Organics™ 240360300, 0.035-0.070 mm, 60 Å).

Nuclear magnetic resonance (NMR) spectra were acquired on a BRUKER 400 MHz instrument. Chemical shifts ($\delta$) are reported in ppm and referenced to residual non-deuterated solvent peaks ($^{1}H/^{13}C$): DMSO (2.50/39.52), $MeOD_4$ (3.31/49.00), and $CDCl_3$ (7.26/77.16). Multiplicities are abbreviated as: s = singlet, d = doublet, t = triplet, q = quartet, br = broad, m = multiplet.

High-resolution (35,000) mass spectrometry was submitted to Portland State University’s BioAnalytical Mass Spectra Facility. Data were acquired on a vanquish UHPLC/HPLC system coupled to a Q-Exactive MS equipped with an electrospray ionization source operating in the positive mode.

### 2.4.2. UV-Vis spectroscopy

The sample was placed in a 1 mL Quartz cuvettes (10 mm light path) and illumined with a deuterium-halogen light source (Ocean Optics, DH-2000). The transmitted light was collected by a Flame UV-Vis-ES spectrophotometer (FLMT05021, Ocean Insight) and the data were acquired with OceanView (Version 2.0.7) Software. Purified SNAP-tags (for Fig. S3) were

purchased from New England Biolabs and labelled with our probes according to the manufacturer's instructions. Uncaging was achieved using 365 nm (Thorlabs M365FP1), 415 nm (Thorlabs M415F3), 470 nm (Thorlabs M470F4) and 565 nm (M565F3) LEDs guided through a fibre-optic cable (Thorlabs #FP400URT, 400 μm diameter, 0.50 numerical aperture) and optical cannula (400 μm, Thorlabs). The cannula tip was pointed directly into the top of the sample. LED power was quantified by a power meter (Thorlabs, PM100D) with its photodiode power sensor (Thorlabs, S120VC,) positioned directly at the fibre tip. **OCT-PEA** (20 μM in DMSO) was irradiated for up to 5 min, and adsorption spectra were acquired every 2 s. When **OCT-PEA** was conjugated to SNAP-tag purified protein, absorbance spectra were acquired every 5 s up to 10 min. The data were analyzed using MATLAB. Exponential curve fitting was achieved using MATLAB's Curve Fitting application as:

$$ft = a * e^{(-b*x)} + c$$

### 2.4.3. Cell culture media and solutions

**INS-1 media**: RPMI 1640 with L-glutamine (Gibco, #11875-093) with 10% FBS, Penicillin-strep (1:100) and (in mM) 10 HEPES (Fisher, #BP310-500), 1 sodium pyruvate (Alfa Aesar, #A11148) 0.05 2-mercaptoethanol (BME, Sigma, #M3148).

**Imaging buffer** contains (in mM): 185 NaCl, 1.2 $CaCl_2$, 1.2 $MgCl_2$, 1.2 $K_2HPO_4$, 20 HEPES. Adjusted to pH 7.4 with NaOH. Glucose was supplemented accordingly at 3, 11 or 20 mM.

**Phosphate buffer** contains (in mM): 320 $Na_2HPO_4$ (Fisher, #BP332-500), 80 $Na(H_2PO_4)•H_2O$ (Fisher, #S369-1). Adjusted pH to 7.4 with NaOH.

**4% PFA:** paraformaldehyde (2 g, Sigma-Aldrich, #158127), 0.2 M phosphate buffer (25 ml), deionized $H_2O$ (25 ml). Adjusted pH to 7.4. Kept on ice until use (within 24 h).

**Blocking buffer:** Phosphate buffer saline (PBS, Gibco, #70013-032) with 10% w/v bovine serum albumin (Fisher, #BP1605-100, lot #182765), and 0.3% v/v triton X-100 (Fisher, #BP151-100).

### 2.4.4. Cell culture

INS-1 832/13 cells[66] were grown in INS-1 media and incubated at 37 °C and 5% $CO_2$. Cells between passages 60-80 were used in experiments. For $Ca^{2+}$ imaging, INS-1 cells were plated at a density of 100,000-150,000 cells per well on 8-well glass bottom chambered coverslips (Ibidi, #0827-90). 18-24 h later, they were starved in Opti-MEM™ (250 μl) for 2 h. A transfection mixture containing (20 μl per well): 1 μl Lipofectamine-2000 (Fisher Scientific, #11668019), 250 ng R-GECO or 125 ng R-GECO + 250 ng pDisplay™-SNAP / 250 ng pDisplay™-HALO / 250 ng pDisplay™-SNAP$^{C145A}$ in Opti-MEM™ was mixed and incubated for 20 min at room temperature. Following starvation, 230 μl fresh Opti-MEM™ was placed on the cells, followed by 20 μl transfection mixture. The cells were then incubated at 37 °C and 5% $CO_2$ for 18-24 h before exchanging the transfection mixture with INS-1 media. Microscopy experiments were performed 60-72 h post transfection.

Use of conditioned imaging buffer (supplements the INS-1 secreted factors) prior to $Ca^{2+}$ imaging was necessary to achieve a stable baseline recording. The media on a separate petri dish of INS-1 cells (6 cm, 80% confluence) was exchanged for imaging buffer with 20 mM glucose and incubated at 37 °C and 5% $CO_2$ for at least 1 h. This conditioned imaging buffer was added to the cells as the final wash directly before imaging.

For siRNA transfection, an siRNA (Invitrogen, Table 2.3): Oligofectamine™ (Invitrogen, #12252-011) complexes were prepared separately (1 μl of 20 μM siRNA : 16 μl Opti-MEM™ for siRNA complex and 0.8 μl Oligofectamine™ : 3 μl Opti-MEM™ for Oligofectamine™ complex per well) and incubated for 7 min at room temperature. The Oligofectamine™ complex mixture

was added to the siRNA complex mixture and incubated together for 20 min at room temperature, then added to INS-1 cells freshly seeded at 100,000 cells per well on 8-well glass bottom chambered coverslips. INS-1 cells were transfected with R-GECO and pDisplay™-SNAP the following day as described above, and imaged 60-72 h post transfection.

*Table 2.3. siRNA GPR55 sequence and Catalog number*

| **Abbreviation** | **Cat No. / Lot No.** | **5' → 3' Sequence** |
|---|---|---|
| siRNA GPR55 A | 10620318 / 439644 A06 | CCUAUAGGAGCAUUCACAUUCUACU |
| siRNA GPR55 B | 10620318 / 439644 B07 | CCAUUGCUACCAAUCUUGUCGUCUU |
| siRNA Scramble | 12935-200<br>Stealth RNAi™ siRNA Negative Control, Low GC Duplex | - |

### 2.4.5. cDNA constructs and site-directed mutagenesis

SNAP-tags and HaloTags were inserted into the pDisplay™ vector (ThermoFisher #V66020) using Gibson cloning. Site-directed mutagenesis to create the C145A mutation of the pDisplay™-SNAP construct was achieved using the QuikChange XL Site-Directed Mutagenesis Kit from Agilent Technologies with forward primer 5'-TTCTGATCCCGGCACACCGTGTGGT-3' and reverse primer 5'-ACCACACGGTGTGCCGGGATCAGAA-3'. After amplification, success of cloning was confirmed via Sanger sequencing.

### 2.4.6. Cell viability assay - MTT

INS-1 cells were plated in a 96-well plate (Corning #3596) with 50,000 cells per well in INS-1 media, and then were incubated for 48-72 h until they reached 70-80% confluence. For

application of uncaged probe, **OCT-PEA** (10 μl, 40 mM in DMSO) was irradiated for 5 min as described above in the “UV-Vis spectroscopy” section. The media in the 96-well plate of cells was exchanged with 100 μl of INS-1 media with DMSO (0.1% v/v) and without BME. Afterwards, the compounds were added, and the cells were incubated at 37 °C and 5% $CO_2$ for 24 h. The media was aspirated from the wells and washed in 100 μl PBS. 3-(4,5-Dimethyl-2-thiazolyl)-2,5-diphenyltetrazolium bromide (MTT, TCI Chemicals, #D0801) was added to the wells at 5 mg/ml and incubated at 37 °C and 5% $CO_2$ for 4 h. The media was gently removed and then 100 μl DMSO was added to each well. The plate was placed in the dark on an orbital shaker for 15 min at 100 rpm. Absorbance at 590 nm was recorded on a CLARIOstar$^{PLUS}$ plate reader (BMG Labtech, 0430) and the data were processed in Microsoft Excel and MATLAB.

### 2.4.7. Immunofluorescence microscopy

INS-1 cells were plated on acid-etched glass coverslips (12 mm, #1.5) at a density of 100,000 cells per well in a 24-well plate (Fisherbrand, #FB012929). The cells were fixed with ice-cold PFA (4%, 20 min, room temperature, orbital shaker 100 rpm), and then washed 2× with PBS (5 min). Fixed INS-1 cells on coverslips were incubated in the blocking buffer (1 h). Cells were then incubated in 1° antibody solution (diluted in blocking buffer). The plate was sealed and incubated overnight (12-14 h, 4 °C, orbital shaker 100 rpm) in the dark. The coverslips were then washed 3× with PBS (5 min, RT, orbital shaker 100 rpm). They were then transferred to the 2° antibody solution (diluted in blocking buffer, 1 h, RT) and shaken in the dark. Details of the specific antibodies and dilutions are provided in Table 2.4. The coverslips were washed 3× with PBS (5 min) and then incubated in the dark with DAPI (Thermo, #D1206, 36 nM, 10 min) on the orbital shaker, and then washed 2× with deionized water (5 min). The coverslips were mounted on a microscope slide (VWR® Superfrost® Plus Micro Slide, 75×25×1 mm, #48311-703) and

sealed with mounting solution (Fluoromount™). Slides remained in the dark overnight and then imaged within one week.

Fixed cell microscopy was performed on a Zeiss LSM880 confocal laser scanning microscope with Airyscan with a 63× oil objective at 2048×2048 resolution. DAPI excitation was performed with a 405 nm laser. Green fluorophores were excited with a 488 nm laser. Red fluorophores were excited with a 550 nm laser.

*Table 2.4. Corresponding primary and secondary antibodies for immunofluorescence.*

| Protein Target | Primary Antibody | Secondary Antibody |
|---|---|---|
| GPR55 | GPR55 rabbit polyclonal antibody (Bioss Antibodies, ca # BS-768R, lot # VK3136032A); 1:200 dilution | Alexa Fluor 488 conjugated donkey anti-rabbit (Life Technologies, cat # A21206); 1:2000 dilution |
| Insulin | Insulin guinea pig polyclonal antibody (Abcam, cat # ab7842, lot #GR3322969-1); 1:250 dilution | IgG (H+L) Highly Cross-Adsorbed Goat anti-Guinea Pig, Alexa Fluor™ 594 (Invitrogen, cat # A11076, lot #2160074); 1:250 dilution |
| Myc-tag | Myc-tag mouse mAB (Cell Signaling Technology, cat #2276, lot 24), 1:8000 | Cy™3 AffiniPure Donkey anti-Mouse IgG (H+L) (Jackson ImmunoResearch Laboratories, cat #715-165-151, log #130991), 1:1000 |

### 2.4.8. Live-cell confocal fluorescence microscopy

Live cell imaging was performed on an Olympus Fluoview 1200 laser scanning confocal microscope at 37 °C and 5% $CO_2$. Images were acquired with a 63× oil objective and 2048x2048 pixel resolution, and videos were acquired with a 20× objective, 512×512-pixel resolution, and scan rate of 4 s per frame. R-GECO excitation was performed with a 559 nm laser and emission was collected at 570-670 nm. SNAP-Surface® Alexa Fluor® 488 (NEB, #S9129S) excitation was performed with a 488 nm laser and emission was collected at 500-545 nm. Hoechst-33342 excitation was performed with a 405 nm laser and emission was collected at 425-460 nm. Photo-activation was performed with a 375 nm laser (PicoQuant, PDL 800-D, ~95 μW output from the objective) triggered using the quench function in the Olympus software. For SNAP-tag dye labeling, the cells were washed once, labeled with SNAP-Surface® Alexa Fluor® 488 (1 μM, 30 min) in INS-1 media (without BME), washed once, then incubated with Hoechst-33342 (10 μM, 5 min) in 20 mM glucose imaging buffer. The cells were washed 2× and imaged in 20 mM glucose imaging buffer. For **OCT-PEA** $Ca^{2+}$ imaging, cells were incubated with **OCT-PEA** (5 μM, 2 h) in INS-1 media without BME at 37 °C and 5% $CO_2$. Control experiments involved incubation with CID16020046 (5 μM, 30 min, Tocris, #4959), U73122 (5 μM, 30 min, Tocris, #1268), U73343 (5 μM, 30 min, Tocris, #4133), or SNAP-Cell® Block (10 μM, 20 min, NEB, #S9106S) in INS-1 media without BME. Cells were washed, and equilibrated for at least 20 min with conditioned imaging buffer 37 °C and 5% $CO_2$.

### 2.4.9. Data analysis and code availability

For $Ca^{2+}$ imaging experiments, regions-of-interest were manually drawn around oscillating cells using the Fiji software[76], and the resulting data were analyzed with MATLAB scripts written in-house. All data and codes used for analysis are available on request. Unless otherwise described, all data are presented as mean ± S.E.M, which is calculated as:

$$\text{S. E. M.} = \frac{\text{standard deviation}}{\sqrt{\text{N}}}$$

For $Ca^{2+}$ imaging experiments depicting the averages over time, N is the total number of cells (technical replicates over all videos), and T is the number of independent experiments (biological replicates). Oscillations were calculated in MATLAB using the 'findpeaks' function with an x threshold of 2 and y threshold of 1.25. Following cell selection, the total number of oscillations across the field of view was counted from the beginning of the video to the first stimulus (PEA addition, or UV-A irradiation in the case of **OCT-PEA**). Separately, the total number of oscillations were counted for over an equivalent time post-stimulation. The sum of the peaks was normalized against the number of cells per video (to quantify "oscillations per cell" for each trial and condition), and then the mean fold change for post/pre-stimulation was calculated alongside the S.E.M. In the case of these oscillation frequency counts, N is the number of independent trials (biological replicates). Statistical significance was assessed using Matlab (Mathworks). For the comparison between two groups in oscillation frequency analysis, Welch's two-sample t-test was used, with significance threshold placed at *P<0.05, **P<0.01, ns = P>0.05.

## 2.5. Detailed Synthetic Methods

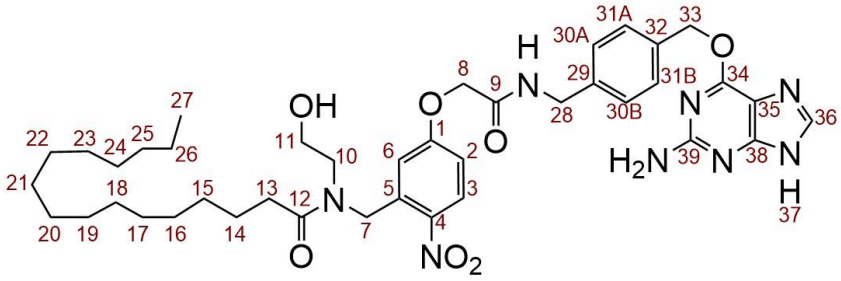


*Figure 2.14. Numbering system utilized in the NMR assignments for **OCT-PEA**.*

### 2.5.1. Synthesis of Ethyl 2-(3-formyl-4-nitrophenoxy) acetate (1).

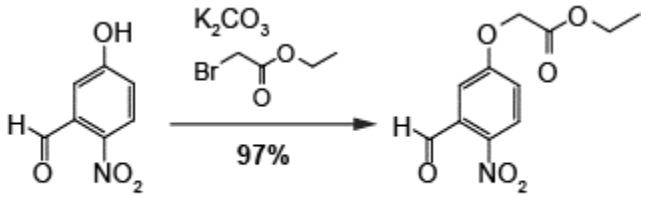


1

Ethyl 2-(3-formyl-4-nitrophenoxy) acetate (**1**) was prepared using a procedure as described by Heinbockel *et al.*[47] 5-hydroxy-2-nitrobenzaldehyde (0.53 g, 3.2 mmol, 1.0 equiv.) and anhydrous $K_2CO_3$ (0.32 g, 2.3 mmol, 0.70 equiv.) were dissolved in dry acetonitrile (5 ml) under an Ar atmosphere. Ethylbromoacetate (0.40 ml, 3.6 mmol, 1.1 equiv.) was added dropwise and the reaction mixture was stirred overnight at room temperature (RT). The reaction was filtered, and the filtrate was concentrated *in vacuo*. The residue was purified by flash column chromatography (hexane/EtOAc 95:5→80:20) to yield **ethyl 2-(3-formyl-4-nitrophenoxy) acetate** (**1**) (0.78 g, 3.1 mmol, 97%) as a yellow solid. Analytical data were comparable to those reported in Heinbockel *et al.*[47]

**TLC (4:1 hexane:EtOAc):** $R_f$ = 0.20. **$^1$H NMR ($CDCl_3$, 400 MHz, 25° C):** δ 10.48 (s, 1 H, CHO), 8.17 (d, 1 H, H3, *J* = 9.1 Hz), 7.31 (d, 1H, H6, *J* = 3.0 Hz), 7.20 (dd, 1 H, H2, *J* = 8.8, 3.0 Hz), 4.77 (s, 2 H, $H8_{A,B}$), 4.29 (q, 2 H, $\underline{CH_2}CH_3$, *J* = 7.1 Hz), 1.32 (t, 3 H, $CH_2\underline{CH_3}$, *J* = 7.3 Hz).

### 2.5.2. Synthesis of (2-*tert*-butoxyethyl)-(5-ethoxycarbonylmethoxy-2-nitrobenzyl)amine (2).

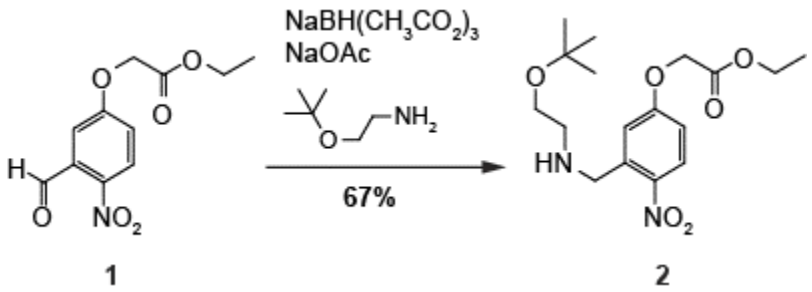


1 2

**(2-*tert*-butoxyethyl)-(5-ethoxycarbonylmethoxy-2-nitrobenzyl)amine** (**2**) was prepared as described by Heinbockel *et al.*[47] 2-(*tert*-butoxy)-ethanamine (69 mg, 0.59 mmol, 1.5 equiv.) and ethyl 2-(3-formyl-4-nitrophenoxy) acetate (**1**) (0.10 g, 0.40 mmol, 1.0 equiv.) were dissolved in dry 1,2-dichloroethane (2 ml) under an Ar atmosphere. Anhydrous NaOAc (34 mg, 0.41 mmol, 1.0 equiv.) was then added, and the reaction mixture was stirred at RT for 1 h. $NaBH(CH_3CO_2)_3$ (0.21 g, 1.0 mmol, 2.5 equiv.) was added in one portion, and the reaction mixture was stirred overnight at RT. The reaction was diluted with $CH_2Cl_2$ (5 ml) and quenched with a saturated aqueous $NaHCO_3$ solution. The organic phase was separated, washed 2× with a saturated aqueous $NaHCO_3$ solution, once with saturated brine, and then dried over anhydrous $MgSO_4$. Following filtration and concentration *in vacuo*, the residue was purified *via* flash column chromatography (10 g silica, hexane/EtOAc 90:10→65:35 with 1 vol% $Et_3N$) to yield **(2-*tert*-butoxyethyl)-(5-ethoxycarbonylmethoxy-2-nitrobenzyl)amine** (**2**) (95 mg, 0.27 mmol, 67%) as a yellow oil. Analytical data were comparable to those reported in Heinbockel *et al.*[47].

**TLC (1:1 hexane:EtOAc):** $R_f$ = 0.15. **$^1$H NMR ($CDCl_3$, 400 MHz, 25 °C):** δ 8.08 (d, 1 H, H3, *J* = 9.0 Hz), 6.84 (dd, 1 H, H2, *J* = 9.0, 2.9 Hz), 4.71 (s, 2 H, $H8_{A,B}$), 4.28 (q, 2 H, $\underline{CH_2}CH_3$, *J* = 7.1 Hz), 4.13 (s, 2 H, $H7_{A,B}$), 3.49 (t, 2 H, $H10_{A,B}$, *J* = 5.3 Hz), 2.75 (t, 2 H, $H11_{A,B}$, *J* = 5.3 Hz), 1.73 (b, NH), 1.31 (t, 3 H, $CH_2\underline{CH_3}$, *J* = 7.1 Hz), 1.20 (s, 9 H, *t*-Bu $CH_3$).

### 2.5.3. Synthesis of *N*-(*2-tert*-butoxyethyl)-*N*-(5-ethoxycarbonylmethoxy-2-nitrobenzyl) palmitoylamide (3).

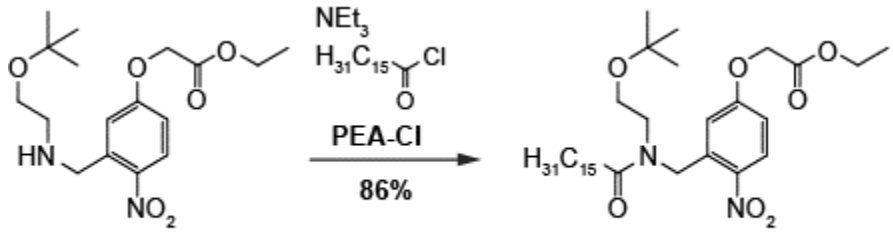


Oxalyl chloride (0.36 ml, 4.2 mmol, 1.5 equiv.) was added to a solution of palmitic acid (0.718 g, 2.8 mmol, 1.0 equiv.) in dry $CH_2Cl_2$ (35 ml) under an Ar atmosphere. A drop of N,N-dimethylformamide was added, and the reaction mixture was stirred for 70 min at room temperature. The reaction was concentrated *in vacuo* to yield a yellow-orange oil. To ensure complete removal of oxalyl chloride, the product was 2× dissolved in $CH_2Cl_2$, concentrated *in vacuo*, and then dried under high vacuum (<1 mbar) for 20 min. The oil was dissolved in anhydrous $CH_2Cl_2$ (9 ml) immediately before use in the following reaction.

**(2-*tert*-butoxyethyl)-(5-ethoxycarbonylmethoxy-2-nitrobenzyl)amine** (**2**) (0.55 g, 1.6 mmol, 1.0 equiv.) was dissolved in dry $CH_2Cl_2$ (30 ml) under an Ar atmosphere, followed by dropwise addition of the above described palmitoyl chloride solution (9 ml, 1.8 equiv.) and then $Et_3N$ (0.39 ml, 2.8 mmol, 1.8 equiv.). The reaction mixture was stirred for 90 min at room temperature, then diluted with $CH_2Cl_2$ (20 ml). The organic phase was washed 2× with a saturated aqueous $NaHCO_3$ solution, once with saturated brine, and then dried over anhydrous $MgSO_4$. Following filtration and concentration *in vacuo*, the residue was purified *via* flash column chromatography (50 g silica, hexane/EtOAc 95:5→90:10→85:15), to yield ***N*-(*2-tert*-butoxyethyl)-*N*-(5-ethoxycarbonylmethoxy-2-nitrobenzyl)palmitoylamide** (**3**) (0.82 g, 1.38 mmol, 86%), as a yellow oil. The product was isolated as a mixture of *E* and *Z* amide isomers.

**TLC (3:1 hexane:EtOAc):** $R_f$ = 0.35. **$^1$H NMR ($CDCl_3$, 400 MHz, 25 °C):** δ 8.23 (d, 0.5 H, H3, *J* = 9.3 Hz), 8.12 (d, 0.5 H, H3, *J* = 9.5 Hz), 6.91-6.72 (m, 2 H, H2, H6), 5.14 (s, 1 H, $H7_A$), 5.01 (s, 1 H, $H7_B$), 4.66 (d, 2 H, $H8_{A,B}$, *J* = 9.5 Hz), 4.32-4.23 (m, 2 H, $C\underline{H_2}CH_3$), 3.60-3.43 (m, 4 H, $H10_{A,B}$, $H11_{A,B}$), 2.54 (t, 1 H, $H13_A$, *J* = 7.6 Hz), 2.19 (t, 1 H, $H13_B$, *J* = 7.6 Hz), 1.75-1.57 (m, 2 H, $H14_{A,B}$), 1.41-1.19 (m, 24 H, H15-H26, $CH_2C\underline{H_3}$), 1.16 (d, 9H, *t*-Bu $CH_3$, *J* = 4.3 Hz), 0.88 (t, 3H, $H27_{A,B,C}$). **$^{13}$C NMR ($CDCl_3$, 101 MHz, 25 °C):** δ 174.62 + 174.25 (C12), 167.92 + 167.63 (C9), 162.51 + 162.00 (C1), 142.22 + 141.46 (C4), 137.81 + 137.52 (C5), 128.78 + 128.13 (C3), 114.58 + 113.68 (C6), 112.97 + 112.55 (C2), 73.62 + 73.31 ($\underline{C}(CH_3)_3$), 65.59 + 65.50 (C8), 62.04 + 61.90 ($\underline{C}H_2CH_3$), 60.76 + 59.85 (C10, C11), 51.49 (C7), 49.13-47.50 (C10, C11), 33.28 +33.24 (C13), 32.07-29.51 (C15-C26), 27.56 + 27.48 ($C(\underline{C}H_3)_3$), 25.51 + 25.40 (C14), 22.84 ($CH_2\underline{C}H_3$), 14.29 + 14.27 (C27). **HRMS (ESI$^+$):** *m/z* calculated for $[C_{33}H_{56}N_2O_7]^+$ = 593.4160, observed = 593.4149 ($[M+H]^+$)

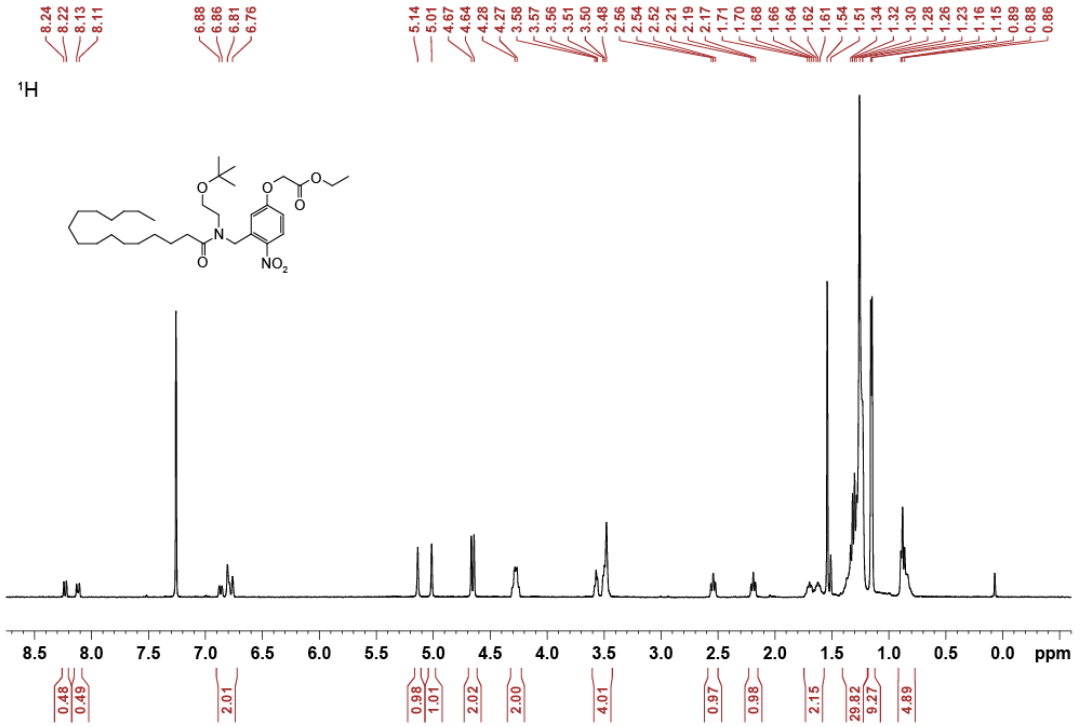
8.24
8.22
8.13
8.11
6.88
6.86
6.81
6.76
5.14
5.01
4.67
4.64
4.28
4.27
3.58
3.57
3.56
3.51
3.50
3.48
2.56
2.54
2.52
2.21
2.19
2.17
1.71
1.70
1.68
1.66
1.64
1.62
1.61
1.54
1.51
1.34
1.32
1.30
1.28
1.26
1.23
1.16
1.15
0.89
0.88
0.86
1H
NO2
8.5 8.0 7.5 7.0 6.5 6.0 5.5 5.0 4.5 4.0 3.5 3.0 2.5 2.0 1.5 1.0 0.5 0.0 ppm
0.48
0.49
2.01
0.98
1.01
2.02
2.00
4.01
0.97
0.98
2.15
29.82
9.27
4.89

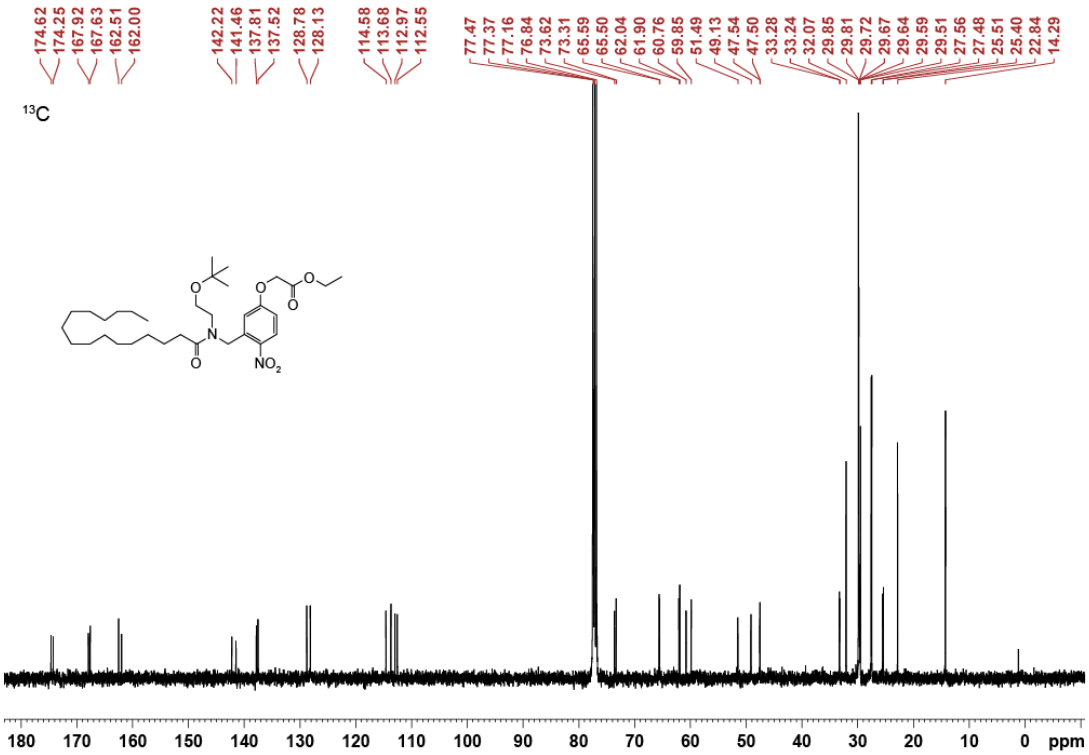
174.62
174.25
167.92
167.63
162.51
162.00
142.22
141.46
137.81
137.52
128.78
128.13
114.58
113.68
112.97
112.55
77.47
77.37
77.16
76.84
73.62
73.31
65.59
65.50
62.04
61.90
60.76
59.85
51.49
49.13
47.54
47.50
33.28
33.24
32.07
29.85
29.81
29.72
29.67
29.64
29.59
29.51
27.56
27.48
25.51
25.40
22.84
14.29
13C
NO2
180 170 160 150 140 130 120 110 100 90 80 70 60 50 40 30 20 10 0 ppm

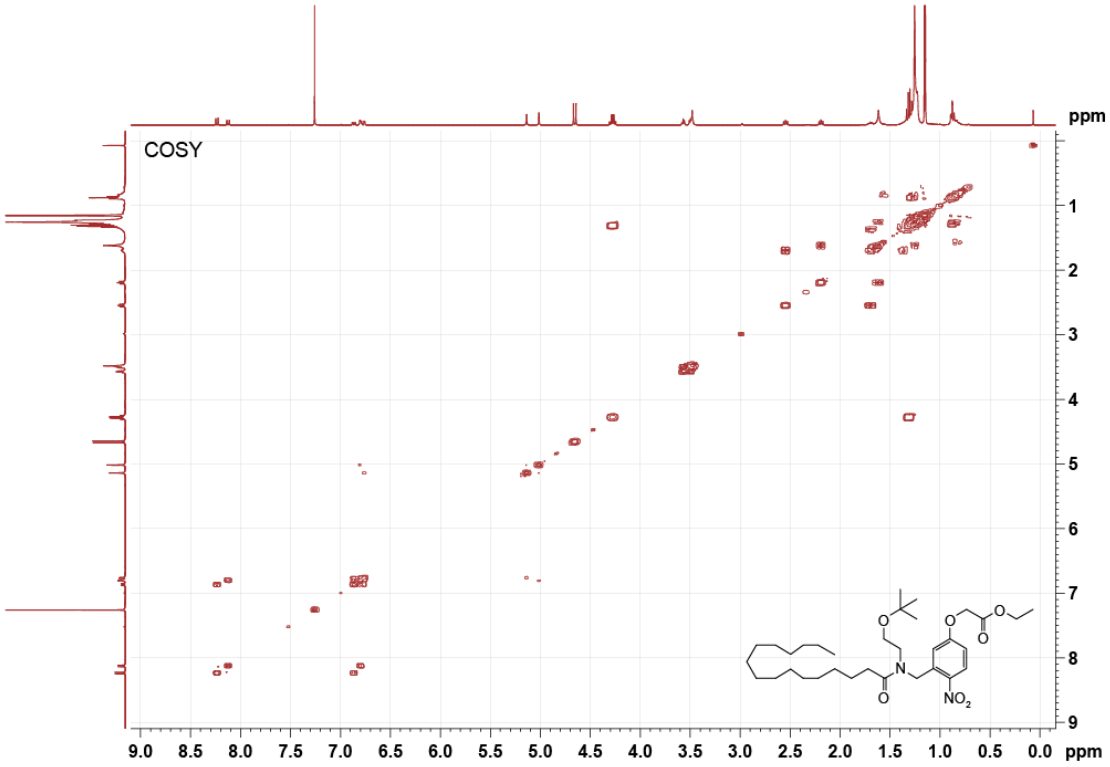
COSY
ppm
9.0 8.5 8.0 7.5 7.0 6.5 6.0 5.5 5.0 4.5 4.0 3.5 3.0 2.5 2.0 1.5 1.0 0.5 0.0 ppm
1 2 3 4 5 6 7 8 9
O
O
O
O
O
N
O
NO2

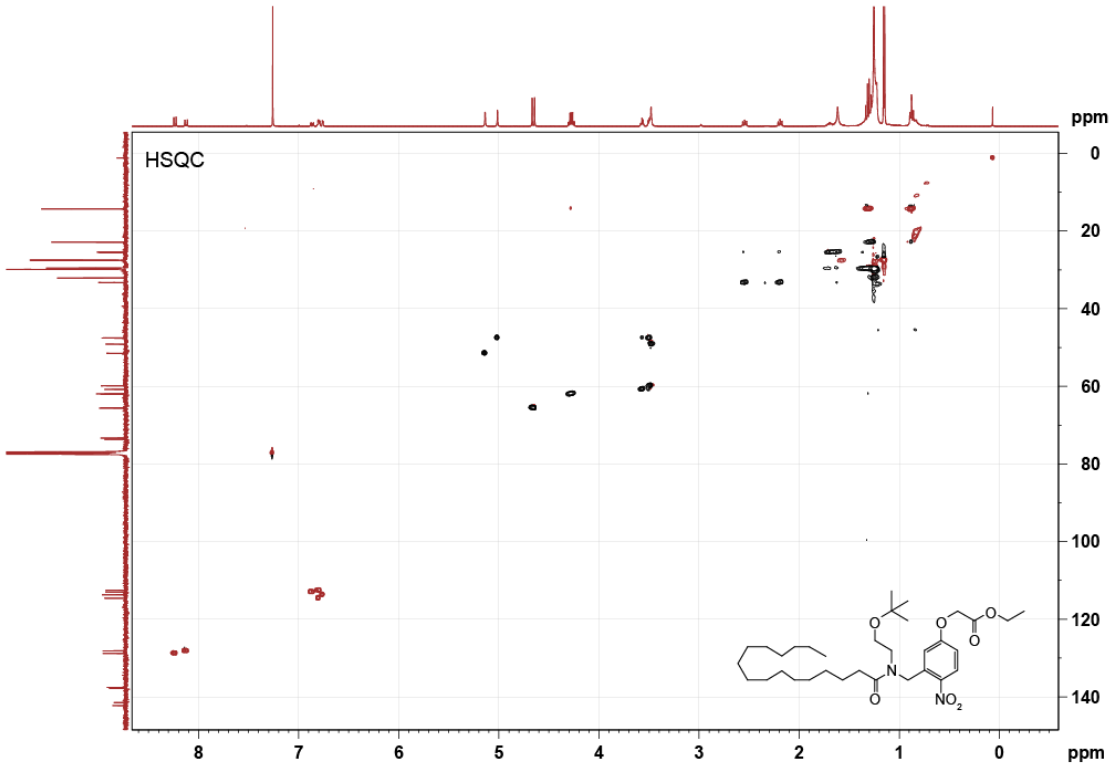
HSQC
ppm
8 7 6 5 4 3 2 1 0 ppm
0 20 40 60 80 100 120 140
O
O
O
O
O
N
O
NO2

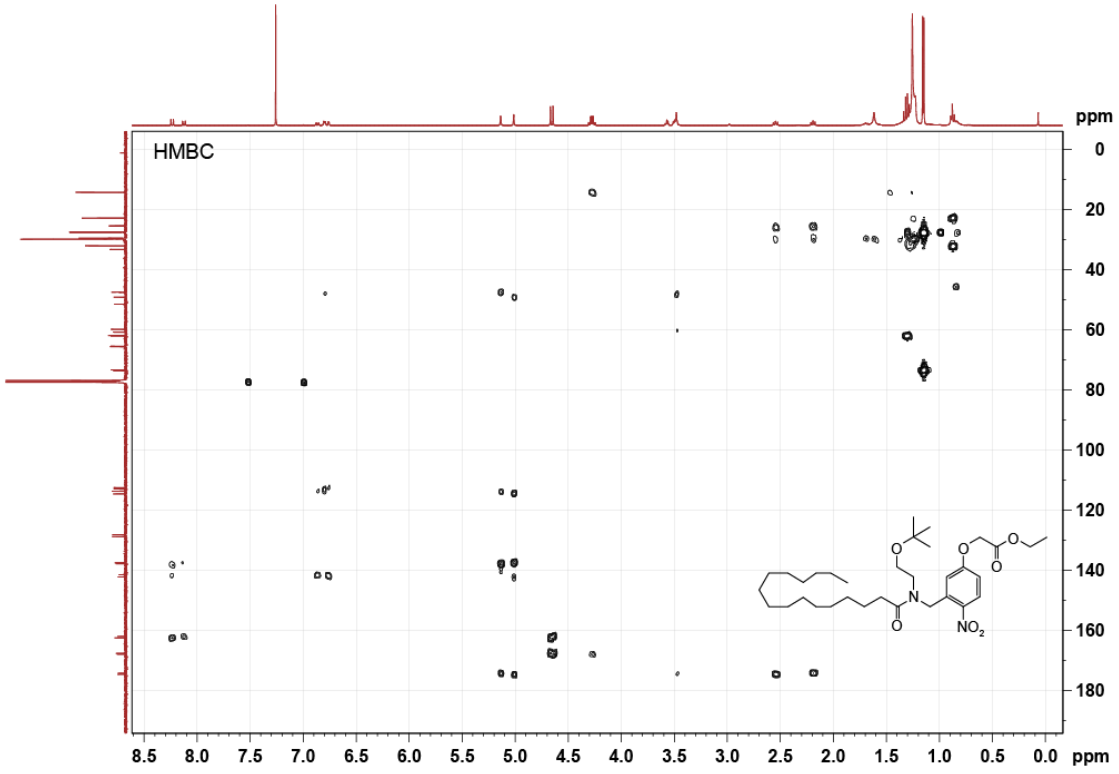
HMBC
ppm
0
20
40
60
80
100
120
140
160
180
8.5
8.0
7.5
7.0
6.5
6.0
5.5
5.0
4.5
4.0
3.5
3.0
2.5
2.0
1.5
1.0
0.5
0.0
ppm
O
O
O
O
O
N
O
NO2

### 2.5.4. Synthesis of *N*-(2-*tert*-butoxyethyl)-*N*-(5-carboxymethoxy-2-nitrobenzyl) palmitoylamide (4).

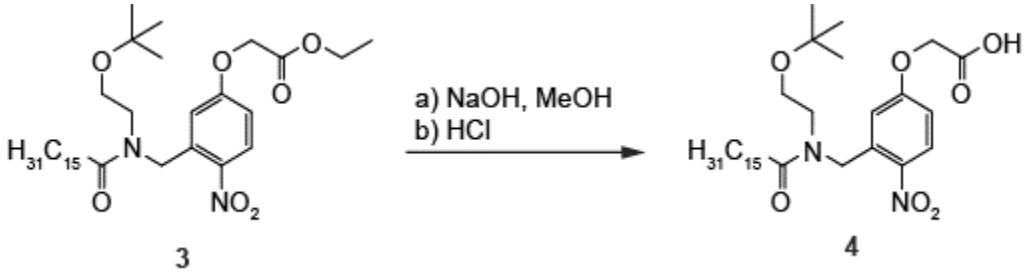


***N*-(*2-tert*-butoxyethyl)-*N*-(5-ethoxycarbonylmethoxy-2-nitrobenzyl)palmitoylamide** (**3**) (0.55 g, 0.93 mmol, 1.0 equiv.) was dissolved in MeOH (7.4 ml) and cooled in an ice-water bath for 5 min. 1 M aqueous NaOH (2.0 ml, 2.0 mmol, 2.0 equiv.) was added dropwise over 3 min, and the reaction continued for 1 h while gradually warming to room temperature. The reaction was again cooled in an ice-water bath and then neutralized with 1 M HCl (1.5 ml, 1.5 mmol, 1.5 equiv.). The reaction was diluted in EtOAc (5 ml), and the aqueous phase was 2× back-extracted with EtOAc and 2× with $Et_2O$. The combined organic extracts were then washed 2× with brine and dried over anhydrous $MgSO_4$. Filtration and concentration *in vacuo* yielded ***N*-(2-*tert*-butoxyethyl)-*N*-(5-carboxymethoxy-2-nitrobenzyl)palmitoylamide** (**4**) (0.55 g, 0.98 mmol) as a white powder, which was immediately used in the next step without purification.

### 2.5.5. Synthesis of *N*-(2-*tert*-butoxyethyl)-*N*-(5-methoxy-6-((4-(aminomethyl)benzyl)oxy)-*9H*-purin-2-carbamoyl-2-nitrobenzyl)palmitoylamide (5).

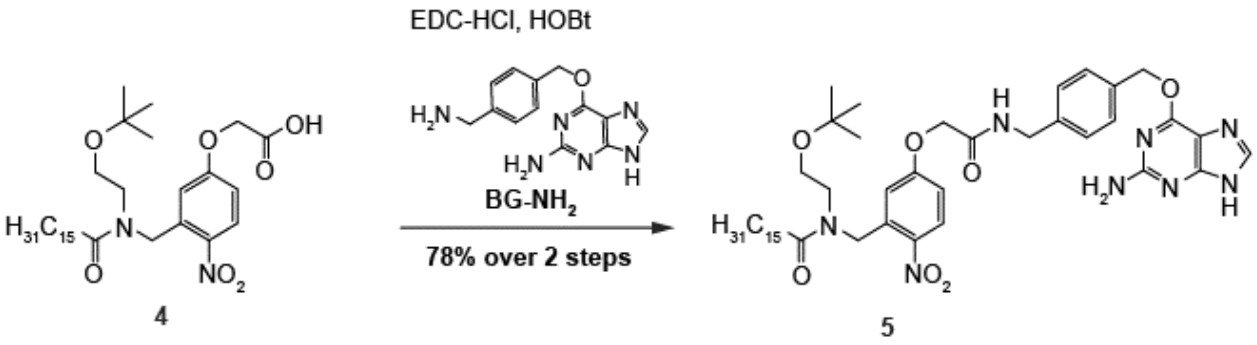


**6-((4-(aminomethyl)benzyl)oxy)-*9H*-purin-2-amine (BG-$NH_2$)** was prepared using a procedure described in Keppler *et al.*[55]

1-Hydroxybenzotriazole (HOBt) (0.15 g, 1.1 mmol, 1.1 equiv.) and 1-(3-dimethylaminopropyl)-3-ethylcarbodiimide hydrochloride (EDC-HCl) (0.21 g, 1.1 mmol, 1.1 equiv.) were added to ***N*-(2-*tert*-butoxyethyl)-*N*-(5-carboxymethoxy-2-nitrobenzyl) palmitoylamide** (**4**) (0.55 g, 0.98 mmol, 1.0 equiv.). The mixture was dissolved in dry *N,N*-dimethylformamide (30 ml) under an Ar atmosphere and was stirred for 45 min in an ice-water bath. Separately, BG-$NH_2$ (0.34 g, 1.24 mmol, 1.3 equiv.) was dissolved in dry *N,N*-dimethylformamide (15 ml) under an Ar atmosphere. The BG-$NH_2$ solution was added dropwise to the reaction flask over 15 min and stirred overnight, while slowly warming to room temperature. After diluting the reaction in EtOAc (40 ml), the organic phase was washed 2× with a saturated aqueous $NaHCO_3$ solution (100 ml), 2× with 0.1 M aqueous HCl (100 ml), 2× with $H_2O$ (100 ml), and once with saturated brine. The organic phase was dried over anhydrous $MgSO_4$, filtered, and then concentrated *in vacuo*. The residue was purified *via* flash column chromatography (60.12 g silica, $CH_2Cl_2$/MeOH 99:1→97:3→95:5) to yield ***N*-(2-*tert*-butoxyethyl)-*N*-(5-methoxy-6-((4-(aminomethyl) benzyl)oxy)-*9H*-purin-2-carbamoyl-2-nitrobenzyl)palmitoylamide** (**5**) (0.59 g, 0.72 mmol, 78% over two steps) as a yellow oil. The product was isolated as a mixture of *E* and *Z* amide isomers.

**TLC (95:5 $CH_2Cl_2$:MeOH):** $R_f$ = 0.36. **$^1$H NMR (DMSO, 400 MHz, 25 °C):** δ 8.90-8.68 (m, 1.0 H, CONH), 8.22 (d, 0.3 H, H3, *J* = 9.0Hz), 8.13 (d, 0.7 H, H3 *J* = 9.3 Hz), 7.84 (s, 1 H, H36), 7.46 (d, 2 H, $H31_{A,B}$, *J* = 8.1 Hz), 7.30 (d, 2 H, $H30_{A,B}$, *J* = 8.1 Hz), 7.09 (dd, 0.3 H, H2, *J* = 9.1, 2.8 Hz), 7.05 (dd, 0.7 H, H2, *J* = 9.0, 2.7 Hz), 6.79 (d, 0.3 H, H6, *J* = 2.4 Hz), 6.76 (d, 0.7 H, H6, *J* = 2.4 Hz), 6.26 (s, 1 H, NH), 5.48 (s, 2 H, $H33_{A,B}$), 5.08 (s, 0.6 H, $H7_A$), 4.89 (s, 1.4 H, $H7_{A,B}$), 4.70 (s, 2 H, $H8_{A,B}$), 4.37 (s, 2 H, $H28_{A,B}$), 3.44(s, 4 H, $H10_{A,B}$, $H11_{A,B}$), 2.54 (t, 1.5 H, $H13_{A,B}$, *J* = 7.1 Hz), 2.19 (t, 0.7 H, $H13_B$, *J* = 7.0 Hz), 1.67-1.45 (m, 2 H, $14_{A,B}$), 1.44-1.13 (m, 24 H, H15-H26), 1.09 (d, 9 H, *t*-Bu $CH_3$, *J* = 5.4 Hz), 0.84 (t, 3 H, $H27_{A,B,C}$, *J* = 6.8 Hz). **$^{13}$C NMR (DMSO, 101 MHz, 25 °C):** δ 173.28 (C12), 166.85 (C9), 161.99 (C1), 159.63 (C34), 141.30 (C4), 138.89 (C29), 138.28 (C36), 137.12 (C5), 135.42 ($C32_{E/Z}$), 128.46 (3 C, $C32_{E/Z}$, $C30_{A,B}$), 127.78 (C3), 127.40 (3 C, C29, $C31_{A,B}$), 113.85 (C6), 112.90 (C2), 72.60 ($\underline{C}(CH_3)_3$), 667.28(C8), 66.59 (C33), 59.69 (2 C, C10,C11), 46.58 (C7), 41.70 (C28), 32.04 (C13), 31.39 + 29.17 + 22.17 (12 C, C15-C26), 27.0371 ($C(\underline{C}H_3)_3$), 24.75 (C14), 13.88 (C27). **HRMS (ESI$^+$):** *m/z* calculated for $[C_{44}H_{64}N_8O_7]^+$ = 817.4971, observed = 817.4951 ($[M+H]^+$).

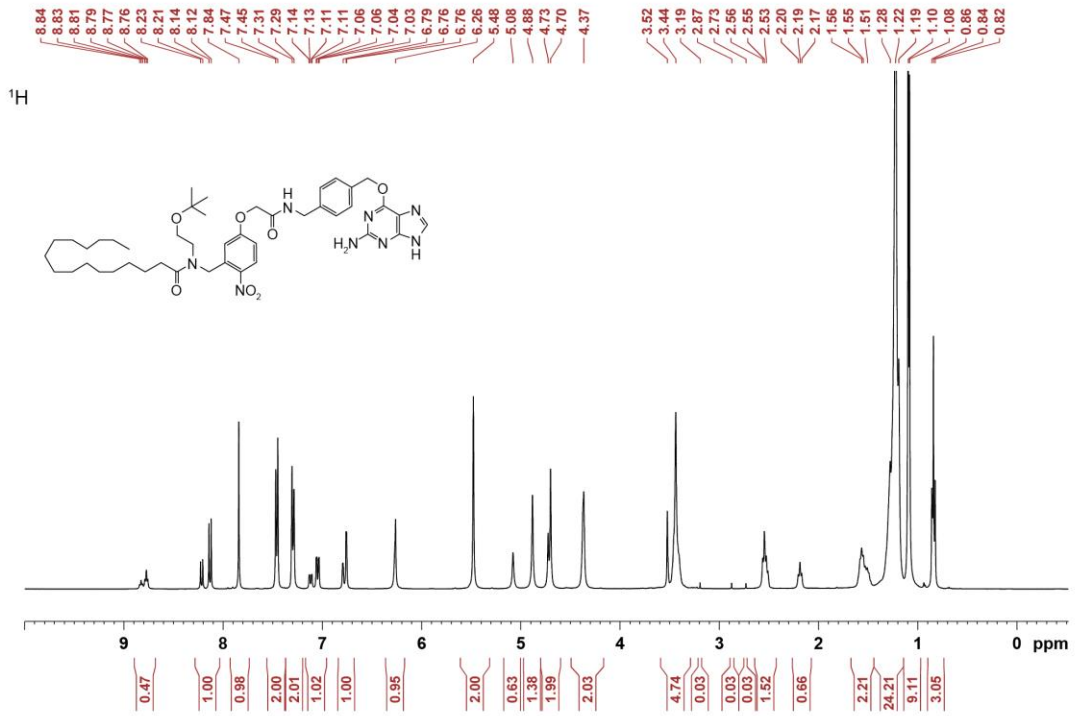
8.84
8.83
8.81
8.79
8.77
8.76
8.23
8.21
8.14
8.12
7.84
7.47
7.45
7.31
7.29
7.14
7.13
7.11
7.11
7.06
7.06
7.04
7.03
6.79
6.76
6.76
6.26
5.48
5.08
4.88
4.73
4.70
4.37
3.52
3.44
3.19
2.87
2.73
2.56
2.55
2.53
2.20
2.19
2.17
1.56
1.55
1.51
1.28
1.22
1.19
1.10
1.08
0.86
0.84
0.82
1H
9
8
7
6
5
4
3
2
1
0 ppm
0.47
1.00
0.98
2.00
2.01
1.02
1.00
0.95
2.00
0.63
1.38
1.99
2.03
4.74
0.03
0.03
0.03
1.52
0.66
2.21
24.21
9.11
3.05

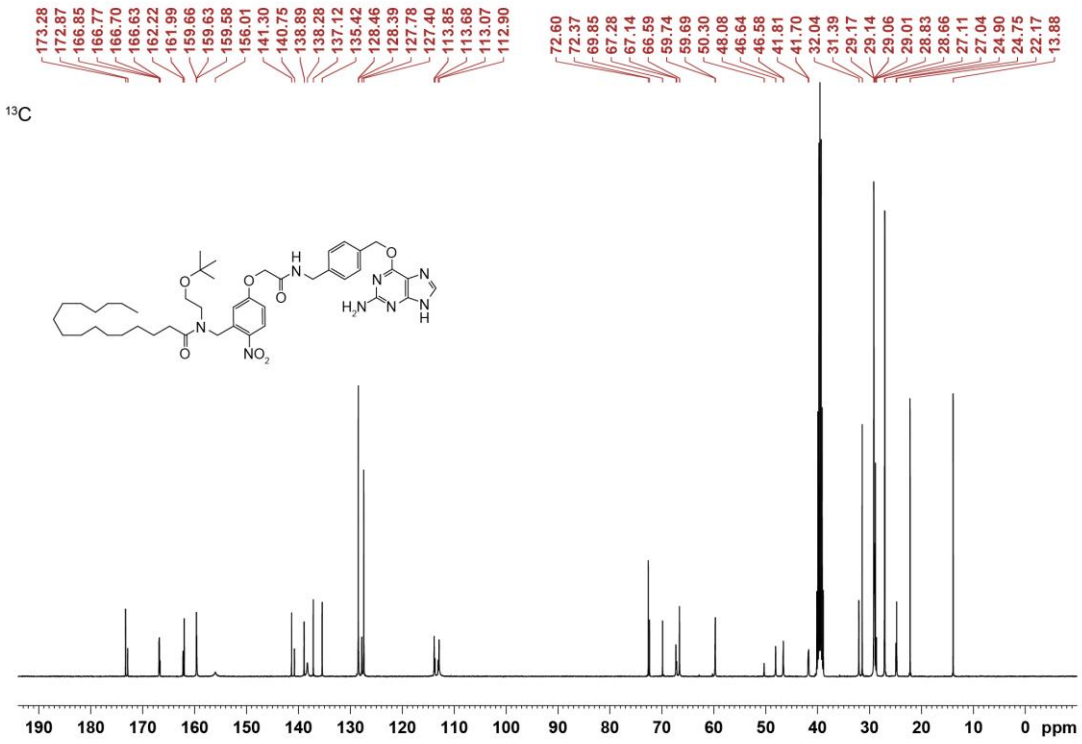
173.28
172.87
166.85
166.77
166.70
166.63
162.22
161.99
159.66
159.63
159.58
156.01
141.30
140.75
138.89
138.28
137.12
135.42
128.46
128.39
127.78
127.40
113.85
113.68
113.07
112.90
72.60
72.37
69.85
67.28
67.14
66.59
59.74
59.69
50.30
48.08
46.64
46.58
41.81
41.70
32.04
31.39
29.17
29.14
29.06
29.01
28.83
28.66
27.11
27.04
24.90
24.75
22.17
13.88
13C
190
180
170
160
150
140
130
120
110
100
90
80
70
60
50
40
30
20
10
0 ppm

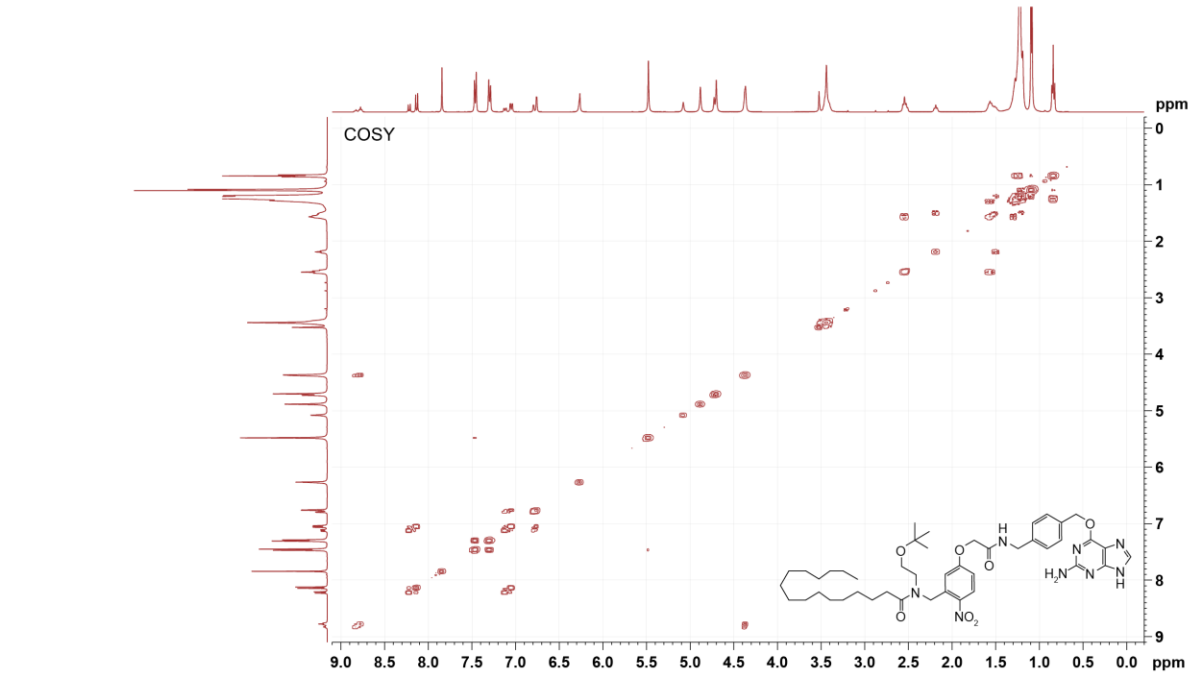
COSY
ppm
9.0 8.5 8.0 7.5 7.0 6.5 6.0 5.5 5.0 4.5 4.0 3.5 3.0 2.5 2.0 1.5 1.0 0.5 0.0 ppm
0 1 2 3 4 5 6 7 8 9

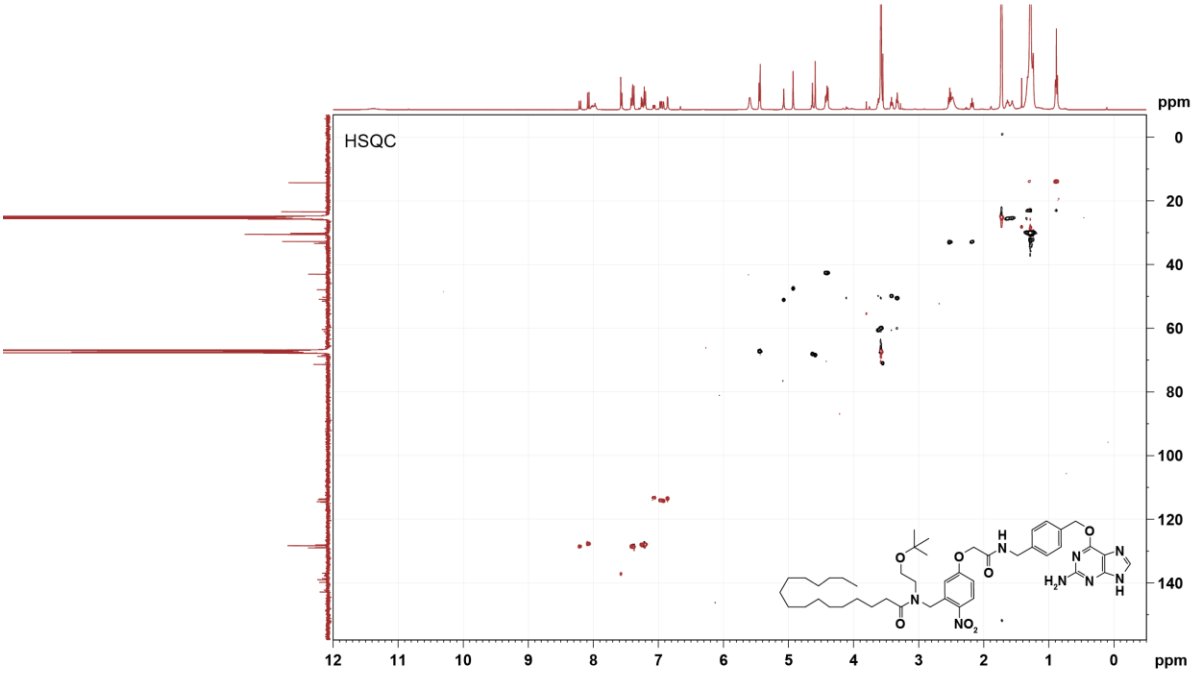
HSQC
ppm
12 11 10 9 8 7 6 5 4 3 2 1 0 ppm
0 20 40 60 80 100 120 140

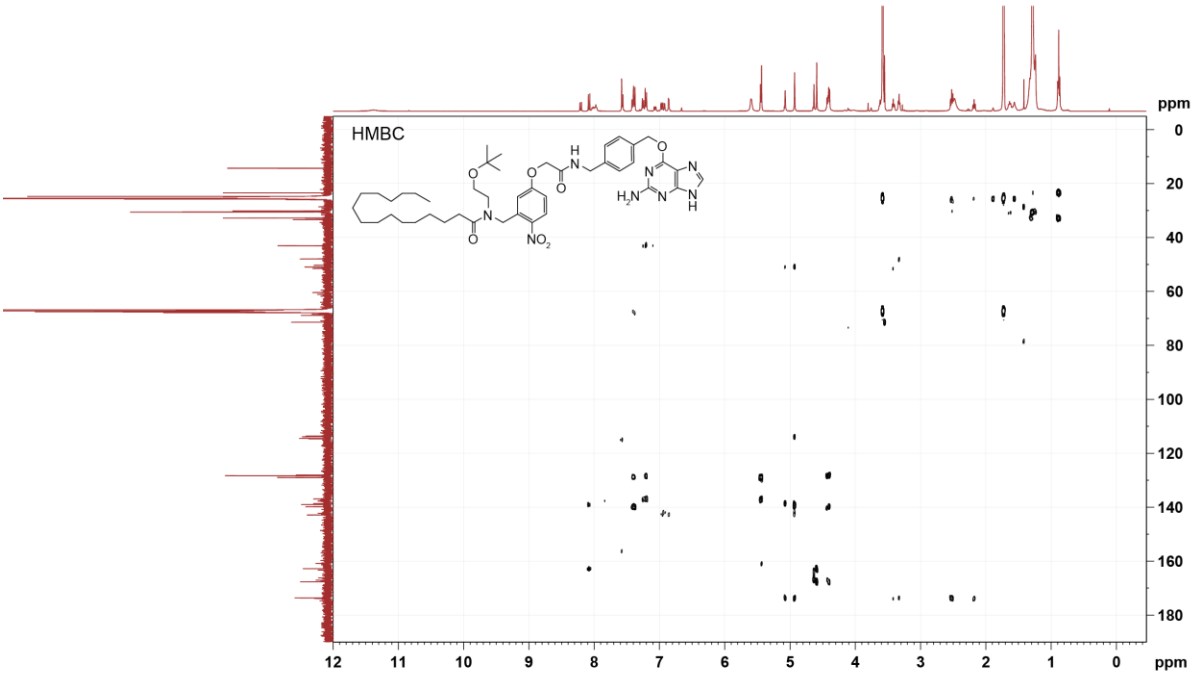
HMBC
ppm
0
20
40
60
80
100
120
140
160
180
12
11
10
9
8
7
6
5
4
3
2
1
0
ppm

### 2.5.6. Synthesis of *N*-(ethyl-2-ol)-*N*-(5-methoxy-6-((4-(aminomethyl)benzyl)oxy)-*9H*-purin-2-carbamoyl-2-nitrobenzyl)palmitoylamide (OCT-PEA).

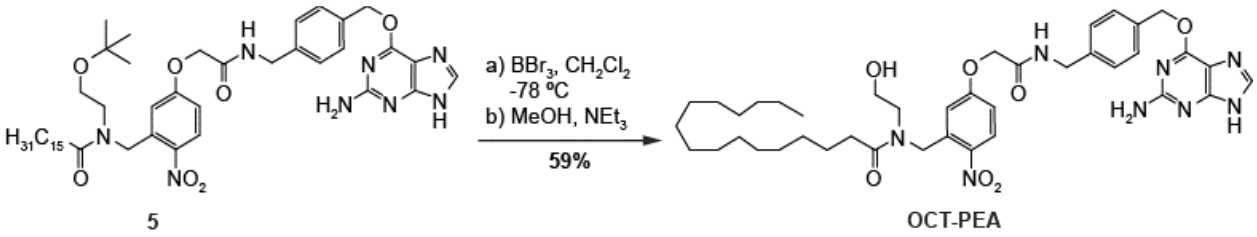


***N*-(2-*tert*-butoxyethyl)-*N*-(5-methoxy-6-((4-(aminomethyl)benzyl)oxy)-*9H*-purin-2-carbamoyl-2-nitrobenzyl)palmitoylamide** (**5**) (0.11 g, 0.14 mmol, 1.0 equiv.) was dissolved in dry $CH_2Cl_2$ (6.5 ml) under an Ar atmosphere, and then cooled in a dry ice / acetone bath. $BBr_3$ (1.0 M in $CH_2Cl_2$, 0.56 ml, 0.56 mmol, 4.0 equiv.) was added over 5 min and the reaction continued for 50 min. The reaction was quenched with 4:1 MeOH:$Et_2O$ (3 ml), and stirred vigorously for 5 min. The reaction mixture was neutralized with $Et_3N$ (0.3 ml, 2.1 mmol) and diluted in $CH_2Cl_2$ (42 ml). The reaction mixture was washed 2× with $H_2O$ (50 ml) and 2× with saturated brine (50 ml). The organic phase was concentrated *in vacuo* and purified *via* flash column chromatography (15 g silica, $CH_2Cl_2$/MeOH 93:7), yielding compound ***N*-(ethyl-2-ol)-N-(5-methoxy-6-((4-(aminomethyl)benzyl)oxy)-*9H*-purin-2-carbamoyl-2-nitrobenzyl) palmitoylamide** (**OCT-PEA**, 0.063 g, 82 μmol, 59%) as a yellow oil. The product was isolated as a mixture of *E* and *Z* amide isomers.

**TLC (9:1 $CH_2Cl_2$:MeOH):** $R_f$ = 0.40. **$^1$H NMR (THF-D8, 400 MHz, 25 °C):** δ 11.38 (b), 8.21 (d, 0.3 H, H3, *J* = 9.2 Hz), 8.08 (d, 0.6 H, H3, *J* = 9.5 Hz), 8.05-7.91 (m, 1 H, HNCO), 7.57 (d, 1 H, H36, *J* = 7.9 Hz), 7.40 (t, 2 H, $H31_{A,B}$, *J* = 8.7 Hz), 7.32 (dd, 2 H, $H30_{A,B}$, *J* = 17.9, 7.7 Hz), 7.07 (dd, 0.4 H, H2, *J* = 9.2, 2.6 Hz), 6.96 (dd, 0.6 H, H2, *J* = 9.2, 2.6 Hz), 6.92 (d, 0.4 H, H6, *J* = 2.3 Hz), 6.86 (d, 0.6 H, H6, *J* = 2.3 Hz), 5.59 (b), 5.44 (d, 2 H, H33, *J* = 6.9 Hz), 5.07 (s, 0.8 H, $H7_A$), 4.93 (s, 1.2 H, $H7_{A,B}$), 4.61 (d, 2 H, $H8_{A,B}$, *J* = 17.1 Hz), 4.48-4.34 (m, 2 H, $H28_{A,B}$), 3.46-3.29 (m,

2 H, $H10_A/H11_A$), 2.52 (t, $H13_A$, $J$ = 7.4 Hz), 2.31-2.13 (m, 1 H, $H13_B$), 1.69-1.51 (m, 2 H, $H14_{A,B}$), 1.38-1.19 (m, 24 H, H15-H26), 0.88 (t, 3 H, $H27_{A,B,C}$, $J$ = 6.7 Hz). **$^{13}$C NMR (THF-D8, 101 MHz, 25 °C):** δ 173.87 ($C12_{E/Z}$), 173.28 ($C12_{E/Z}$), 167.86 ($C9_{E/Z}$), 167.34 ($C9_{E/Z}$), 162.78 (C1), 142.67 (C5), 138.79 (C4), 138.02 (C36), 136.62 (C32), 129.18 (2 C, $C31_{A,B}$), 128.89 ($C3_{E/Z}$), 128.42 (3 C, C29 + $C30_{A,B}$), 128.06 ($C3_{E/Z}$), 114.32 ($C6_{E/Z}$), 113.99 ($C6_{E/Z}$), 113.71 ($C2_{E/Z}$), 68.67 (C28), 68.37 (C8), 60.94 ($\underline{C}(CH_3)_3$) 51.50 ($C7_{E/Z}$), 51.04 (C10), 50.24 (C11), 48.04 ($C7_{E/Z}$), 43.10 (C28), 33.34 (C13), 33.25 + 30.49 +23.36 (12 C, C15-C26), 14.26 (C27). **HRMS (ESI$^+$):** *m/z* calculated for $[C_{40}H_{56}N_8O_7]^+$ = 761.4345, observed = 761.4341 ($[M+H]^+$)

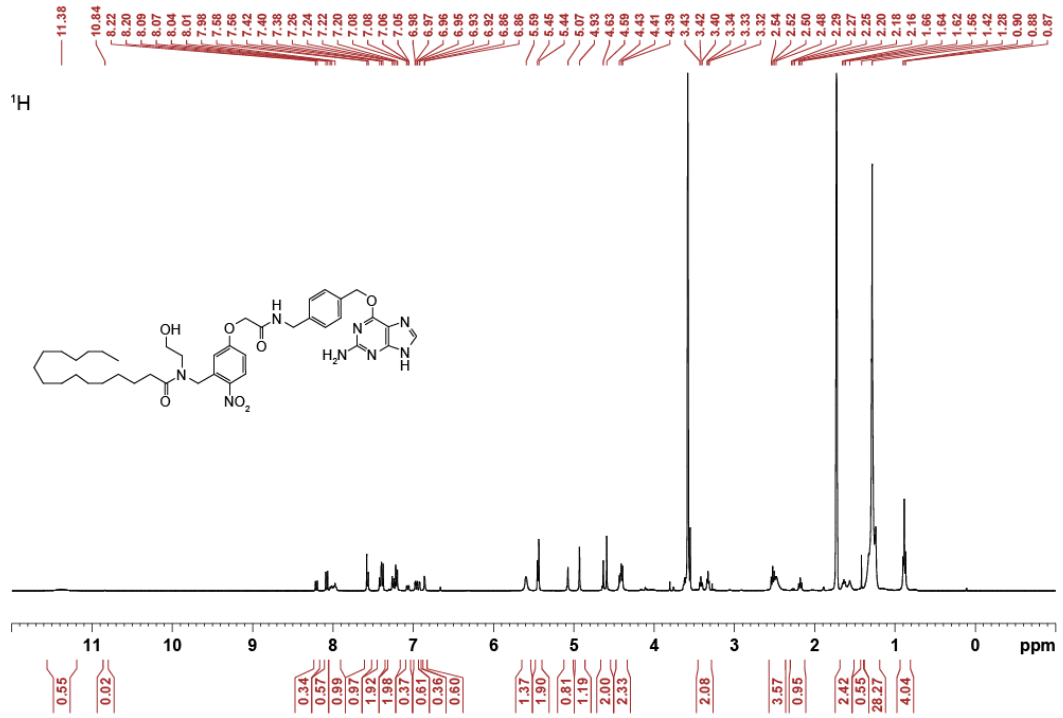
11.38
10.84
8.22
8.20
8.09
8.07
8.04
8.01
7.98
7.58
7.56
7.42
7.40
7.38
7.26
7.24
7.22
7.20
7.08
7.08
7.06
7.05
6.98
6.97
6.96
6.95
6.93
6.92
6.86
6.86
5.59
5.45
5.44
5.07
4.93
4.63
4.59
4.43
4.41
4.39
3.43
3.42
3.40
3.34
3.33
3.32
2.54
2.52
2.50
2.48
2.29
2.27
2.25
2.20
2.18
2.16
1.66
1.64
1.62
1.56
1.42
1.26
0.90
0.88
0.87
1H
OH
O
H
N
O
N
N
N
N
H
H2N
O
N
O
NO2
11
10
9
8
7
6
5
4
3
2
1
0
ppm
0.55
0.02
0.34
0.57
0.99
0.97
1.92
1.98
0.37
0.61
0.36
0.60
1.37
1.90
0.81
1.19
2.00
2.33
2.08
3.57
0.95
2.42
0.55
28.27
4.04

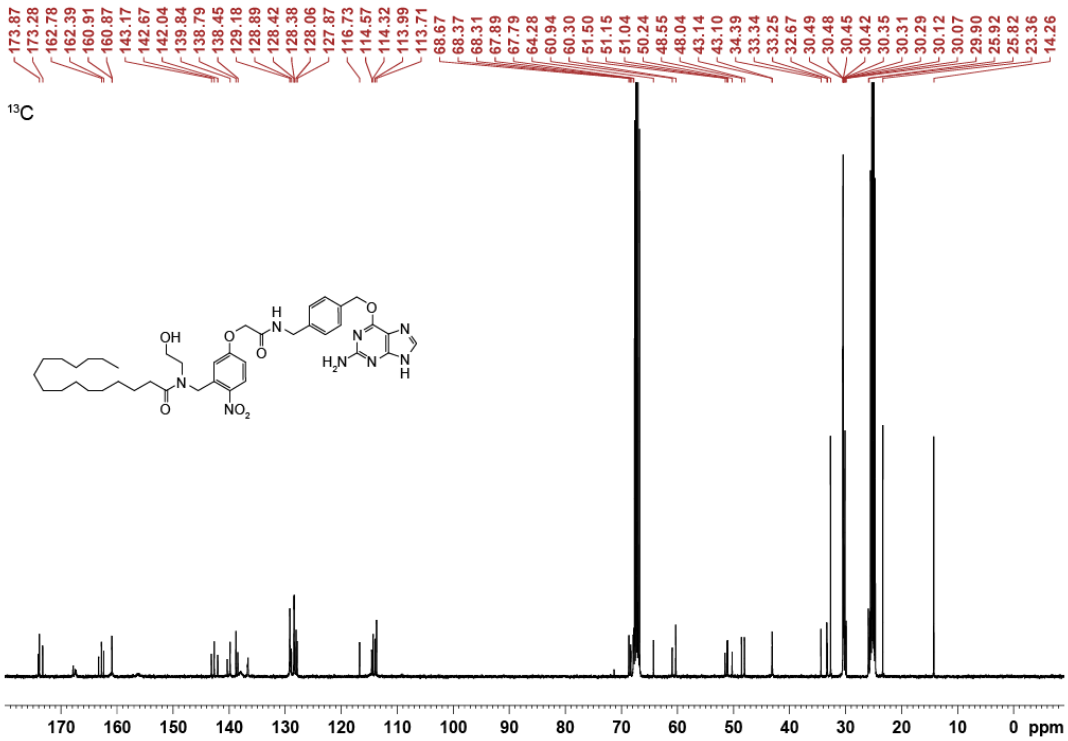
173.87
173.28
162.78
162.39
160.91
160.87
143.17
142.67
142.04
139.84
138.79
138.45
129.18
128.89
128.42
128.38
128.06
127.87
116.73
114.57
114.32
113.99
113.71
68.67
68.37
68.31
67.89
67.79
64.28
60.94
60.30
51.50
51.15
51.04
50.24
48.55
48.04
43.14
43.10
34.39
33.34
33.25
32.67
30.49
30.48
30.45
30.42
30.35
30.31
30.29
30.12
30.07
29.90
25.92
25.82
23.36
14.26
13C
OH
O
H
N
O
N
N
N
N
H
H2N
O
N
O
NO2
170
160
150
140
130
120
110
100
90
80
70
60
50
40
30
20
10
0
ppm

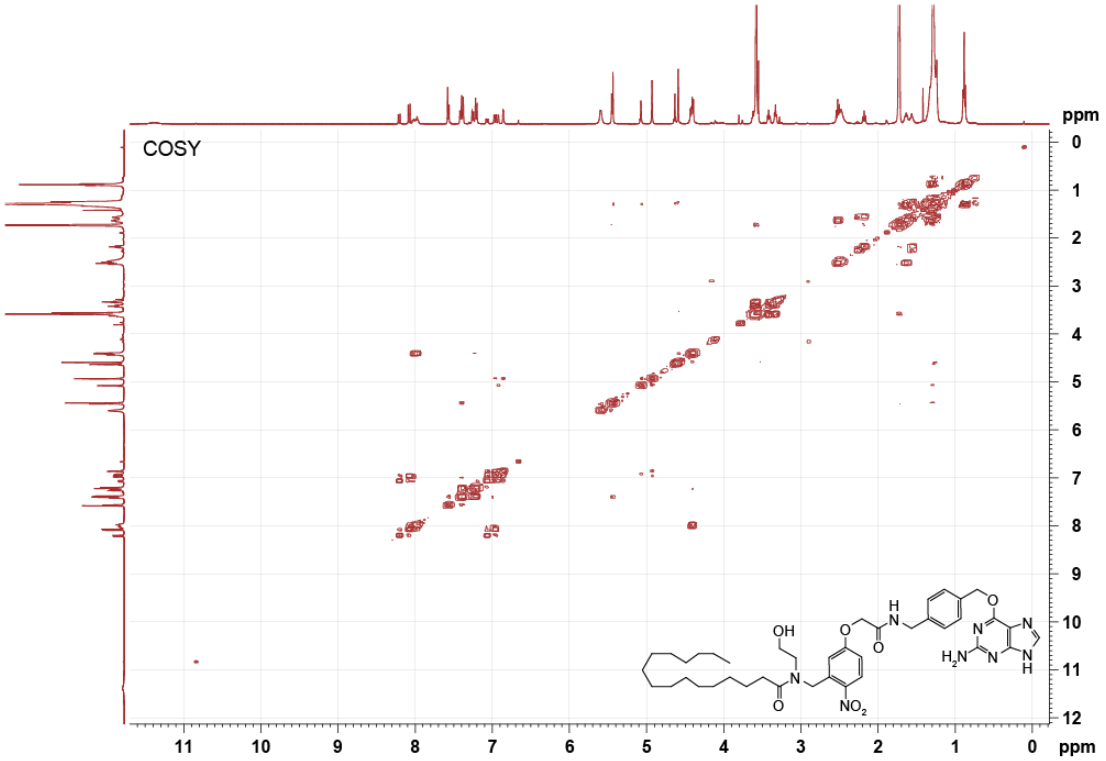
COSY
ppm
0
1
2
3
4
5
6
7
8
9
10
11
12
11
10
9
8
7
6
5
4
3
2
1
0
ppm
OH
O
H
N
O
N
N
N
H
$H_2N$
N
O
N
O
$NO_2$

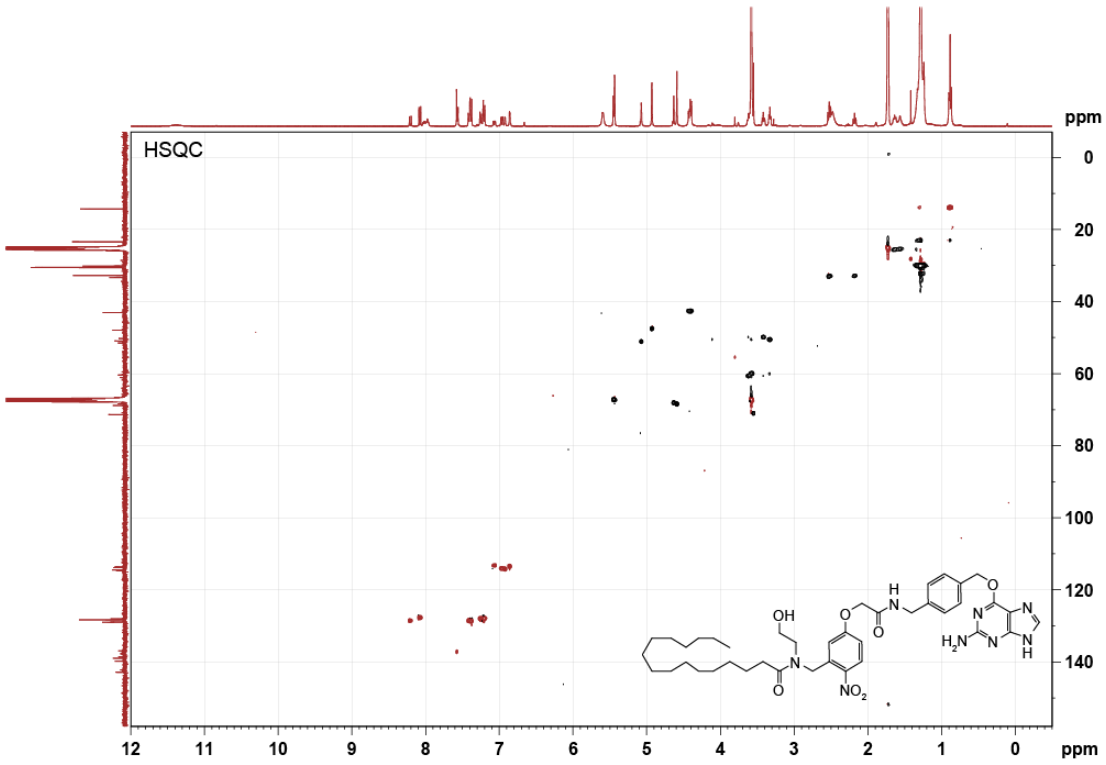
HSQC
ppm
0
20
40
60
80
100
120
140
12
11
10
9
8
7
6
5
4
3
2
1
0
ppm
OH
O
H
N
O
N
N
N
H
$H_2N$
N
O
N
O
$NO_2$

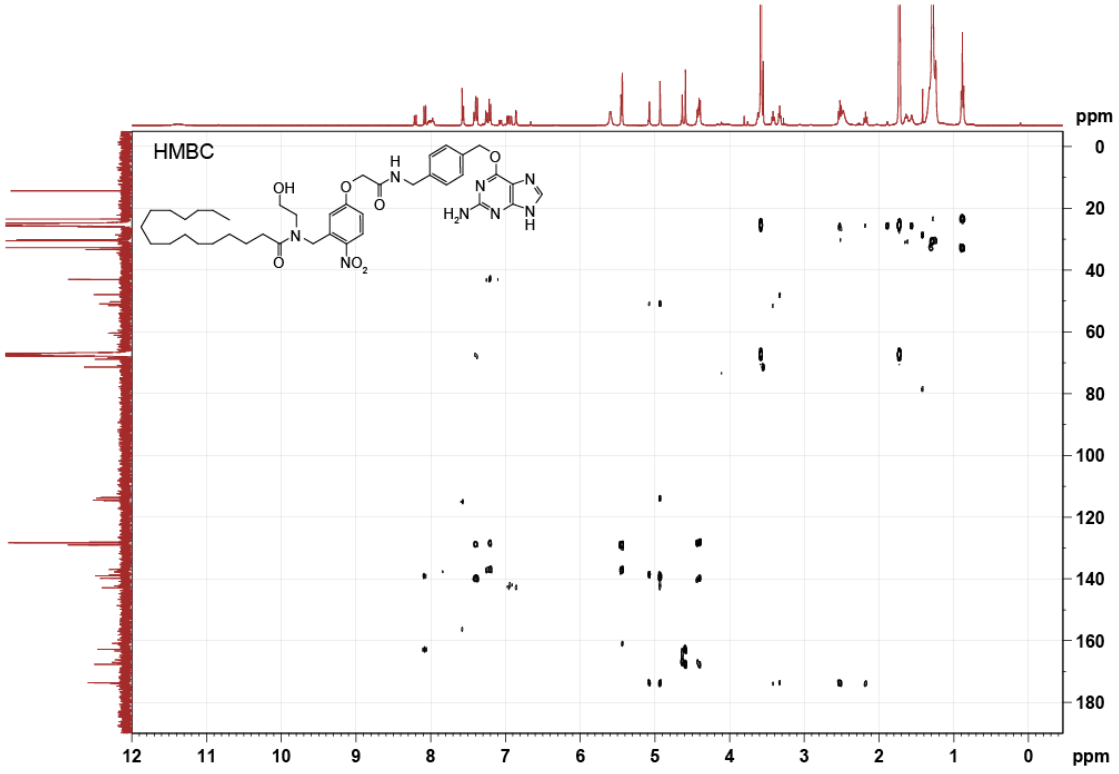
HMBC
OH
O
H
N
O
N
O
N
N
N
N
H
$H_2N$
N
O
$NO_2$
ppm
0
20
40
60
80
100
120
140
160
180
12
11
10
9
8
7
6
5
4
3
2
1
0
ppm

# Chapter 3. Optical control of endocannabinoid signaling in human pancreatic islets with tethered photopharmacology.

Janelle M. Tobias[1], Alexander E.G. Viray[1], Sunghee Chai and James A. Frank[1]

[1] Department of Chemical Physiology & Biochemistry, Oregon Health & Science University, Portland, OR, USA.

Author contribution:

**J.M.T.** and J.A.F. conceived and coordinated the study. **J.M.T.** synthesized and characterized the compounds, performed INS-1 imaging experiments, and performed insulin ELISA. A.E.G.V. and S.C designed and generated the AAV viruses. A.E.G.V. characterized the AAV viruses, and carried out the cytotoxicity assay. J.A.F. performed live islet imaging, and **J.M.T.** processed the islet data. **J.M.T.** wrote MATLAB codes for $Ca^{2+}$ and UV-Vis data analysis. **J.M.T.** and J.A.F. wrote the manuscript with contributions from other co-authors.

A manuscript is in preparation for the work presented in this chapter, and the figures have been adapted for this thesis.

## 3.1. Introduction

Pancreatic β-cell excitability and insulin secretion are regulated by a plethora of GPCRs, including the cannabinoid receptors (CBRs), which respond to lipids called *N*-acylethanolamines (NAEs)[22,77]. However, NAEs' complex pharmacology and hydrophobicity make them difficult to control in time and space after application to cells. This complicates our understanding of NAE signaling in β-cells, and prevents us from investigating the CBR pathways which potentially play a role in metabolic disorders. Building on previous work, we wanted to use the the Optically-Cleavable Targeted (OCT)-ligand approach[59] to investigate NAE signaling in intact human islets. OCT-ligands allow NAEs to be first targeted, and then released on genetically-defined membranes (**Figure 3.1 A**). Previously, we synthesized a probe—coined OCT-PEA—that tethers to SNAP-tags and releases the saturated NAE, palmitoylethanolamide (PEA) at the site of SNAP-tag expression, to activate nearby endogenous receptors. We showed that uncaging OCT-PEA on the surface of the INS-1 pancreatic β-cell line, stimulated $Ca^{2+}$ oscillations through GPR55 and phospholipase C. While this study set the stage for targeted cannabinoid photopharmacology, the application of this probe remained limited to a model β-cell line, INS-1 cells. The low solubility and slow labeling kinetics of OCT-PEA, coupled with our inability to express SNAP-tags in primary pancreatic tissue prevented us from applying this tool to more complex biological systems, such as the pancreatic islet.

In this work, we describe the second-generation of OCT-ligands and their application to manipulate cannabinoid signaling in intact human islets (**Figure 3.1 B**). We chemically modified OCT-PEA to target HaloTags, which have faster labeling kinetics relative to SNAP-tags[78], and identified a HaloTag-targeted OCT-PEA (**hOCT-PEA**) with improved labeling relative to the parent molecule OCT-PEA. To use our probes in human islets, we developed a novel adeno-associated virus (AAV) that allowed us to express HaloTags exclusively on the β-cell surface in intact human islets. Coined AAV-Halo, we expressed HaloTags on human β-cells and showed

that PEA uncaging on human β-cells stimulated $Ca^{2+}$ oscillations. The fusion of improved OCT-ligands and AAV-Halo tools allow us to target CBRs in intact human islets with enhanced spatiotemporal precision.

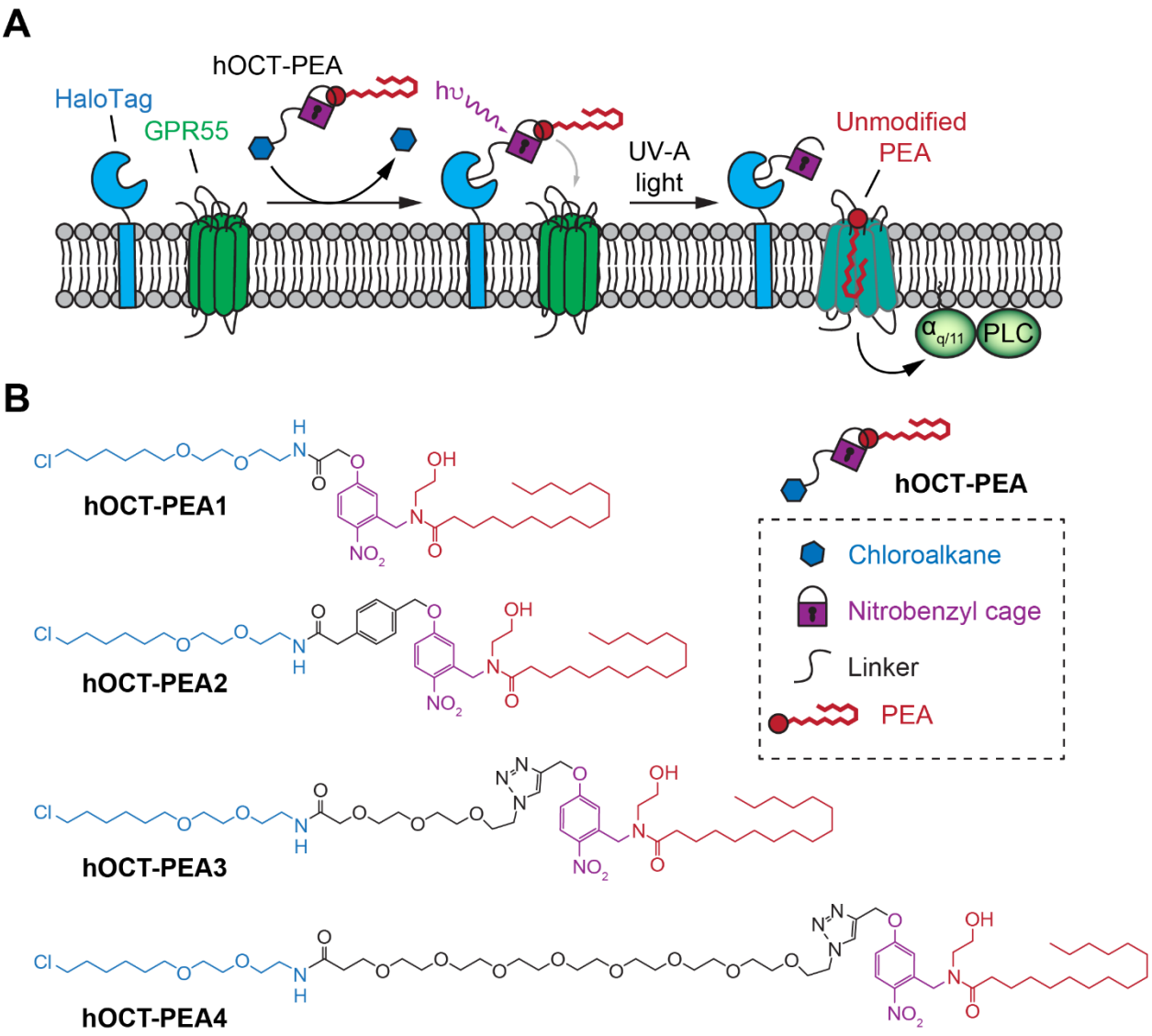


*Figure 3.1. OCT-palmitoylethanolamide (PEA) labels HaloTags and activates GPR55. (**A**) Schematic depiction of **hOCT-PEA**, which activates GPR55 through $G\alpha_{q/11}$ and PLC. (**B**) Chemical structures of **hOCT-PEA1-4** which contains: a chloroalkane tag, linker, nitrobenzyl cage, and PEA ligand.*

## 3.2. Results

### 3.2.1. Design and synthesis of hOCT-PEA derivatives

To increase the labeling efficiency of our OCT-ligands, I prepared probes that target the HaloTag system (HaloTag7)[56], which is known to label more rapidly when compared to SNAP-tags[78]. Previous studies have shown that the linker region proximal to the chloroalkane is important for labeling efficiency[79], so I synthesized four HaloTag-targeting probes (hOCT-ligands) that differ in the linker length and degree of hydrophilicity, denoted as **hOCT-PEA1-4** (**Figure 3.1**).

**hOCT-PEA1** and **hOCT-PEA2** contain a short amide linker attached to the chloroalkane motif, and were synthesized in a similar fashion to the original SNAP-targeted compound, **OCT-PEA** (**Figure 3.2 A**). 5-hydroxy-2-nitrobenzaldehyde was reacted with a bromated linker ($X_1R_1$ = ethyl 2-bromoacetate, $X_2R_2$ = methyl 2-(4-(bromomethyl) phenyl)acetate) under basic conditions to form a phenolic ethers **1** and **5**, respectively. Reductive amination with 2-(*t*-butyloxy)-ethanamine formed amines **2** and **6**, followed by acylation with palmitoyl chloride to yield the tertiary amides **3** and **7**, respectively. The ester protecting group ($R_1$ = $CH_2CH_3$ or $R_2$ = $CH_3$) was hydrolyzed under basic conditions to form the corresponding carboxylic acids, which were directly coupled to **2-(2-(chloromethoxy)ethoxy)ethan-1-amine** (CA) to afford *t*Bu-ether protected OCT-ligands **4** and **8**. Finally, the *t*Bu-ether was removed in neat trifluoroacetic acid to afford **hOCT-PEA1** in 38% overall yield (**Detailed synthetic methods, Figure 3.14 A**) and **hOCT-PEA2** in 23% overall yield (**Detailed synthetic methods, Figure 3.15 A**).

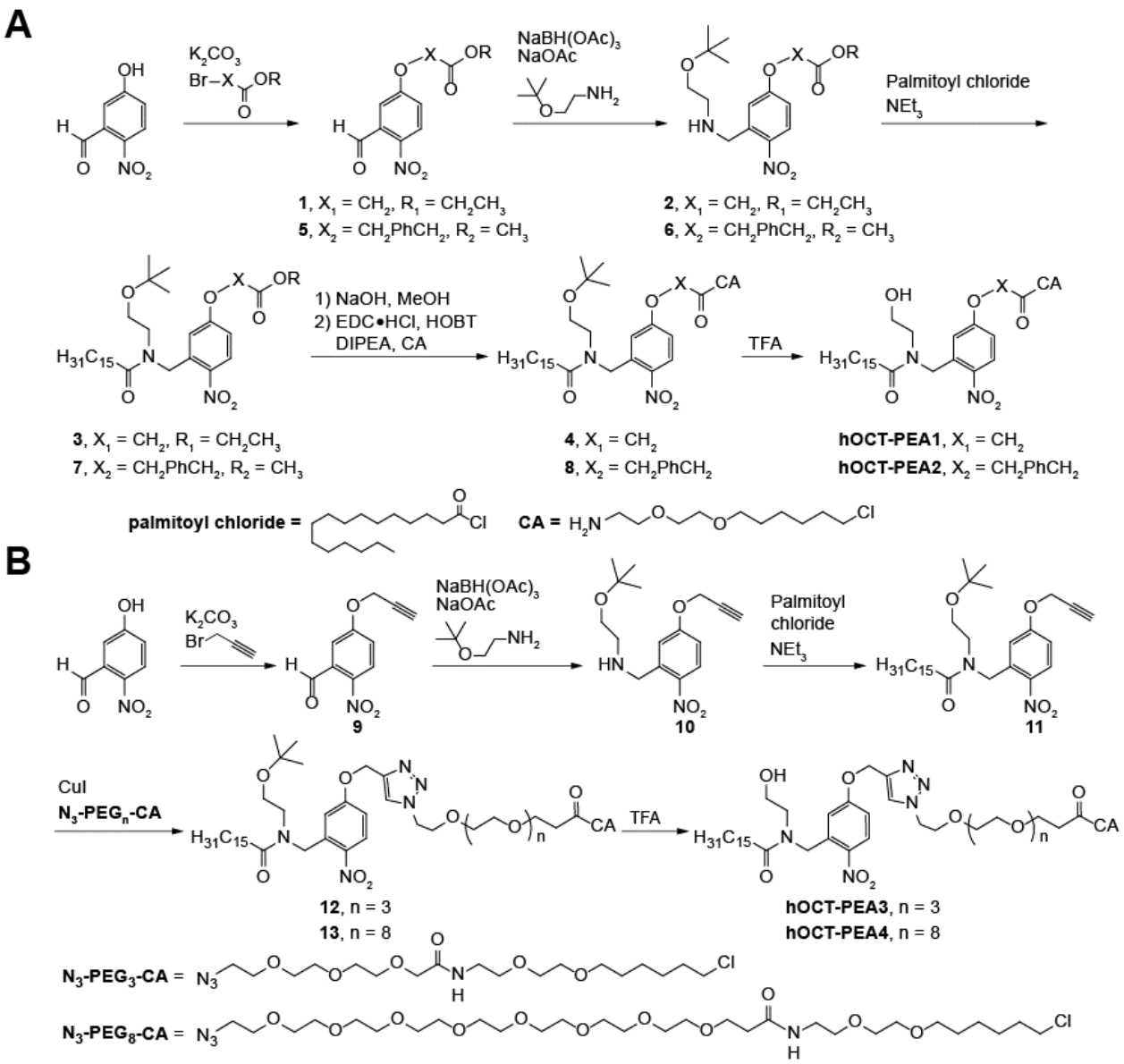


*Figure 3.2. Synthetic scheme for hOCT-PEA derivatives.*
*(**A**) Chemical synthesis of **hOCT-PEA1** and **hOCT-PEA2**, which proceeded over 6 steps in 38% and 23% overall yields, respectively. (**B**) Chemical synthesis of **hOCT-PEA3** and **hOCT-PEA4**, which proceeded over 5 steps in 16% and 14% overall yields, respectively.*

**hOCT-PEA3** and **hOCT-PEA4** were designed to contain long polyethylene glycol (PEG) linkers to improve their aqueous solubility. These were synthesized using copper-catalyzed click chemistry to incorporate different linker lengths and the CA in a single step (**Figure 3.2 B**). First,

5-hydroxy-2-nitrobenzaldehyde was reacted with 3-bromoprop-1-yne under basic conditions to form phenolic ether **9**. Reductive amination with 2-(*t*-butyloxy)-ethanamine formed amine **10**, followed by acylation with palmitoyl chloride to yield the tertiary amide **11**. To prepare the extended PEG-CA linkers, amide coupling of the PEG acids with the **CA** led to **$N_3$-$PEG_n$-CA** (n = 3,8). The extended PEG-linkers (**$N_3$-$PEG_3$-CA** and **$N_3$-$PEG_8$-CA**) were clicked onto alkyne **11** to afford triazoles **12** and **13**, respectively. Finally, deprotection of the *t*Bu-ether afforded **hOCT-PEA3** in 16% overall yield (**Detailed synthetic methods, Figue 3.16 A**), or **hOCT-hPEA4** in overall 14% yield (**Detailed synthetic methods, Figure 3.17 A**), respectively. This use of click-chemistry opens the door for straightforward functionalization of the linker and bioconjugation motifs of our OCT-ligands, which can be used to prepare a library of unique OCT-ligands in futures studies.

We studied the photophysical properties of **hOCT-PEA1-4** by UV-Vis spectroscopy. To assess the kinetics of the uncaging reaction, we exposed each compound to 365 nm LED light (**Figure 3.3 A**, ~26 mW). In the dark, $\lambda_{max}$ for each compound was **hOCT-PEA1** = 306 nm; **hOCT-PEA2** = 313 nm; **hOCT-PEA3** = 310 nm; and **hOCT-PEA4** = 310 nm (**Figure 3.3 B**). Further, irradiation led to a bathochromic wavelength shift for each compound, consistent with the uncaged product which contains an extended electron $\pi$-network of the uncaged nitroso-aldehyde. The uncaging reaction for **hOCT-PEA1-4** proceeded with a $\tau$ = 22 s, 22 s, 26 s, and 25 s, respectively (**Figure 3.3 C**). Together, these data show that the chosen linkers did not impact the uncaging kinetics of the nitrobenzyl photocage *in vitro*.

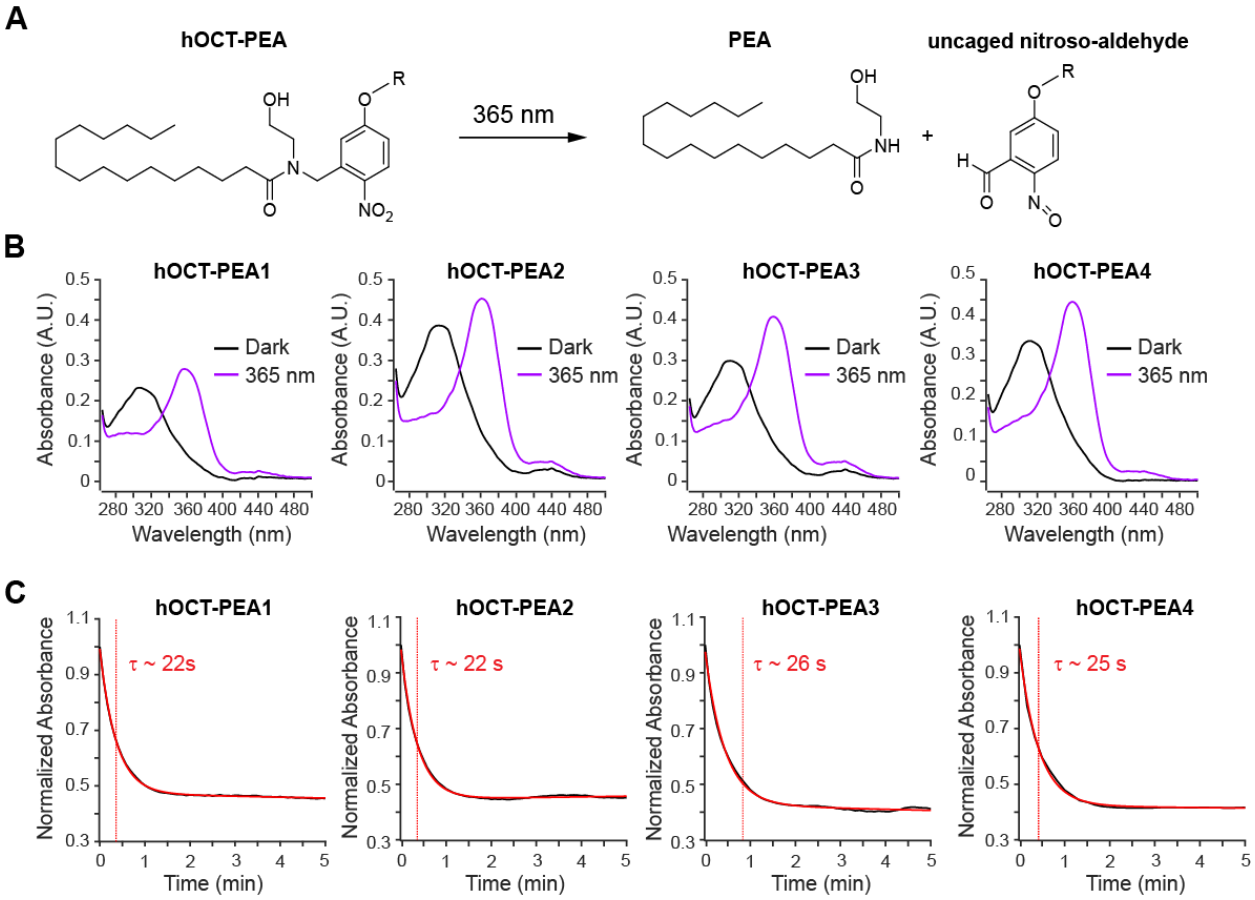


*Figure 3.3. Photophysical characterization of hOCT-PEA derivatives by UV-Vis spectroscopy. (**A**) Chemical structures showing the uncaging reaction for hOCT-PEA derivatives. Uncaging OCT-PEA releases PEA and the nitroso-aldehyde attached to R, where R is the linker that differs across hOCT-PEA derivatives. (**B**) UV-Vis absorbance spectra of four hOCT-PEA derivatives in the dark (black) and 1 min after 365 nm LED exposure (magenta). (**C**) Kinetics of uncaging reaction for four hOCT-PEA derivatives. Data for each compound is normalized against the absorbance at $\lambda_{max}$, and plotted over 5 min of 365 nm irradiation. The $\lambda_{max}$ for each compound are: **hOCT-PEA1** = 306 nm; **hOCT-PEA2** = 313 nm; **hOCT-PEA3** = 310 nm; **hOCT-PEA4** = 310 nm.*

Next, we wanted to confirm that **hOCT-PEA4** was compatible for use with longer wavelengths. I adjusted the power of four LEDs (365 nm, 415 nm, 470 nm, and 565 nm) to ~16 mW, and exposed **hOCT-PEA4** to each LED for 5 min (**Figure 3.4 A**). After 365 nm light exposure, the main absorbance peak of **hOCT-hPEA4** is at λ = 312 nm, which is red-shifted

after 365 nm light exposure, and proceeded with $\tau$ = 43 s. Irradiation with longer wavelengths (415 nm, 470 nm, and 565 nm) did not efficiently uncage **hOCT-hPEA4** (**Figure 3.4 B**), demonstrating that the probe is compatible for use in fluorescence microscopy with blue and green biosensors.

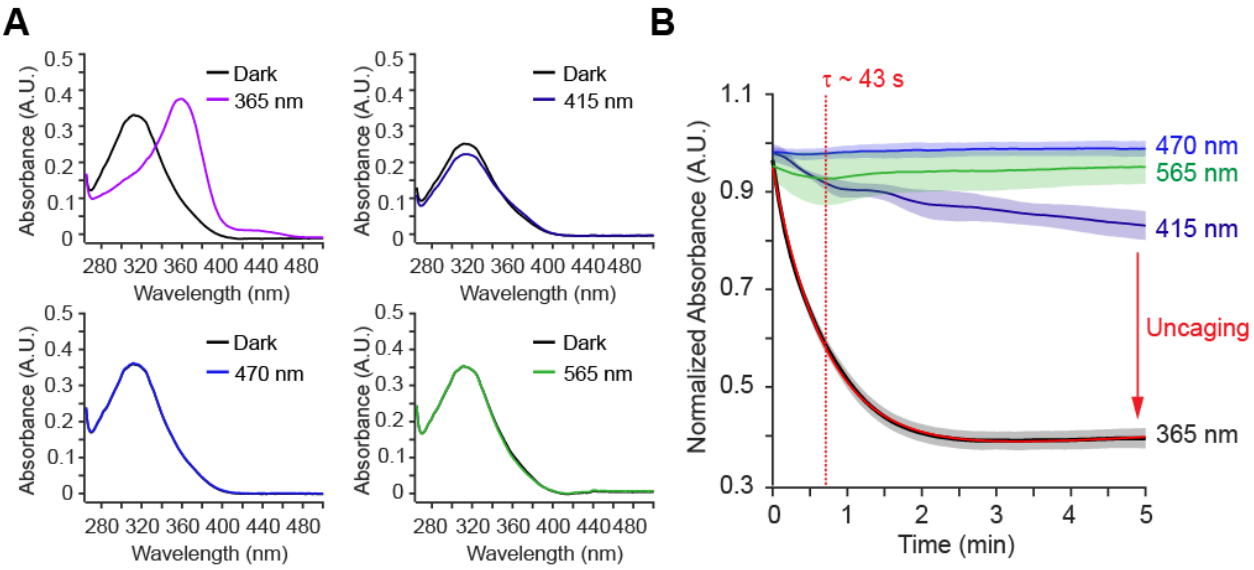


*Figure 3.4. Comparing uncaging across LEDs.*
*(**A**) UV-Vis absorbance spectra of **hOCT-PEA4** (40 $\mu$M in DMSO) in the dark (black) and after 2.5 min of 365 nm (magenta, top left, ~16 mW), 405 nm (navy, top right, ~15 mW), 470 nm (blue, bottom left, ~16 mW), or 565 nm (green, bottom right, ~21 mW) LED exposure . (**B**) Normalized absorbance at $\lambda$ = 312 nm over time of **hOCT-PEA4** (40 $\mu$M in DMSO) after exposure to 365 nm LED (black, ~16 mW), 405 nm (navy, ~15 mW), 470 nm (blue, ~16 mW), or 565 nm (green, ~21 mW) light. Absorbance data is normalized against the absorbance at t = 0 min. N = 3 samples for each condition. Shaded error bars = mean ± SEM.*

### 3.2.2. Comparing hOCT-PEA derivatives' labeling efficiency and toxicity in INS-1 cells

With four OCT-ligands in hand, we wanted to compare their labeling efficiency at surface-expressed HaloTags. To this end, I constructed a reporter plasmid CMV-pDisplayHaloTag7-T2A-EGFP (pDisplayHalo-EGFP), that allows for quantification of probe labeling through the co-

expression of cytosolic EGFP and surface-targeted HaloTags (**Figure 3.5 A**). I also prepared a control plasmid with a mutated HaloTag, pDisplayHalo7$^{D107A}$-EGFP (**Figure 3.5 B**). Both plasmids have a Myc-tag on the HaloTag which can be used to visualize protein expression. However, the D107A mutation prevents the HaloTag from labeling the chloroalkane motif, and thus HaloTag dyes or hOCT-ligands.

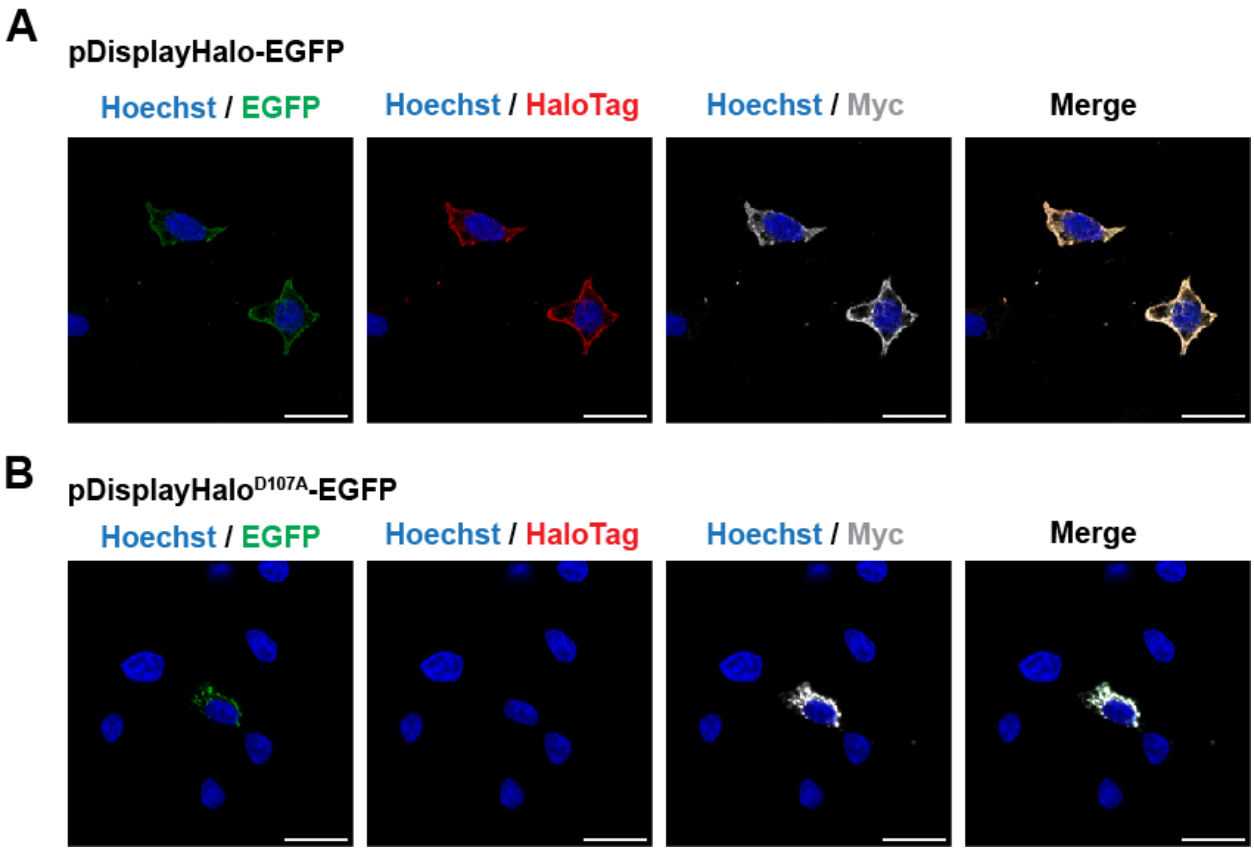


*Figure 3.5. Expression of pDisplayHalo-EGFP and pDisplayHalo$^{D107A}$-EGFP in INS-1 cells. INS1 cells were transfected with pDisplayHalo-EGFP or pDisplayHalo$^{D107A}$-EGFP and labelled with Hoechst-33342 (10 μM, blue) and jFHalo549i (500 nM, red) for 10 min. Cells were fixed, then probed for Myc-tag (grey). EGFP (green) serves as a transfection marker. (**A**) INS1 cells transfected with pDisplayHalo-7-T2A-EGFP have surfaced-labeled Halo-tags in cells that are positive for EGPF and Myc. (**B**) In contrast, INS-1 cells transfected with the inactive pDisplayHalo$^{D107A}$-EGFP did not have jFHalo549i fluorescenc but maintained Myc staining in the EGFP positive cells. Scale bar 15 mm.*

INS-1 β-cells were transfected with pDisplayHalo-EGFP, preincubated with vehicle or **hOCT-PEA** derivatives for 1 h at increasing concentrations, then labeled with a fluorescent HaloTag dye (jFHalo549i) to fluorescently label any free HaloTags. The cells were fixed and imaged, where fluorescence of jFHalo549i was normalized to the EGFP fluorescence. Since the **hOCT-PEAs** and jFHalo549i dye covalently label the same residue (D107) in the HaloTag protein, successful **hOCT-PEA** labeling decreases jFHalo549i fluorescence (**Figure 3.6 A**). Surprisingly, **hOCT-PEA1**, which has the same linker as the original SNAP-tag targeted OCT-PEA, and **hOCT-PEA2**, which has a sterically bulkier linker, did not efficiently label the HaloTags up to 8 μM. However, **hOCT-PEA3** and **hOCT-PEA4**, which incorporated flexible PEG linkers of different lengths, showed improved labeling relative to **hOCT-PEA1** and **hOCT-PEA2** (**Figure 3.6 B**). We found that **hOCT-PEA4** labeled pDisplay-HaloTags much more effectively than the other 3 **hOCT-PEA** derivatives. Complete labeling was achieved at 2 μM for 1 h which was a shorter incubation and lower dose relative to the original OCT-PEA probe, which required labeling of 5 μM probe for 2 h. Because **hOCT-PEA4** showed superior labeling, it was used as the lead compound the subsequent experiments.

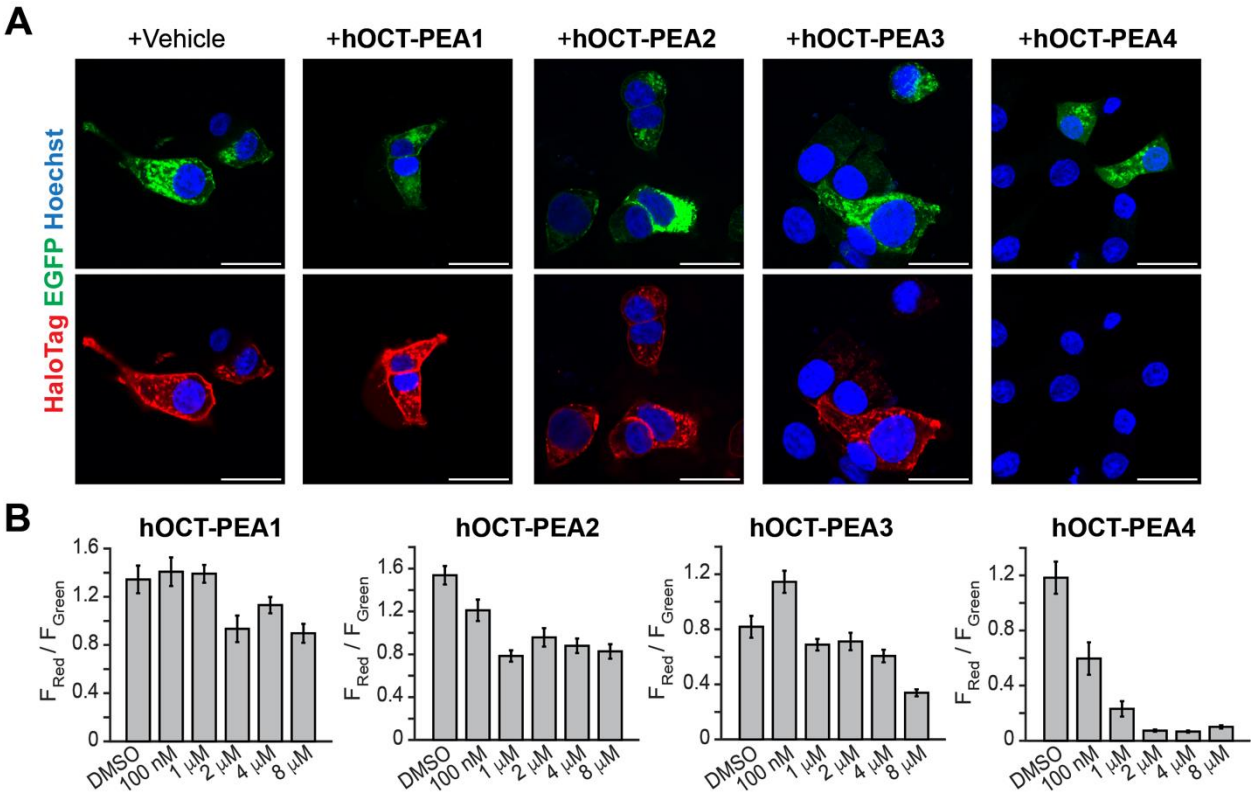


*Figure 3.6. Evaluating **hOCT-PEA** labeling in INS-1 β-cells.*
*(**A**) INS-1 cells were transfected with pDisplayHalo-EGFP, treated with vehicle or **hOCT-PEA** derivatives (2 μM), then incubated with jfHalo549i (red, 500 nM) to label any free HaloTags and Hoechst-33342 (blue, 10 μM) to label nuclei. EGFP (green) served as a transfection marker and for normalization purposes. Shown are representative images from each condition. Scale bar = 20 μm. (**B**) Quantification of competition labeling. Bar graph shows the ratio of the jFHalo549i fluorescence intensity relative to the EGFP fluorescence.*

Next, we assessed whether treatment of **hOCT-PEA4** impacted INS-1 cell viability (**Figure 3.7**). We incubated INS-1 cells overnight with intact **hOCT-PEA4** or probe that had been uncaged by 365 nm LED light, then subjected them to 3-(4,5-dimethylthiazol-2-yl)-2,5-diphenyltetrazolium bromide (MTT assay). We did not detect any cytotoxic effects from the intact or uncaged **hOCT-PEA4** probe at concentrations up 40 μM, which is near the solubility limit of the probe. As a positive control, we applied KCl, which killed the INS-1 cells in a dose-

dependent manner. This result demonstrates that **hOCT-PEA4** is not cytotoxic to β-cells, even during long incubations.

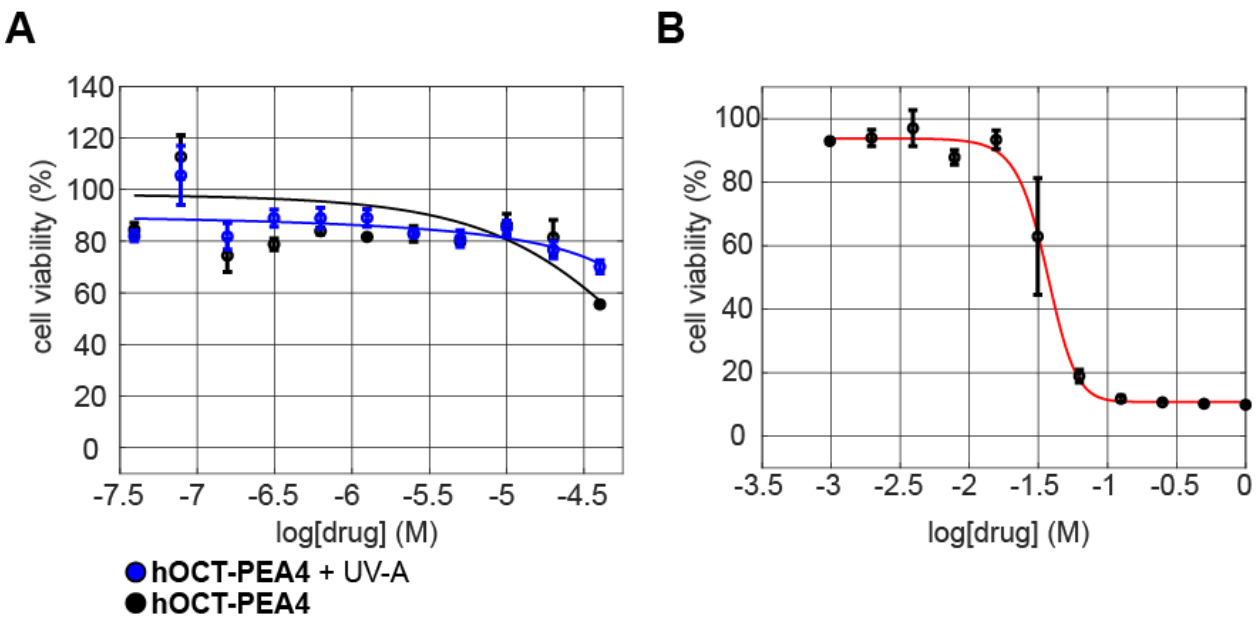


*Figure 3.7. Evaluating prolonged **hOCT-PEA4** treatment on INS-1 cell viability. (**A**) INS-1 cells were incubated with intact or UV-A-uncaged **hOCT-PEA4** for 24 h, then evaluated by the 3-(4,5-dimethylthiazol-2-yl)-2,5-diphenyltetrazolium bromide (MTT) assay. INS-1 cell viability was stable when the cells were incubated with **hOCT-PEA4** (caged, black), UV-A irradiated **hOCT-PEA4** (uncaged, blue) up to 40 μM, near its solubility limit in physiological buffer. (**B**) As a positive control for the viability assay in **A**, INS-1 cells were incubated with KCl for 24 h. Four biological replicates were performed for each condition. Error bars = mean ± S.E.M.*

### 3.2.3. Plasma membrane uncaging of hOCT-PEA4 in INS-1 cells

To assess the impact of **hOCT-PEA4** uncaging on β-cell $Ca^{2+}$ signaling, we co-transfected INS-1 cells with cDNA encoding pDisplayHalo-EGFP and RGECO[68], which allows intracellular $Ca^{2+}$ levels to be monitored in real-time. Cells were preincubated with **hOCT-PEA4**, washed, and then evaluated via confocal microscopy (**Figure 3.8 A**). Relative to vehicle, uncaging **hOCT-**

**PEA4** increased the number of $Ca^{2+}$ oscillations after 375 nm stimulation relative to baseline (**Figure 3.8 B**). When a GPR55 inhibitor (CID160020046, 5 μM) was present in the bath, the $Ca^{2+}$ stimulation caused by uncaging **hOCT-PEA4** was not significantly reduced (**Figure 3.8 B**). To evaluate the impact of untethered **hOCT-PEA4** that had accumulated in the cells, we used the control pDisplayHalo7$^{D107A}$-EGFP plasmid with an inactive HaloTag that cannot tether our probe (**Figure 3.8 B**). INS-1 cells transfected with the mutant plasmid had a reduced probe effect on $Ca^{2+}$ stimulation relative to the standard conditions, demonstrating the importance of probe tethering to the cell surface. Together, these data show that **hOCT-PEA4** stimulates $Ca^{2+}$ in INS-1 cells partially through GPR55 and requires HaloTag expression and compound tethering. This result sets the stage for application of **hOCT-PEA4** in more complex biological settings, such as intact human islets.

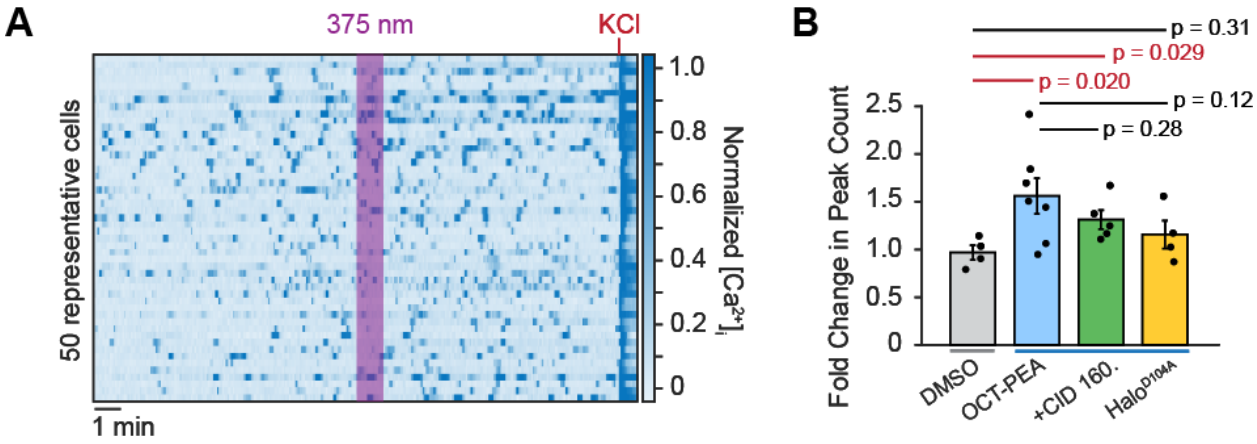


*Figure 3.8. Uncaging **hOCT-PEA4** on the INS-1 cell surface.*
*(**A**) Heat map showing $Ca^{2+}$ traces from 50 individual INS-1 cells co-transfected with RGECO and pDisplayHalo-EGFP and preincubated with **hOCT-PEA4** (2 μM, 1 h). Each video included a baseline recording, irradiation with 375 nm (60 s), and a positive control addition (25 mM KCl) for data normalization. (**B**) Comparison bar graph showing the fold change in the number of $Ca^{2+}$ oscillations counted after 375 nm irradiation relative to baseline. Uncaging **hOCT-PEA4** (blue, N = 199, T= 7) led to an increased fold change relative to vehicle (grey, N = 114, T = 4). Uncaging in the presence of CID16020046 (green, N = 148, T = 5) and in INS-1 cells*

*transfected with pDisplayHalo$^{D107A}$-EGFP (yellow, N = 90, T = 4) reduced the probe's fold change effect on $Ca^{2+}$. Each dot represents the average data from a video, T. Error bars = mean ± SEM.*

### 3.2.4. Endocannabinoids mediate $Ca^{2+}$ and insulin release in intact human islets

Before applying our tools to islets, we wanted to evaluate how modulating the ECS tone affected [$Ca^{2+}$] and insulin secretion in human islets. To assess the health and glucose-responsiveness of different human islet batches, we transduced islets with AdV-RIP-GCaMP6s, an adenovirus that expressed the cytosolic $Ca^{2+}$ indicator GCaMP6s. The virus has a rat insulin promoter (RIP) that drives GCaMP6s expression in β-cells. The islets were then exposed to increasing glucose concentrations (2, 11, and 20 mM) and glucose-stimulated $Ca^{2+}$ oscillations were monitored by confocal microscopy. (**Figure 3.9**). We observed increased $Ca^{2+}$ oscillations at the 11 mM and 20 mM glucose conditions, relative to 2 mM, confirming the glucose-sensitivity and health of our islet cultures.

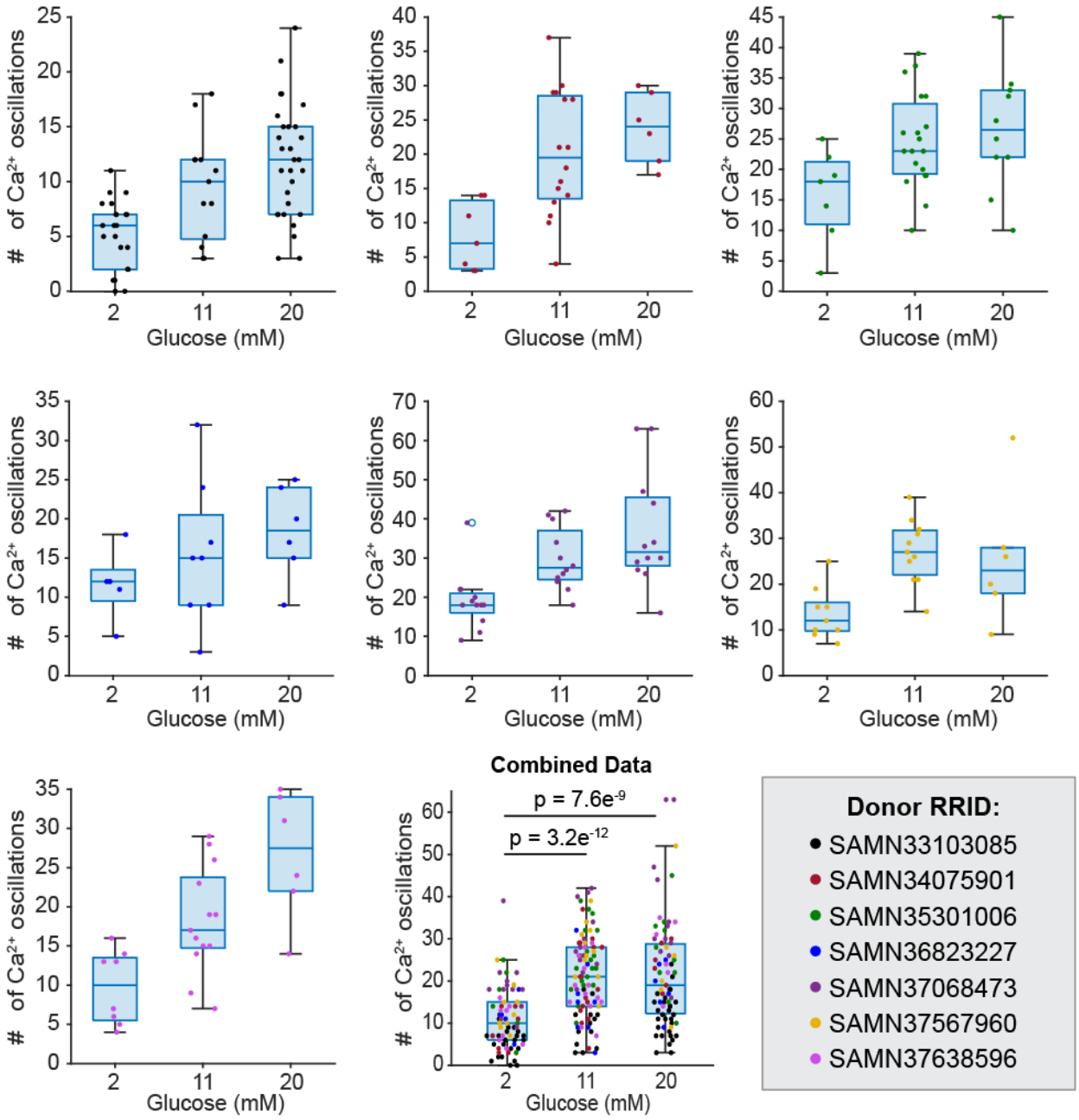


*Figure 3.9. $Ca^{2+}$ imaging to evaluate glucose sensitivity across donors.*
*Human islets were transduced with AdV-RIP-GCaMP6s, which expresses a green $Ca^{2+}$ sensor in $\beta$-cells. Comparison bar graph showing the number of $Ca^{2+}$ events detected at increasing glucose concentrations (2 mM, 11 mM and 20 mM). Data is separated by donor, and combined in a summary graph.*

Next, we treated islets with inhibitors for enzymes responsible for NAE biosynthesis and degradation—*N*-acylphosphatidylethanolamine phospholipase D (NAPE-PLD) inhibitor LEI401, and N-acylethanolamine acid amidase (NAAA, degradation) inhibitor ARN726. NAPE-PLD is responsible for the biosynthesis of a variety of NAEs[80], whereas NAAA preferentially degrades PEA[81]. In both cases, we observed fewer $Ca^{2+}$ oscillations at 11 mM glucose compared to no drug (**Figure 3.10 A**), suggesting that endogenous NAE metabolism plays a role in mediating human islet $Ca^{2+}$-handling. We also evaluated the impact of the NAE signaling on insulin release from human islets in two donors (**Figure 3.10 B**). Under high glucose (11 mM) conditions, islets treated with PEA (10 μM) or a NAPE-PLD inhibitor (LEI401, 10 μM) significantly stimulated insulin secretion relative to vehicle. Exendin-4 (100 nM)—which activates glucagon-like peptide-1 receptor, a known stimulator of GSIS[82]—was used as a positive control but did not significantly stimulate insulin release (p value = 0.0596). However, insulin stimulation from exendin-4 treatment was trending towards significance. Further, treatment with a GPR55 inhibitor CID16020046 (10 μM) did not affect insulin secretion under high glucose conditions.

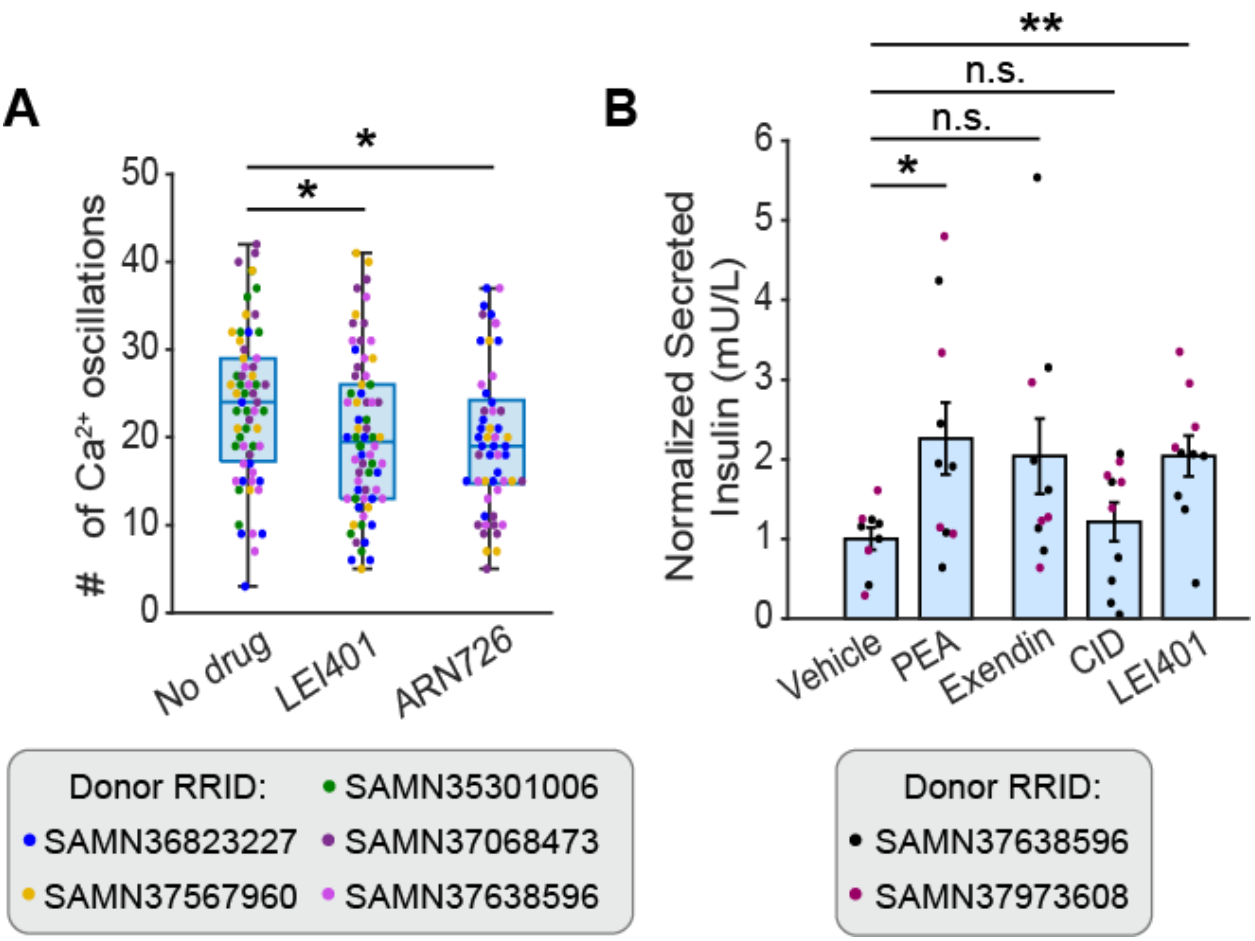


*Figure 3.10. Evaluating ECS tone in human islets.*

*(**A**) Comparison bar graph showing the number of $Ca^{2+}$ events detected in GCaMP6s-expressing human islets in response to a NAPE-PLD inhibitor (LEI401, 5 $\mu$M) and NAAA inhibitor (ARN 726, 5 $\mu$M). Data collected from 5 donors. (**B**) Comparison bar graph showing the normalized secreted insulin (mU/L) from human islets in response to vehicle (0.1% v/v DMSO), PEA (10 $\mu$M), exendin-4 (100 nM), CID16020046 (10 $\mu$M) and NAPE-PLD inhibitor (LEI401, 10 $\mu$M). Data collected from 2 donors. Significance threshold placed at *P<0.05, **P<0.01, ns = P>0.05.*

### 3.2.5. HaloTag AAV virus and targeted hOCT-PEA4 uncaging in islets

To illuminate the role of NAE signaling in the context of human β-cell function, we sought to apply the OCT-ligand approach to uncage NAEs in intact human islets. Because our current approach relied on HaloTag cDNA transfection, we generated a HaloTag AAV for transducing

human β-cells, coined AAV-INSx2-pDisplay-Halo (AAV-Halo). This AAV is built on previous AAV technology that allowed for the expression of transgenes in human β-cells without leaky α-cell expression[83] (**Figure 3.11**, top). We also generated the control catalytically inactive Halo-tag AAV (AAV-Halo$^{D107A}$), which maintains pDisplay surface HaloTag expression in β-cells but cannot label the chloroalkane biorthogonal motif (**Figure 3.11**, bottom).

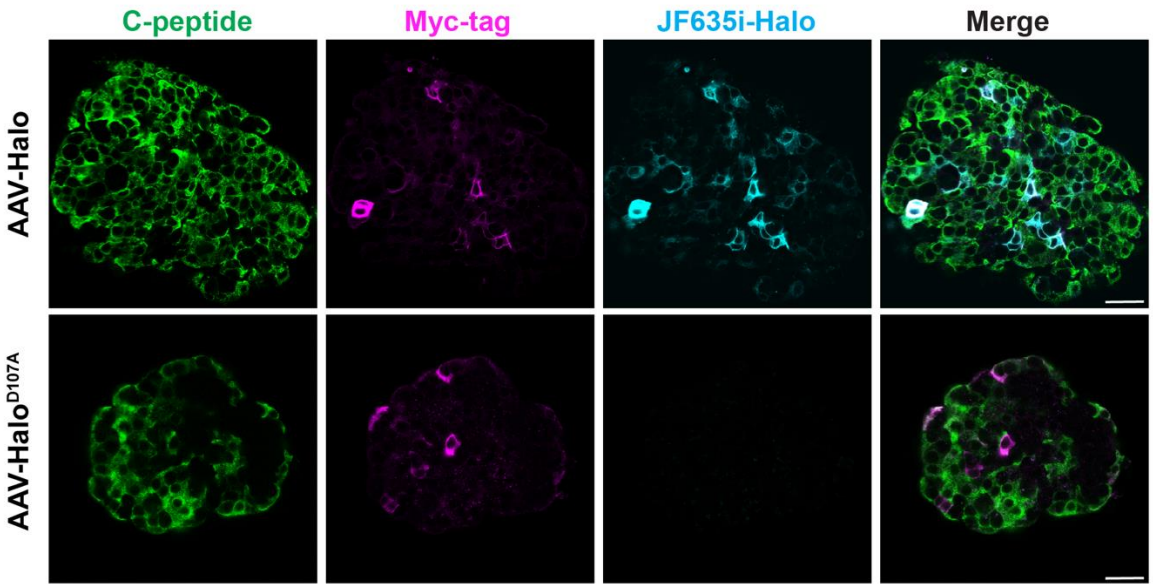


*Figure 3.11. Expression of AAV-Halo and AAV-Halo$^{D107A}$ in human islets.*
*Human islets were transduced with either AAV-Halo or AAV-Halo$^{D107A}$, stained with JF635i-HaloTag (2 μM, 1 h, cyan), fixed, and then probed for C-peptide (green) and Myc-tag (magenta). The D107A mutation prevents the HaloTag from labeling the HaloTag dye. Islets transduced with AAV-Halo have β-cells (marked by C-peptide) that have Myc and HaloTag staining (**top**). In contrast, islets transduced with AAV-Halo$^{D107A}$ have Myc staining in C-peptide positive cells, but lacks HaloTag staining (**bottom**). Scale bar 30 μm.*

With improved OCT-ligands and AAV-Halo in hand, we are now in position to interrogate the effects of PEA on human islets. We combined **hOCT-PEA4** and AAV-Halo to assess the impact of PEA release on β-cell $Ca^{2+}$ dynamics in intact human islets. We were unable to use the GCaMP6s sensor for uncaging experiments due to a photoswitching artefact induced by 375

nm irradiation (data not shown). Instead, live human islets were transduced with AAV-Halo alongside a β-cell-specific adenovirus to express jRGECO1a (AdV-RIP-jRGECO1a), a red-shifted $Ca^{2+}$ sensor. We observed robust jRGECO1a expression across the islet, which overlapped with HaloTag labeling and C-peptide staining in immunohistochemistry experiments (**Figure 3.12 A**). Together, these viruses allowed us to target OCT-ligands to β-cells and record the complimentary $Ca^{2+}$ event. To confirm that **hOCT-PEA4** was able to label HaloTags expressed on human islet β-cells, we performed a competitive labeling assay between **hOCT-PEA4** and Halo-JF635i dye. Islets that were pre-incubated with vehicle prior to the JF635i-HaloTag showed robust HaloTag fluorescence on the β-cell membranes (**Figure 3.12 B**, top); however, pre-incubation with **hOCT-PEA4** (5 μM, 90 min) blocked the HaloTag dye labeling (**Figure 3.12 B**, bottom). This result confirms that our probe successfully tethered the HaloTags in the islets.

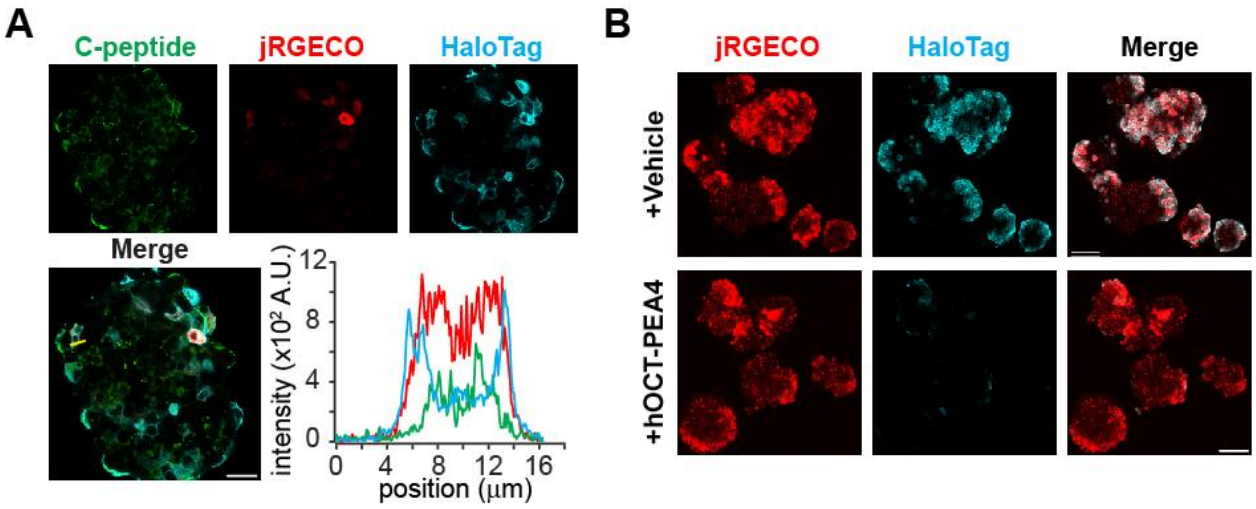


*Figure 3.12. Targeting β-cells in intact human islets.*
*(**A**) Immnofluorescent staining of human islet transduced with AAV-Halo (cyan) and jRGECO (red), and probed for C-peptide (green) to label β-cells. An intensity plot is shown across the white arrow in the merged image. (**B**) Competitive labeling of AAV-Halo transduced islets between **hOCT-PEA4** (5 μM, 90 min) and Halo-JF635i dye. Islets preincubated with **hOCT-PEA4**, had reduced jFHalo-635i dye fluorescence relative to vehicle (0.1% v/v DMSO).*

Finally, we monitored $Ca^{2+}$ dynamics in β-cells in intact islets stimulated with 11 mM glucose. Islets co-transduced with jRGECO1a and AAV-Halo were preincubated with **hOCT-PEA4**. Uncaging **hOCT-PEA4** on β-cells caused an increase in the number of $Ca^{2+}$ oscillations relative to vehicle (**Figure 3.13 A**,**B**). In cells pre-treated with vehicle only, no increase was observed, confirming that this $Ca^{2+}$ increase was not an artefact caused by the UV-A irradiation. This result demonstrates that PEA uncaging on β-cells increases human islet $Ca^{2+}$ oscillations; and more generally, demonstrates the suitability of our technology to target endocannabinoid signaling on human β-cells. Interestingly, uncaging **hOCT-PEA4** with GPR55 inhibitor CID16020046 in the bath during imaging also caused an increase in $Ca^{2+}$ oscillations, suggesting that **hOCT-PEA4** is stimulating $Ca^{2+}$ in islets in a GPR55-independent mechanism.

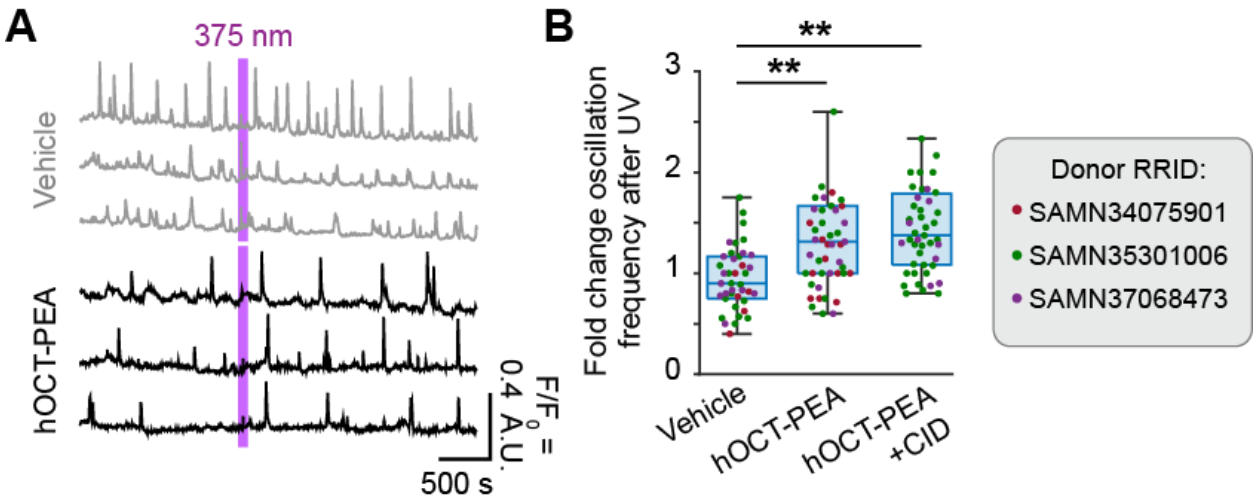


*Figure 3.13. Uncaging hOCT-PEA4 on β-cells in human islets.*
*(**A**) Three representative jRGECO $Ca^{2+}$ traces of islets treated with vehicle (0.1% v/v DMSO) or **hOCT-PEA4** (5 μM, 90 min). 375 nm irradiation is indicated by the purple bar. (**B**) Comparison bar graph showing fold change in $Ca^{2+}$ oscillation counts after 375 nm stimulation relative to baseline. Uncaging **hOCT-PEA4** (5 μM, 90 min, N = 48) on cells lead to a higher fold change in $Ca^{2+}$ events relative to vehicle (0.1% v/v DMSO, N = 42) across three donors. Treatment with the GPR55 inhibitor (CID16020046, N = 47) did not reduce $Ca^{2+}$ stimulation from uncaging **hOCT-PEA4**. Significance threshold placed at *P<0.05, **P<0.01, ns = P>0.05.*

## 3.3. Discussion

This study presents a new set of tools to study endocannabinoid signaling in intact human pancreatic islets. Building on our previous OCT-ligand technology that tethered SNAP-tags, we synthesized new **hOCT-PEA** derivatives that label HaloTags, and identified **hOCT-PEA4** to have improved labeling efficiency and solubility compared to the original probe. Using fluorescent $Ca^{2+}$ imaging and insulin assays, we showed that human islets have an endogenous cannabinoid tone which mediates $Ca^{2+}$ dynamics, and that PEA triggers insulin release in human islets. Interestingly, treatment with the NAPE-PLD inhibitor LEI401 decreased $Ca^{2+}$ oscillations, yet stimulated insulin release. NAPE-PLD is responsible for the biosynthesis of multiple NAE species[80,84], which could explain this discrepancy. Also, the $Ca^{2+}$ oscillations following LEI401 treatment were recorded in five different donors, whereas insulin release in response to LEI401 was evaluated in two donors. Further characterization of LEI401's mechanism of action in islets is warranted and more repeats of the insulin ELISA data are needed. Finally, using novel AAV-Halo virus to enrich our probes at the β-cell surface, photorelease of **hOCT-PEA4** allowed for activation of endogenous receptors in human islets in a GPR55-independent manner. To finalize this dataset, uncaging **hOCT-PEA4** in human islets transduced with jRGECO1a and AAV-Halo$^{D107A}$ is needed to assess the contribution of untethered probe on $Ca^{2+}$ dynamics.

A key advance in our technology is the development of a novel AAV to express HaloTags on the surface of human β-cells, and we demonstrated that these transduce intact human islets tissue. Because we are transducing intact islets, we do observe more efficient HaloTag expression on the outer surface of the islet. While this peripheral expression may be limiting for some experiments, it did not prevent the application or tethering of our probes. If future applications require HaloTag-expression on the inner core of the islet, a pseudoislet prep could be utilized, where the islets are dissociated and transduced, then reconstituted[85]. While the

OCT-ligand approach has thus far only been applied to release PEA, the platform is versatile and will allow us to target other compatible probes using the same virus. Our future efforts will include developing OCT-ligands with different endocannabinoids of interest. For example, an OCT-ligand to release anandamide (**Chapter 4**) could target $G_i$-coupled CB1 and TRP channels[3], which would allow us to probe other NAE signaling pathways. Notably, our approach is not limited to endocannabinoids, and our future synthetic efforts will extend to other ligands such as synthetic agonists, neurotransmitters, and small peptides.

One consideration for using our OCT-ligands is that they require UV-A light for activation. For imaging applications, the use of UV-A light is advantageous because it allows them to be used with blue-green fluorescent biosensors. However, we acknowledge that UV-A light can be damaging to cells and tissues when applied for extended periods of time. In future studies, we intend to modify the nitrobenzyl photocage to leverage red-shifted photocages. These modifications will allow photorelease with lower energy irradiation, which penetrates deeper in tissue and is less phototoxic. Such a development will be advantageous for more complex biological settings, such as *in vivo*, where longer-irradiation light could be applied through the skin.

Our current approach leverages a novel AAV-Halo to target β-cells specifically in human islets. We can also modify the promotor sequences of this virus to target alternative islet cell types, such as α-cells. The role of endocannabinoid signaling in α-cells is not described, thus such developments may be important to discover endocannabinoid regulation of α-cell physiology. Additionally, we can use our hOCT-PEA ligands to investigate NAE signaling in other organ systems, such as the brain, where endocannabinoid signaling is abundant, yet still poorly characterized, especially for more exotic NAEs or endocannabinoids with different lipid tails. While we primarily used HaloTags in this study, using AAV-SNAP would allow us to use existing photopharmacological tools, such as PORTL-ligands[57], in human islets.

In summary, this work presents the first application of cell-targeted, photopharmacology in intact human islets. The OCT-ligand approach enables evaluation of endogenous signaling pathways, while the Halo-AAV allows for cell-specific targeting in heterogeneous tissue. Moving forward, these tools offer the potential to increase the sophistication of our experimental design and test the impact of NAE signaling in native tissue environments.

## 3.4. Methods

### 3.4.1. General synthetic methods

Unless otherwise noted, all chemicals were purchased from TCI Chemicals, Fisher Scientific, Sigma-Aldrich, or Acros Organics, and were used without further purification. Dry solvents were purchased as “extra dry” or “anhydrous” and used without further purification. Reactions and chromatography were monitored by analytical thin layer chromatography (TLC) on Merck silica gel 60 $F_{254}$ glass plates. The plates were first visualized under 254 nm UV light, followed by staining with $KMnO_4$ solution or cerium (IV) molybdate solution (Hanessian’s stain) and gentle heating with a heat gun. Flash column chromatography was performed using silica gel (ACROS Organics™ 240360300, 0.035-0.070 mm, 60 A) or a Buchi Pure chromatography system. Nuclear magnetic resonance (NMR) spectra were acquired on a BRUKER 400 MHz instrument. Chemical shifts ($\delta$) are reported in ppm and referenced to residual non-deuterated solvent peaks ($^{1}H/^{13}C$): $MeOD_4$ (3.31/49.00), and $CDCl_3$ (7.26/77.16). Multiplicities are abbreviated as: s = singlet, d = doublet, t = triplet, q = quartet, br = broad, m = multiplet. Data in $^{13}C$ is reported as E/Z isomer, where assignment of isomers are separated by a slash ( / ), and each peak assignment is separated by a semicolon. Separate atom peaks that are merged under one large peak (*i.e.,* acyl PEA chain, PEG linker) are separated by a comma.

High-resolution (35,000) mass spectrometry data were acquired at Portland State University’s BioAnalytical Mass Spectra Facility. Data were acquired on a vanquish UHPLC/HPLC system coupled to a Q-Exactive MS equipped with an electrospray ionization source operating in the positive mode.

### 3.4.2. UV-Vis spectroscopy

Compounds were diluted to 40 $\mu$M in DMSO and placed in a 1 ml Quartz cuvette (10 mm light path). A deuterium-halogen light source (Ocean Optics, DH-2000) transmitted light through the

sample, which was collected by a Flame UV-Vis-ES spectrophotometer (FLMT05021, Ocean Insight) using OceanView (Version 2.0.7) Software. Uncaging was achieved using 365 nm (Thorlabs M365FP1), 415 nm (Thorlabs M415F3), 470 nm (Thorlabs M470F4) and 565 nm (M565F3) fiber-coupled LEDs guided through a fiber-optic cable (Thorlabs #FP400URT, 400 μm diameter, 0.50 numerical aperture) and optical cannula (400 μm, Thorlabs). LED power was quantified by a power meter (Thorlabs, PM100D) with its photodiode power sensor (Thorlabs, S120VC) positioned directly at the fiber tip. The cannula tip was pointed directly into the top of the sample.

### 3.4.3. Cell Culture media and solutions

**INS-1 media** contains: RPMI 1640 with L-glutamine (Gibco, #11875-093) with 10% FBS, Penicillin-strep (1:100) and (in mM) 10 HEPES (Fisher, #BP310-500), 1 sodium pyruvate (Alfa Aesar, #A11148). INS-1 media was filtered and distributed into 50 ml aliquots. 50 μM 2-mercaptoethanol (BME, Sigma, #M3148) was added fresh to each 50 ml aliquot prior to use.

**INS-1 imaging buffer** contains (in mM): 185 NaCl, 1.2 $CaCl_2$, 1.2 $MgCl_2$, 1.2 $K_2HPO_4$, 20 HEPES. Adjusted to pH 7.4 with NaOH. D-glucose was supplemented at 5, 11 or 20 mM.

**INS-1 permeabilization buffer** contains: Phosphate buffered saline (PBS, Gibco, #70013-032) with 5 vol% donkey serum, and 0.3 vol% triton X-100 (Fisher, #BP151-100).

**INS-1 blocking buffer** contains: Phosphate buffered saline (PBS, Gibco, #70013-032) with 5 vol% donkey serum, and 0.1 vol% triton X-100 (Fisher, #BP151-100).

**Islet culture media** contains: RPMI 1640 with L-glutamine (Gibco, #11875-093) with 15 vol% FBS, Penicillin-strep (1:100)

**Islet imaging buffer** contains (in mM): 119 NaCl, 4.7 KCl, 1.0 $CaCl_2$, 1.5 $MgSO_4$, 1.2 $K_2HPO_4$, 10 HEPES. Adjusted to pH 7.35 with NaOH. Glucose was supplemented at 2, 11 or 20 mM.

**Islet blocking buffer** contains 0.3 vol% triton X-100 (Fisher, #BP151-100), 0.1 vol% BSA, 2 vol% donkey serum, phosphate buffer saline (PBS, Gibco, #70013-032)

**HEK culture (D10) media** contains high glucose DMEM (Gibco, #11965-092), 10 vol% FBS (HyClone's USDA tested, #SH30910), 0.5 vol% Penicillin-strep (Gibco, #15070). Sterile filtered and aliquoted.

**Phosphate buffer** contains (in mM): 320 $Na_2HPO_4$ (Fisher, #BP332-500), 80 $Na(PO_4H_2)•H_2O$ (Fisher, #S369-1). Adjusted pH to 7.4 with NaOH.

**4% PFA:** paraformaldehyde (2 g, Sigma-Aldrich, #158127), 0.2 M phosphate buffer (25 ml), deionized $H_2O$ (25 ml). Adjusted pH to 7.4. Kept on ice until use.

### 3.4.4. Cell Culture

INS-1 832/13 (INS-1) cells[66] were grown in INS-1 media and incubated at 37 °C and 5% $CO_2$. Cells were used between passages 65-80. For live-cell $Ca^{2+}$ imaging, INS-1 cells were plated at a density of 150,000 cells per well on 8-well glass bottom chambered coverslips (Ibidi, #0827-90). 18-24 h later, cells were starved in Opti-MEM™ (250 μl) for 2 h before adding the transfection mixture containing (20 μl per well): 1 μl Lipofectamine-2000 (Fisher Scientific, #11668019), 75 ng R-GECO + 225 ng pDisplay-Halo- EGFP, or 75 ng R-GECO + 225 ng pDisplay-Halo7$^{D107A}$-EGFP in Opti-MEM™. The cells were then incubated at 37 °C and 5% $CO_2$ for 18-24 h before exchanging the transfection mixture with INS-1 media. Microscopy experiments were performed 60-72 h post-transfection.

Human pancreatic islets from non-diabetic donors were received from the Integrated Islet Distribution Program (IIDP) funded by the National Institute of Diabetes and Digestive and Kidney Disease (NIDDK). Islets were cultured in islet culture media in non-surface treated 24-well suspension plates (VWR® #10861-558), or non-surface treated 10 cm culture dishes (Falcon® #351029) at 37 °C and 5% $CO_2$ for up to two weeks after receiving the shipment.

Islets were transduced by mixing AAV-Halo only in 200 μl islet culture media in a 15 ml conical centrifuge tube set at ~10° angle for 1 h at 4 °C on an orbital shaker. They were then transferred to 24-well suspension plates or 10 cm culture dishes and cultured for 4 days at 37 °C and 5% $CO_2$ before experiments. For GCaMP6s and jRGECO1a transductions, the islets were placed in a 24-well plate in 2 ml islet media, then 1 μl concentrated AdV solution was added directly to the media of the wells and cultured for 4 days before experiments.

### 3.4.5. INS-1 Competition Labeling Assay

For the **hOCT-PEA** competition labeling assay, a transfection mixture containing (50 μl per well) 1 μl Lipofectamine-2000 and 150 ng pDisplay-Halo-EGFP in Optim-MEM™ was added to acid-etched glass coverslips (12 mm, #1.5) in a 24-well plate. INS-1 cells were then plated at a density of 150,000 cells per well on top of the transfection mixture, and Opti-MEM™ was added to a final volume of 0.5 ml. The cells were then incubated at 37 °C and 5% $CO_2$ for 18-24 h before exchanging the media with fresh INS-1 media. 60-72 h post transfection, the cells were labeled with vehicle or OCT-ligand (100 nM – 8 μM) in INS-1 media (without BME) for 1 h. The cells were washed once with INS-1 media (without BME), then labelled with a dye mixture containing jFHalo549i (500 nM) and Hoechst-33342 (10 μM) for 10 min. The coverslips were washed with cold PBS, fixed in 4% PFA for 5 min at RT, and washed 3× in PBS. The coverslips were mounted on a microscope slide (VWR® Superfrost® Plus Micro Slide, 75×25×1 mm, #48311-703) with mounting solution (Fluoromount™) and sealed with nail polish. Imaging parameters are described below in the “Fixed cell microscopy” section.

Two images per coverslip were acquired with a 20× objective at 1024×1024 pixel resolution for quantification, and one representative image was acquired with a 63× oil objective at 2048×2048 pixel resolution. For quantification, intensity from regions-of-interest drawn using the Fiji software[76] around each EGFP+ cell across 4 images from two biological replicates, and

the intensities from the green and red channels were exported to be analyzed with MATLAB scripts written in-house.

### 3.4.6. rAAV production and purification

We produced and purified the rAAV's using the *Easy AAV production* as previously described[83]. After cloning pDisplay-HaloTag into their AAV vector and verifying insert size from restriction digest and sequencing, we grew and maintained HEK293 cells for two passages before plating them in 10-cm culture dishes in HEK culture media to achieve 90% confluency the following day. For each plate, the media was replaced with 6.5 ml modified HEK culture media featuring DMEM + L-glutamine, 2% FBS, and no antibiotics. 6 μg of each AAV plasmid (AAV-INSx2-pDisplay-HaloTag-3MRE's, pAd5 Adeno Helper, and pAAV-KP1 Rep-Cap[86]) were mixed in a 50 ml conical tube with 54 μl of 1 mg/ml polyethylenemine (PEI, Polysciences MW 2500). 3.5 ml of OptiMEM was added before vigorous mixing with a benchtop vortex mixer, followed by 20 min incubation at RT and addition to the HEK cells. The plates were cultured for 7 days at 37° C and 5% $CO_2$ prior to AAV harvest and purification. The AAV-containing culture media was collected from the plates and placed into a 250 ml conical tube, 2× centrifuged at 1800g for 30 min and then placed into a new conical tube. The filtrate was then passed through a 0.25 μm PES filter into a new 250 ml conical tube before 1 μl of benzonase was added. The tube was gently inverted 10× to mix the solutions. The conical tube was then incubated at 37° C and 5% $CO_2$ for 30 min, followed by centrifugation at 1800g for 30 min. The solution was again filtered through a 0.25 μm PES filter into a new 250 ml conical tube. The filtrate was then mixed with 5× PEG8000 / NaCl to achieve 1× concentration and inverted 50 times. The mixture was stored at 4 °C overnight to precipitate the viral particles. The mixture was again centrifuged at 5000g at 4° C for 1 h before the supernatant was carefully removed. The viral pellet was resuspended in 500 μl PBS and placed on an orbital shaker overnight at 4° C. The virus / PBS mixture was collected

into 1.5 ml tubes and centrifuged at 5000 rpm for 4 min at RT. The viral lysate was then collected and transferred into a new 1.5 ml tube, then aliquoted into 0.5 ml tubes. The viral aliquots were quickly frozen on dry ice, and stored in -80° C for future use.

### 3.4.7. Immunofluorescence staining in cultured β-cells and islets

INS-1 cells were plated on acid-etched glass coverslips (12 mm, #1.5) at a density of 100,000 cells per well in a 24-well plate (Fisherbrand, #FB012929), and transfected as noted in the INS-1 Cell Culture section. The cells were labelled with a dye mixture including jFHalo549i (500 nM) and Hoechst-33342 (10 μM) for 10 min. The coverslips were washed with cold PBS, fixed in ice-cold 4% PFA for 5 min at RT and washed 2× with PBS (5 min). The fixed cells were then incubated in the blocking buffer for 1 h. The cells were then incubated in 1° Myc-tag Mouse mAB antibody (1:8000, Cell Signaling Technology, cat #2276, lot 24) diluted in INS-1 blocking buffer and shook overnight (12-14 h, 4 °C) in the dark. The coverslips were then washed 3× with PBS (5 min, RT), then incubated with 2° donkey anti-mouse Alexa Fluore™647 solution (1:750), diluted in INS-1 blocking buffer for 1 h in the dark shaking at RT. The coverslips were washed 3× with PBS (5 min) and then washed 2× with deionized $H_2O$ (5 min). The coverslips were mounted on a microscope slide (VWR® Superfrost® Plus Micro Slide, 75×25×1 mm, #48311-703) with mounting solution (Fluoromount™) and sealed using nail polish. The slides were kept in the dark until imaging within one week.

Live human islets were transduced with AAV-Halo, then labelled with either JF635i-HaloTag dye at 2 μM for 2 h in islet culture media. The labelled islets were transferred into 1.5 ml tubes and centrifuged at 2000 rpm for 1 min. The media was removed and PBS was added, followed by centrifugation at 2000 rpm for 1 min at RT. The PBS was removed from the pellet, then 4% PFA was added and the islets were incubated at 4° C for 1 h on an orbital shaker. The islets were centrifuged at 2000 rpm for 1 min, and then the solution was removed before adding

islet blocking buffer. The islets were incubated at 4° C for 1 h on an orbital shaker, and then centrifuged at 2000 rpm for 1 min. The buffer was aspirated before co-application of rat monoclonal anti-C-peptide antibody (GN-ID4,DSHB; 1:100 dilution) and mouse anti-Myc-tag mAB antibody (1:1000, Cell Signaling Technology, cat #2276, lot 24) in islet blocking buffer at 4° C for 7 days on an orbital shaker. The islets were centrifuged at 2000 rpm for 1 min, then the primary antibody solution was removed, before washing with PBS, rotating on a benchtop nutator for 30 min at RT, and spun down at 2000 rpm for 1 min. The washing step was repeated 3×. The secondary antibodies were added to the islets; which included goat anti-rat Alexa Fluor 488 (Jackson ImmunoResearch; 1:750 dilution) and anti-Mouse Cy™3 AffiniPure Donkey IgG (H+L) (Jackson ImmunoResearch Laboratories, cat #715-165-151, lot #130991, 1:1000), antibodies in islet blocking buffer at 4° C for 1 week on an orbital shaker. The samples were again centrifuged at 2000 rpm for 1 min, and the antibody solution was removed before washing again with PBS, rotating on a benchtop nutator for 30 min at RT, and spun down at 2000 rpm for 1 min. The washing step was repeated again 3×. For mounting, the islets were spun down, the PBS was removed, and then the islets were resuspended in VectaShield (40 μl) and transferred to the center of a microscope slide (VWR® Superfrost® Plus Micro Slide, 75×25×1 mm, #48311-703). The edges were than sealed with clear nail polish and allowed to dry in the dark at RT for 1 h before imaging.

### 3.4.8. Live-cell confocal microscopy

Live cell and islet imaging was performed on an Olympus Fluoview 1200 laser scanning confocal microscope at 37 °C and 5% $CO_2$. Videos were acquired with a 20× objective, 512×512-pixel resolution, and scan rate of 4 s per frame. R-GECO and jRGECO1a excitation was performed with a 559 nm laser at low laser power (<6%) and emission was collected at 570-670 nm. EGFP and GCaMP6s excitation was performed with a 488 nm laser at low laser

power (<5%) and emission was collected at 500-545 nm. Photo-activation was performed with a 375 nm laser (PicoQuant, PDL 800-D, 100% laser power) triggered using the quench function in the Olympus software.

Control experiments involved incubation with CID16020046 (5 μM, 30 min, Tocris, #4959), LEI401 (5 μM, 30 min, Cayman Chemical, #31108), or ARN726 (5 μM, 30 min, Cayman Chemical, #24259), in imaging buffer.

For dye-labeling experiments in human islets, live human islets were labelled with JF635i-HaloTag dyes at 2 μM for 1 h in islet culture media at 37 °C and 5% $CO_2$. They were then washed with PBS and ~10 islets at a time were transferred into 8-well Ibidi glass bottom chambered coverslip (Ibidi, #0827-90) containing 250 μL of islet imaging buffer and equilibrated for 20 min before imaging.

For $Ca^{2+}$ imaging experiments in human islets, AdV-RIP-jRGECO1a or AdV-RIP-GCaMP6s-expressing islets were transferred to 8-well Ibidi glass bottom chambered coverslips (Ibidi, #0827-90) containing 300 μL of islet imaging buffer. 10-15 islets were added to each chamber, and the chamber was gently swirled to cluster the islets in the center of the chamber. The islets were placed on the microscope and allowed to equilibrate at 37 °C and 5% $CO_2$ for at least 25 min before imaging.

For $Ca^{2+}$ imaging experiments, regions-of-interest were manually drawn around oscillating cells that were EGFP+ (INS-1) or entire islets using the Fiji software, and the resulting data were analyzed with MATLAB scripts written in-house.

### 3.4.9. Fixed cell microscopy

Fixed samples were imaged on a Zeiss LSM880 confocal laser scanning microscope with Airyscan with a 40× oil objective or a 63× oil objective at 2048×2048 pixel resolution. Hoechst-33342 and DAPI excitation were performed with a 405 nm laser at low laser power (<1%).

Green fluorophores were excited with a 488 nm laser at low laser power (<2%). Red fluorophores were excited with a 550 nm laser at low laser power (<10%). Far-red fluorophores were excited with 647 nm laser at laser power (<15%).

### 3.4.10. MTT assay

INS-1 cells were plated in a 96-well plate (Corning #3596) with 50,000 cells/well in INS-1 media, and then were incubated for 48-72 h until they reached 70-80% confluence. To generate the uncaged probe, **hOCT-PEA4** (10 μl, 40 mM in DMSO) was irradiated for 5 min with a 365 nm LED. Next, intact **hOCT-PEA4**, or uncaged **hOCT-PEA4** were added to the wells in INS-1 media without BME, and the cells were incubated at 37 °C and 5% $CO_2$ for 24 h. The media was aspirated from the wells, and then the cells were washed in 100 μl PBS. 3-(4,5-Dimethyl-2-thiazolyl)-2,5-diphenyltetrazolium bromide (MTT, TCI Chemicals, #D0801) was added to the wells at 5 mg/ml and incubated at 37 °C and 5% $CO_2$ for 4 h. The media was gently removed, and then 100 μl DMSO was added to each well. The plate was incubated in the dark on an orbital shaker for 15 min at 100 rpm. Absorbance at 590 nm was recorded on a CLARIOstarPLUS plate reader (BMG Labtech, 0430), and the data were processed in Microsoft Excel and MATLAB.

### 3.4.11. Insulin ELISA assay

Each islet treatment was performed in triplicate or quadruplet per drug stimulation. For one treatment, 20 islets were handpicked and transferred to a 1.5 ml tube. The islets were centrifuged at 310 rcf for 4 min and the media was aspirated. The islets were preconditioned in INS-1 imaging buffer spiked with 5 mM glucose for 1 h at 37 °C and 5% $CO_2$. The islets were again spun at 310 rcf for 4 min, and the buffer was aspirated. The islets were then treated with INS-1 imaging buffer spiked with 11 mM glucose + drug (vehicle, 10 μM PEA, 100 nM Exendin-

4, 10 μM CID16020016, or 10 μM LEI401) for 30 min at 37 °C and 5% $CO_2$. The stimulated islets were centrifuged at 310 rcf for 4 min, then the supernatant was collected and evaluated via a human insulin ELISA assay (Mercodia 10-1113-01) per manufacturer instructions. Absorbance values at 450 nm were recorded using a CLARIOstarPLUS plate reader (BMG Labtech, 0430), and the data was processed using myAssays.com and MATLAB.

### 3.4.12. Data analysis and code availability

Unless otherwise described, all data are presented as mean ± S.E.M, which was calculated as:

$$\mathrm{S.E.M.} = \frac{\text{standard deviation}}{\sqrt{\mathrm{N}}}$$

For $Ca^{2+}$ imaging experiments, N is the total number of cells (technical replicates), and T is the number of independent experiments (biological replicates). Oscillations were calculated in MATLAB using the 'findpeaks' function with a y threshold of 0.5 for RGECO (INS-1 data), a y threshold of 0.2 for jRGECO1a (islet data), and a y threshold of 0.1 for GCamP6s (islet data). For RGECO and jRGECO1a data, the total number of oscillations across the field of view was counted from the beginning of the video to UV-A irradiation. Separately, the total number of oscillations were counted over an equivalent time post-stimulation. The sum of the peaks was normalized against the number of cells per video (to quantify "oscillations per cell" for each trial and condition), and then the mean fold change for post/pre-stimulation was calculated alongside the S.E.M. For GCamP6s data, the total number of oscillations across the entire video was counted.

Statistical significance was assessed using MATLAB (Mathworks) and Excel (Microsoft). For the comparison between two groups in oscillation frequency analysis, a Welch's two-sample t-test was used, with significance threshold placed at *P<0.05, **P<0.01, ns = P>0.05.

## 3.5. Detailed synthetic methods

**A**

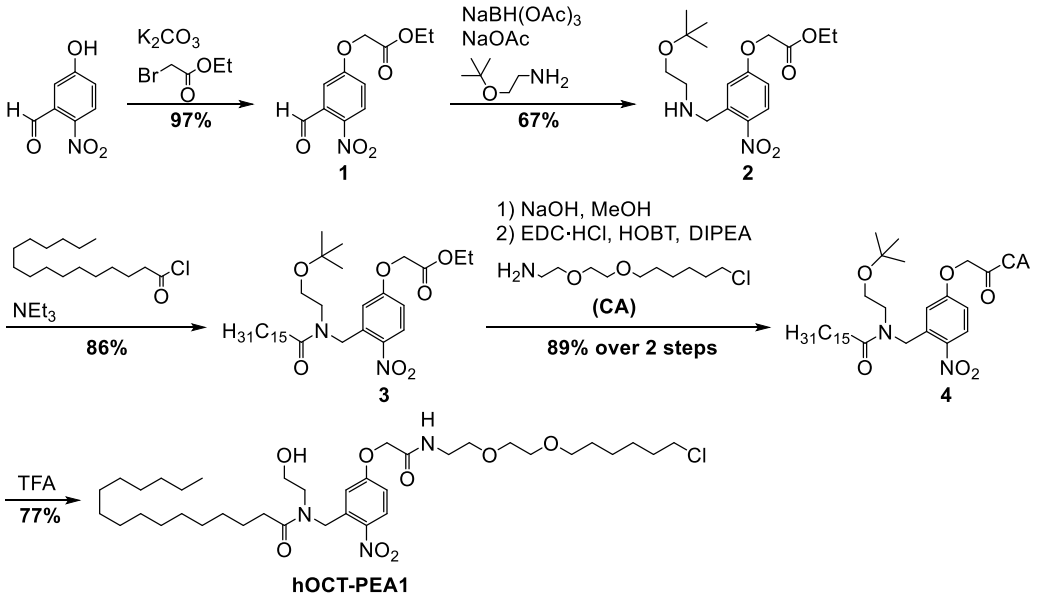


**B**

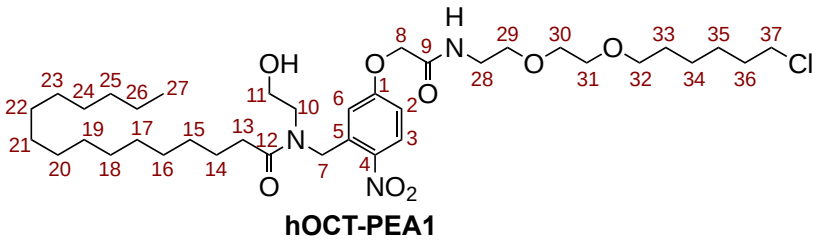


*Figure 3.14. Synthetic scheme of **hOCT-PEA1**.*

*(**A**) Synthesis of **hOCT-PEA1**, which was prepared from in 6 steps and 38% overall yield. (**B**) NMR atom numbering assignment for **hOCT-PEA1**.*

### 3.5.1. Synthesis of *N*-(2-(*tert*-butoxy)ethyl)-*N*-(5-(2-((2-(2-((6-chlorohexyl)oxy) ethoxy)ethyl) amino)-2-oxoethoxy)-2-nitrobenzyl)palmitamide (4)

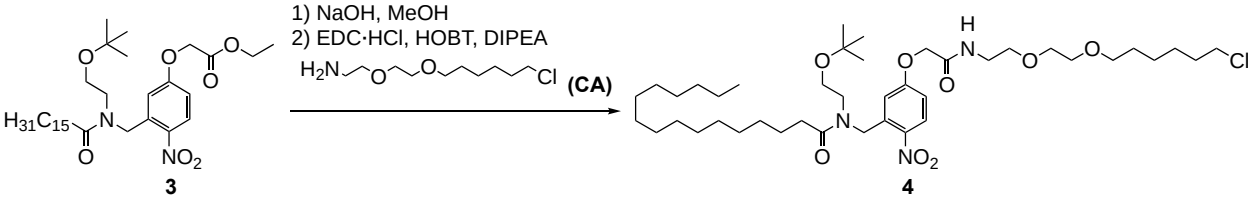


***N*-(*2-tert*-butoxyethyl)-*N*-(5-ethoxycarbonylmethoxy-2-nitrobenzyl)palmitoylamide** (3) was prepared as described in Chapter 2[59] (section **2.5.3**). **2-(2-(Chloromethoxy)ethoxy)ethan-1-amine** (CA) was prepared as described by Liu, Q et al[87].

Compound **3** (38 mg, 0.064 mmol, 1.0 equiv.) was dissolved in MeOH (0.7 ml), and then aqueous NaOH (1 M, 0.13 ml, 0.13 mmol, 2.0 equiv.) was added dropwise over 90 s. The reaction continued for 30 min before the reaction was diluted in MeOH (0.5 ml), and then aqueous HCl (1 M, 0.12 ml, 0.12 mmol, 1.9 equiv.) was added until the mixture was at pH = 7.0. The reaction was diluted in EtOAc (0.5 ml), and the organic layer was 2× extracted with $H_2O$ (2 × 0.3 ml). The organic layer was washed once with saturated brine and dried over anhydrous $MgSO_4$. The crude mixture was filtered, and the solvent was removed *in vacuo*. The crude **2-(3-((*N*-(2-(*tert*-butoxy)ethyl)palmitamido)methyl)-4-nitrophenoxy) acetic acid** (31 mg, 0.055 mmol) was used directly in the next reaction without further purification.

1-hydroxybenzotriazole (HOBt, 10. mg, 0.074 mmol, 1.4 equiv.) and 1-(3-dimethylaminopropyl)-3-ethylcarbodiimide hydrochloride (EDC·HCl, 14 mg, 0.074 mmol, 1.4 equiv.) were added to **2-(3-((*N*-(2-(*tert*-butoxy)ethyl)palmitamido)methyl)-4-nitrophenoxy) acetic acid** (31 mg, 0.055 mmol, 1.0 equiv.) and put under an argon atmosphere. The mixture was dissolved in anhydrous *N,N*-dimethylformamide (DMF, 1.3 ml) and *N,N*-diisopropylethylamine (DIPEA, 17 μl, 0.098 mmol, 1.8 equiv.) was added dropwise. Separately, **2-(2-((6-chlorohexyl)oxy)ethoxy) ethan-1-amine** (**CA**, 43 mg, 0.19 mmol, 3.5 equiv.) was placed under an argon atmosphere, dissolved in anhydrous DMF (0.5 ml), and transferred to the

reaction mixture. The reaction was heated to 50 °C and stirred for 1 h. The reaction was diluted in EtOAc (3 ml), and the organic phase was washed 2× with $H_2O$, once with saturated aqueous LiCl, and once with brine. $SiO_2$ gel was added to the crude product and the solvent removed *in vacuo*, then the product-containing $SiO_2$ gel was loaded onto a $SiO_2$ column and purified by flash column chromatography (EtOAc:Hexane 0:1 → EtOAc:Hexane 1:0). ***N*-(2-(*tert*-butoxy)ethyl)-*N*-(5-(2-((2-(2-((6-chlorohexyl)oxy)ethoxy)ethyl)amino)-2-oxoethoxy)-2-nitrobenzyl)palmitamide** (**4**, 44 mg, 0.057 mol, 89%) was isolated as a yellow oil.

**TLC (MeOH:DCM) 1:19): $R_f$ =** 0.32. **$^1$H NMR ($CDCl_3$, 400 MHz, 25 °C): δ** 8.27 (d, 0.4 H, H3, *J* = 9.1 Hz); 8.13 (d, 0.6 H, H3, *J* = 8.6 Hz); 6.95-6.75 (m, 3 H, NH, H2, H6); 5.15 (s, 0.9 H, $H7_A$); 5.01 (s, 1.2 H, $H7_B$); 4.53 (d, 2 H, $H8_{A,B}$, *J* = 8.6 Hz); 3.73-3.36 (m, 16 H, $H10_{A,B}$, $H11_{A,B}$, H28-H32, H37); 2.56 (t, 1 H, $H13_A$, *J* = 7.6 Hz); 2.20 (t, 1 H, $H13_B$, *J* = 7.8 Hz); 1.81-1.53 (m, 6 H, $H14_{A,B}$, $H33_{A,B}$, $H36_{A,B}$); 1.50-1.19 (m, 28 H, H15-26, $H34_{A,B}$, $H35_{A,B}$); 0.87 (t, 3 H, $H27_{A,B,C}$, *J* = 6.4 Hz). **$^{13}$C NMR ($CDCl_3$, 101 MHz, 25 °C): δ** 174.70 / 174.26 (C12); 166.99 / 166.62 (C9); 161.74 / 161.26 (C1); 142.48 / 141.81 (C4); 137.79 (C5); 129.04 / 128.23 (C3); 114.43 / 114.20 (C6); 113.11 / 112.44 (C2); 73.62 ($\underline{C}(CH_3)_3$); 71.43 (C37); 70.49, 70.21, 70.14, 69.72, 69.68 (C29-31); 67.74 / 67.69 (C8); 60.80 / 59.91 (C11); 51.41 / 47.67 (C7); 49.19 / 47.53 (C10); 45.15 (C32); 39.10 (C28); 33.26 (C13); 32.65 (C33); 32.06, 29.84, 22.83, 29.77, 29.68, 29.65, 29.58, 29.53, 29.51 (C15-26); 27.57 / 27.49 ($C(\underline{C}H_3)_3$); 26.82 (C34); 25.55 (C35); 25.45 / 25.42 (C14); 14.26 (C27). **HRMS (ESI$^+$):** *m/z* calcd. for $[C_{41}H_{73}N_3O_8Cl]^+$: 770.5086, found: 770.5062 ($[M+H]^+$)).

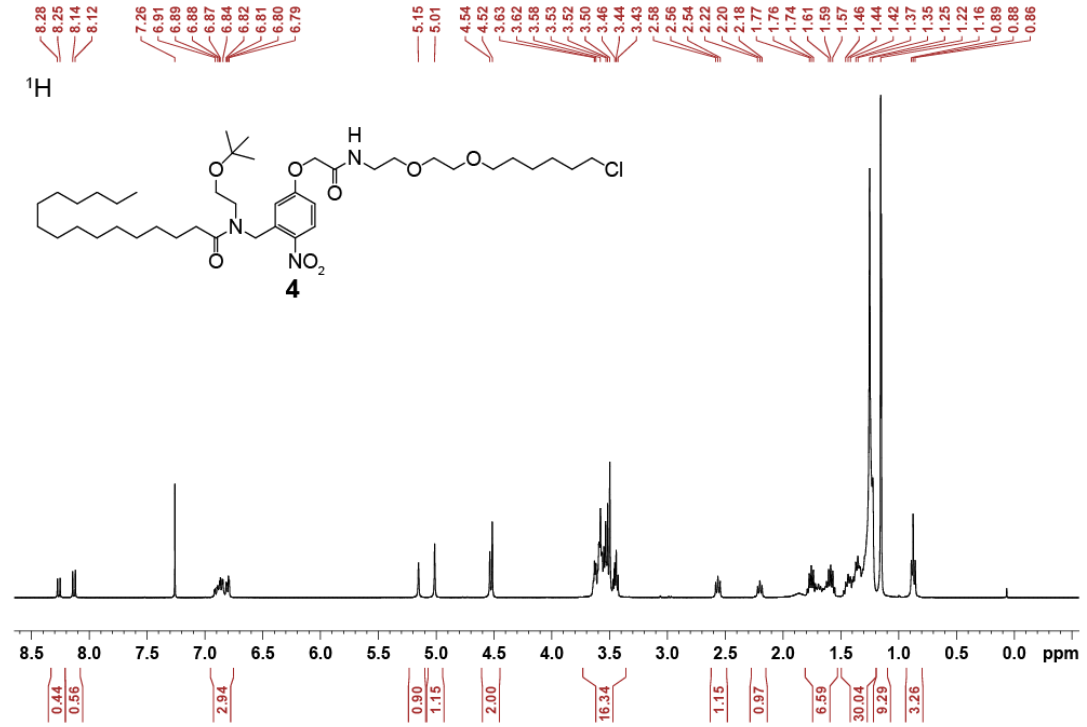
8.28
8.25
8.14
8.12
7.26
6.91
6.89
6.88
6.87
6.84
6.82
6.81
6.80
6.79
5.15
5.01
4.54
4.52
3.63
3.62
3.58
3.53
3.52
3.50
3.46
3.44
3.43
2.58
2.56
2.54
2.22
2.20
2.18
1.77
1.76
1.74
1.61
1.59
1.57
1.46
1.44
1.42
1.37
1.35
1.25
1.22
1.16
0.89
0.88
0.86
1H
4
8.5 8.0 7.5 7.0 6.5 6.0 5.5 5.0 4.5 4.0 3.5 3.0 2.5 2.0 1.5 1.0 0.5 0.0 ppm
0.44
0.56
2.94
0.90
1.15
2.00
16.34
1.15
0.97
6.59
30.04
9.29
3.26

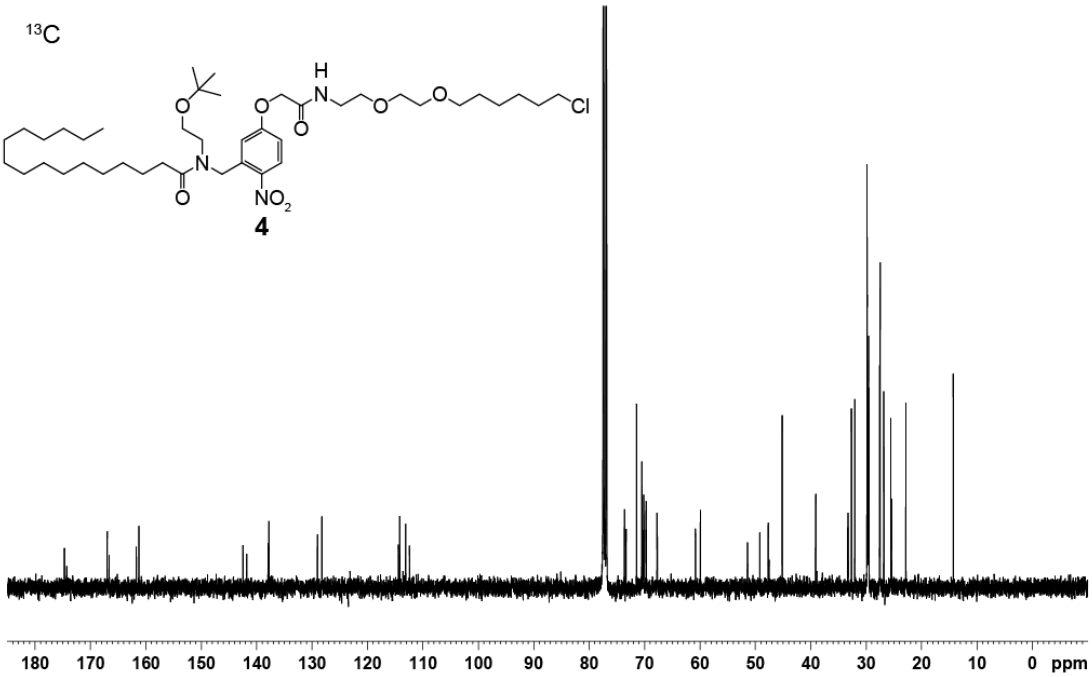
13C
4
180 170 160 150 140 130 120 110 100 90 80 70 60 50 40 30 20 10 0 ppm

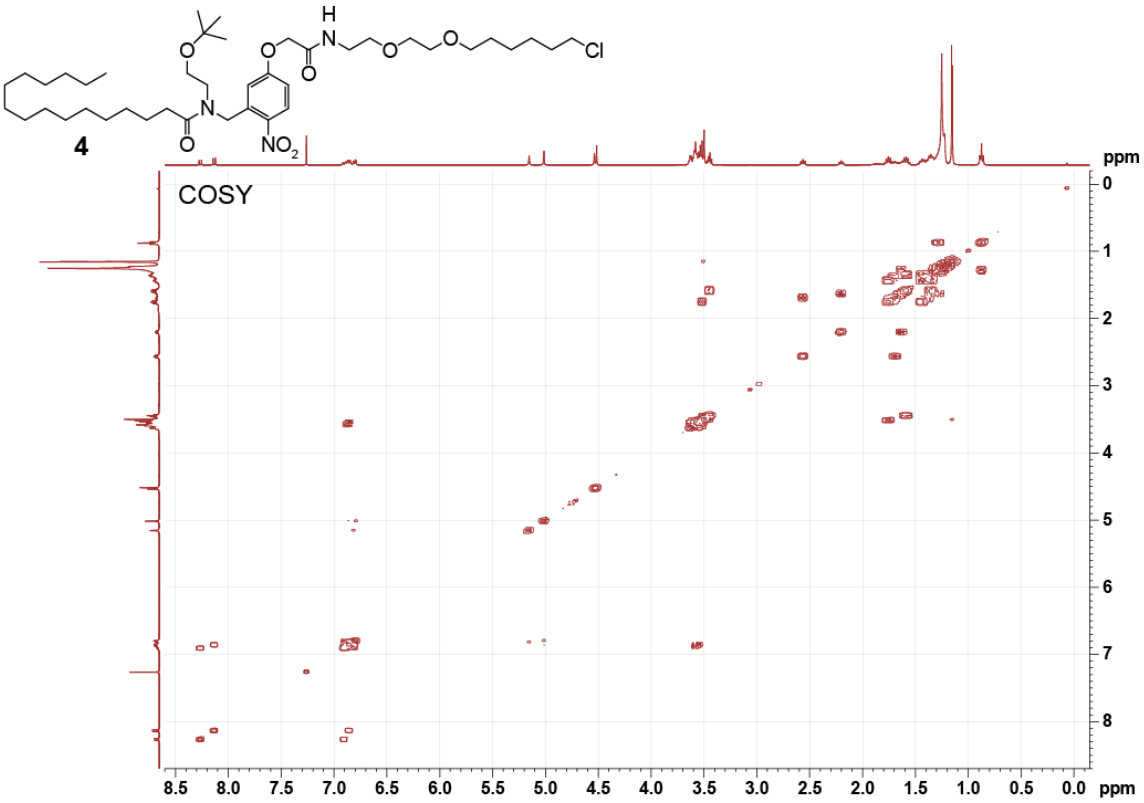
4
COSY
ppm
8.5 8.0 7.5 7.0 6.5 6.0 5.5 5.0 4.5 4.0 3.5 3.0 2.5 2.0 1.5 1.0 0.5 0.0 ppm

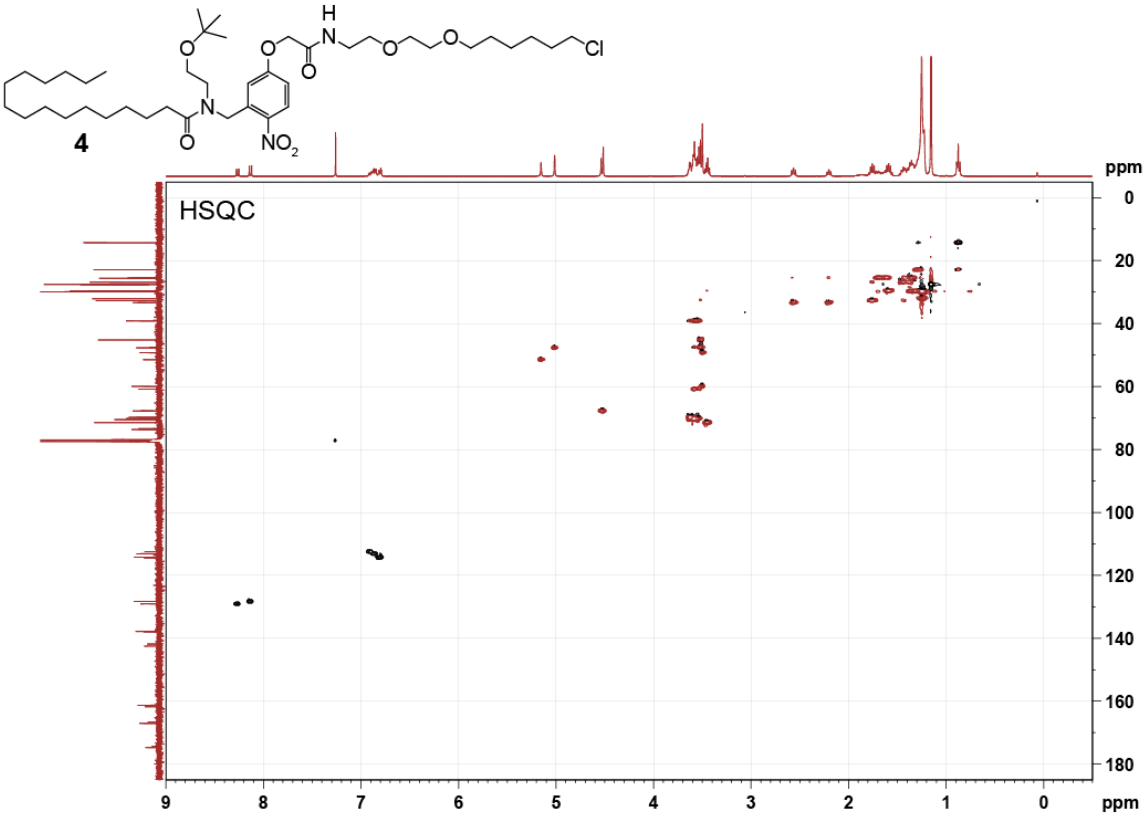
4
HSQC
ppm
9 8 7 6 5 4 3 2 1 0 ppm

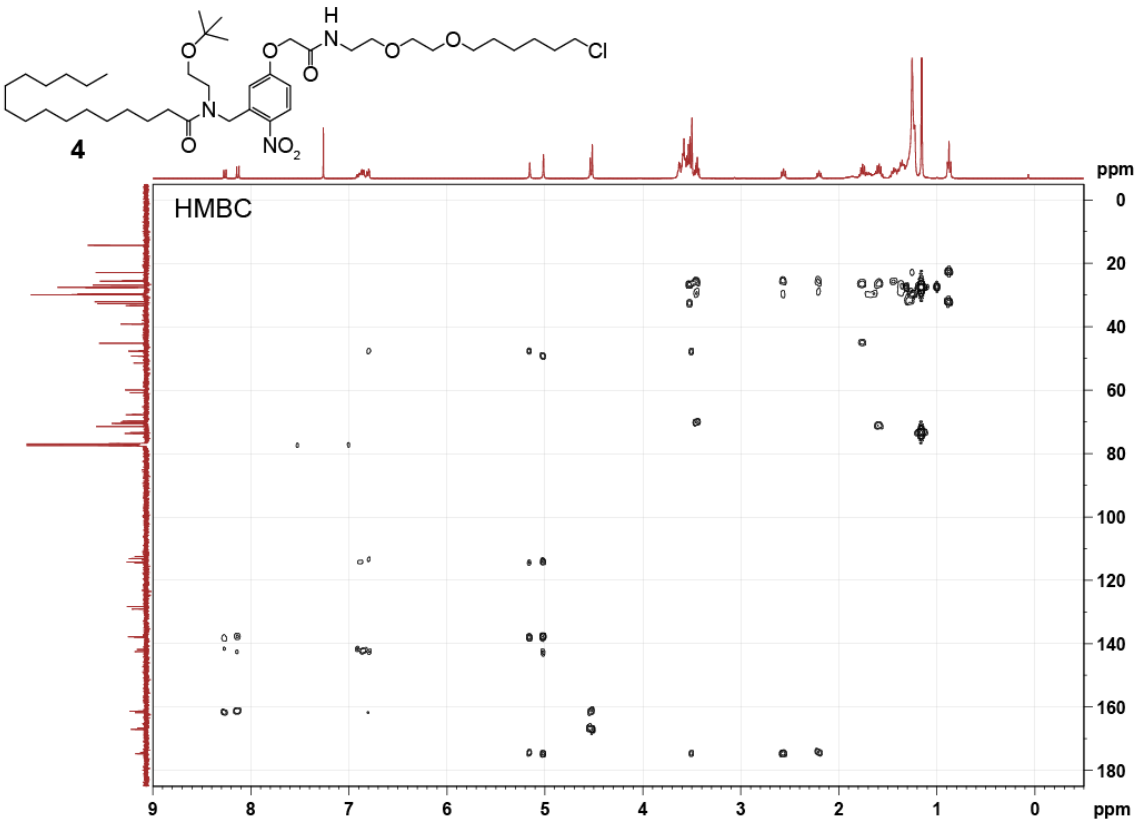
4
HMBC
ppm
0
20
40
60
80
100
120
140
160
180
9
8
7
6
5
4
3
2
1
0
ppm

### 3.5.2. Synthesis of *N*-(5-(2-((2-(2-((6-chlorohexyl)oxy)ethoxy)ethyl)amino)-2-oxoethoxy)-2-nitrobenzyl)-*N*-(2-hydroxyethyl)palmitamide (hOCT-PEA1)

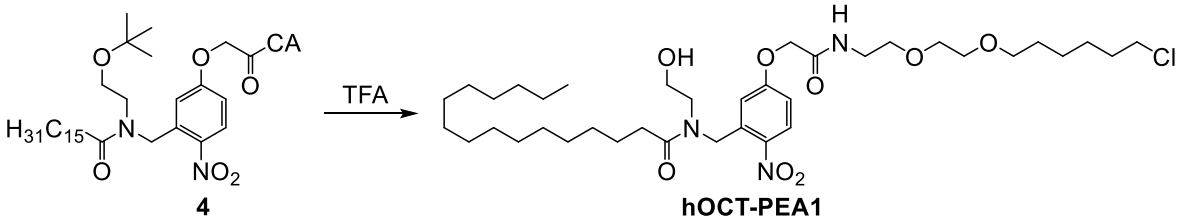


***N*-(2-(*tert*-butoxy)ethyl)-*N*-(5-(2-((2-(2-((6-chlorohexyl)oxy)ethoxy)ethyl) amino)-2-oxoethoxy)-2-nitrobenzyl)palmitamide** (**4**, 14 mg, 0.018 mmol, 1.0 equiv.) was put under an argon atmosphere and trifluoroacetic acid (TFA, 0.50 ml, 6.7 mmol, excess) was added. The reaction stirred for 25 min at RT before the solvent was removed *in vacuo*. The crude product was dissolved in DCM and the solvent was removed *in vacuo*, 2×, to remove residual TFA. The crude product was purified via $SiO_2$ flash column chromatography (EtOAc:hexane 0:1 → EtOAc:hexane 1:0) to yield ***N*-(5-(2-((2-(2-((6-chlorohexyl)oxy)ethoxy) ethyl)amino)-2-oxoethoxy)-2-nitrobenzyl)-*N*-(2-hydroxyethyl)palmitamide** (**hOCT-PEA1**, 10 mg, 0.014 mmol, 77%) as a yellow oil.

**TLC (MeOH:DCM 1:9): $R_f$ =** 0.49. **$^1$H NMR ($CDCl_3$, 400 MHz, 25 °C): δ** 8.28 (d, 0.6 H, H3, *J* = 8.9 Hz); 8.13 (d, 0.4 H, H3, *J* = 9.1 Hz); 6.99-6.79 (m, 3 H, NH, H2, H6); 5.05 (s, 1.2 H, $H7_A$); 4.98 (s, 0.8 H, $H7_B$); 4.57 (d, 2 H, $H8_{A,B}$, *J* = 5.99 Hz); 3.86-3.70 (m, 2 H, $H11_{A,B}$); 3.68-3.49 (m, 12 H, $H10_{A,B}$, H28-H32); 3.45 (q, 2 H, $H37_{A,B}$); 2.57 (t, 0.8 H, $H13_A$, *J* = 7.57 Hz); 2.22 (t, 1.2 H, $H13_B$, *J* = 7.57 Hz, br, 1 H, OH); 1.81-1.52 (m, 6 H, $H14_{A,B}$, $H33_{A,B}$, $H36_{A,B}$); 1.50-1.14 (m, 28 H, H15-26, $H34_{A,B}$, $H35_{A,B}$); 0.87 (t, 3 H, $H27_{A,B,C}$). **$^{13}$C NMR ($CDCl_3$, 101 MHz, 25 °C): δ** 176.30 / 174.67 (C12); 167.53 / 166.65 (C9), 161.98 / 161.35 (C1), 142.16 / 141.57 (C4); 138.11 / 137.24 (C5); 129.08 / 128.14 (C3); 114.06 / 114.00 (C6); 113.43 / 113.35 (C2); 71.42 (C37); 70.73, 70.40, 70.17, 70.10, 69.67 (C29-31); 67.75 / 67.70 (C8); 61.99 / 60.44 (C11); 51.58 / 48.96 (C7);

51.27 / 50.73 (C10); 45.16 (C32); 39.13 (C28); 33.43 / 33.36 (C13); 32.64 (C33); 32.07, 29.84, 29.80, 29.76, 29.70, 29.69, 29.62, 29.56, 29.50, 22.84 (C15-26 + C36); 26.80 (C34); 25.53 (C35); 25.39 / 25.29 (C14); 14.26 (C27). **HRMS (ESI$^+$):** *m/z* calcd. for $[C_{37}H_{65}N_3O_8Cl]^+$: 714.4460, found: 714.4443 ($[M+H]^+$).

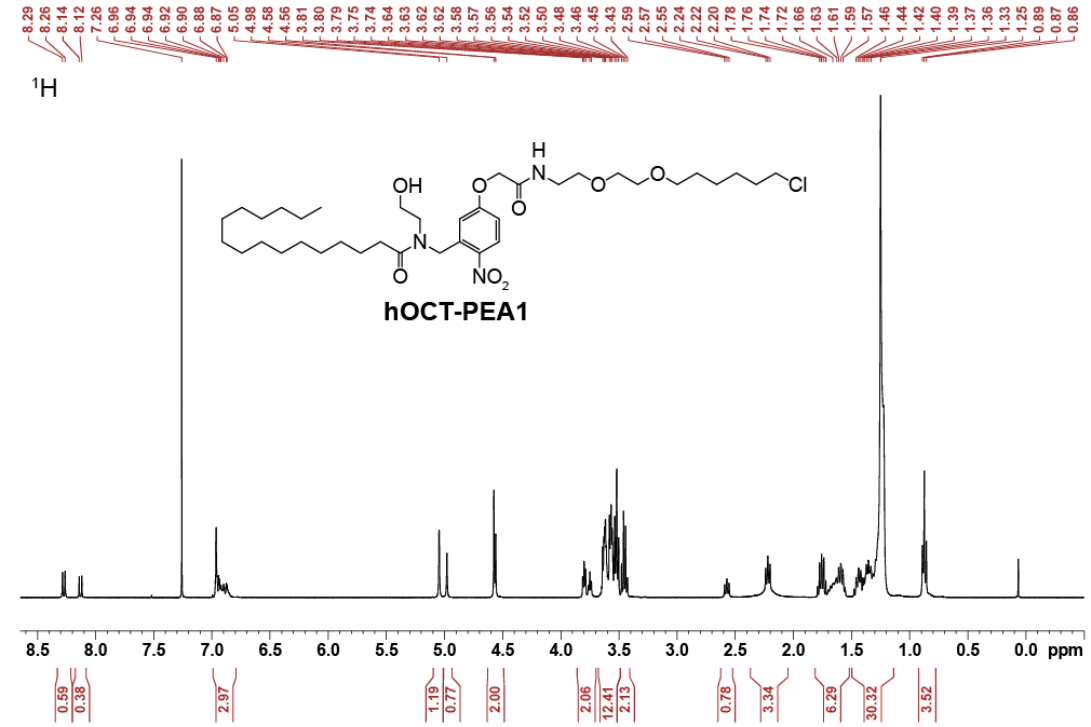
8.29 8.26 8.14 8.12 7.26 6.96 6.94 6.94 6.92 6.90 6.88 6.87 5.05 4.98 4.58 4.56 3.81 3.80 3.79 3.75 3.74 3.64 3.63 3.62 3.62 3.58 3.57 3.56 3.54 3.52 3.50 3.48 3.46 3.45 3.43 2.59 2.57 2.55 2.24 2.22 2.20 1.78 1.76 1.74 1.72 1.66 1.63 1.61 1.59 1.57 1.46 1.44 1.42 1.40 1.39 1.37 1.36 1.33 1.25 0.89 0.87 0.86
1H
OH
O
H
N
O
O
O
Cl
N
O
NO2
hOCT-PEA1
8.5 8.0 7.5 7.0 6.5 6.0 5.5 5.0 4.5 4.0 3.5 3.0 2.5 2.0 1.5 1.0 0.5 0.0 ppm
0.59 0.38 2.97 1.19 0.77 2.00 2.06 12.41 2.13 0.78 3.34 6.29 30.32 3.52

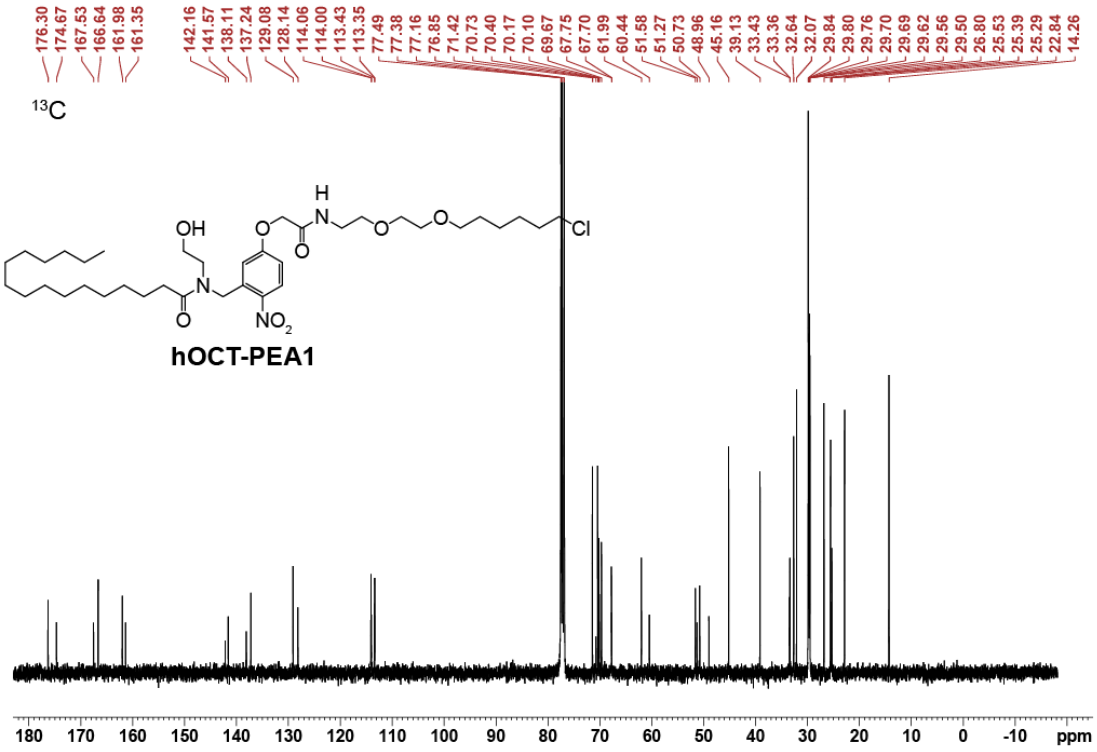
176.30 174.67 167.53 166.64 161.98 161.35 142.16 141.57 138.11 137.24 129.08 128.14 114.06 114.00 113.43 113.35 77.49 77.38 77.16 76.85 71.42 70.73 70.40 70.17 70.10 69.67 67.75 67.70 61.99 60.44 51.58 51.27 50.73 48.96 45.16 39.13 33.43 33.36 32.64 32.07 29.84 29.80 29.76 29.70 29.69 29.62 29.56 29.50 26.80 25.53 25.39 25.29 22.84 14.26
13C
OH
O
H
N
O
O
O
Cl
N
O
NO2
hOCT-PEA1
180 170 160 150 140 130 120 110 100 90 80 70 60 50 40 30 20 10 0 -10 ppm

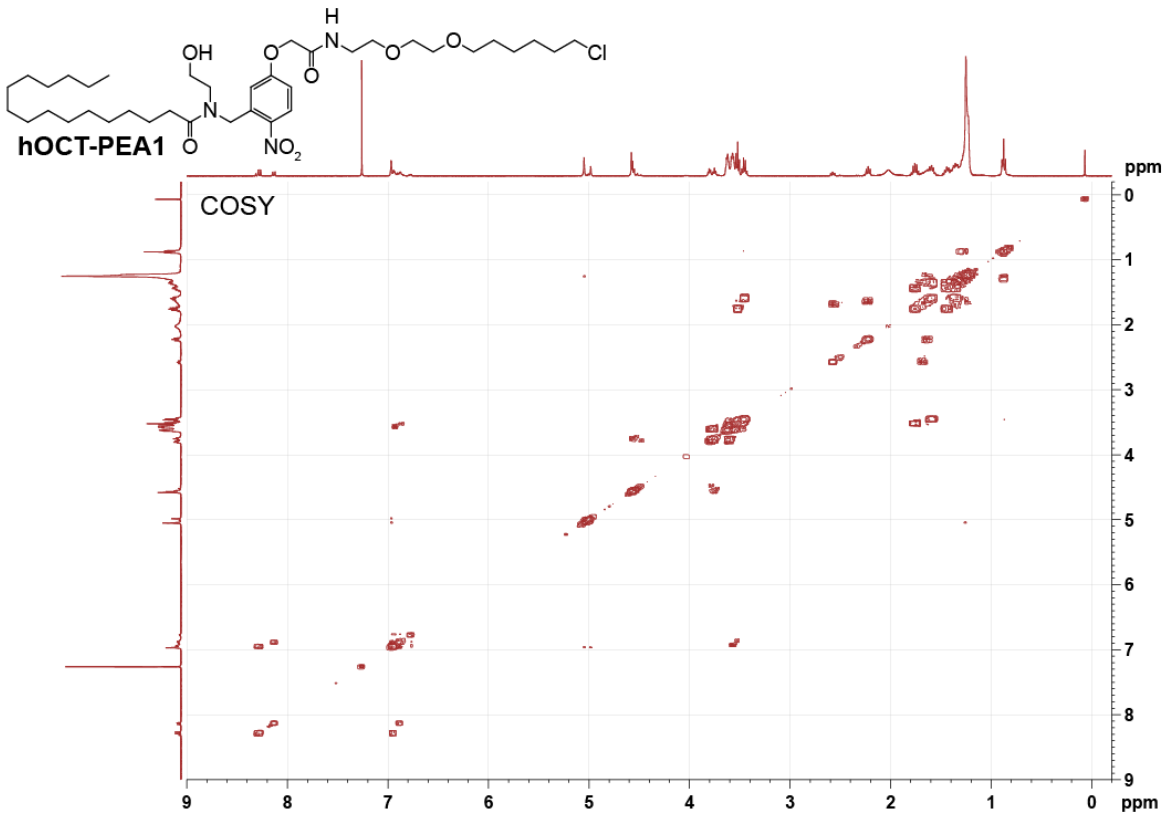
hOCT-PEA1
COSY
ppm

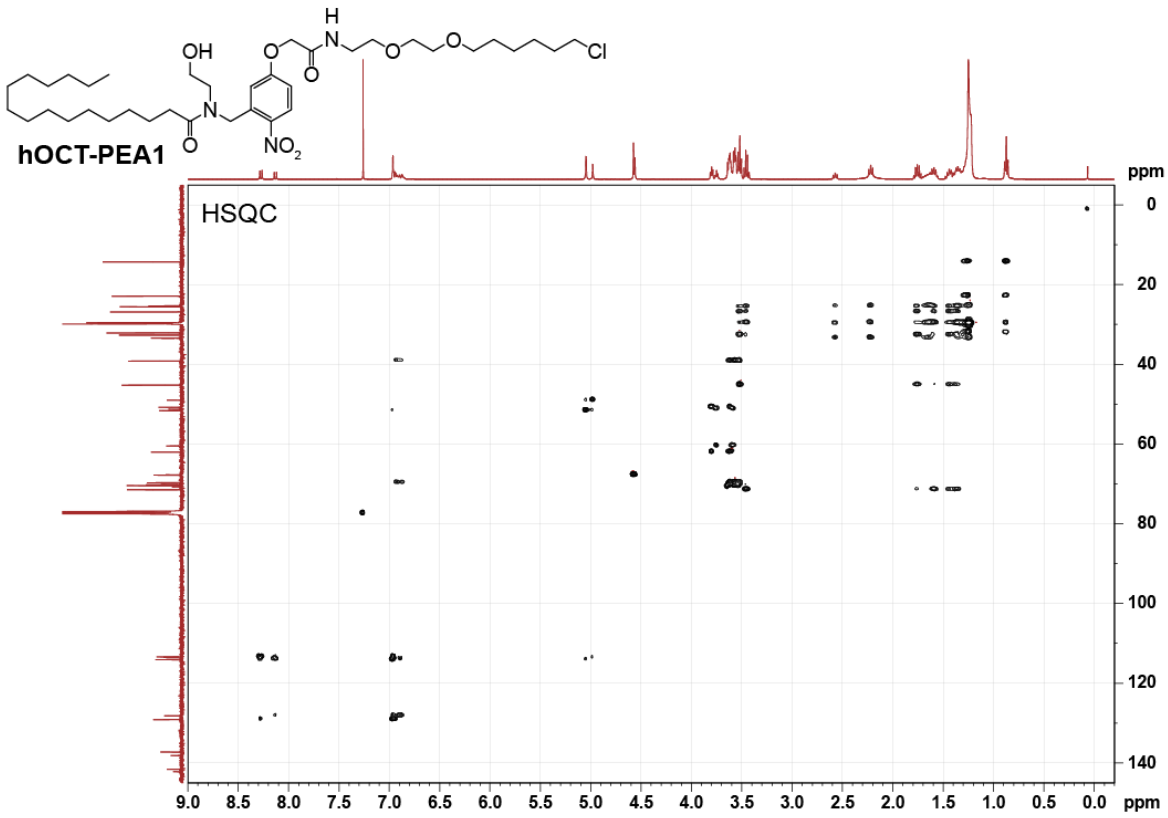
hOCT-PEA1
HSQC
ppm

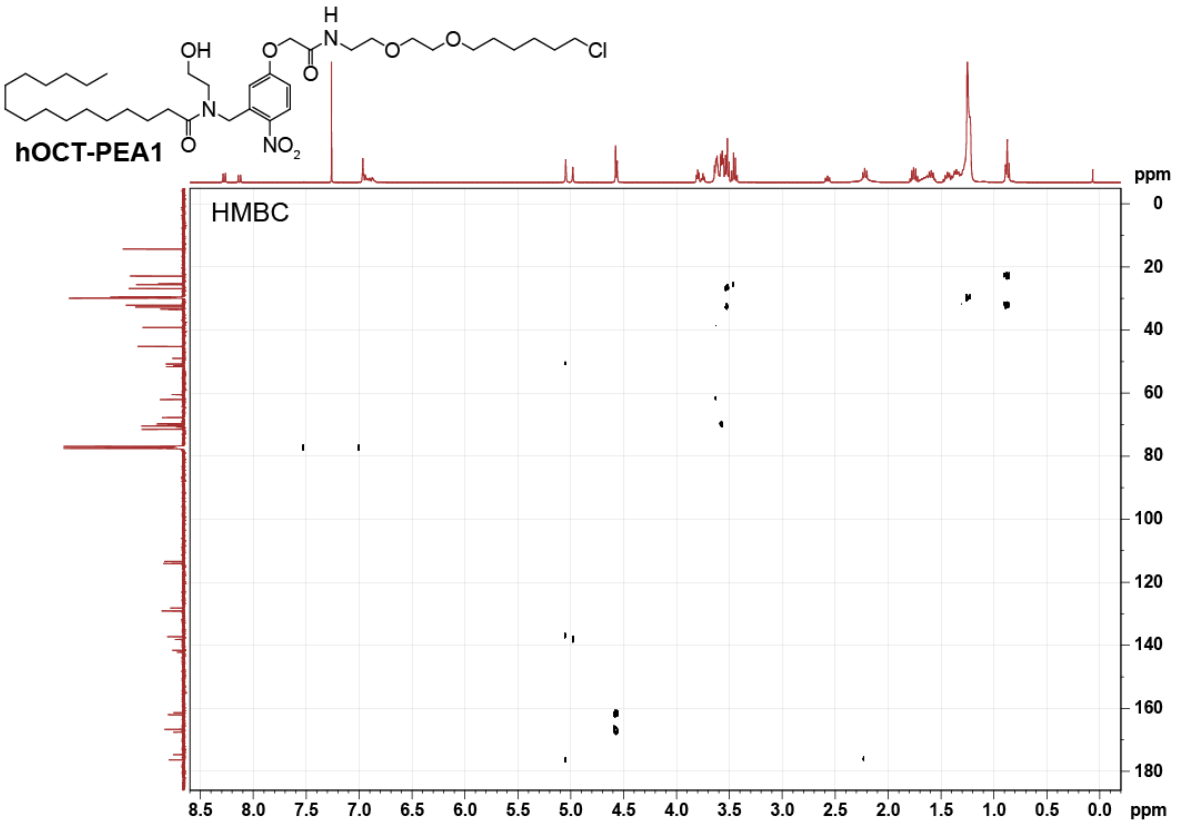
hOCT-PEA1
HMBC
ppm
8.5 8.0 7.5 7.0 6.5 6.0 5.5 5.0 4.5 4.0 3.5 3.0 2.5 2.0 1.5 1.0 0.5 0.0 ppm
0 20 40 60 80 100 120 140 160 180

**A**

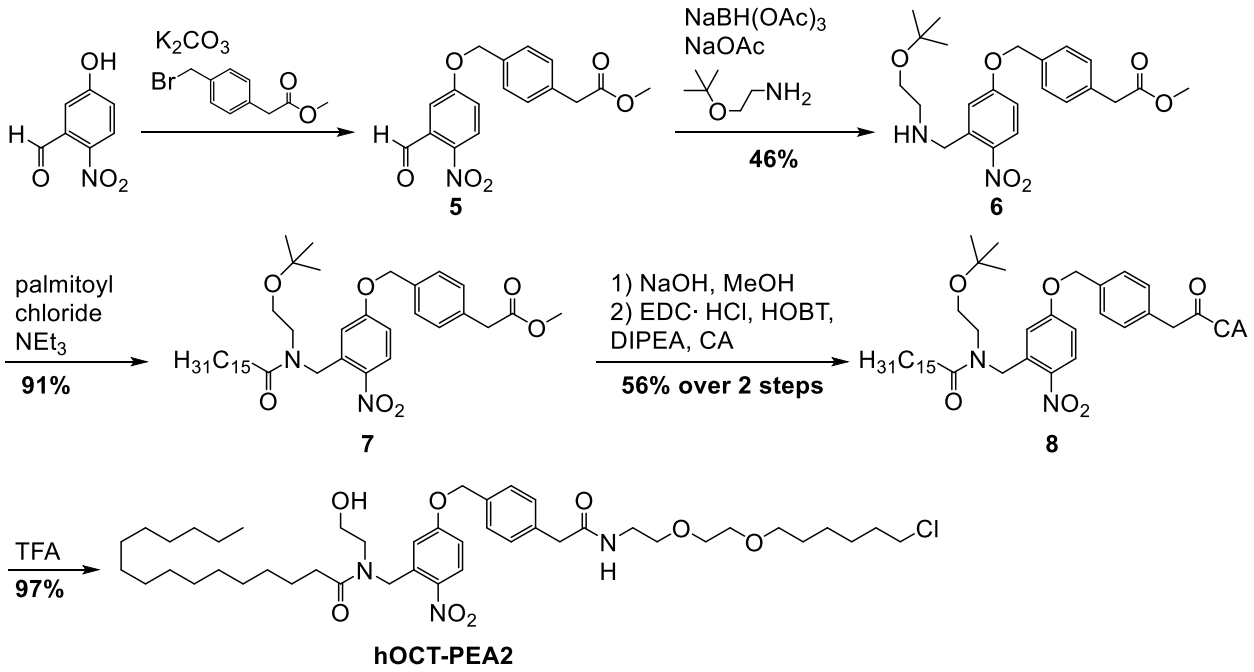


**B**

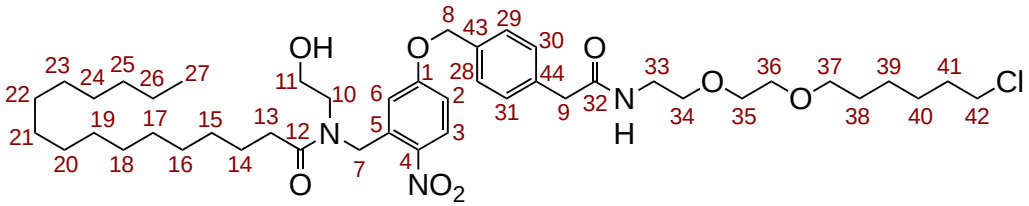


*Figure 3.15. Synthetic scheme of **hOCT-PEA2**.*

*(**A**) Chemical synthesis of **hOCT-PEA2**, which was prepared in 5 steps from compound **5** and 23% overall yield. (**B**) NMR atom numbering assignment for **hOCT-PEA2**.*

### 3.5.3. Synthesis of methyl 2-(4-((3-(((2-(*tert*-butoxy)ethyl)amino)methyl)-4-nitrophenoxy) methyl) phenyl)acetate (6)

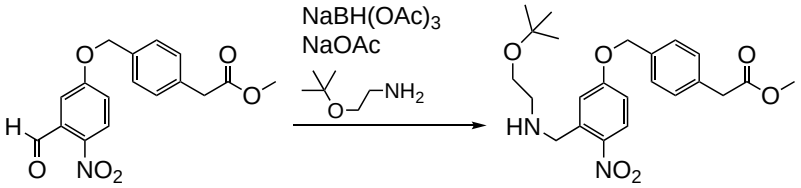


**5** **6**

**2-(4-((3-formyl-4-nitrophenoxy)methyl)phenyl)acetate** (**5**, 57 mg, 0.17 mmol, 1.0 equiv.), 2-*t*-butoxyethylamine (26 mg, 0.22 mmol, 1.3 equiv.), and NaOAc (15 mg, 0.18 mmol, 1.0 equiv.) were added to a reaction vial, alongside a stir bar and then placed under an argon atmosphere. The reaction mixture was dissolved in anhydrous 1,2-dichloroethane (DCE, 1 ml) and stirred for 1 h before adding $NaBH(OAc)_3$ (94 mg, 0.44 mmol, 2.5 equiv.) in one portion. The reaction was stirred overnight at RT, then diluted with DCM (3 ml) and quenched with saturated $NaHCO_3$ (3 ml) and transferred to a separatory funnel. The organic phase was washed 2× with saturated aqueous $NaHCO_3$ and once with brine. The organic phase was dried over anhydrous $MgSO_4$, filtered, and the solvent removed *in vacuo*. The crude product was purified by $SiO_2$ flash column chromatography (EtOAc:Hexane 1:9 → EtOAc:Hexane 1:0). **Methyl 2-(4-((3-(((2-(*tert*-butoxy)ethyl)amino)methyl)-4-nitrophenoxy)methyl)phenyl) acetate** (**6**, 35 mg, 0.081 mmol, 46%) was isolated as an oil.

**TLC (EtOAc:Hexane, 1:1): $R_f$ =** 0.15. **$^1$H NMR ($CDCl_3$, 400 MHz, 25 °C)**: δ 8.07 (d, 1 H, H3, *J* = 9.1 Hz); 7.42-7.27 (m, 5H, H6, H28-31, 5 H); 6.89 (dd, 1 H, H2, *J* = 9.1, 2.8 Hz); 5.14 (s, $H8_{A,B}$, 2 H); 4.13 (s, $H7_{A,B}$, 2 H); 3.70 (s, 3 H, $OC\underline{H}_3$); 3.64 (s, $H9_{A,B}$, 2 H); 3.48 (t, 2 H, $H11_{A,B}$, *J* = 5.3 Hz); 2.74 (t, 2 H, $H10_{A,B}$, *J* = 5.3 Hz); 2.01 (br, N$\underline{H}$, 1 H); 1.19 (s, $C(C\underline{H}_3)_3$, 9 H). **$^{13}$C NMR ($CDCl_3$, 101 MHz, 25 °C)**: δ 171.90 (C32); 162.69 (C1); 141.92 (C5); 139.89 (C4); 134.74 (C43); 134.37 (C44); 129.80 (C30, C31); 127.94 (C3, C28, C29); 116.18 (C6); 113.34 (C2); 72.98

($\underline{C}(CH_3)_3$); 70.30 (C8); 61.02 (C11); 52.24 ($O\underline{C}H_3$); 51.17 (C7); 49.63 (C10); 40.99 (C9); 27.73 ($C(\underline{C}H_3)_3$). **HRMS (ESI$^+$):** *m/z* calcd. for $[C_{23}H_{31}N_2O_6]^+$: 431.2182, found: 431.2174 ($[M+H]^+$).

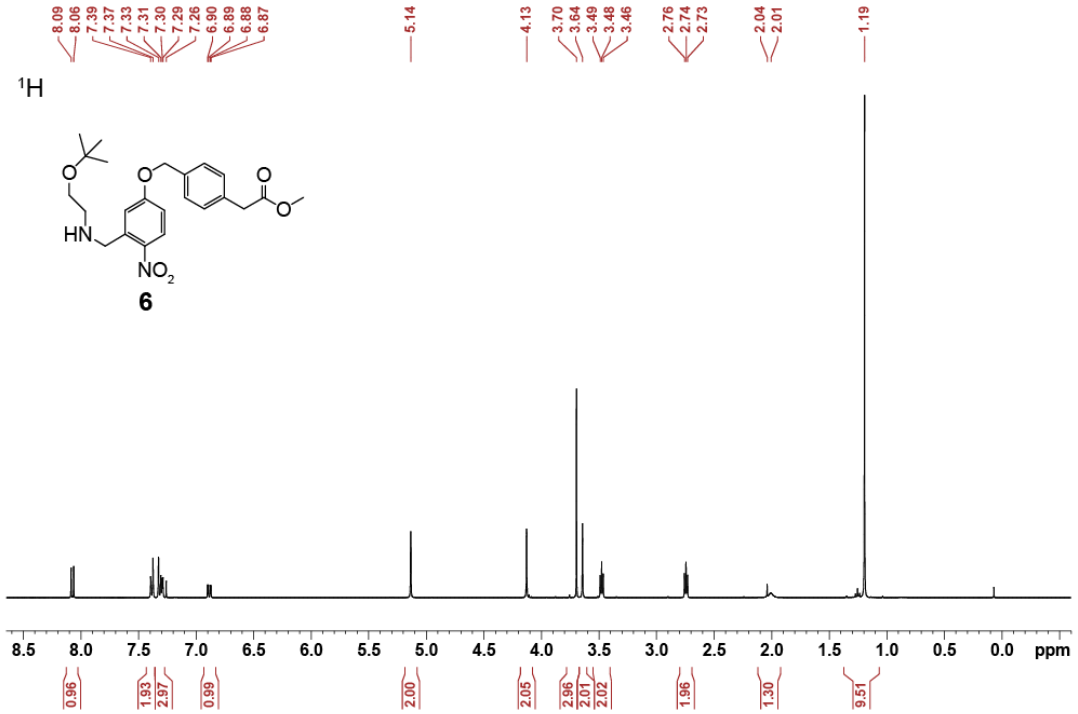
8.09
8.06
7.39
7.37
7.33
7.31
7.30
7.29
7.26
6.90
6.89
6.88
6.87
5.14
4.13
3.70
3.64
3.49
3.48
3.46
2.76
2.74
2.73
2.04
2.01
1.19
1H
HN
NO2
6
8.5 8.0 7.5 7.0 6.5 6.0 5.5 5.0 4.5 4.0 3.5 3.0 2.5 2.0 1.5 1.0 0.5 0.0 ppm
0.96
1.93
2.97
0.99
2.00
2.05
2.96
2.01
2.02
1.96
1.30
9.51

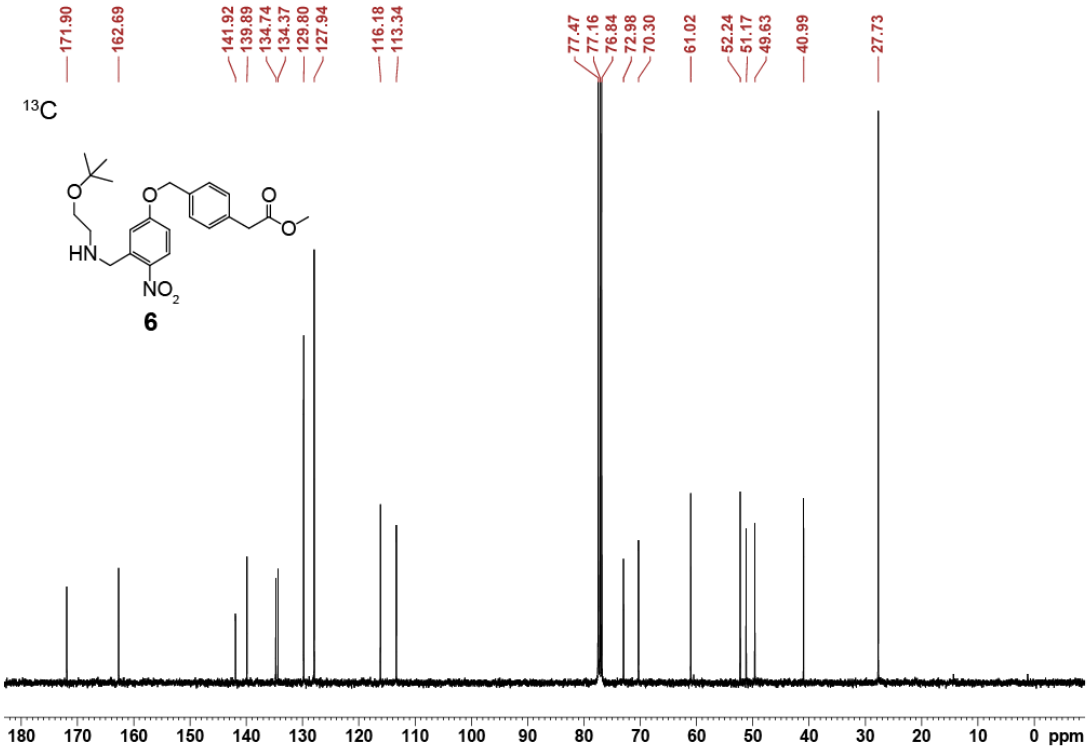
171.90
162.69
141.92
139.89
134.74
134.37
129.80
127.94
116.18
113.34
77.47
77.16
76.84
72.98
70.30
61.02
52.24
51.17
49.63
40.99
27.73
13C
HN
NO2
6
180 170 160 150 140 130 120 110 100 90 80 70 60 50 40 30 20 10 0 ppm

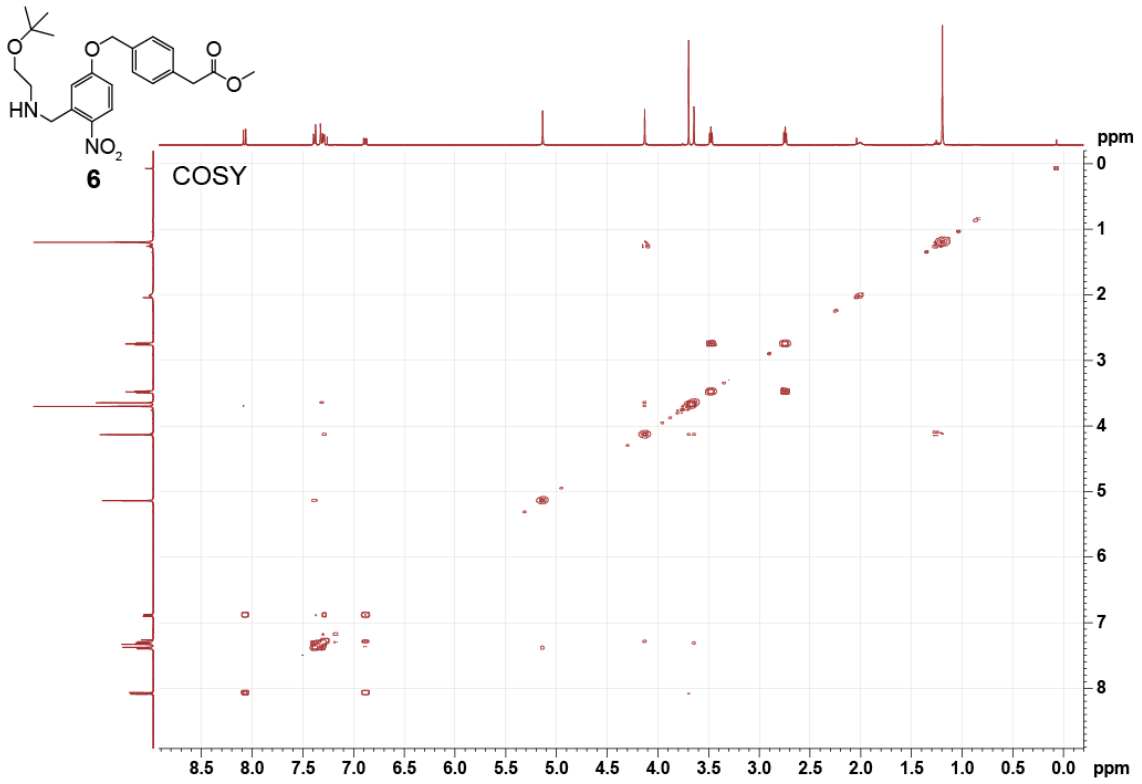
HN
O
O
O
O
NO2
6
COSY
ppm
0
1
2
3
4
5
6
7
8
8.5
8.0
7.5
7.0
6.5
6.0
5.5
5.0
4.5
4.0
3.5
3.0
2.5
2.0
1.5
1.0
0.5
0.0
ppm

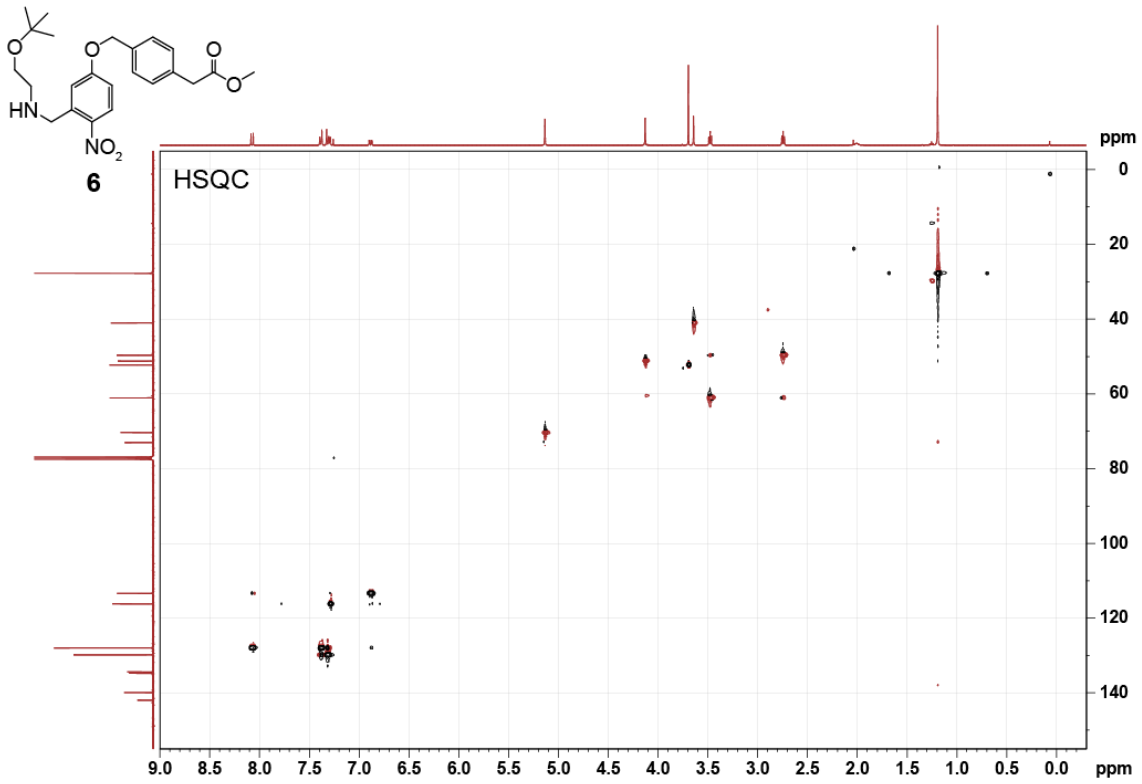
HN
O
O
O
O
NO2
6
HSQC
ppm
0
20
40
60
80
100
120
140
9.0
8.5
8.0
7.5
7.0
6.5
6.0
5.5
5.0
4.5
4.0
3.5
3.0
2.5
2.0
1.5
1.0
0.5
0.0
ppm

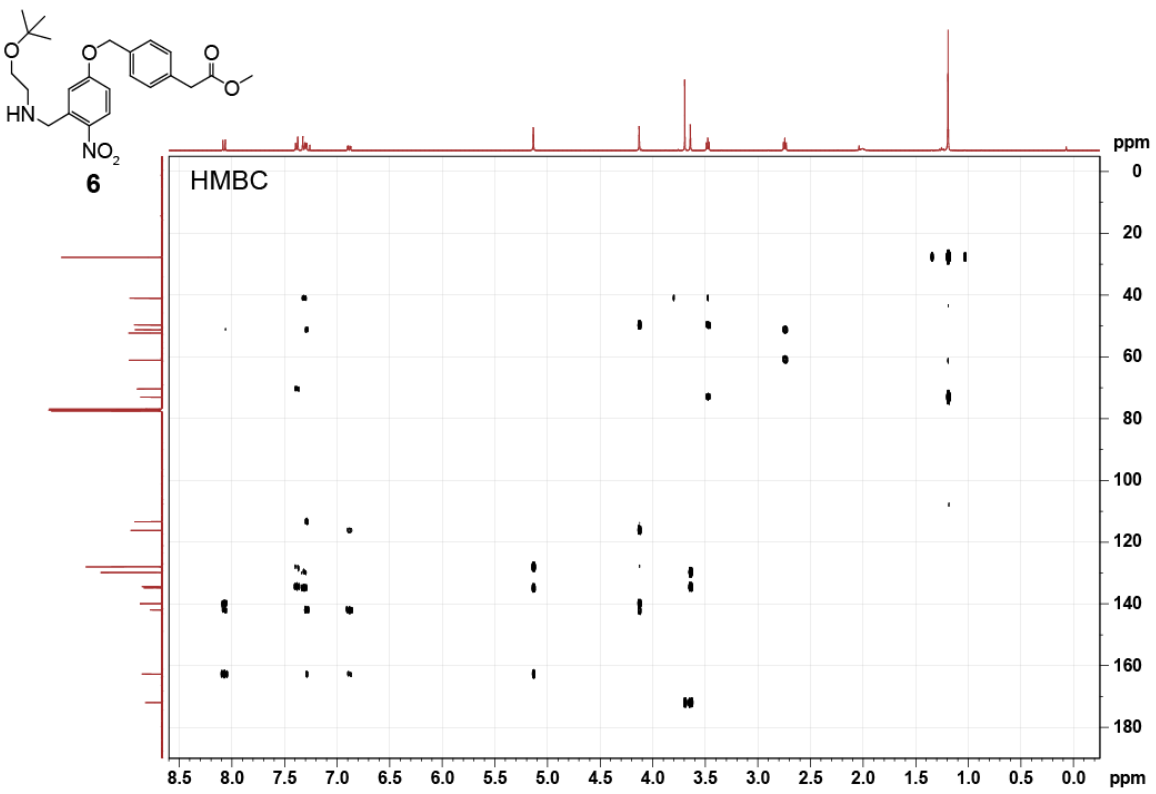
HN
NO2
6
HMBC
ppm
0
20
40
60
80
100
120
140
160
180
8.5
8.0
7.5
7.0
6.5
6.0
5.5
5.0
4.5
4.0
3.5
3.0
2.5
2.0
1.5
1.0
0.5
0.0
ppm

### 3.5.4. Synthesis of methyl 2-(4-((3-((*N*-(2-(*tert*-butoxy)ethyl)palmitamido)methyl)-4-nitrophenoxy)methyl)phenyl)acetate (7)

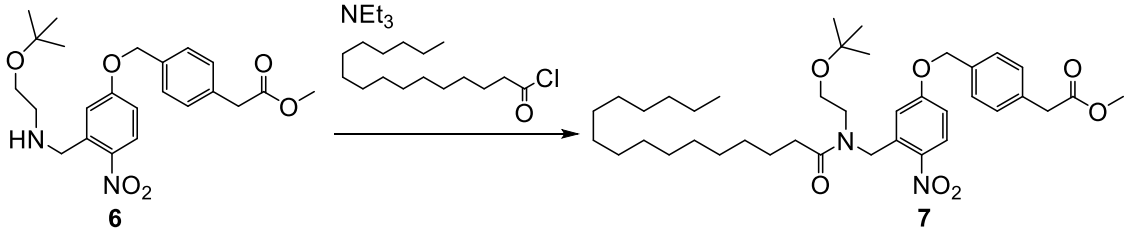


Palmitic acid (62 mg, 0.24 mmol, 3.1 equiv.) was placed under an argon atmosphere, dissolved in anhydrous DCM (0.5 ml), then oxalyl chloride (30 μl, 0.35 mmol, 4.3 equiv.) and a drop of DMF were added to initiate the reaction. The reaction was stirred for 1 h at RT, concentrated *in vacuo,* then re-dissolved in DCM and concentrated *in vacuo* 3×. The crude palmitoyl chloride was placed under an argon atmosphere and re-dissolved in anhydrous DCM (1 ml). **Methyl 2-(4-((3-(((2-(*tert*-butoxy)ethyl)amino)methyl)-4-nitrophenoxy)methyl)phenyl)acetate** (**6**, 34 mg, 0.078 mmol, 1.0 equiv.) was separately placed under an argon atmosphere and dissolved in anhydrous DCM (2 ml), then the palmitoyl chloride solution was transferred to the amine solution via cannula. $NEt_3$ (23 μl, 0.17 mmol, 2.1 equiv.) was added dropwise while stirring. After 90 min the reaction was diluted in DCM (3 ml) and transferred to a separatory funnel. The reaction was quenched with saturated aqueous $NaHCO_3$, then the organic phase was washed 2× with saturated aqueous $NaHCO_3$ and once with brine. The organic phase was separated, dried over anhydrous $MgSO_4$, and then filtered. $SiO_2$ gel was added to the filtered product and the solvent was removed *in vacuo*, then the product-containing $SiO_2$ gel was loaded onto a $SiO_2$ column and purified by flash column chromatography (EtOAc:Hexane 0:1 → EtOAc:Hexane 1:1). **Methyl 2-(4-((3-((*N*-(2-(*tert*-butoxy)ethyl)palmitamido)methyl)-4-nitrophenoxy) methyl)phenyl)acetate** (**7**, 49 mg, 0.074 mmol, 91%) was isolated as a yellow oil.

**TLC (EtOAc:Hexane 1:4): $R_f$ =** 0.17. **$^1$H NMR ($CDCl_3$, 400 MHz, 25 °C)**: δ 8.23 (d, 0.5 H, H3, *J* = 9.1 Hz); 8.12 (d, 0.5 H, H3, *J* = 9.0 Hz); 7.41-7.28 (m, 4 H, H28-31); 6.94 (dd, 0.5 H, H2, *J* = 9.0, 2.8 Hz); 6.87 (dd, 0.5 H, H2, *J* = 9.1, 2.7 Hz); 6.83-6.75 (m, 1 H, H6); 5.16-5.09 (d, 2 H, $H7_A$ + $H8_A$); 5.08 (s, 1 H, $H8_B$); 5.01 (s, 1 H, $H7_B$); 3.70 (s, 3 H, $OC\underline{H}_3$); 3.64 (s, 2 H, $H9_{A,B}$); 3.58-3.35 (m, 4 H, $H10_{A,B}$ + $11_{A,B}$); 2.52 (t, 1 H, $H13_A$, *J* = 7.7 Hz); 2.16 (t, 1 H, $H13_B$, *J* = 7.6 Hz); 1.78-1.52 (m, 2 H, $H14_{A,B}$); 1.44-1.18 (m, 24 H, H15-26); 1.14 (s, 9 H, $C(C\underline{H}_3)_3$); 0.92-0.81 (m, 3 H, $H27_{A,B,C}$). **$^{13}$C NMR ($CDCl_3$, 101 MHz, 25 °C)**: δ 174.56 / 174.21 (C12); 171.86 (C32); 163.44 / 162.99 (C1); 141.60 / 140.83 (C4); 137.70 / 137.40 (C5); 134.66, 134.53, 134.43, 134.31 (C43, C44); 129.93, 129.84 (C30, C31); 128.82 / 128.19 (C3); 127.92,127.86 (C28, C29); 114.48 (C6); 113.55, 113.48 (C6, C2); 112.94 (C2); 73.56 / 73.29 ($\underline{C}(CH_3)_3$); 70.49 / 70.37 (C8); 60.73 / 59.80 (C11); 52.25 (C33); 51.54 (C7); 49.01 (C10); 47.51, 47.47 (C7, C10); 40.97 (C9); 33.25 / 33.20 (C13); 32.06, 30.03-29.17, 22.83 (C15-26); 27.55 / 27.47 ($C(\underline{C}H_3)_3$); 25.51 / 25.40 (C14); 14.26 (C27). **HRMS (ESI$^+$):** *m/z* calcd. for $[C_{39}H_{61}N_2O_7]^+$: 669.4479, found: 669.4475 ($[M+H]^+$).

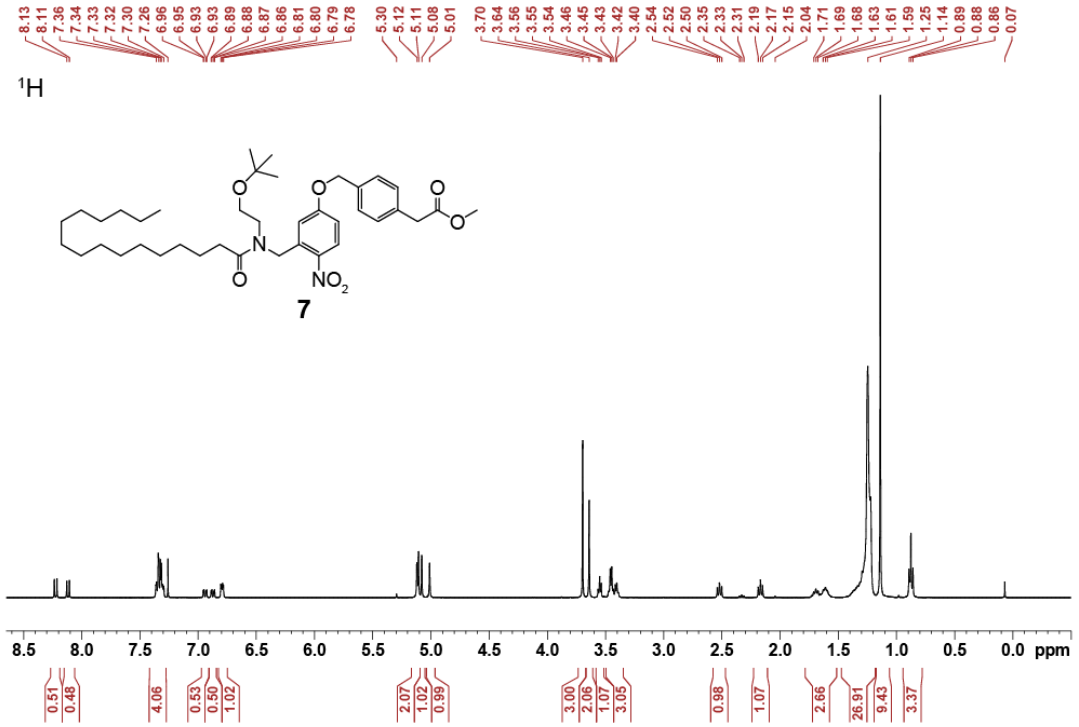
8.13
8.11
7.36
7.34
7.33
7.32
7.30
7.26
6.96
6.95
6.93
6.93
6.89
6.88
6.87
6.86
6.81
6.80
6.79
6.78
5.30
5.12
5.11
5.08
5.01
3.70
3.64
3.56
3.55
3.54
3.46
3.45
3.43
3.42
3.40
2.54
2.52
2.50
2.35
2.33
2.31
2.19
2.17
2.15
2.04
1.71
1.69
1.68
1.63
1.61
1.59
1.25
1.14
0.89
0.88
0.86
0.07
1H
O
O
O
O
N
O
O
NO2
7
8.5
8.0
7.5
7.0
6.5
6.0
5.5
5.0
4.5
4.0
3.5
3.0
2.5
2.0
1.5
1.0
0.5
0.0 ppm
0.51
0.48
4.06
0.53
0.50
1.02
2.07
1.02
0.99
3.00
2.06
1.07
3.05
0.98
1.07
2.66
26.91
9.43
3.37

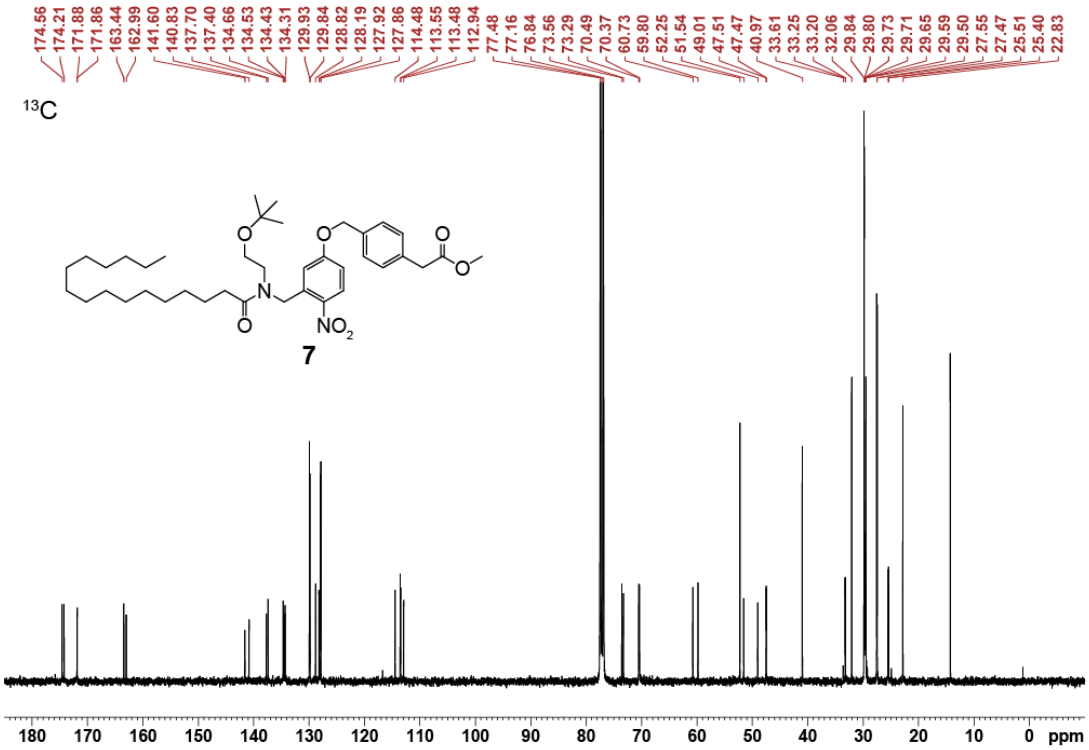
174.56
174.21
171.88
171.86
163.44
162.99
141.60
140.83
137.70
137.40
134.66
134.53
134.43
134.31
129.93
129.84
128.82
128.19
127.92
127.86
114.48
113.55
113.48
112.94
77.48
77.16
76.84
73.56
73.29
70.49
70.37
60.73
59.80
52.25
51.54
49.01
47.51
47.47
40.97
33.61
33.25
33.20
32.06
29.84
29.80
29.73
29.71
29.65
29.59
29.50
27.55
27.47
25.51
25.40
22.83
13C
O
O
O
O
N
O
O
NO2
7
180
170
160
150
140
130
120
110
100
90
80
70
60
50
40
30
20
10
0 ppm

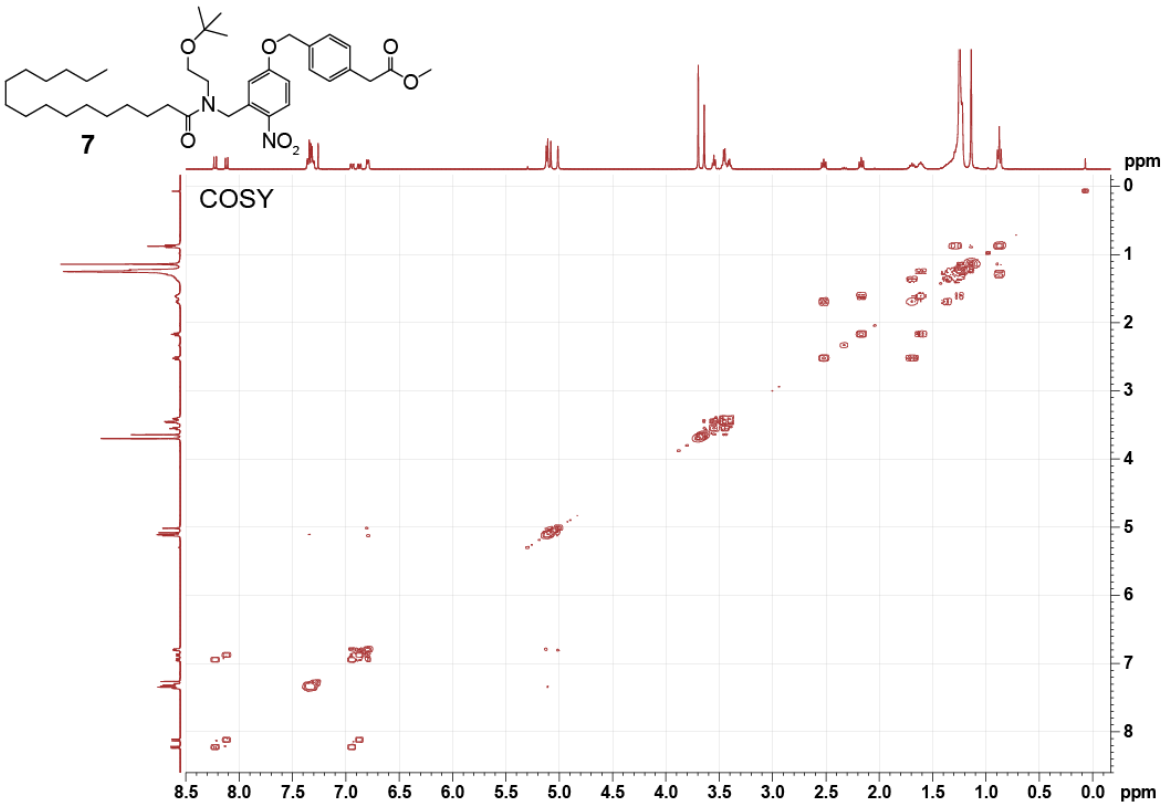
7
COSY
ppm
8.5 8.0 7.5 7.0 6.5 6.0 5.5 5.0 4.5 4.0 3.5 3.0 2.5 2.0 1.5 1.0 0.5 0.0 ppm
0 1 2 3 4 5 6 7 8

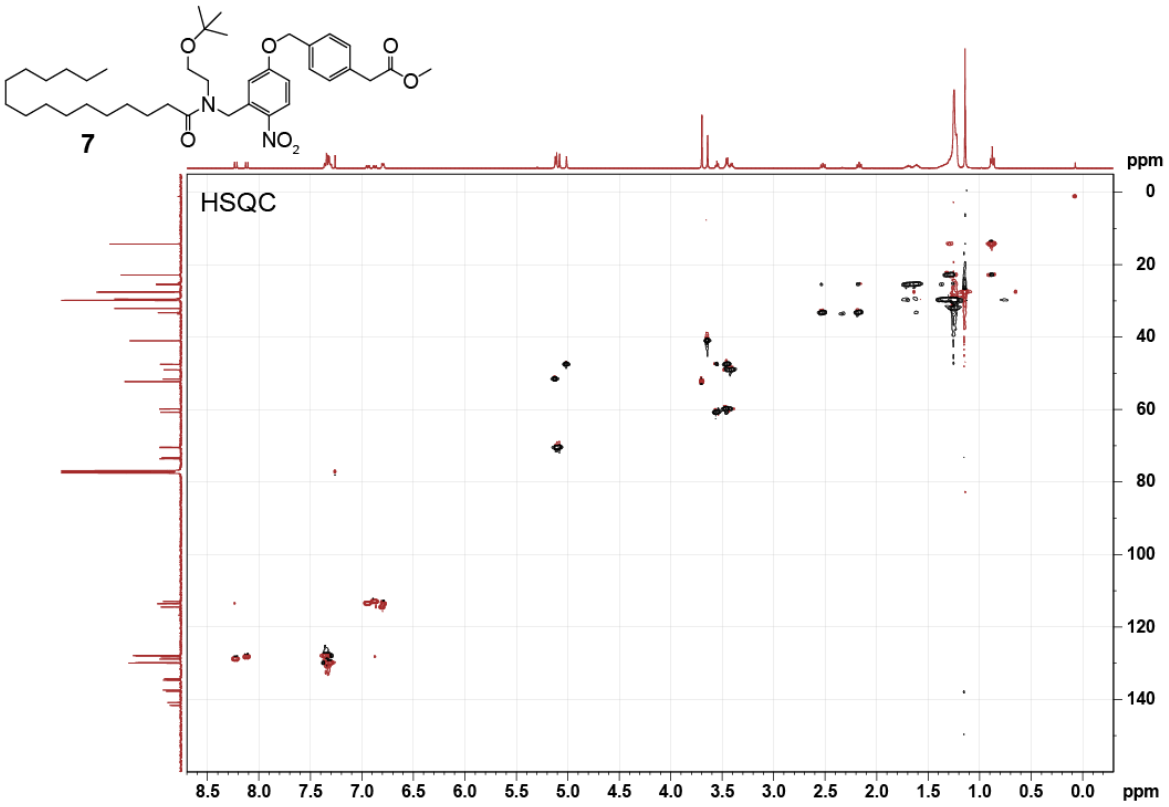
7
HSQC
ppm
8.5 8.0 7.5 7.0 6.5 6.0 5.5 5.0 4.5 4.0 3.5 3.0 2.5 2.0 1.5 1.0 0.5 0.0 ppm
0 20 40 60 80 100 120 140

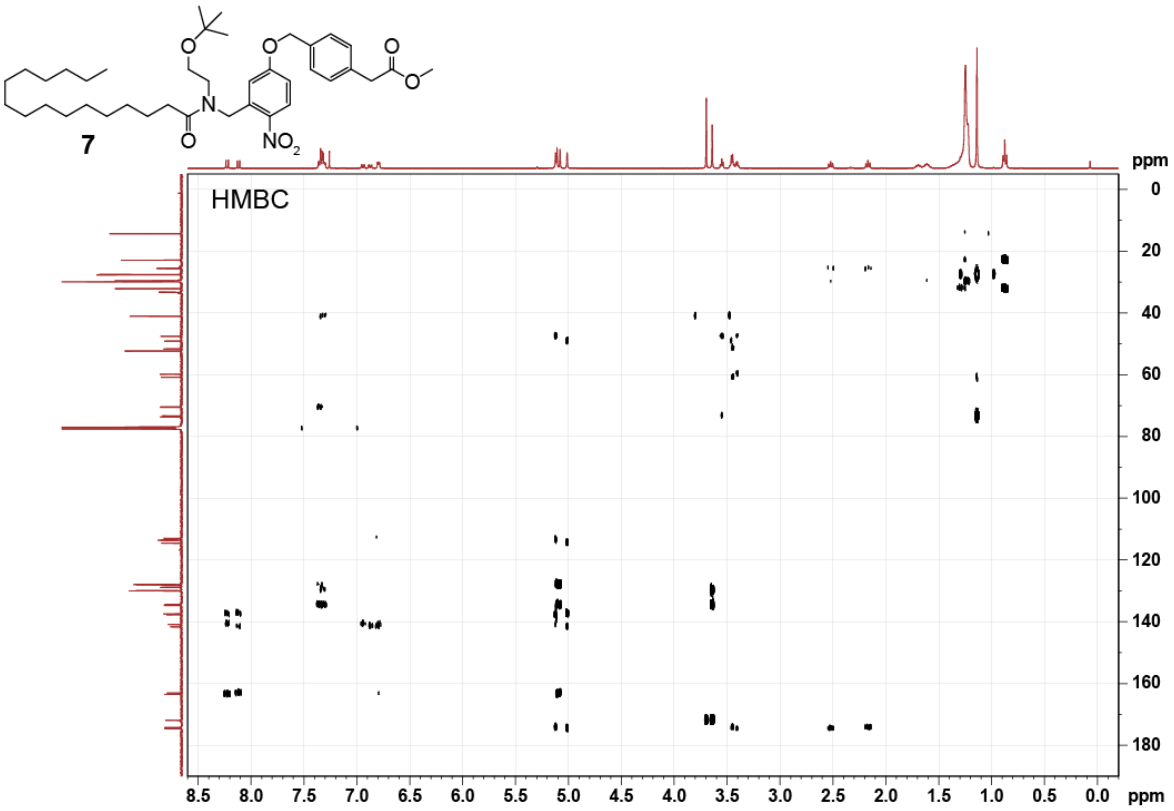
7
HMBC
ppm
0
20
40
60
80
100
120
140
160
180
8.5
8.0
7.5
7.0
6.5
6.0
5.5
5.0
4.5
4.0
3.5
3.0
2.5
2.0
1.5
1.0
0.5
0.0
ppm

### 3.5.5. Synthesis of *N*-(2-(*tert*-butoxy)ethyl)-*N*-(5-((4-(2-((2-(2-((6-chlorohexyl) oxy)ethoxy)ethyl) amino)-2-oxoethyl)benzyl)oxy)-2-nitrobenzyl)palmitamide (8)

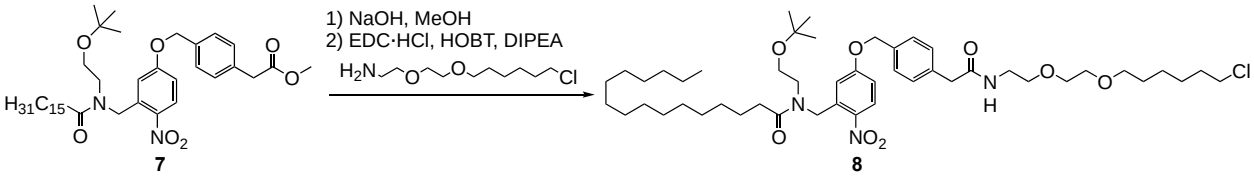


**Methyl 2-(4-((3-((*N*-(2-(*tert*-butoxy)ethyl)palmitamido)methyl)-4-nitrophenoxy)methyl) phenyl)acetate** (**7,** 63 mg, 0.095 mmol, 1.0 equiv.) was placed under an argon atmosphere and dissolved in anhydrous tetrahydrofuran (1 ml). Aqueous NaOH (1 M, 0.19 ml, 0.19 mmol, 2.0 equiv.) was added dropwise, and the reaction was heated to 50 °C. The reaction continued for 110 min, and then aqueous HCl (1 M) was added dropwise until pH = 7.0. The reaction was diluted in DCM (5 ml), and the organic layer was extracted 2× with $H_2O$. The organic phase was washed once with brine and then dried over anhydrous $MgSO_4$. The crude mixture was filtered and the solvent removed *in vacuo*. The crude **2-(4-((3-((*N*-(2-(*tert*-butoxy)ethyl) palmitamido)methyl)-4-nitrophenoxy)methyl)phenyl)acetic acid** (53 mg, 0.080 mmol) was carried directly into the next reaction without further purification.

HOBt (20. mg, 0.15 mmol, 1.9 equiv.) and EDC·HCl (27 mg, 0.14 mmol, 1.8 equiv.) were added to **2-(4-((3-((*N*-(2-(*tert*-butoxy)ethyl)palmitamido)methyl)-4-nitrophenoxy)methyl) phenyl)acetic acid** (53 mg, 0.080 mmol, 1.0 equiv.) and placed under an argon atmosphere. The mixture was dissolved in anhydrous DMF (3 ml) and DIPEA (33 μl, 0.19 mmol, 2.4 equiv.) was added dropwise. The reaction was heated to 50 °C and stirred for 1 h. Separately, **2-(2-((6-chlorohexyl)oxy)ethoxy)ethan-1-amine** (**CA**, 43 mg, 0.19 mmol, 2.4 equiv.) was placed under an argon atmosphere, dissolved in anhydrous DMF (1 ml), and transferred to reaction mixture. The reaction stirred for 2.5 h before diluting in DCM. The organic phase was washed 2× with $H_2O$, once with saturated aqueous LiCl, and once with brine. $SiO_2$ gel was added to the crude product, and the solvent was removed *in vacuo*. The product-containing $SiO_2$ gel was loaded

onto a $SiO_2$ column and purified by flash chromatography (MeOH:DCM 0:1→ MeOH: DCM 1:9). ***N*-(2-(*tert*-butoxy)ethyl)-*N*-(5-((4-(2-((2-(2-((6-chlorohexyl)oxy)ethoxy)ethyl) amino)-2-oxoethyl)benzyl)oxy)-2-nitrobenzyl)palmitamide** (**8**, 46 mg, 0.053 mol, 56%) was isolated as a yellow oil.

**TLC (MeOH:DCM 1:19): $R_f$ =** 0.30. **$^1$H NMR ($CDCl_3$, 400 MHz, 25 °C)**: δ 8.23 (d, 0.5 H, H3, *J* = 9.1 Hz); 8.11 (d, 0.5 H, H3, *J* = 9.1 Hz); 7.39-7.28 (m, 4 H, H28-31); 6.94 (dd, 0.5 H, H2, *J* = 9.1, 2.7 Hz); 6.87 (dd, 0.5 H, H2, *J* = 9.1, 2.7 Hz); 6.80 (m, 1 H, H6, *J* = 10.6, 2.6 Hz); 5.99 (br, 1 H, N<u>H</u>); 5.16-5.09 (d, 2 H, $H7_A$ + $H8_A$); 5.08 (s, 1 H, $H8_B$); 5.01 (s, 1 H, $H7_B$); 3.67-3.36 (m, 16 H, $H9_{A,B}$, H10-11, H33-37, $H42_{A,B}$), 2.52 (t, 1 H, $H13_A$, *J* = 7.6 Hz); 2.16 (t, 1 H, $H13_B$, *J* = 7.5 Hz); 1.83-1.54 (m, 6 H, $H14_{A,B}$, $H38_{A,B}$, $H41_{A,B}$); 1.52-1.17 (m, 28 H, H15-26, H39-H40); 1.14 (s, 9 H, C(C<u>H</u>$_3$)$_3$); 0.92-0.81 (m, 3 H, $H27_{A,B,C}$). **$^{13}$C NMR ($CDCl_3$, 101 MHz, 25 °C)**: δ 174.56 / 174.20 (C12), 170.63 (C32); 163.43 / 162.94 (C1); 141.61 / 140.86 (C4); 137.71 / 137.40 (C5); 135.58 / 135.48 (C44); 134.65 / 134.34 (C43); 129.93, 129.84 (C30, C31); 128.83 / 128.18 (C3); 128.13, 128.04 (C28, C29); 114.52 / 113.54 (C6); 113.42 / 112.87 (C2); 73.55 / 73.27 (<u>C</u>(CH$_3$)$_3$); 71.45 / 71.38 (C42); 70.49 / 70.32 (C8); 70.39-69.83 (C34-36); 60.69 / 59.80 (C11); 51.53 / 47.51 (C7); 49.05 / 47.48 (C10); 45.13 (C37); 43.53 (C9); 39.53 (C33); 33.24 / 33.19 (C13); 32.62 (C38); 32.05, 30.04-29.54, 22.82 (C15-26); 29.49 (C41); 27.55 / 27.46 (C(<u>C</u>H$_3$)$_3$); 26.79 (C39); 25.54 (C40); 25.40 (C14); 14.25 (C27). **HRMS (ESI$^+$):** *m/z* calcd. for $[C_{48}H_{79}N_3O_8Cl]^+$: 860.5556, found: 860.5551 ($[M+H]^+$).

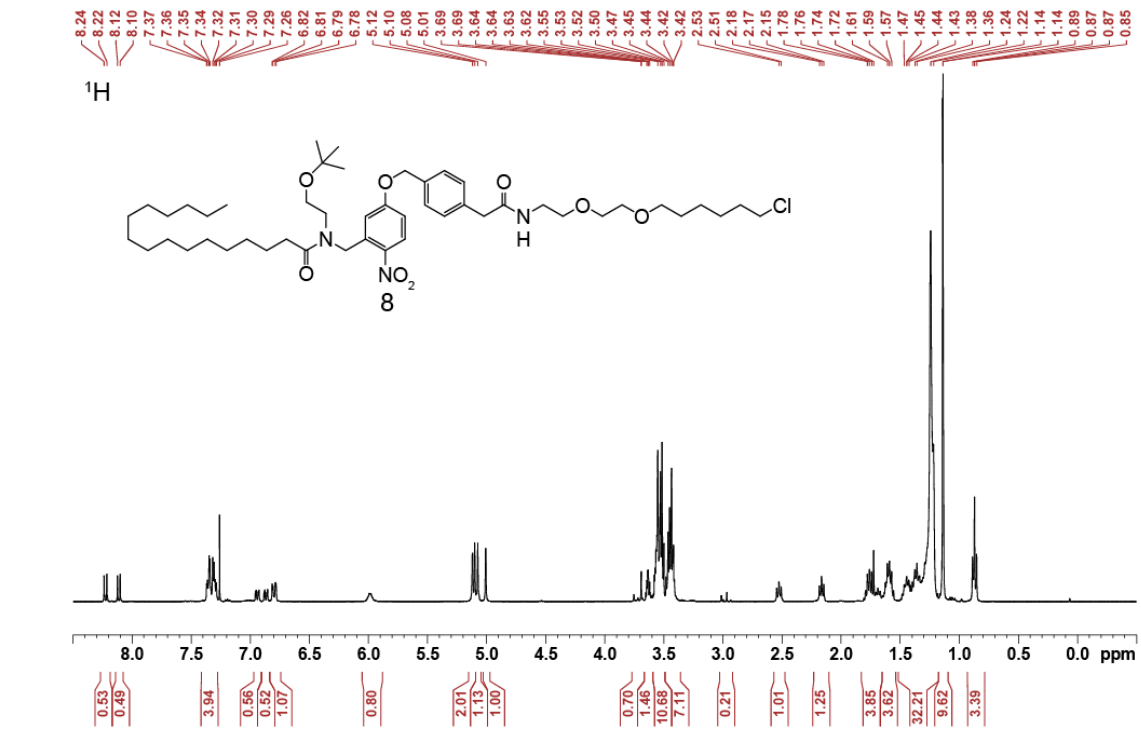
8.24
8.22
8.12
8.10
7.37
7.36
7.35
7.34
7.32
7.31
7.30
7.29
7.26
6.82
6.81
6.79
6.78
5.12
5.10
5.08
5.01
3.69
3.69
3.64
3.64
3.63
3.62
3.55
3.53
3.52
3.50
3.47
3.45
3.44
3.42
3.42
2.53
2.51
2.18
2.17
2.15
1.78
1.76
1.74
1.72
1.61
1.59
1.57
1.47
1.45
1.44
1.43
1.38
1.36
1.24
1.22
1.14
1.14
0.89
0.87
0.87
0.85
1H
Cl
NO2
8
8.0
7.5
7.0
6.5
6.0
5.5
5.0
4.5
4.0
3.5
3.0
2.5
2.0
1.5
1.0
0.5
0.0
ppm
0.53
0.49
3.94
0.56
0.52
1.07
0.80
2.01
1.13
1.00
0.70
1.46
10.68
7.11
0.21
1.01
1.25
3.85
3.62
32.21
9.62
3.39

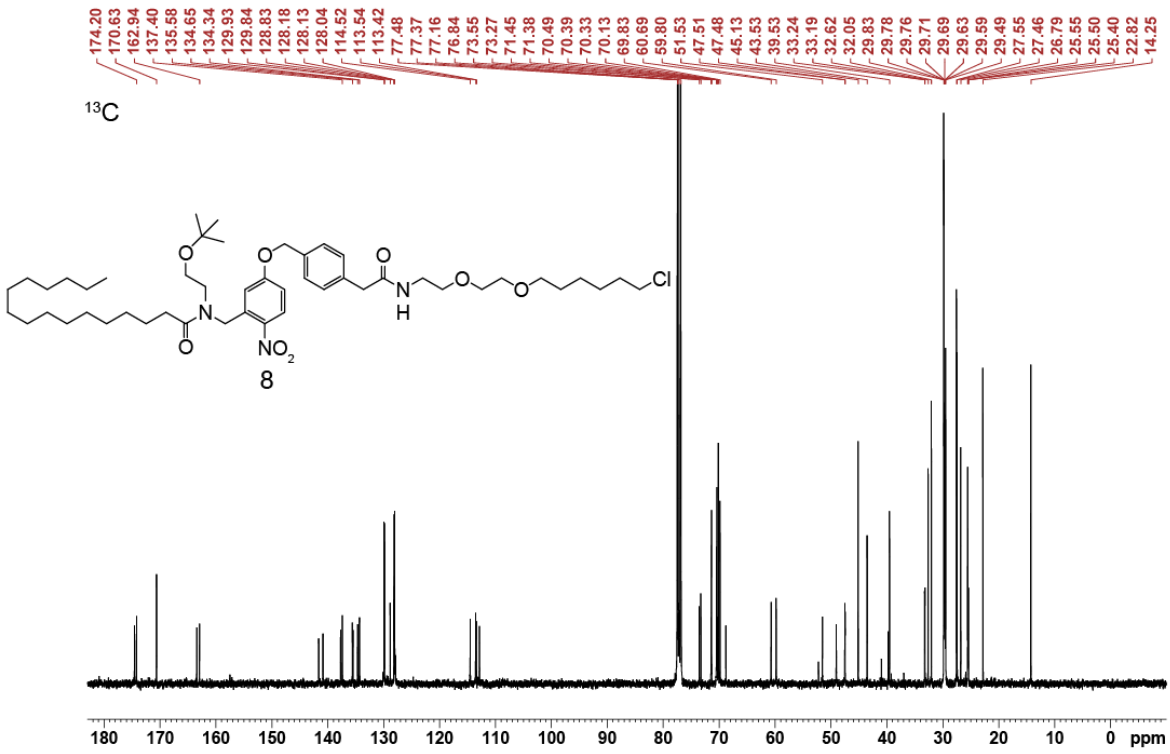
174.20
170.63
162.94
137.40
135.58
134.65
134.34
129.93
129.84
128.83
128.18
128.13
128.04
114.52
113.54
113.42
77.48
77.37
77.16
76.84
73.55
73.27
71.45
71.38
70.49
70.39
70.33
70.13
69.83
60.69
59.80
51.53
47.51
47.48
45.13
43.53
39.53
33.24
33.19
32.62
32.05
29.83
29.78
29.76
29.71
29.69
29.63
29.59
29.49
27.55
27.46
26.79
25.55
25.50
25.40
22.82
14.25
13C
Cl
NO2
8
180
170
160
150
140
130
120
110
100
90
80
70
60
50
40
30
20
10
0
ppm

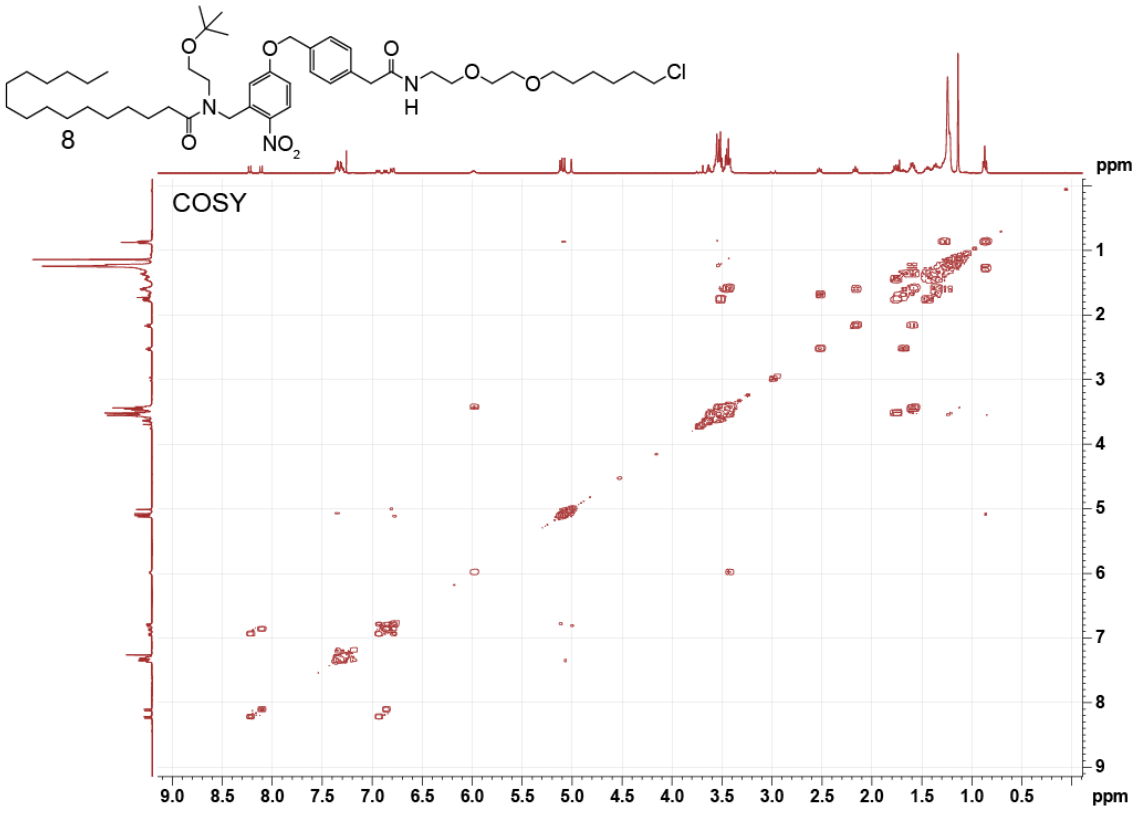
8
O
O
N
H
O
O
Cl
O
O
N
O
NO2
COSY
ppm
1
2
3
4
5
6
7
8
9
9.0
8.5
8.0
7.5
7.0
6.5
6.0
5.5
5.0
4.5
4.0
3.5
3.0
2.5
2.0
1.5
1.0
0.5
ppm

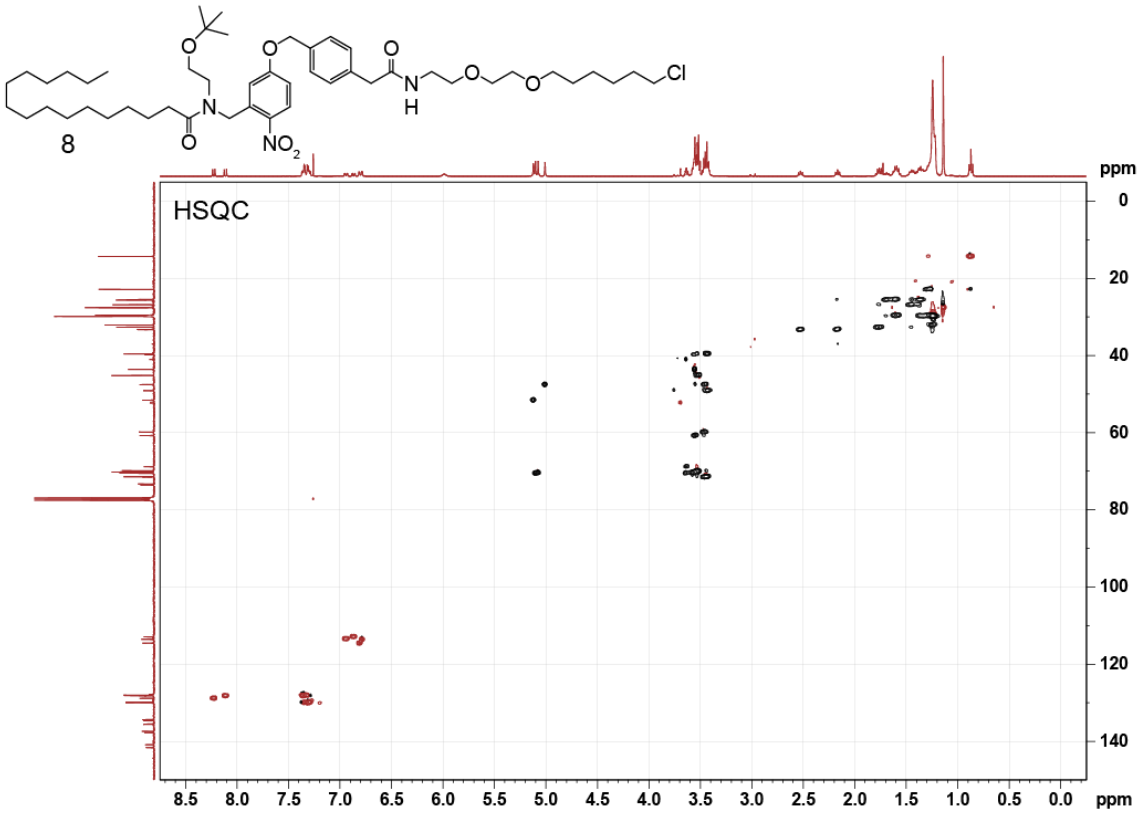
8
O
O
N
H
O
O
Cl
O
O
N
O
NO2
HSQC
ppm
0
20
40
60
80
100
120
140
8.5
8.0
7.5
7.0
6.5
6.0
5.5
5.0
4.5
4.0
3.5
3.0
2.5
2.0
1.5
1.0
0.5
0.0
ppm

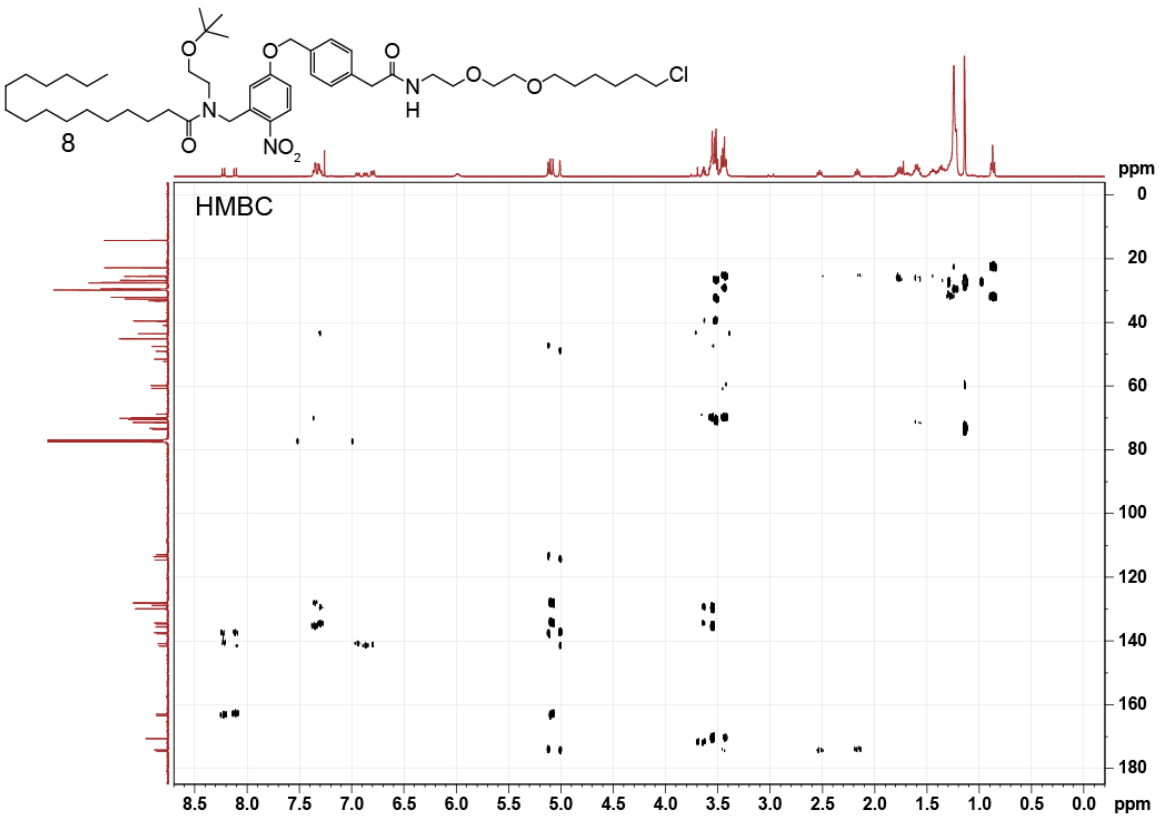
8
HMBC
ppm
0
20
40
60
80
100
120
140
160
180
8.5
8.0
7.5
7.0
6.5
6.0
5.5
5.0
4.5
4.0
3.5
3.0
2.5
2.0
1.5
1.0
0.5
0.0
ppm

### 3.5.6. Synthesis of *N*-(5-((4-(2-((2-(2-((6-chlorohexyl)oxy)ethoxy)ethyl)amino)-2-oxoethyl)benzyl)oxy)-2-nitrobenzyl)-*N*-(2-hydroxyethyl)palmitamide (hOCT-PEA2)

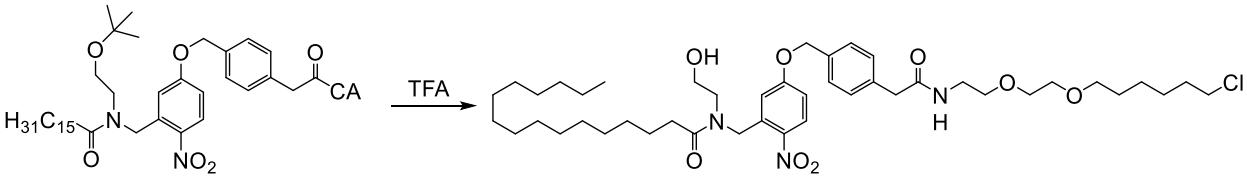


***N*-(2-(*tert*-butoxy)ethyl)-*N*-(5-((4-(2-((2-(2-((6-chlorohexyl)oxy)ethoxy)ethyl) amino)-2-oxoethyl)benzyl)oxy)-2-nitrobenzyl)palmitamide** (**8**, 26 mg, 0.030 mmol, 1.0 equiv.) was placed under an argon atmosphere and then TFA (0.50 ml, 6.7 mmol, excess) was added. The reaction continued for 2 h at RT, then the solvent was removed *in vacuo*. The crude product was re-dissolved in DCM, and the solvent was removed *in vacuo,* 3×, to remove residual TFA. The crude product was purified via $SiO_2$ flash chromatography (MeOH:DCM 1:99 → MeOH:DCM 1:19). ***N*-(5-((4-(2-((2-(2-((6-chlorohexyl)oxy)ethoxy)ethyl)amino)-2-oxoethyl)benzyl)oxy)-2-nitrobenzyl)-*N*-(2-hydroxyethyl)palmitamide** (**hOCT-PEA2**, 23 mg, 0.029 mmol, 97%) was isolated as a yellow oil.

**TLC (MeOH:DCM 1:19): $R_f$ =** 0.30. **$^1$H NMR ($CDCl_3$, 400 MHz, 25 °C): δ** 8.24 (d, 0.7 H, H3, *J* = 9.1 Hz); 8.12 (d, 0.3 H, H3, *J* = 9.1 Hz); 7.39-7.27 (m, 4 H, H28-31); 7.00 (dd, 0.7 H, H2, *J* = 9.1, 2.7 Hz); 6.94 (dd, 0.3 H, H2, *J* = 9.1, 2.7 Hz); 6.79 (d, 0.7 H, H6, *J* = 2.6 Hz); 6.55 (d, 0.3 H, H6, *J* = 2.6 Hz); 6.30 + 6.14 (br, 1 H, NH); 5.19 (s, 0.6 H, $H8_A$); 5.17 (s, 1.3 H, $H8_{A,B}$); 4.98 (s, 1.3 H, $H7_{A,B}$); 4.92 (s, 0.7, $H7_B$); 3.69 (t, 1.4 H, $H11_{A,B}$, *J* = 5.4 Hz); 3.63-3-49 (m, 10 H, $H9_{A,B}$ + H33-36); 3.49-3.33 (m, 6 H, $H11_B$ + $H10_{A,B}$ + $H33_{A,B}$ + $H37_{A,B}$ + $H42_{A,B}$); 3.14 (t, 0.7 H, $H10_B$, *J* = 6.7 Hz); 2.43 (t, 0.9 H, $H13_A$, *J* = 7.6 Hz); 2.18 (t, 2 H, OH + $H13_B$, *J* = 7.5 Hz); 1.81-1.72 (m, 2 H, $H38_{A,B}$); 1.72-1.65 (m, 0.7 H, $H14_A$); 1.65-1.55 (m, 3.6 H, $H14_{A,B}$ + $H41_{A,B}$); 1.51-1.18 (m, 30 H, $H39_{A,B}$ + $H40_{A,B}$ + H15-26); 0.87 (t, 3 H, $H27_{A,B,C}$, *J* = 6.8 Hz). **$^{13}$C NMR ($CDCl_3$, 101 MHz, 25 °C): δ** 176.04 (C12); 174.20, 171.06 / 170.71 (C32); 163.49 / 162.60 (C1); 140.70 (C4);

137.19 / 136.85 (C5); 135.61 (C44); 135.23; 135.18 / 134.35 (C43); 130.01 (C30 + C31); 128.91 / 128.13 (C3); 127.73 (C28, C29); 126.99; 115.14 / 114.71 (C2); 112.97 / 112.93 (C6); 71.38 (C42); 70.59 / 70.07 (C8); 70.35 / 70.11 / 69.86 / 69.76 (C34-36); 61.64 / 59.93 (C11); 51.47 / 48.13 (C7); 50.30 (C10); 45.17 (C37); 43.42 / 43.17 (C9); 39.65 / 39.57 (C33); 33.20 (C13); 32.64 (C38); 32.06, 29.84, 29.82, 29.79, 29.76, 29.64, 29.50, 22.84 (C15-26); 29.57 (C41); 26.81 (C39); 25.54 (C40); 25.27 (C14); 14.26 (C27). **HRMS (ESI$^+$):** *m/z* calcd. for $[C_{44}H_{71}N_3O_8Cl]^+$: 804.4930, found: 804.4916 ($[M+H]^+$).

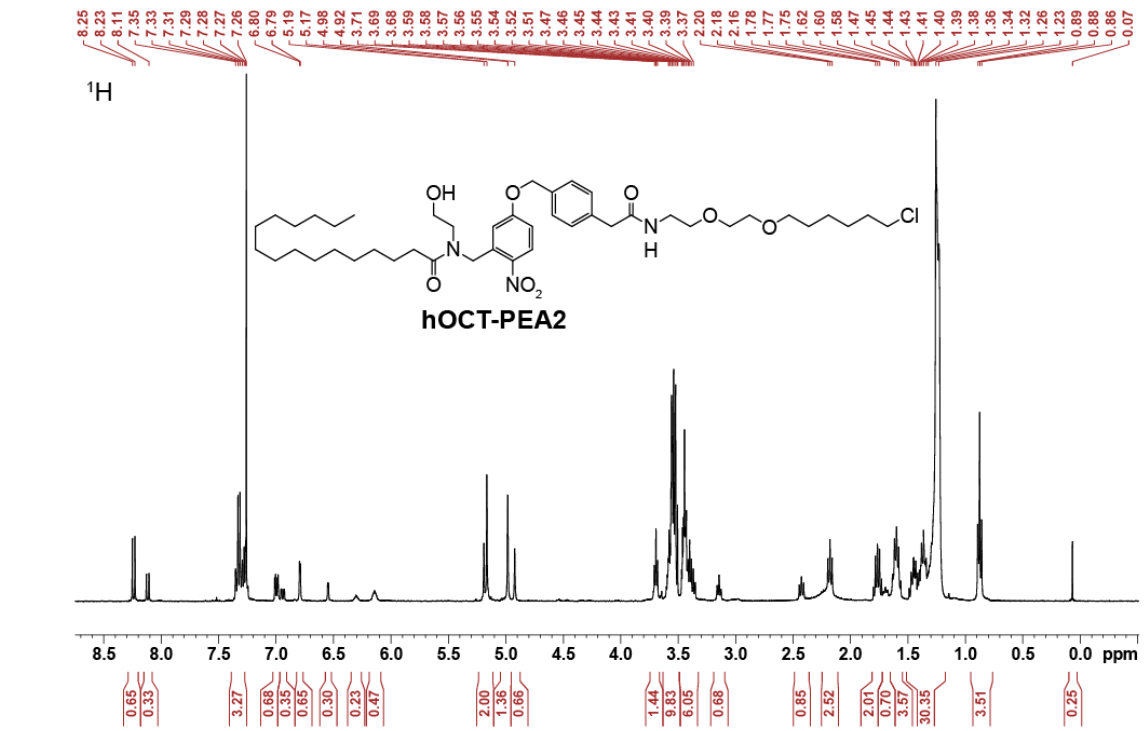
8.25 8.23 8.11 7.35 7.33 7.31 7.29 7.28 7.27 7.26 6.80 6.79 5.19 5.17 4.98 4.92 3.71 3.69 3.68 3.59 3.58 3.57 3.56 3.55 3.54 3.52 3.51 3.47 3.46 3.45 3.44 3.43 3.41 3.40 3.39 3.37 2.20 2.18 2.16 1.78 1.77 1.75 1.62 1.60 1.58 1.47 1.45 1.44 1.43 1.41 1.40 1.39 1.38 1.36 1.34 1.32 1.26 1.23 0.89 0.88 0.86 0.07
1H
OH
O
O
N
O
O
O
O
N
H
Cl
NO2
hOCT-PEA2
8.5 8.0 7.5 7.0 6.5 6.0 5.5 5.0 4.5 4.0 3.5 3.0 2.5 2.0 1.5 1.0 0.5 0.0 ppm
0.65 0.33 3.27 0.68 0.35 0.65 0.30 0.23 0.47 2.00 1.36 0.66 1.44 9.83 6.05 0.68 0.85 2.52 2.01 0.70 3.57 30.35 3.51 0.25

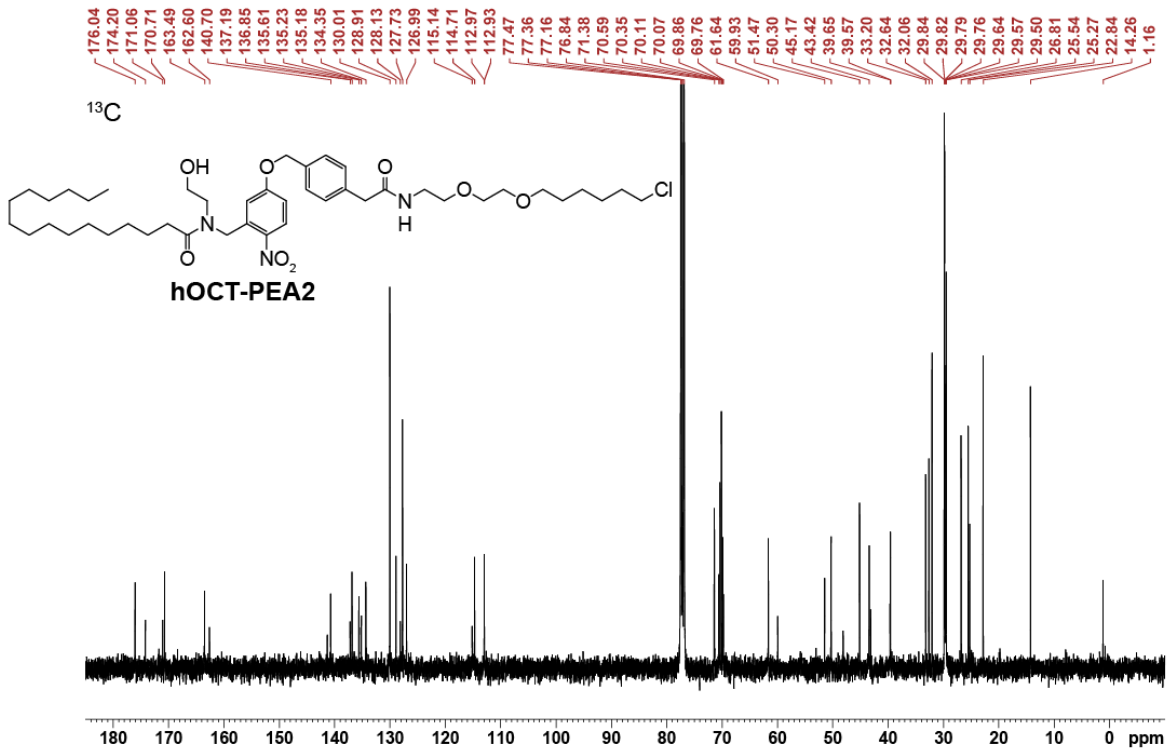
176.04 174.20 171.06 170.71 163.49 162.60 140.70 137.19 136.85 135.61 135.23 135.18 134.35 130.01 128.91 128.13 127.73 126.99 115.14 114.71 112.97 112.93 77.47 77.36 77.16 76.84 71.38 70.59 70.35 70.11 70.07 69.86 69.76 61.64 59.93 51.47 50.30 45.17 43.42 39.65 39.57 33.20 32.64 32.06 29.84 29.82 29.79 29.76 29.64 29.57 29.50 26.81 25.54 25.27 22.84 14.26 1.16
13C
OH
O
O
N
O
O
O
O
N
H
Cl
NO2
hOCT-PEA2
180 170 160 150 140 130 120 110 100 90 80 70 60 50 40 30 20 10 0 ppm

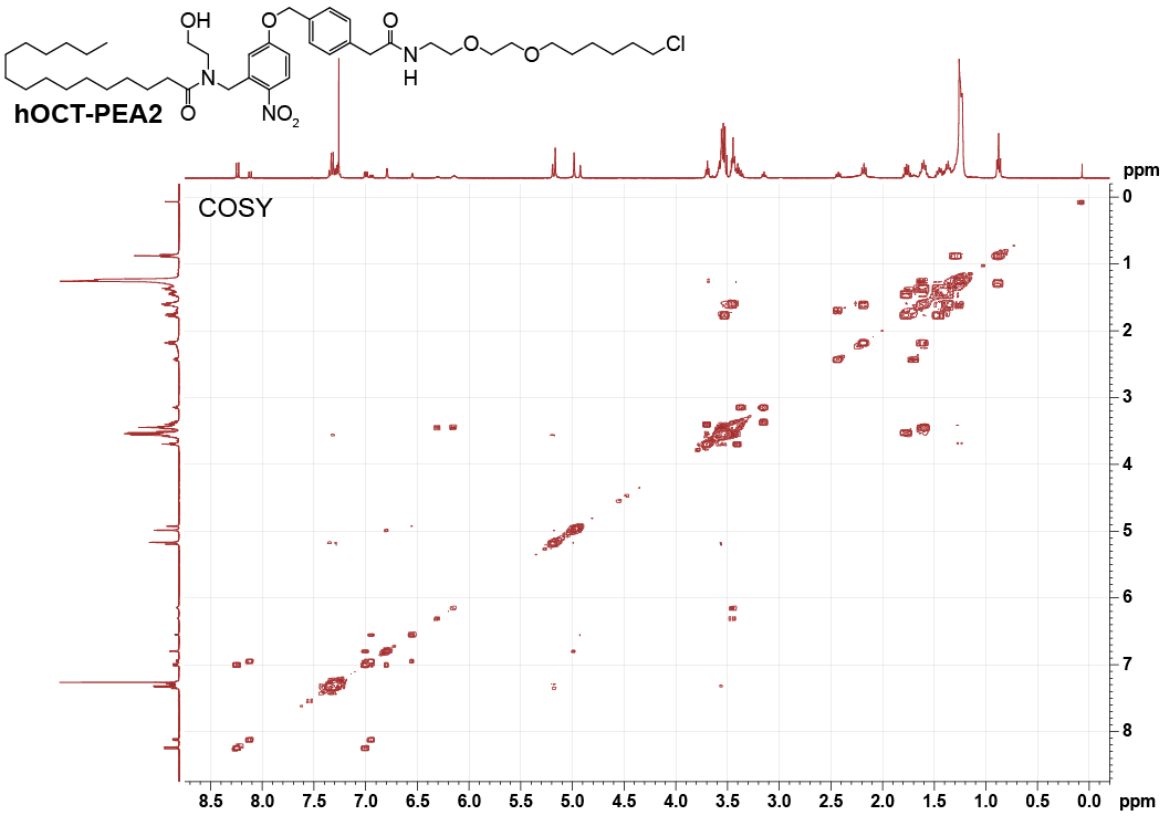
hOCT-PEA2
COSY
ppm

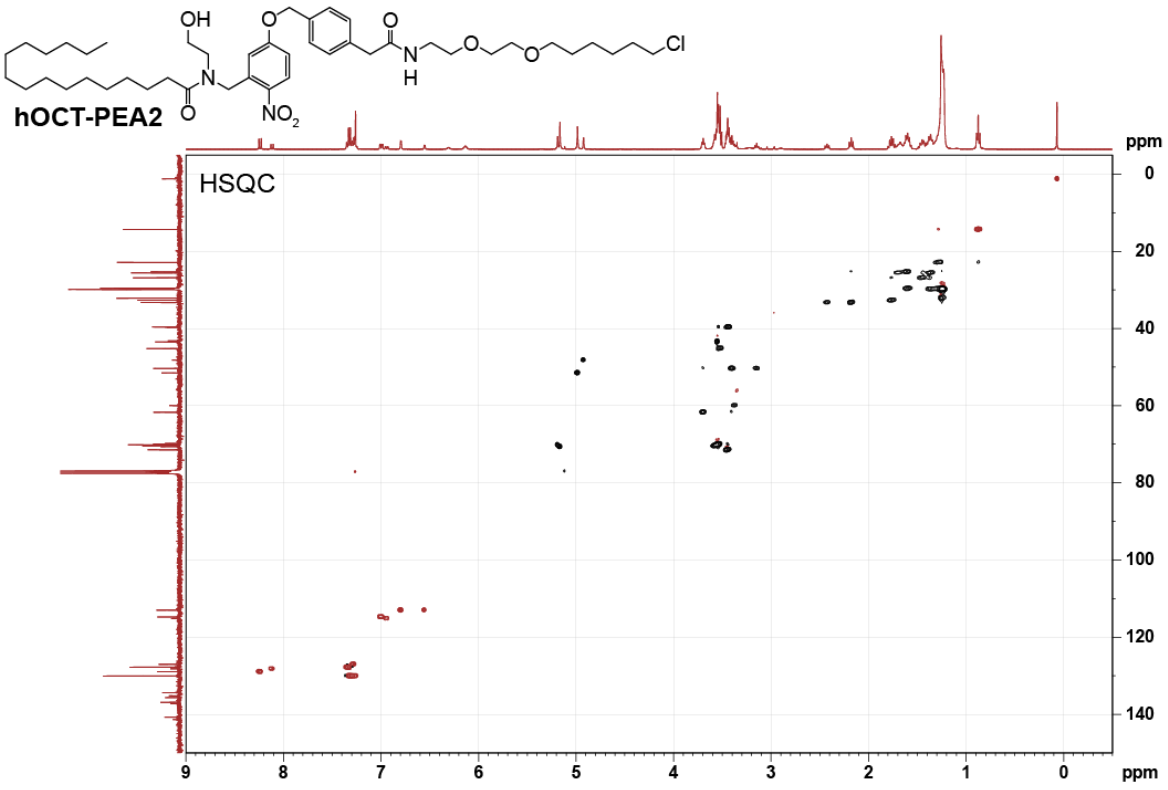
hOCT-PEA2
HSQC
ppm

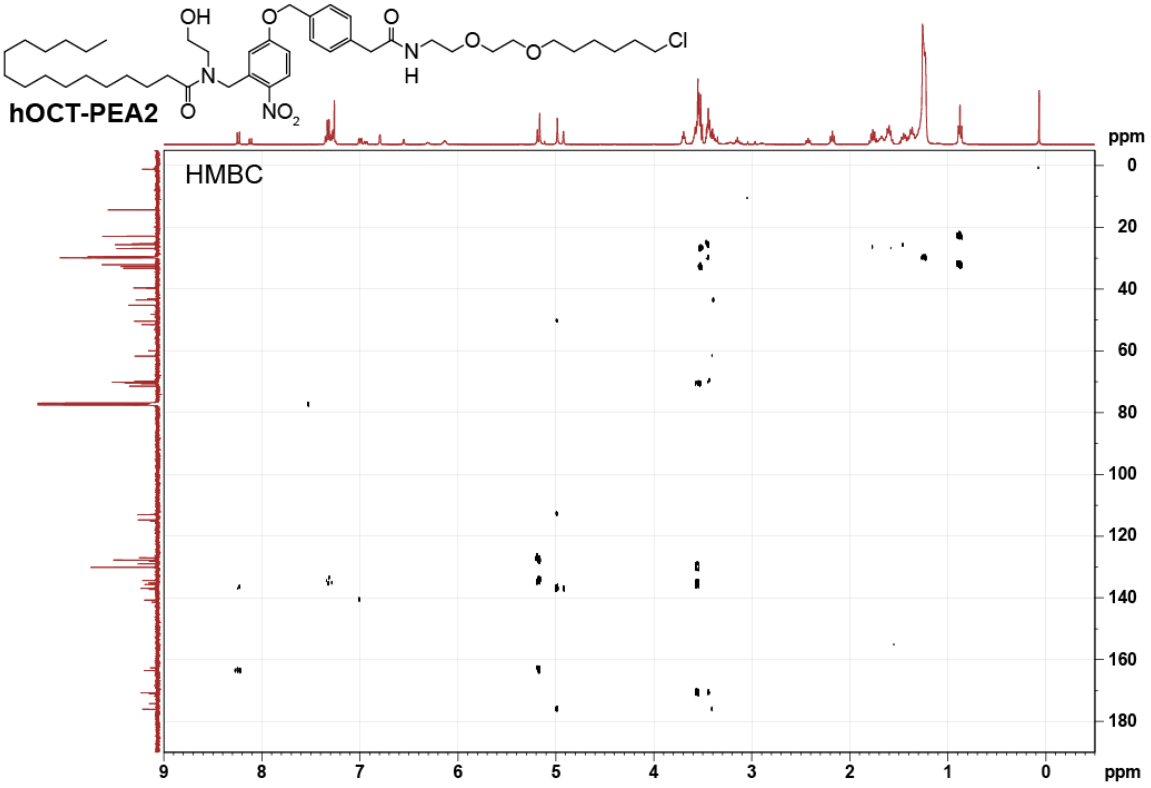
hOCT-PEA2
OH
O
O
N
H
Cl
N
O
O
NO2
HMBC
ppm
0
20
40
60
80
100
120
140
160
180
9
8
7
6
5
4
3
2
1
0
ppm

**A**

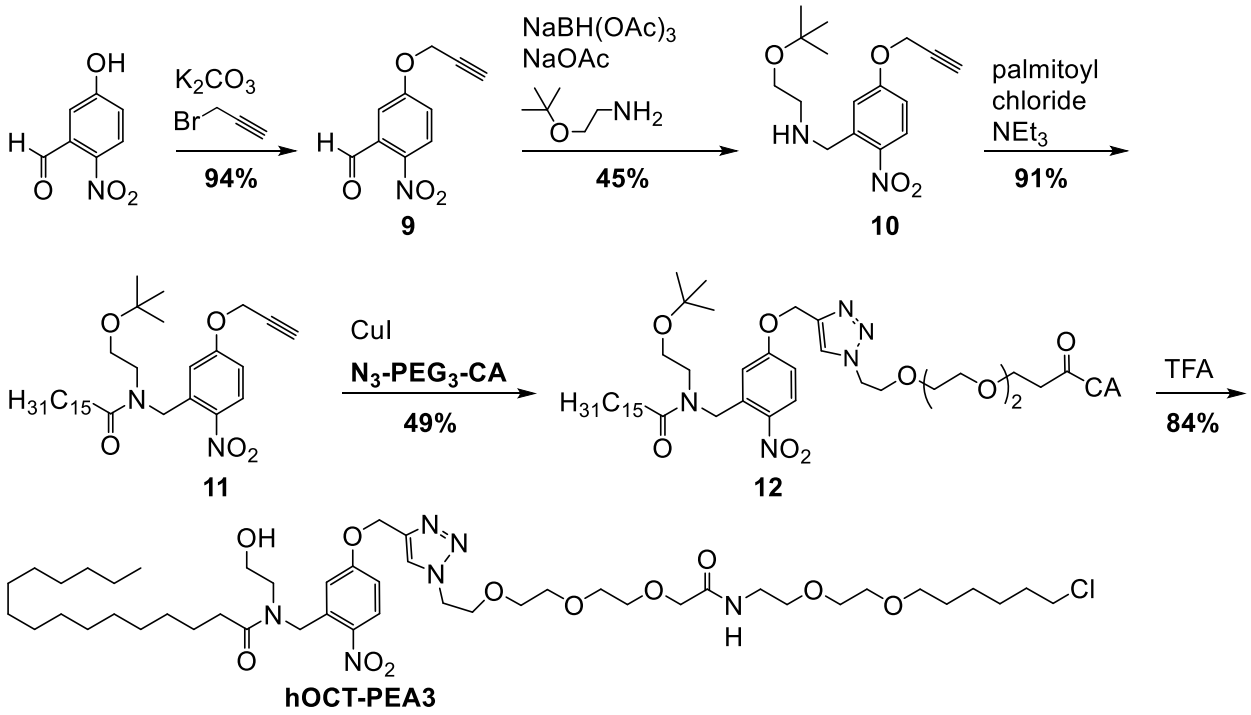


**B**

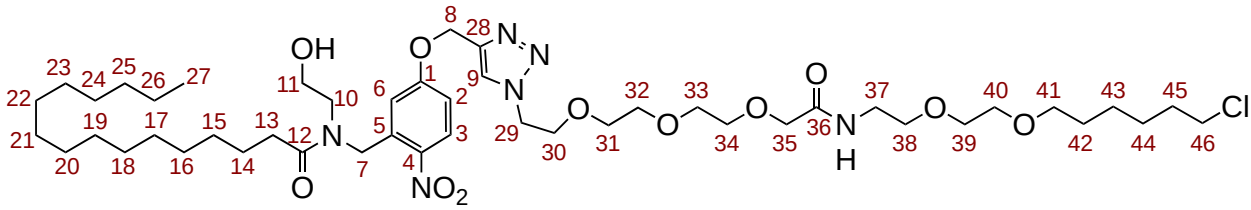


*Figure 3.16. Synthetic scheme of **hOCT-PEA3**.*

*(**A**) Chemical synthesis of **hOCT-PEA3**, which was prepared in 5 steps and 16% yield. (**B**) NMR atom numbering assignment for **hOCT-PEA3**.*

### 3.5.7. Synthesis of 2-(*tert*-butoxy)-*N*-(2-nitro-5-(prop-2-yn-1-yloxy)benzyl)ethan-1-amine (10)

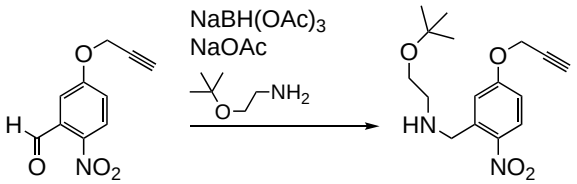


**9** **10**

**2-Nitro-5-(prop-2-yn-1-yloxy)benzaldehyde** (**9**) was prepared as described by Li et. al[88]. Aldehyde **9** (0.1001 g, 0.488 mmol, 1.0 equiv.), 2-*t*-butoxyethylamine (68.9 mg, 0.588 mmol, 1.2 equiv.), and NaOAc (40.3 mg, 0.491 mmol, 1.0 equiv.) were added to a reaction vial and placed under an argon atmosphere. The reaction mixture was dissolved in anhydrous DCE (2 ml), stirred for 1 h before adding $NaBH(OAc)_3$ (0.2577 g, 1.22 mmol, 2.5 equiv.) in one portion, and then stirred overnight. The reaction was diluted reaction with DCM (5 ml), quenched with saturated $NaHCO_3$ (5 ml), and transfered to a separatory funnel. The organic phase was washed 2× with saturated $NaHCO_3$ and once with brine. The organic phase was dried over anhydrous $MgSO_4$, filtered and the solvent was removed *in vacuo*. The crude product was purified by $SiO_2$ flash chromatography (EtOAc:Hexane 3:7→ EtOAc:Hexane 4:1). **2-(*tert*-butoxy)-*N*-(2-nitro-5-(prop-2-yn-1-yloxy)benzyl)ethan-1-amine** (**10**, 67.8 mg, 0.221 mmol, 45%) was isolated as a an oil.

**TLC (EtOAc:Hexane, 1:1 ): $R_f$ =** 0.25. **$^1$H NMR ($CDCl_3$, 400 MHz, 25 °C)**: δ 8.09 (d, 1 H, H3, *J* = 9.1 Hz); 7.31 (d, 1 H, H6, *J* = 2.8 Hz); 6.93 (dd, 1 H, H2, *J* = 9.1, 2.9 Hz); 4.79 (d, 2 H, $H8_{A,B}$, *J* = 2.4 Hz); 4.14 (s, 2 H, $H7_{A,B}$); 3.49 (t, 2 H, $H11_{A,B}$, *J* = 5.3 Hz); 2.77 (t, 2 H, $H10_{A,B}$, J = 5.3 Hz); 2.56 (t, 1 H, H9, *J* = 2.4 Hz); 1.91 (br, 1 H, N<u>H</u>); 1.20 (s, 9 H, $C(C\underline{H}_3)_3$). **$^{13}$C NMR ($CDCl_3$, 101 MHz, 25 °C)**: δ 161.35 (C1); 142.40 (C4); 139.86 (C5); 127.75 (C3); 116.21 (C6); 113.42 (C2); 77.36 (C28); 76.61 (C9); 72.97 ($\underline{C}(CH_3)_3$); 61.03 (C11); 56.25 (C8); 51.04 (C7); 49.57 (C10); 27.69 ($C(\underline{C}H_3)_3$).

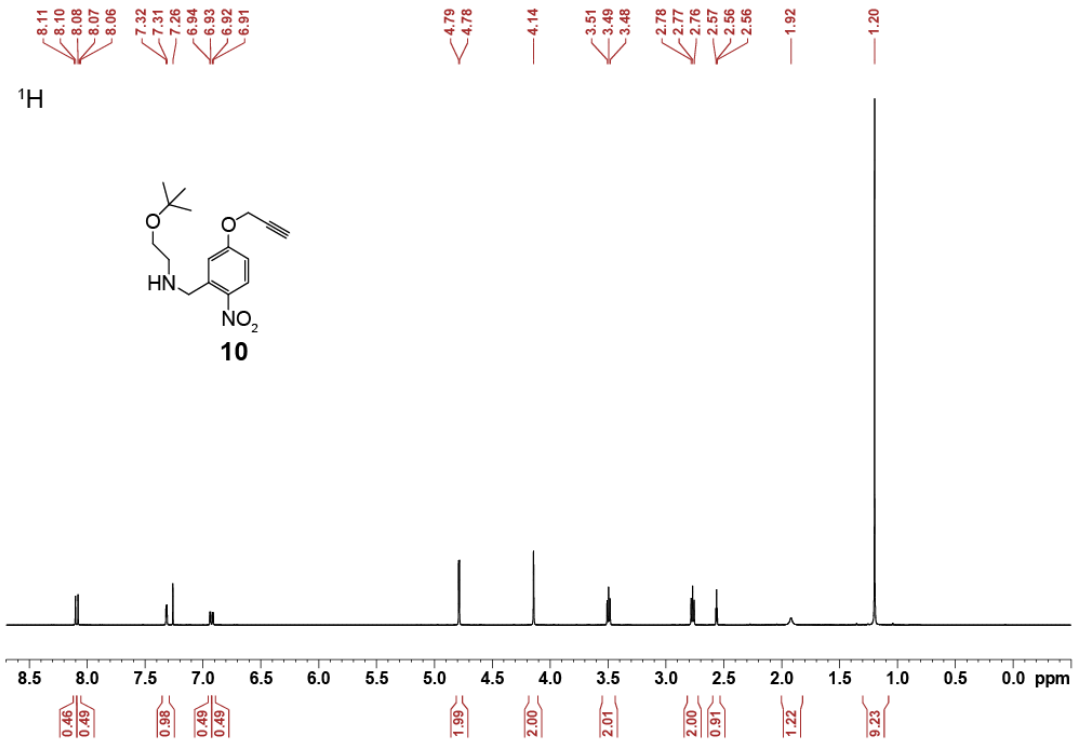
8.11
8.10
8.08
8.07
8.06
7.32
7.31
7.26
6.94
6.93
6.92
6.91
4.79
4.78
4.14
3.51
3.49
3.48
2.78
2.77
2.76
2.57
2.56
2.56
1.92
1.20
1H
O
O
HN
NO2
10
8.5 8.0 7.5 7.0 6.5 6.0 5.5 5.0 4.5 4.0 3.5 3.0 2.5 2.0 1.5 1.0 0.5 0.0 ppm
0.46
0.49
0.98
0.49
0.49
1.99
2.00
2.01
2.00
0.91
1.22
9.23

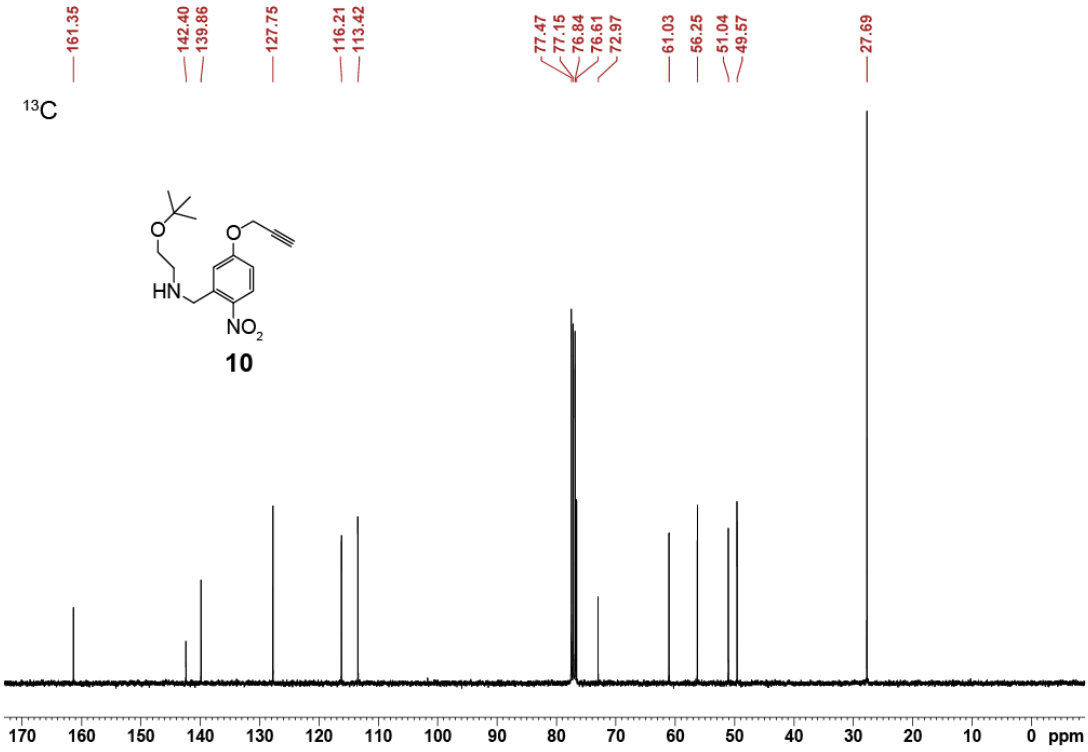
161.35
142.40
139.86
127.75
116.21
113.42
77.47
77.15
76.84
76.61
72.97
61.03
56.25
51.04
49.57
27.69
13C
O
O
HN
NO2
10
170 160 150 140 130 120 110 100 90 80 70 60 50 40 30 20 10 0 ppm

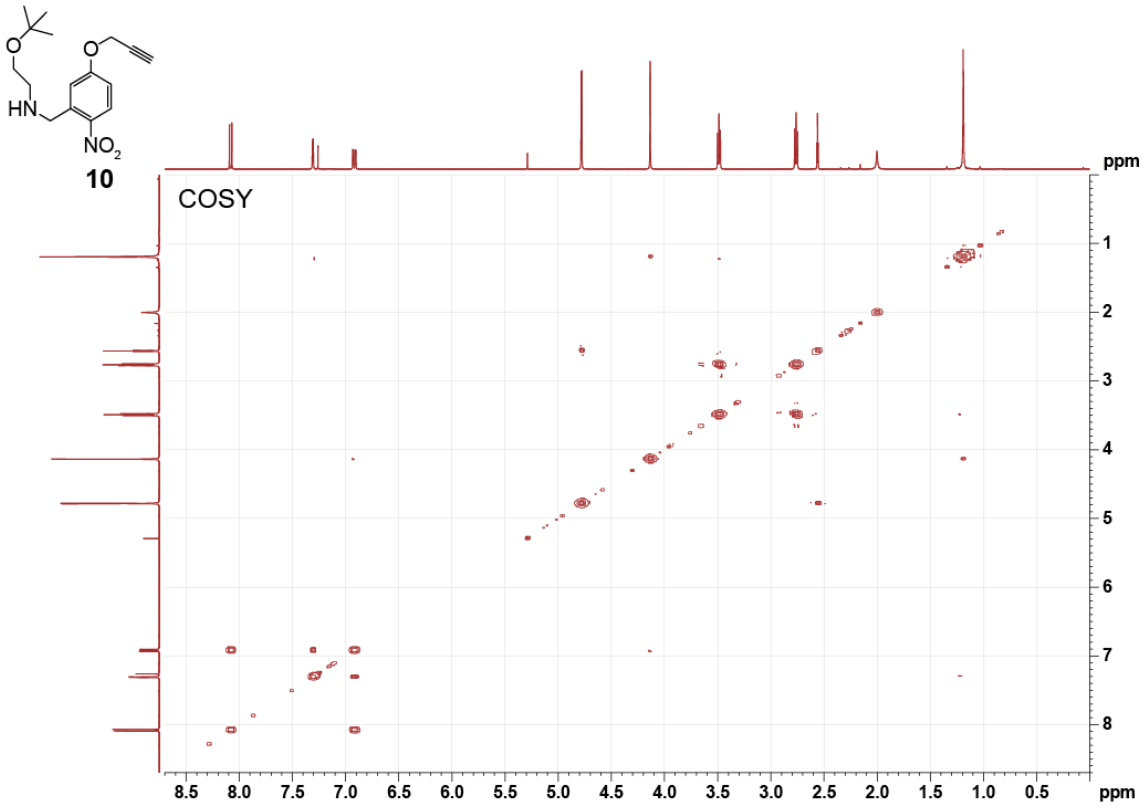
10
COSY
ppm
8.5 8.0 7.5 7.0 6.5 6.0 5.5 5.0 4.5 4.0 3.5 3.0 2.5 2.0 1.5 1.0 0.5
ppm
1 2 3 4 5 6 7 8

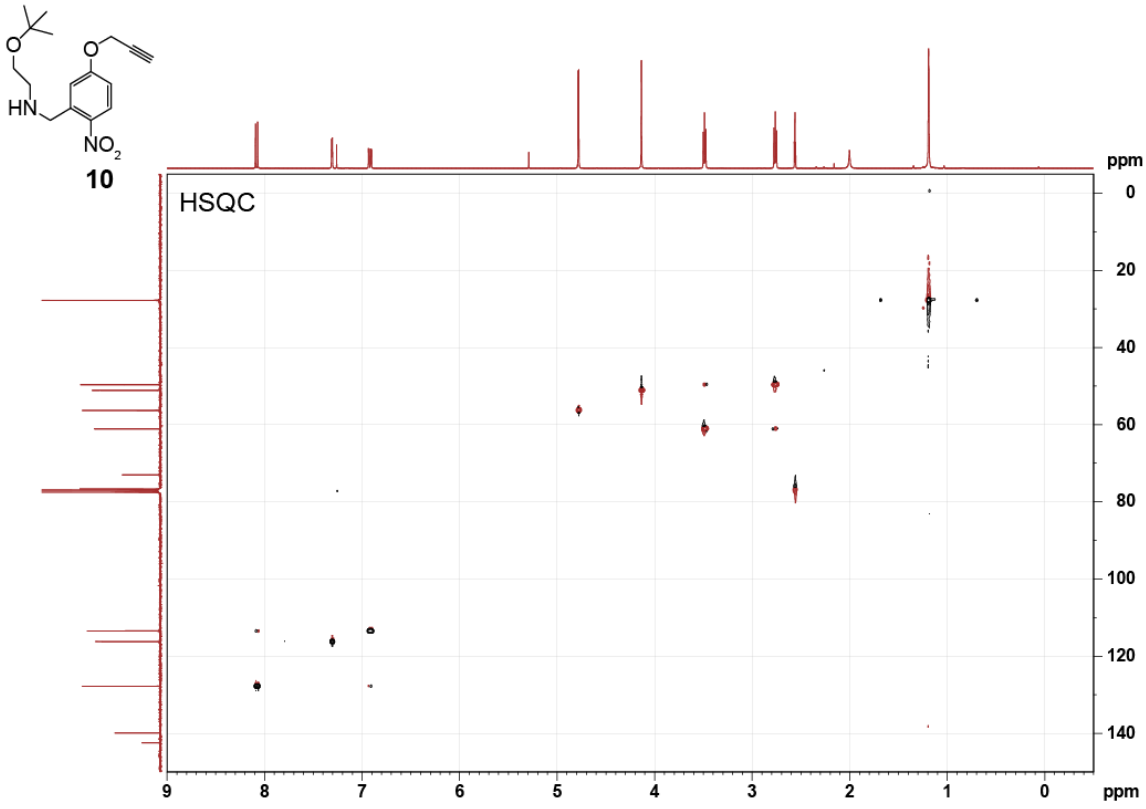
10
HSQC
ppm
9 8 7 6 5 4 3 2 1 0
ppm
0 20 40 60 80 100 120 140

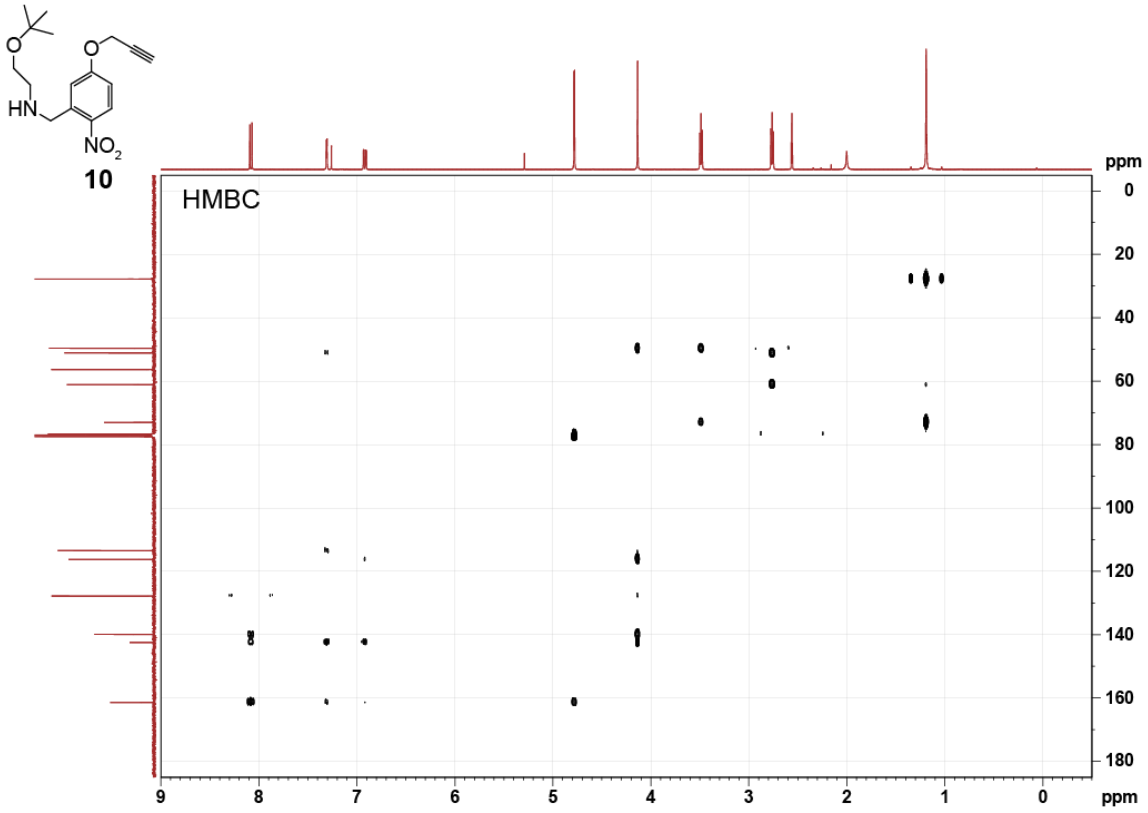
HN
NO2
10
HMBC
ppm
0
20
40
60
80
100
120
140
160
180
9
8
7
6
5
4
3
2
1
0
ppm

### 3.5.8. Synthesis of *N*-(2-(*tert*-butoxy)ethyl)-*N*-(2-nitro-5-(prop-2-yn-1-yloxy) benzyl)palmitamide (11)

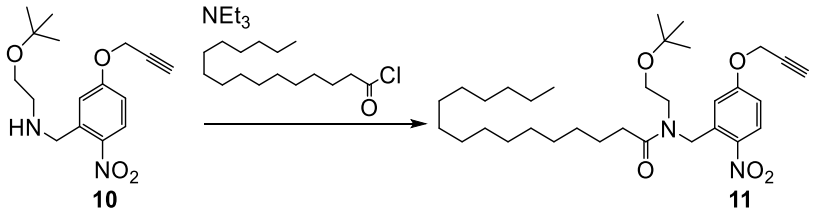


Palmitic acid (89.3 mg, 0.348 mmol, 3.0 equiv.) was placed under an argon atmosphere, dissolved in anhydrous DCE (7 ml), and oxalyl chloride (45 μl, 0.524 mmol, 4.4 equiv.) was added. A drop of anhydrous DMF was added to initiate the reaction. The reaction was stirred for 1 h at RT before the solvent was removed *in vacuo*. The crude product was re-dissolved in DCM 3×, then 2× in toluene, and the solvent was removed *in vacuo,* accordingly. The crude palmitoyl chloride was placed under an argon atmosphere and then dissolved in anhydrous DCE (2 ml).

Separately, **2-(*tert*-butoxy)-*N*-(2-nitro-5-(prop-2-yn-1-yloxy)benzyl) ethan-1-amine** (**10**, 36 mg, 0.12 mmol, 1.0 equiv.) was placed under an argon atmosphere and dissolved in anhydrous DCE (2.5 ml). The amine was transferred to the acid chloride solution, then $NEt_3$ (33 μl, 0.237 mmol, 2.0 equiv.) was added dropwise. After 90 min, the reaction was diluted in DCM (3 ml), and the reaction was quenched with saturated $NaHCO_3$. The organic phase was extracted, washed 2× with saturated aqueous $NaHCO_3$ and once with brine. $SiO_2$ gel was added to the crude product, and the solvent was removed *in vacuo*, then the product-containing $SiO_2$ gel was loaded onto a $SiO_2$ column (4.1 g) and purified by flash column chromatography (7.5% → 15% EtOAc / Hexane). ***N*-(2-(*tert*-butoxy)ethyl)-*N*-(2-nitro-5-(prop-2-yn-1-yloxy)benzyl)palmitamide** (**11**, 57.4 mg, 0.105 mmol, 91%) was isolated as a yellow oil.

**TLC (EtOAc:Hexane, 1:4): $R_f$ =** 0.28. **$^1$H NMR ($CDCl_3$, 400 MHz, 25 °C):** δ 8.25 (d, 0.5 H, H3, *J* = 9.1 Hz); 8.14 (d, 0.5 H, H3, *J* = 9.1 Hz); 6.98 (dd, 0.5 H, H2, *J* = 9.1, 2.8 Hz); 6.92 (dd, 0.5 H,

H2, *J* = 9.1, 2.8 Hz); 6.85 (dd, 1 H, H6, J = 8.2, 2.7 Hz); 5.14 (s, 1 H, $H7_A$); 5.03 (s, 1 H, $H7_B$); 4.74 (dd, 2 H, $H8_{A,B}$, *J* = 11.2, 2.4 Hz); 3.61-3.45 (m, 4 H, $H10_{A,B}$ + $11_{A,B}$); 2.59-2.52 (m, 1.8 H, H9 + $H13_A$); 2.33 (t, 0.2 H, $H13_A$, *J* = 7.5 Hz); 2.20 (t, 1 H, $H13_B$, *J* = 7.5 Hz); 1.77-1.53 (m, 2 H, $H14_{A,B}$); 1.44-1.18 (m, 24 H, H15-26); 1.15 (d, 9 H, $C(C\underline{H}_3)_3$, *J* = 4.1 Hz); 0.92-0.81 (m, 3 H, $H27_{A,B,C}$). **$^{13}$C NMR ($CDCl_3$, 101 MHz, 25 °C):** δ 174.58 / 174.22 (C12); 162.17 / 161.70 (C1); 142.02 / 141.35 (C4); 137.70 / 137.38 (C5); 128.67 / 128.09 (C3); 114.42 / 113.85 (C6); 113.48 / 113.03 (C2); 73.61 / 73.30 ($\underline{C}(CH_3)_3$); 60.80 / 59.85 (C11); 56.41 / 56.23 (C8); 51.52 (C7); 47.60 / 47.56 (C10); 33.30 / 33.23 (C13); 32.06, 30.03-29.28, 22.83 (C15-26); 27.56 / 27.47 ($C(\underline{C}H_3)_3$); 25.54 / 25.39 (C14); 14.26 (C27). **HRMS (ESI$^+$):** *m/z* calcd. for $[C_{32}H_{53}N_2O_5]^+$: 545.3954, found: 545.3945 ($[M+H]^+$).

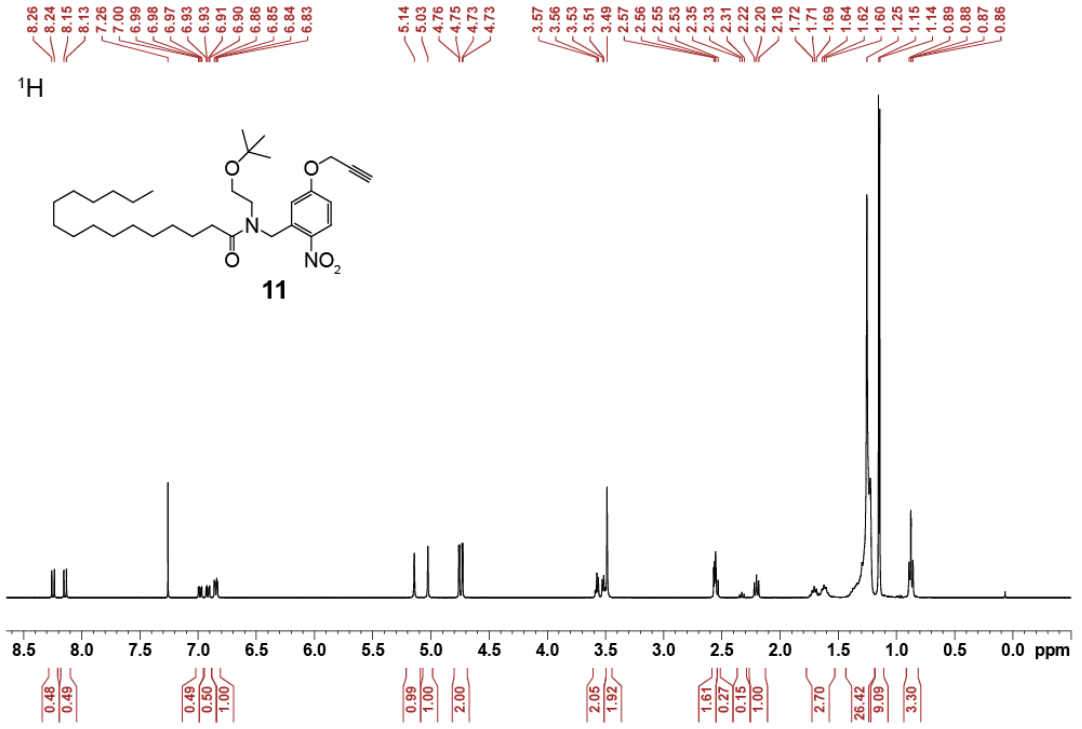
8.26
8.24
8.15
8.13
7.26
7.00
6.99
6.98
6.97
6.93
6.93
6.91
6.90
6.86
6.85
6.84
6.83
5.14
5.03
4.76
4.75
4.73
4.73
3.57
3.56
3.53
3.51
3.49
2.57
2.56
2.55
2.53
2.35
2.33
2.31
2.22
2.20
2.18
1.72
1.71
1.69
1.64
1.62
1.60
1.25
1.15
1.14
0.89
0.88
0.87
0.86
1H
11
8.5 8.0 7.5 7.0 6.5 6.0 5.5 5.0 4.5 4.0 3.5 3.0 2.5 2.0 1.5 1.0 0.5 0.0 ppm
0.48
0.49
0.49
0.50
1.00
0.99
1.00
2.00
2.05
1.92
1.61
0.27
0.15
1.00
2.70
26.42
9.09
3.30

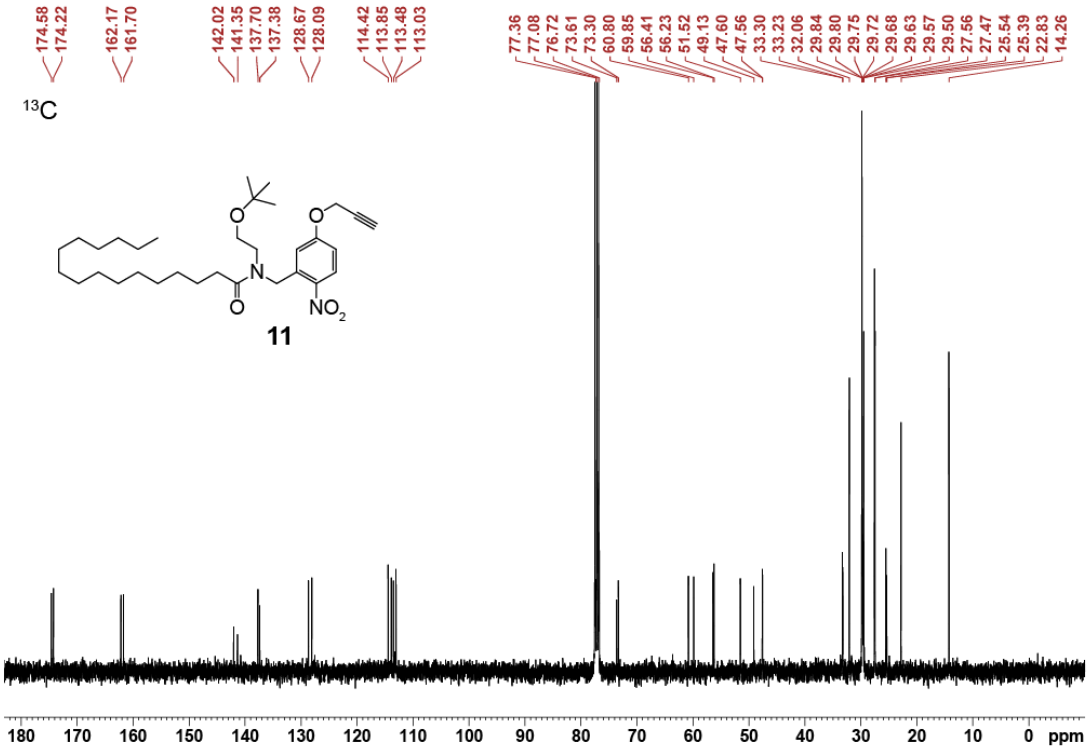
174.58
174.22
162.17
161.70
142.02
141.35
137.70
137.38
128.67
128.09
114.42
113.85
113.48
113.03
77.36
77.08
76.72
73.61
73.30
60.80
59.85
56.41
56.23
51.52
49.13
47.60
47.56
33.30
33.23
32.06
29.84
29.80
29.75
29.72
29.68
29.63
29.57
29.50
27.56
27.47
25.54
25.39
22.83
14.26
13C
11
180 170 160 150 140 130 120 110 100 90 80 70 60 50 40 30 20 10 0 ppm

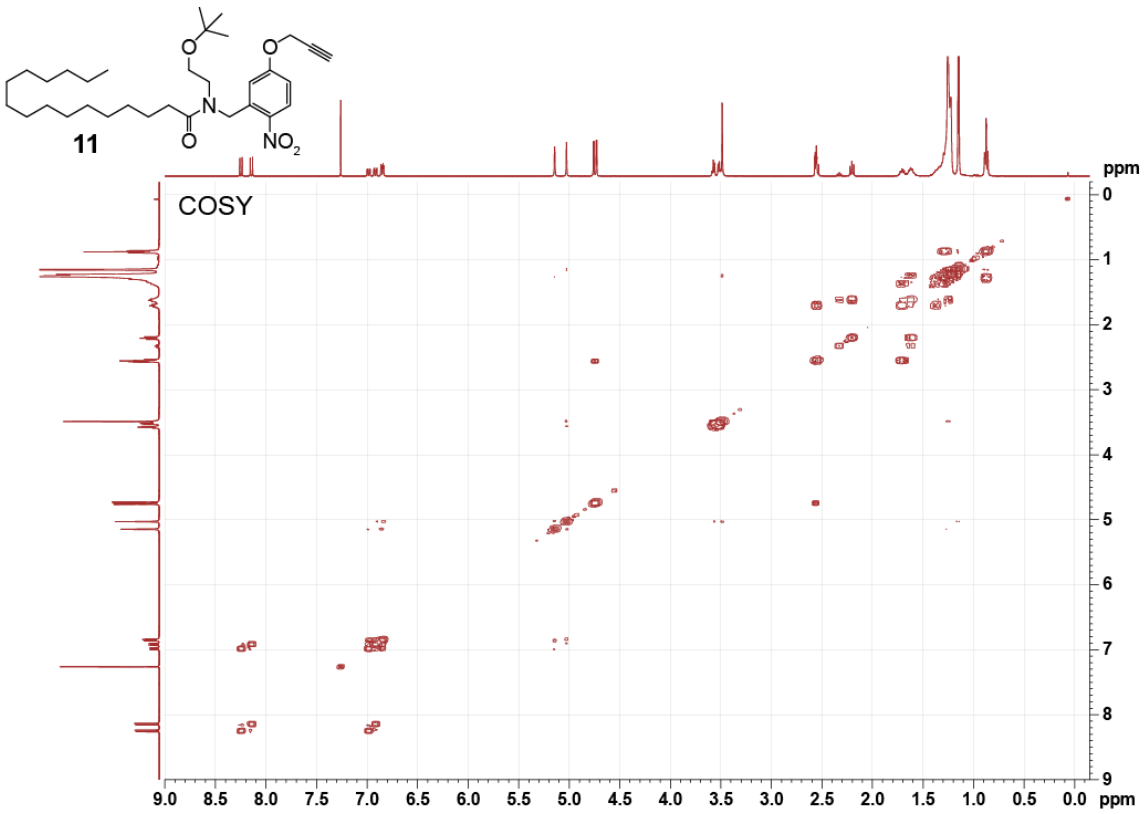
11
COSY
ppm
9.0 8.5 8.0 7.5 7.0 6.5 6.0 5.5 5.0 4.5 4.0 3.5 3.0 2.5 2.0 1.5 1.0 0.5 0.0 ppm
0 1 2 3 4 5 6 7 8 9

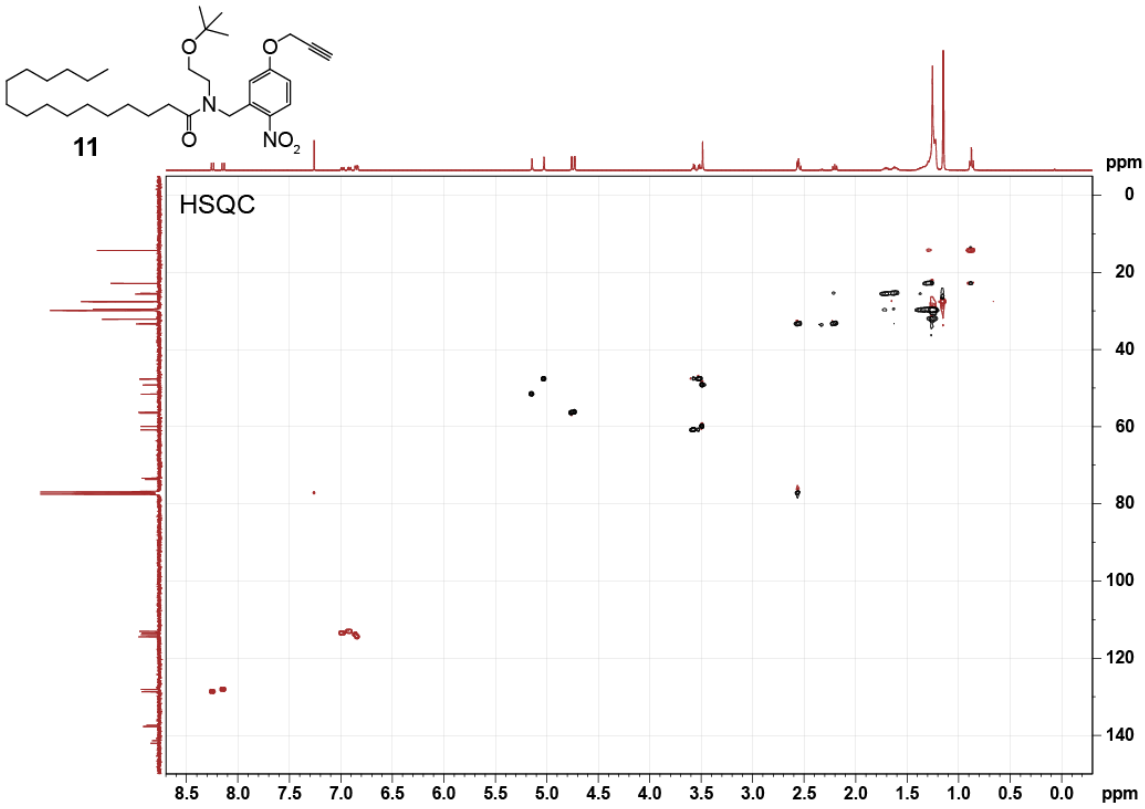
11
HSQC
ppm
8.5 8.0 7.5 7.0 6.5 6.0 5.5 5.0 4.5 4.0 3.5 3.0 2.5 2.0 1.5 1.0 0.5 0.0 ppm
0 20 40 60 80 100 120 140

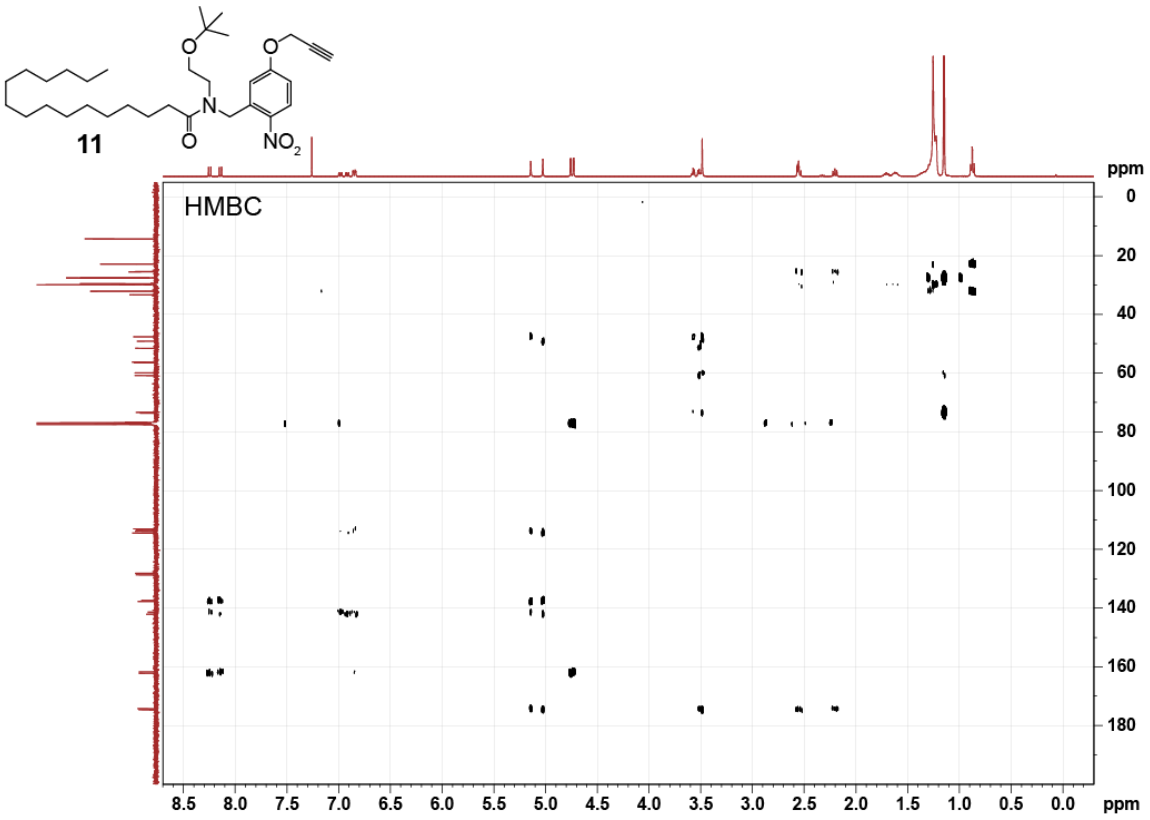
11
HMBC
ppm
0
20
40
60
80
100
120
140
160
180
8.5
8.0
7.5
7.0
6.5
6.0
5.5
5.0
4.5
4.0
3.5
3.0
2.5
2.0
1.5
1.0
0.5
0.0
ppm

### 3.5.9. Synthesis of 2-(2-(2-(2-azidoethoxy)ethoxy)ethoxy)-*N*-(2-(2-((6-chlorohexyl)oxy)ethoxy) ethyl)acetamide ($N_3$-$PEG_3$-CA)

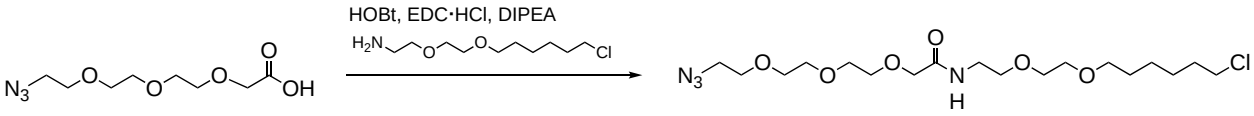


**$N_3$-$PEG_3$-CA**

HOBt (15.7 mg, 0.116 mmol, 1.5 equiv.) and EDC·HCl (22.6 mg, 0.118 mmol, 1.6 equiv.) were added to 11-azido-3,6,9-trioxaundecanoic acid (17.7 mg, 0.0759 mmol, 1.0 equiv.), and put under an argon atmosphere. The reaction was dissolved in anhydrous DMF (2 ml). Separately, **CA** (38.3 mg, 0.171 mmol, 2.3 equiv.) was placed under an argon atmosphere and dissolved in anhydrous DMF (1 ml). The amine was transferred to the acid reaction mixture, DIPEA (27 μl, 0.155 mmol, 2.0 equiv.) was added, and the reaction stirred at RT for 5.5 h. The reaction was directly loaded onto a C18 reverse phase column and purified by flash chromatography (MeOH:$H_2O$ 1:1 → MeOH:$H_2O$ 4:1), followed by $SiO_2$ flash column chromatography (MeOH:DCM 1:99 → MeOH:DCM 1:19). **2-(2-(2-(2-azidoethoxy)ethoxy) ethoxy)-*N*-(2-(2-((6-chlorohexyl)oxy)ethoxy)ethyl)acetamide** (**$N_3$-$PEG_3$-CA**, 21.3 mg, 0.0485 mmol, 64% yield) was isolated as a yellow oil.

**TLC (MeOH:DCM, 1:9): $R_f$ =** 0.54. **$^1$H NMR ($CDCl_3$, 400 MHz, 25 °C)**: δ 7.12 (br, 1 H, NH); 4.00 (s, 2 H, $H35_{A,B}$); 3.68 (s, 10 H, H30-34); 3.63-3.48 (m, 10 H, H37-41); 3.45 (t, 2 H , $H46_{A,B}$, *J* = 6.65); 3.39 (t, 2 H , $H29_{A,B}$, *J* = 5.03); 1.77 (q, 2 H, $H42_{A,B}$, *J* = 7.09); 1.60 (q, 2 H, $H45_{A,B}$, *J* = 7.07); 1.51-1.31 (m, 4 H, $H43_{A,B}$ + $H44_{A,B}$). **$^{13}$C NMR ($CDCl_3$, 101 MHz, 25 °C)**: δ 170.08 (C36); 71.40 (C46); 71.09, 70.87, 70.82, 70.75, 70.59, 70.47 (C35, C30-34); 70.24, 70.19, 69.99 (C38-40); 50.82 (C29); 45.20 (C41); 38.75 (C37); 32.67 (C42); 29.62 (C45); 26.84 (C43); 25.58 (C44). **HRMS (ESI$^+$):** *m/z* calcd. for $[C_{18}H_{36}N_4O_6Cl]^+$: 439.2323, found: 439.2317 ($[M+H]^+$).

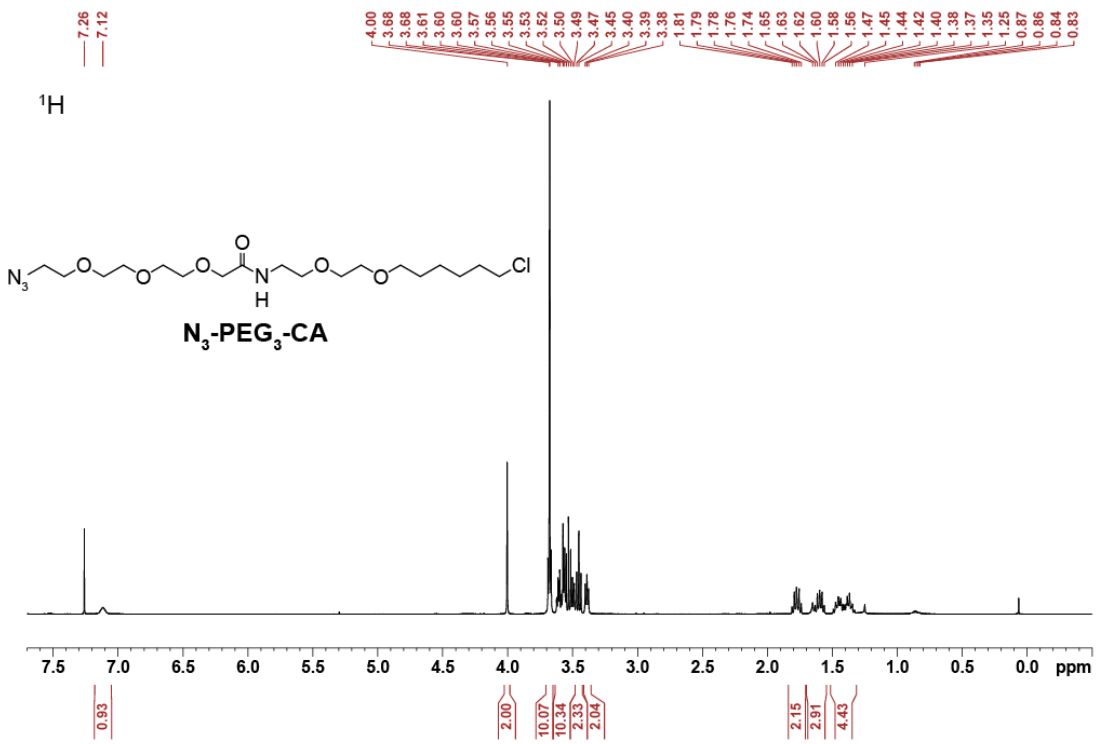
7.26
7.12
4.00
3.68
3.68
3.61
3.60
3.60
3.57
3.56
3.55
3.53
3.52
3.50
3.49
3.47
3.45
3.40
3.39
3.38
1.81
1.79
1.78
1.76
1.74
1.65
1.63
1.62
1.60
1.58
1.56
1.47
1.45
1.44
1.42
1.40
1.38
1.37
1.35
1.25
0.87
0.86
0.84
0.83
1H
N3
O
N
H
Cl
N3-PEG3-CA
7.5 7.0 6.5 6.0 5.5 5.0 4.5 4.0 3.5 3.0 2.5 2.0 1.5 1.0 0.5 0.0 ppm
0.93
2.00
10.07
10.34
2.33
2.04
2.15
2.91
4.43

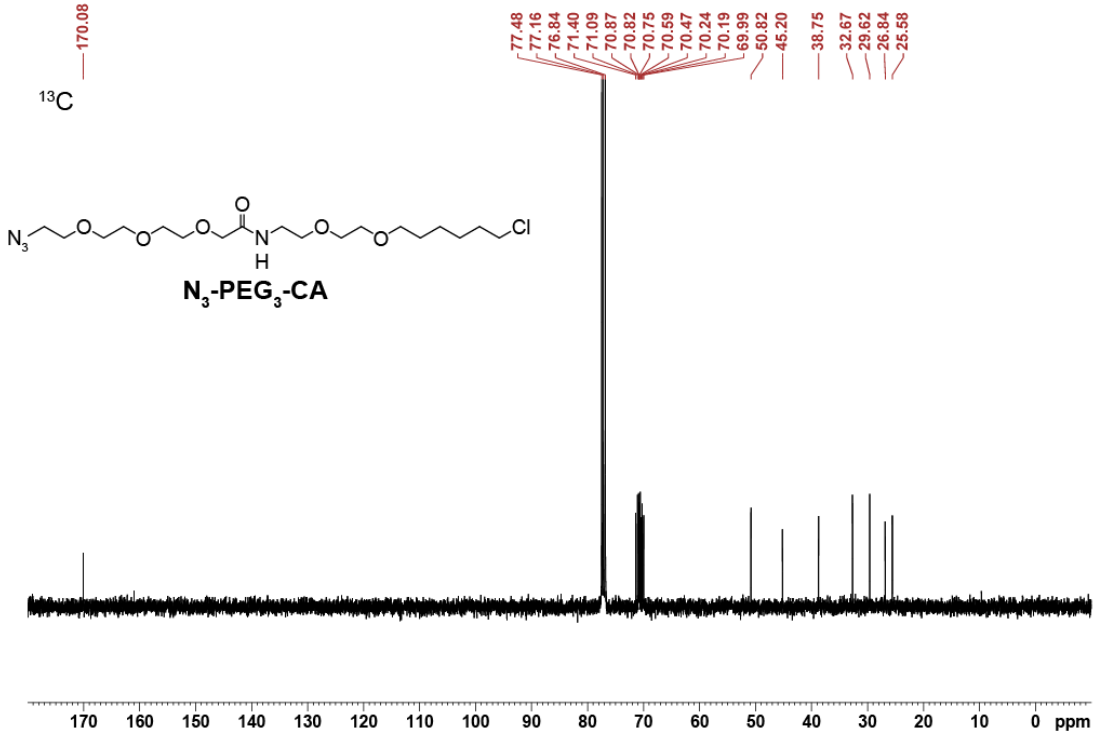
170.08
77.48
77.16
76.84
71.40
71.09
70.87
70.82
70.75
70.59
70.47
70.24
70.19
69.99
50.82
45.20
38.75
32.67
29.62
26.84
25.58
13C
N3
O
N
H
Cl
N3-PEG3-CA
170 160 150 140 130 120 110 100 90 80 70 60 50 40 30 20 10 0 ppm

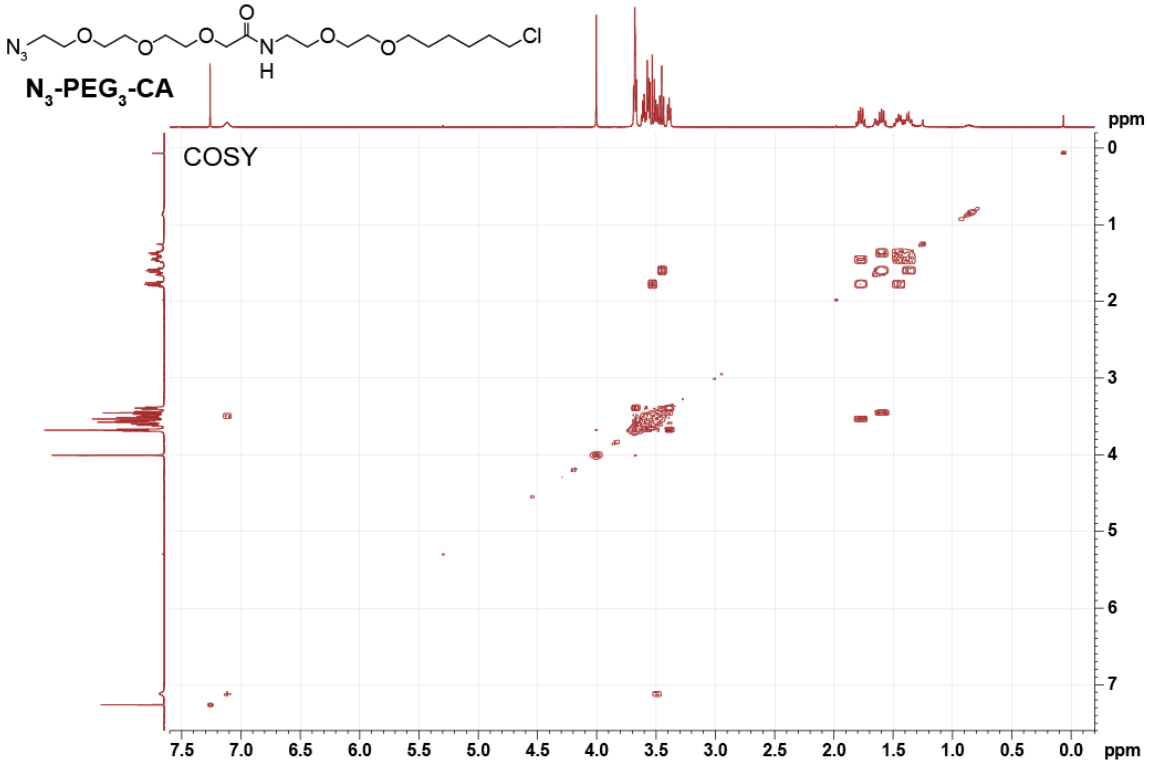
N3
O
O
O
O
N
H
O
O
Cl
N3-PEG3-CA
COSY
ppm
0
1
2
3
4
5
6
7
7.5
7.0
6.5
6.0
5.5
5.0
4.5
4.0
3.5
3.0
2.5
2.0
1.5
1.0
0.5
0.0
ppm

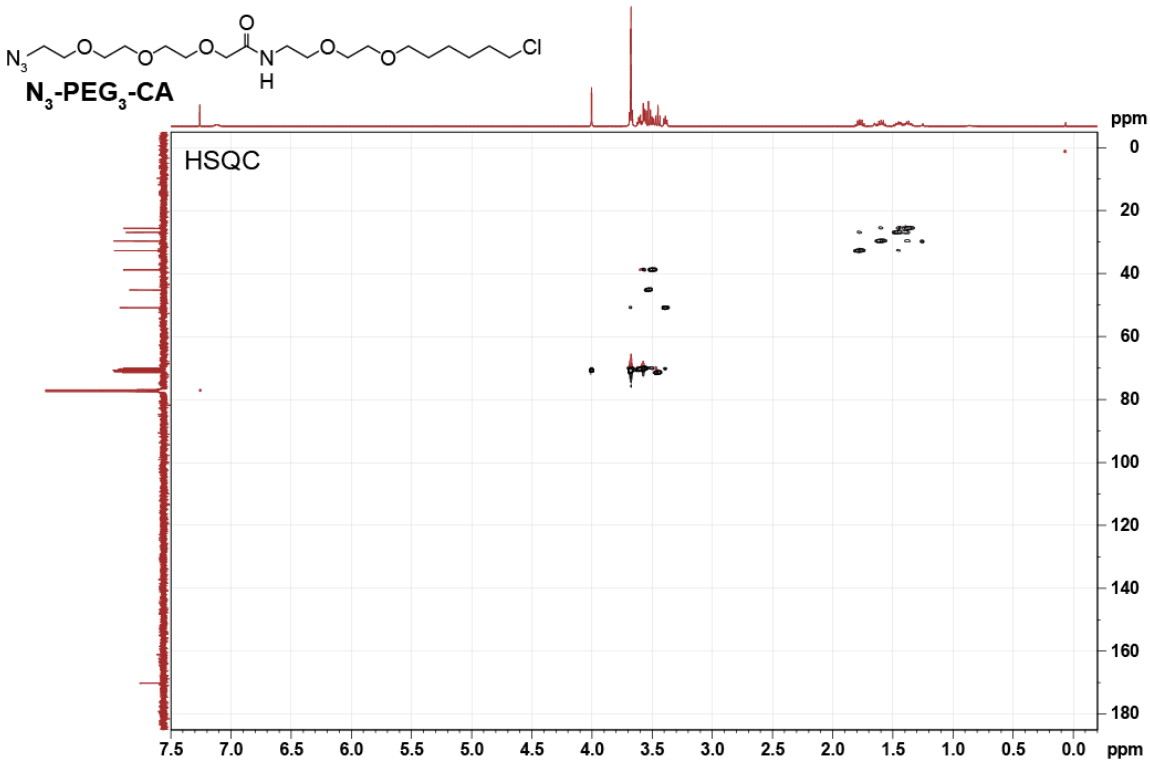
N3
O
O
O
O
N
H
O
O
Cl
N3-PEG3-CA
HSQC
ppm
0
20
40
60
80
100
120
140
160
180
7.5
7.0
6.5
6.0
5.5
5.0
4.5
4.0
3.5
3.0
2.5
2.0
1.5
1.0
0.5
0.0
ppm

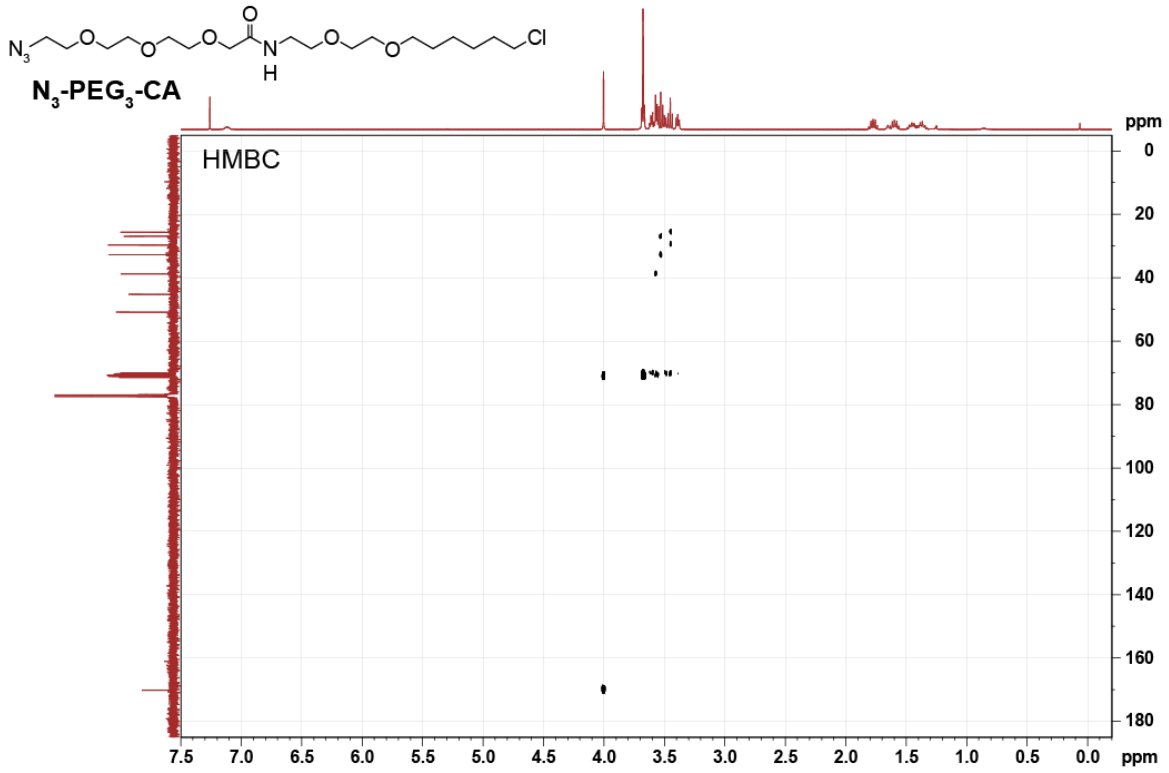
N3-PEG3-CA
HMBC
ppm
0
20
40
60
80
100
120
140
160
180
7.5
7.0
6.5
6.0
5.5
5.0
4.5
4.0
3.5
3.0
2.5
2.0
1.5
1.0
0.5
0.0
ppm

### 3.5.10. Synthesis of *N*-(2-(*tert*-butoxy)ethyl)-*N*-(5-((1-(24-chloro-11-oxo-3,6,9,15,18-pentaoxa-12-azatetracosyl)-1*H*-1,2,3-triazol-4-yl)methoxy)-2-nitrobenzyl)palmitamide (12)

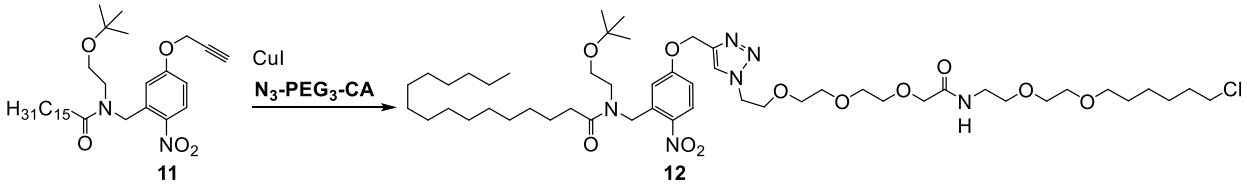


CuI (3.2 mg, 0.013 mmol, 0.5 equiv.) and sodium ascorbate (5.6 mg, 0.028 mmol, 1.1 equiv.) were added to **2-(2-(2-(2-azidoethoxy)ethoxy)ethoxy)-*N*-(2-(2-((6-chlorohexyl)oxy)ethoxy) ethyl)acetamide** ($N_3$-$PEG_3$-CA, 11 mg, 0.025 mmol, 1.0 equiv.), and the mixture was placed under an argon atmosphere. Separately, ***N*-(2-(*tert*-butoxy)ethyl)-*N*-(2-nitro-5-(prop-2-yn-1-yloxy)benzyl)palmitamide** (**11**, 15 mg, 0.027 mmol, 1.1 equiv.) was dissolved in anhydrous DMF (0.5 ml) and transferred to **$N_3$-$PEG_3$-CA** mixture. The reaction was stirred overnight, and loaded directly onto a C18 reverse phase column for purification (ACN:$H_2O$ 0:1 → ACN:$H_2O$ 1:0). ***N*-(2-(*tert*-butoxy)ethyl)-*N*-(5-((1-(24-chloro-11-oxo-3,6,9,15,18-pentaoxa-12-azatetracosyl)-1*H*-1,2,3-triazol-4-yl)methoxy)-2-nitrobenzyl)palmitamide** (**12**, 15 mg, 0.012 mmol, 49%) was isolated as a yellow oil.

**TLC (MeOH:DCM, 1:19): $R_f$ =** 0.24. **$^1$H NMR ($CDCl_3$, 400 MHz, 25 °C):** δ 8.24 (d, 0.5 H, H3, *J* = 9.1 Hz); 8.11 (d, 0.5 H, H3, *J* = 8.8 Hz); 7.83 (d, 1 H, H9, *J* = 8.2 Hz); 7.17-6.66 (m, 3 H, H2 + H6 + N<u>H</u>); 5.24 (s, 1.5 H, $H8_{A,B}$); 5.16 (s, 0.5 H, $H8_B$); 5.13 (s, 1 H, $H7_A$); 5.01 (s, 1 H, $H7_B$); 4.56 (q, 2 H, $H10_{A,B}$, *J* = 5.2 Hz); 3.99 (s, 2 H, $H35_{A,B}$); 3.89 (q, 2 H, $H11_{A,B}$, *J* = 5.0 Hz); 3.69-3.36 (m, 24 H, H29-34 + H37-41 + $H46_{A,B}$); 2.57 (t, 1 H, $H13_A$, *J* = 7.8 Hz); 2.19 (t, 1 H, $H13_B$, *J* = 7.8 Hz); 1.83-1.52 (m, 6 H, $H14_{A,B}$ + $H42_{A,B}$ + $H45_{A,B}$); 1.50-1.19 (m, 28 H, H43-44 + H15-26); 1.14 (s, 9 H, $C(C\underline{H}_3)_3$); 0.87 (t, 3 H, $H27_{A,B,C}$, *J* = 6.9 Hz). **$^{13}$C NMR ($CDCl_3$, 101 MHz, 25 °C):** δ 174.70 / 174.29 (C12); 170.03 (C36); 163.11 / 162.52 (C1); 142.69 / 142.37 (C28); 141.69 / 141.04 (C5); 139.25; 137.57 / 137.40 (C4); 136.66; 129.41; 128.90 / 128.13 (C3); 124.60 /

124.53 (C9); 115.32 / 114.18 (C6); 113.24; 113.11 / 112.71 (C2); 73.54; 73.36; 73.27 ($\underline{C}(CH_3)_3$); 71.36 (C46); 70.94; 70.84; 70.74 (C35); 70.64; 70.56; 70.41; 70.13; 69.92; 69.49; 69.46 / 69.30 (C11); 62.49; 62.31 / 52.15 (C8), 60.72; 60.34; 59.88; 51.49 / 47.56 (C7); 50.54 / 50.50 (C10); 49.00; 47.94; 47.50; 45.16 (C41); 38.76 (C37), 33.27 / 33.18 (C13); 32.63 (C42); 32.05; 29.83; 29.78; 29.67; 29.62; 29.48; 29.40; 29.36; 22.81; 29.58 (C45); 27.55 / 27.50 / 27.46 ($C(\underline{C}H_3)_3$); 26.80 + 25.62 (C43); 25.53 (C44); 25.44 + 25.41 (C14); 14.25 (C27). **HRMS (ESI$^+$):** *m/z* calcd. for $[C_{50}H_{88}ClN_6O_{11}]^+$: 983.6200, found: 983.6193 ($[M+H]^+$).

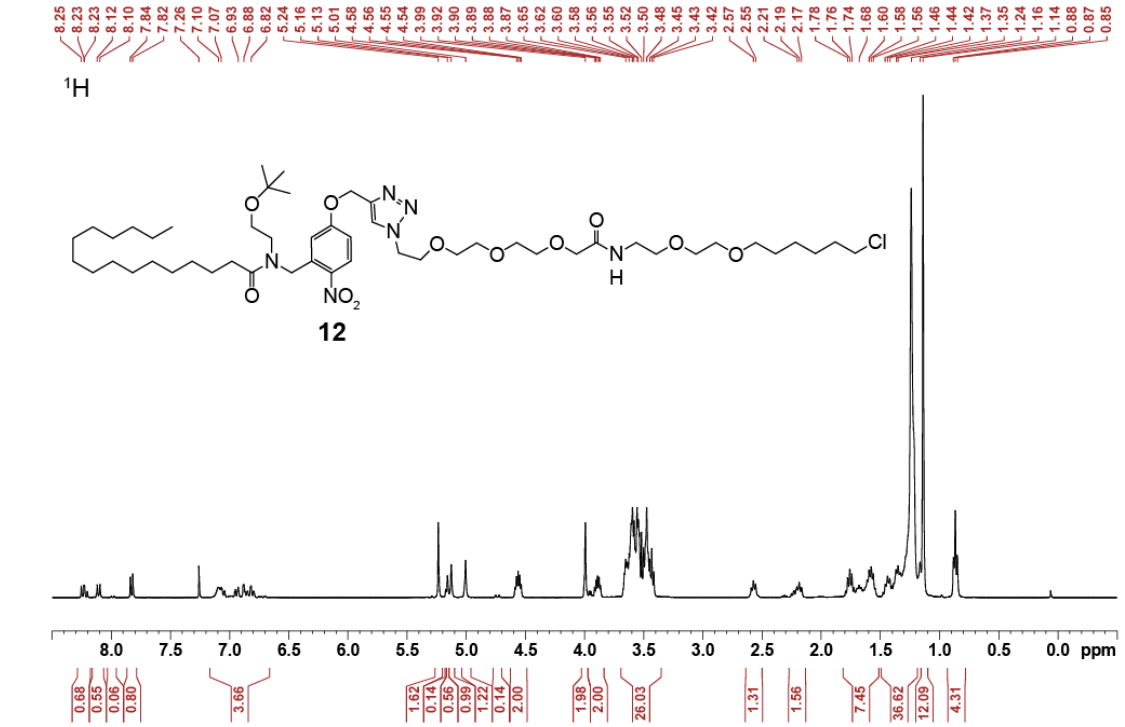
8.25 8.23 8.23 8.12 8.10 7.84 7.82 7.26 7.10 7.07 6.93 6.88 6.82 5.24 5.16 5.13 5.01 4.58 4.56 4.55 4.54 3.99 3.92 3.90 3.89 3.88 3.87 3.65 3.62 3.60 3.58 3.56 3.55 3.52 3.50 3.48 3.45 3.43 3.42 2.57 2.55 2.21 2.19 2.17 1.78 1.76 1.74 1.68 1.60 1.58 1.56 1.46 1.44 1.42 1.37 1.35 1.24 1.16 1.14 0.88 0.87 0.85
1H
Cl
NO2
12
8.0 7.5 7.0 6.5 6.0 5.5 5.0 4.5 4.0 3.5 3.0 2.5 2.0 1.5 1.0 0.5 0.0 ppm
0.68 0.55 0.06 0.80 3.66 1.62 0.14 0.56 0.99 1.22 0.14 2.00 1.98 2.00 26.03 1.31 1.56 7.45 36.62 12.09 4.31

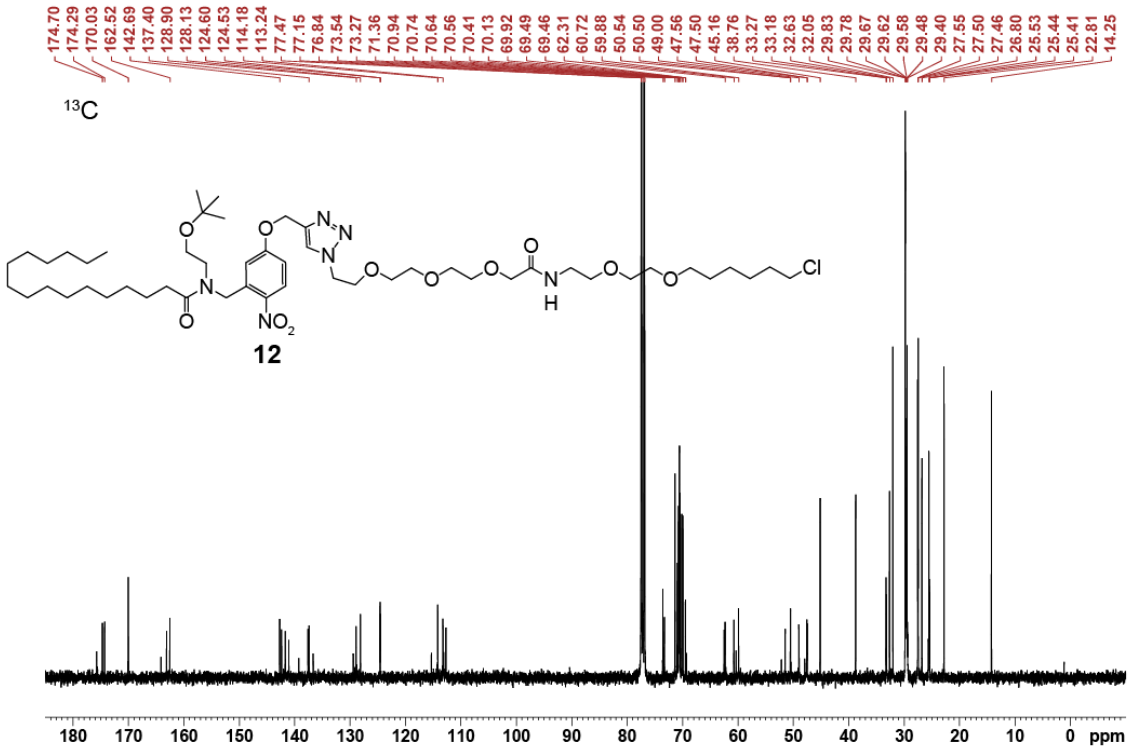
174.70 174.29 170.03 162.52 142.69 137.40 128.90 128.13 124.60 124.53 114.18 113.24 77.47 77.15 76.84 73.54 73.27 71.36 70.94 70.74 70.64 70.56 70.41 70.13 69.92 69.49 69.46 62.31 60.72 59.88 50.54 50.50 49.00 47.56 47.50 45.16 38.76 33.27 33.18 32.63 32.05 29.83 29.78 29.67 29.62 29.58 29.48 29.40 27.55 27.50 27.46 26.80 25.53 25.44 25.41 22.81 14.25
13C
Cl
NO2
12
180 170 160 150 140 130 120 110 100 90 80 70 60 50 40 30 20 10 0 ppm

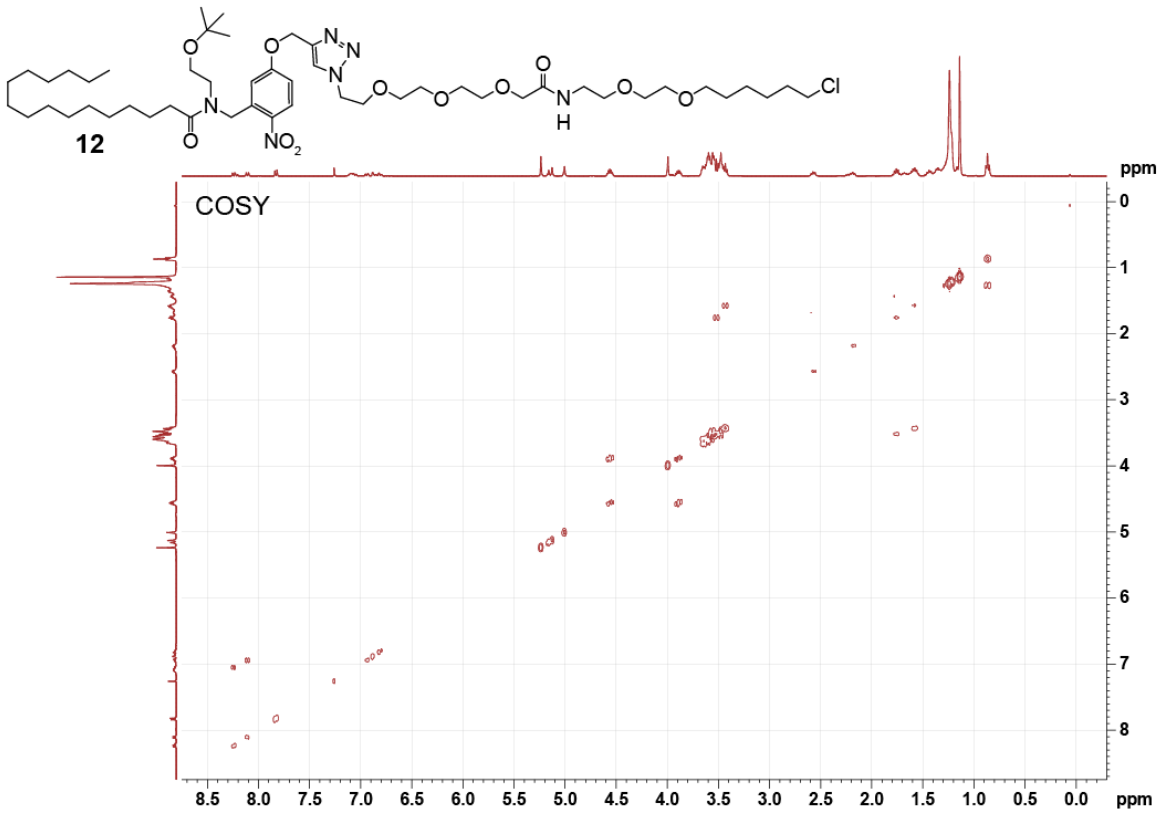
12
COSY
ppm
8.5 8.0 7.5 7.0 6.5 6.0 5.5 5.0 4.5 4.0 3.5 3.0 2.5 2.0 1.5 1.0 0.5 0.0 ppm
0 1 2 3 4 5 6 7 8

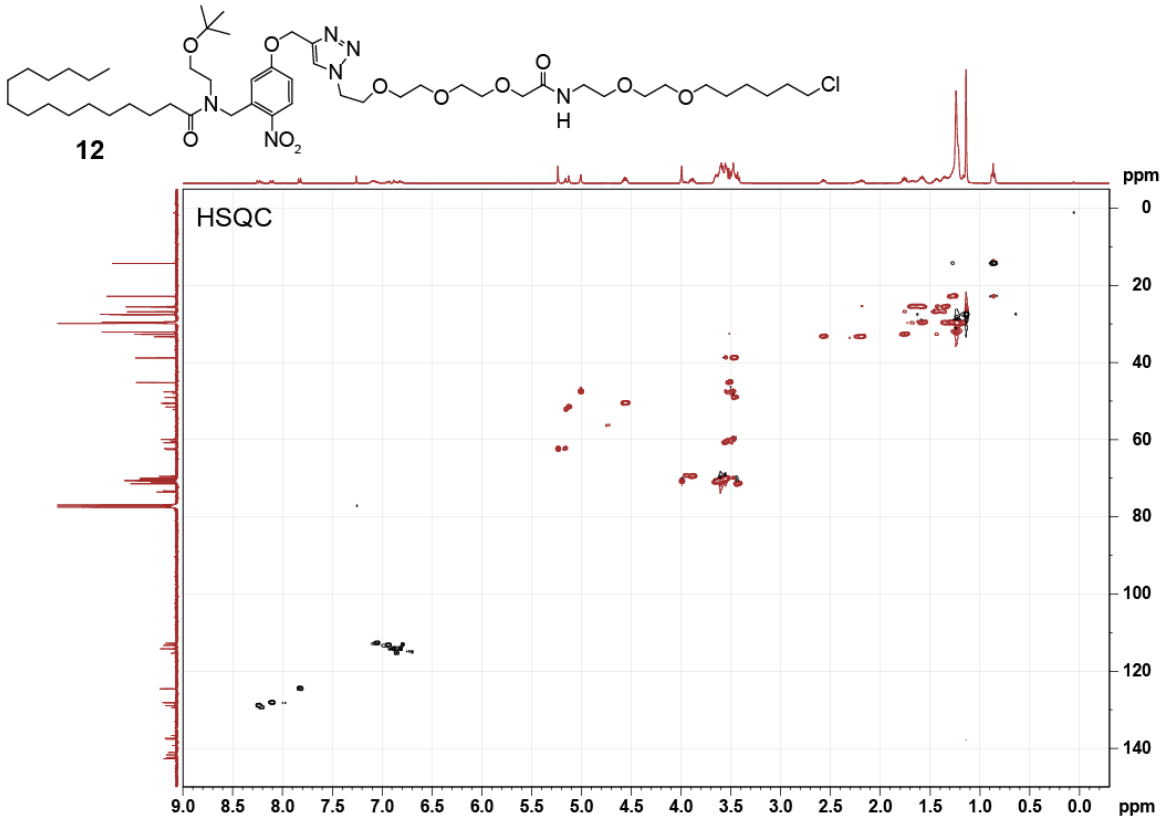
12
HSQC
ppm
9.0 8.5 8.0 7.5 7.0 6.5 6.0 5.5 5.0 4.5 4.0 3.5 3.0 2.5 2.0 1.5 1.0 0.5 0.0 ppm
0 20 40 60 80 100 120 140

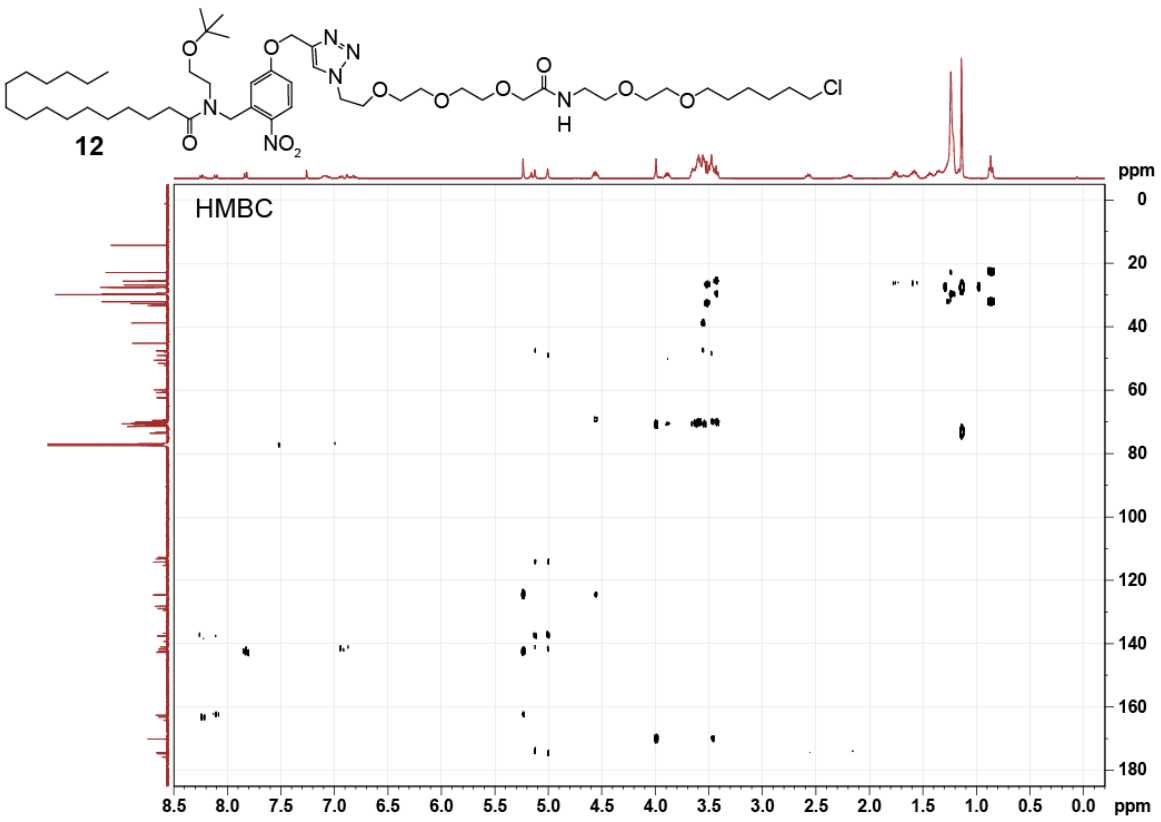
12
HMBC
ppm
0
20
40
60
80
100
120
140
160
180
8.5
8.0
7.5
7.0
6.5
6.0
5.5
5.0
4.5
4.0
3.5
3.0
2.5
2.0
1.5
1.0
0.5
0.0
ppm

### 3.5.11. Synthesis of *N*-(5-((1-(24-chloro-11-oxo-3,6,9,15,18-pentaoxa-12-azatetracosyl)-1*H*-1,2,3-triazol-4-yl)methoxy)-2-nitrobenzyl)-*N*-(2-hydroxyethyl) palmitamide (hOCT-PEA3)

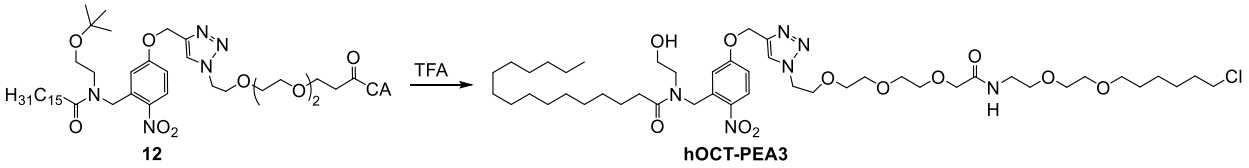


***N*-(2-(*tert*-butoxy)ethyl)-*N*-(5-((1-(24-chloro-11-oxo-3,6,9,15,18-pentaoxa-12-azatetracosyl)-1*H*-1,2,3-triazol-4-yl)methoxy)-2-nitrobenzyl)palmitamide** (12, 28 mg, 0.029 mmol, 1.0 equiv.) was put under an argon atmosphere and neat TFA (0.5 ml, 6.7 mmol, excess) was added. The reaction was stirred for 40 min at RT, before it was diluted with DCM (1.5 ml). The solvent was removed *in vacuo*, re-dissolve 2× in DCM and solvent was removed *in vacuo* accordingly to remove residual TFA. The crude product was purified via $SiO_2$ flash chromatography (MeOH:DCM 1:99 → MeOH:DCM 1:19). ***N*-(5-((1-(24-chloro-11-oxo-3,6,9,15,18-pentaoxa-12-azatetracosyl)-1*H*-1,2,3-triazol-4-yl)methoxy)-2-nitrobenzyl)-*N*-(2-hydroxyethyl)palmitamide** (**hOCT-hPEA3**, 22 mg, 0.024 mmol, 84%) was isolated as a yellow oil.

**TLC (MeOH:DCM, 1:19): $R_f$ =** 0.16. **$^1$H NMR ($MeOD_4$, 400 MHz, 25 °C):** δ 8.28 (d, 0.3 H, H3, *J* = 9.1 Hz); 8.18 (d, 0.6 H, H3, *J* = 1.8 Hz); 8.16 (d, 1 H, H9, *J* = 1.9 Hz); 7.22 (dd, 0.3 H, H2, *J* = 4.0 Hz); 7.10 (dd, 0.6 H, H2, *J* = 4.0 Hz); 7.05 (d, 0.1 H, *J* = 2.7 Hz); 6.99 (d, 0.5 H, H6, *J* = 2.7 Hz); 6.94 (d, 0.1 H, H6, *J* = 2.6 Hz); 6.90 (d, 0.3 H, *J* = 2.7 Hz); 5.33 (s, 0.5 H, $H8_A$); 5.31 (s, 1 H, $H8_B$); 5.28 (s, 0.2 H, $H8_A$); 5.25 (s, 0.3 H, $H8_A$); 5.15 (s, 0.7 H, $H7_A$); 5.00 (s, 1.3 H, $H7_{A,B}$); 4.63 (q, 2 H, $H10_{A,B}$, *J* = 4.88 Hz); 3.98 (s, 2 H, $H35_{A,B}$); 3.93 (q, 2 H, $H11_{A,B}$, *J* = 4.57 Hz); 3.74 (q, 2 H, *J* = 4.70 Hz); 3.70-3.38 (m, 24 H, H29-34 + H37-41 + $H46_{A,B}$); 2.67 (t, 1.2 H, $H13_{A,B}$, *J* = 7.6 Hz); 2.29 (t, 0.8 H, $H13_B$, *J* = 7.4 Hz); 1.82-1.64 (m, 3 H, $H42_{A,B}$ + $H14_A$); 1.64-1.53 (m, 3 H,

$H14_B$ + $H45_{A,B}$); 1.53-1.20 (m, 28 H, H43-44 + H15-26); 0.92 (t, 3 H, $H27_{A,B,C}$, *J* = 6.8 Hz). **$^{13}$C NMR ($MeOD_4$, 101 MHz, 25 °C):** δ 177.00 / 176.92 (C12); 172.74 (C36); 164.28 / 163.89 (C1); 143.86 (C28); 142.83 (C5); 142.41; 138.02 / 137.96 (C4); 129.77 / 129.05 (C3); 126.51 (C9); 115.11; 115.00 / 114.83 (C6); 114.54 (C2); 72.18 (C46); 71.99; 71.69; 71.59; 71.52; 71.43; 71.40; 71.29 (C35); 71.27; 71.18; 70.48; 70.29; 70.23 (C11); 63.12 / 63.01 (C8); 60.94; 60.70; 52.41 (C7); 51.96 / 51.51 (C10); 50.64; 49.00; 45.73 (C41); 39.81 (C37); 34.04 / 33.99 (C13); 33.75 (C42); 33.08; 30.81; 30.78; 30.71; 30.63; 30.49; 30.45; 30.29; 23.74; 30.58 (C45); 27.75 (C43, C14); 26.51 (C14); 14.46 (C27). **HRMS (ESI$^+$):** *m/z* calcd. for $[C_{46}H_{80}N_6O_{11}Cl]^+$: 927.5574, found: 927.5565 ($[M+H]^+$).

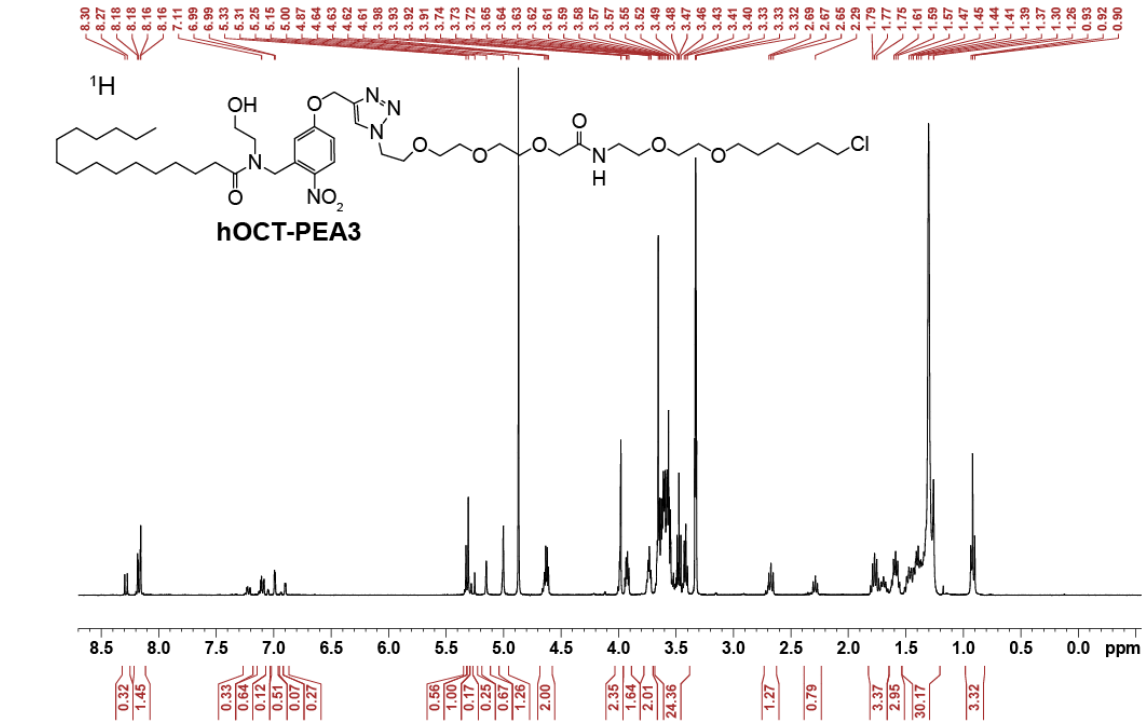
$^{1}$H
hOCT-PEA3

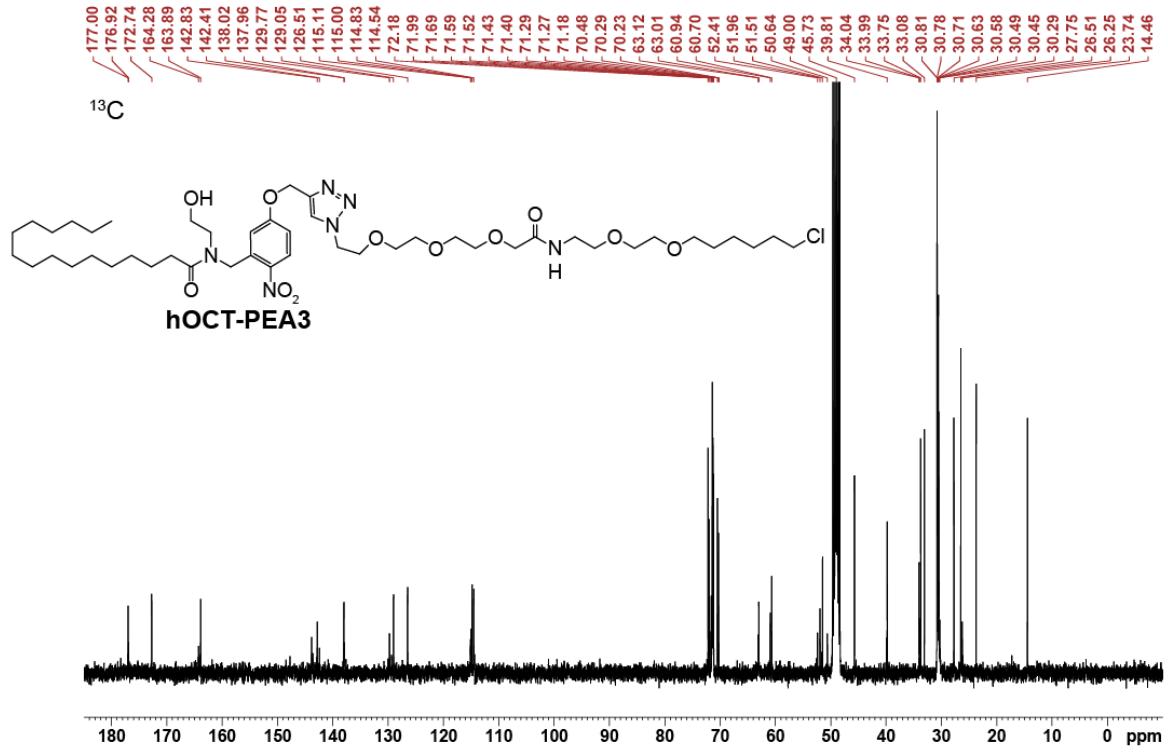
$^{13}$C
hOCT-PEA3

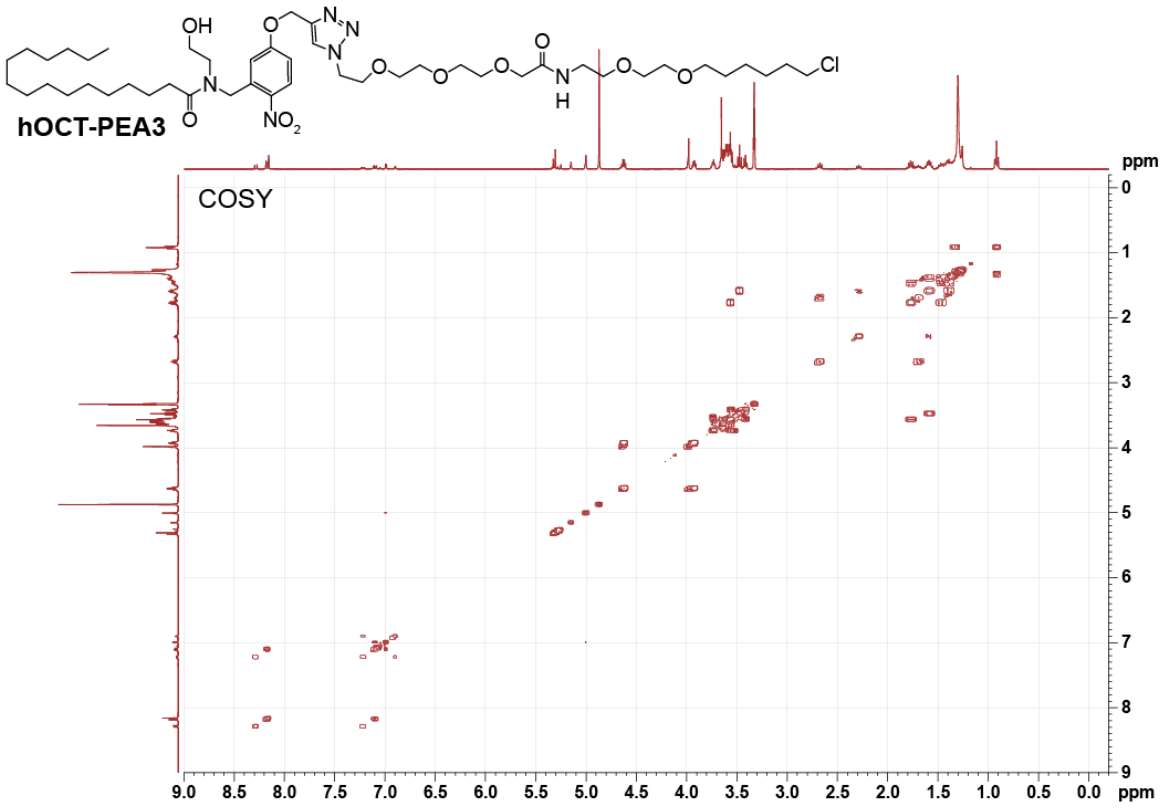
hOCT-PEA3
COSY
ppm
9.0 8.5 8.0 7.5 7.0 6.5 6.0 5.5 5.0 4.5 4.0 3.5 3.0 2.5 2.0 1.5 1.0 0.5 0.0 ppm

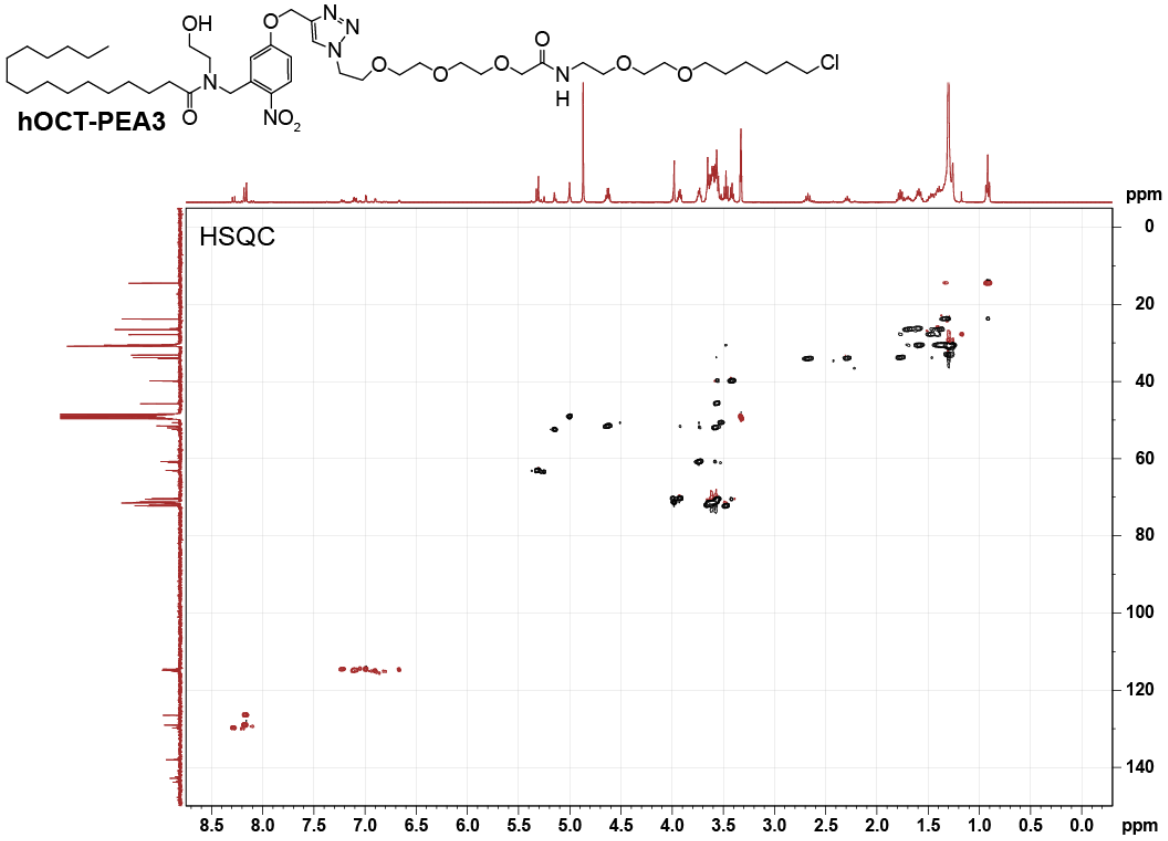
hOCT-PEA3
HSQC
ppm
8.5 8.0 7.5 7.0 6.5 6.0 5.5 5.0 4.5 4.0 3.5 3.0 2.5 2.0 1.5 1.0 0.5 0.0 ppm

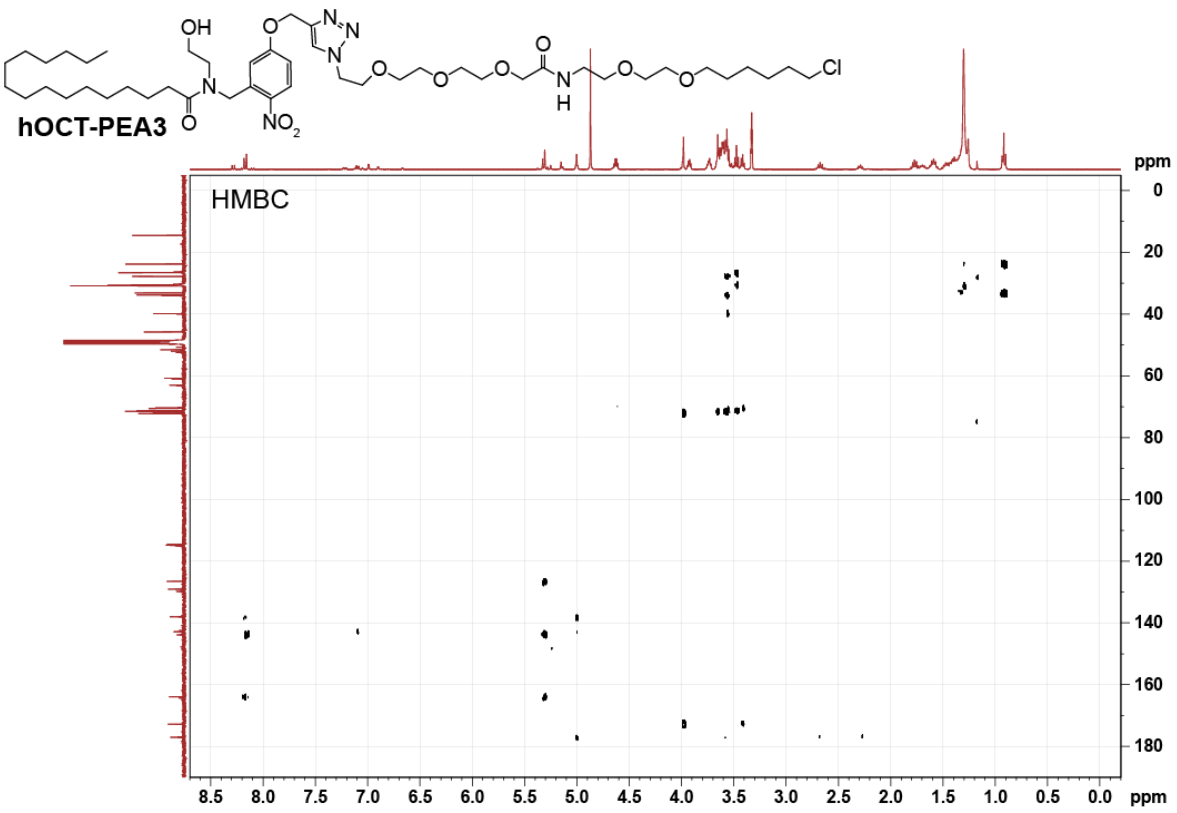
hOCT-PEA3
HMBC
ppm
8.5 8.0 7.5 7.0 6.5 6.0 5.5 5.0 4.5 4.0 3.5 3.0 2.5 2.0 1.5 1.0 0.5 0.0 ppm
0 20 40 60 80 100 120 140 160 180

**A**

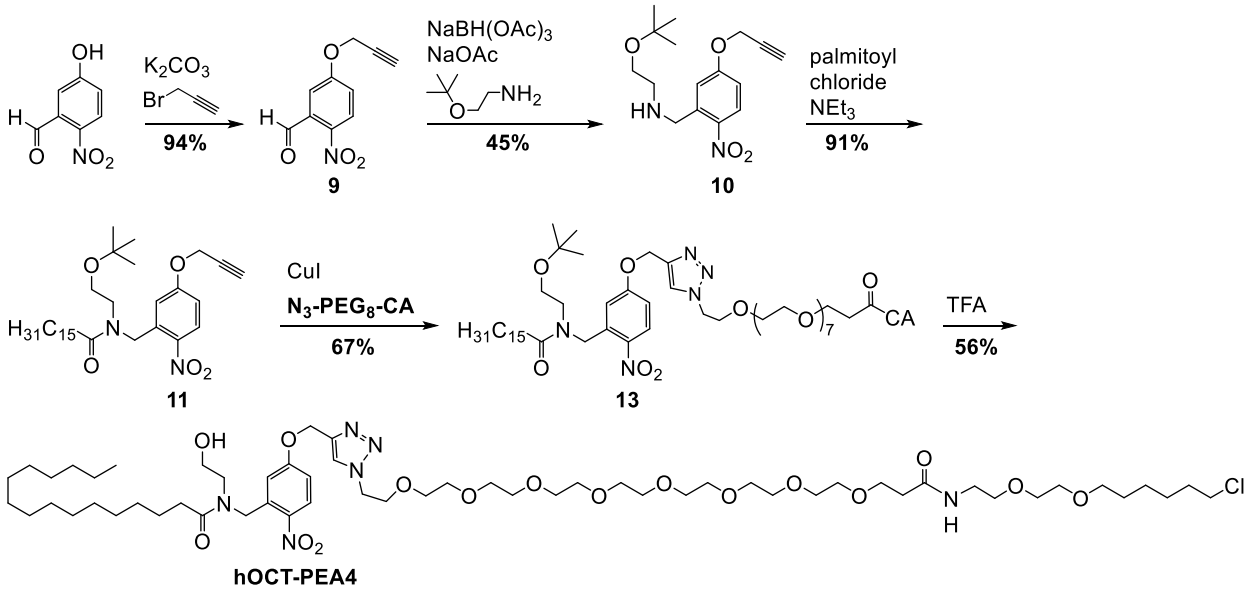


**B**

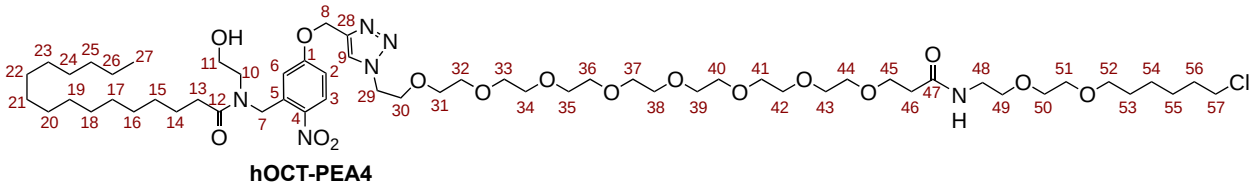


*Figure 3.17. Synthetic scheme of **hOCT-PEA4**.*

*(**A**) Chemical synthesis of **hOCT-PEA4**, which prepared in 5 steps and 14% yield. (**B**) NMR atom numbering assignment for **hOCT-PEA4**.*

### 3.5.12. Synthesis of 1-azido-*N*-(2-(2-((6-chlorohexyl)oxy)ethoxy)ethyl)-3,6,9,12,15,18,21,24-octaoxaheptacosan-27-amide ($N_3$-$PEG_8$-CA)

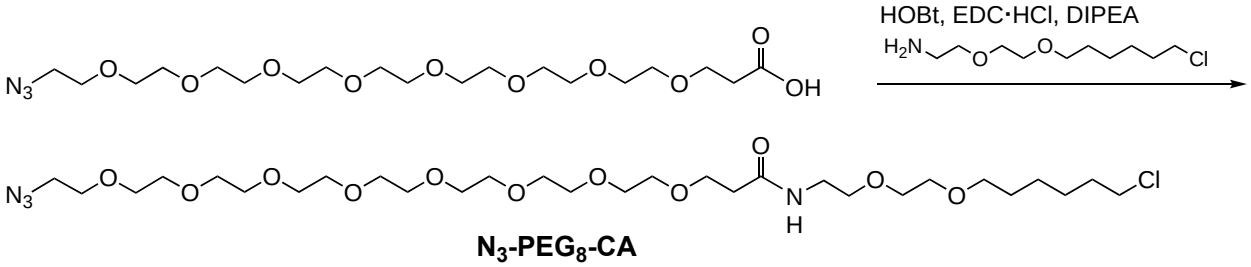


**$N_3$-$PEG_8$-CA**

HOBt (21 mg, 0.16 mmol, 1.6 equiv.) and EDC·HCl (33 mg, 0.17 mmol, 1.7 equiv.) were added to azido-PEG8-acid (47 mg, 0.10 mmol, 1.0 equiv.), and put under an argon atmosphere, then dissolved in anhydrous DMF (3 ml). Separately, **CA** (44 mg, 0.20 mmol, 1.9 equiv.) was placed under an argon atmosphere and dissolved in anhydrous DMF (1.5 ml). The amine was transferred to the acid reaction mixture, then DIPEA (37 μl, 0.21 mmol, 2.1 equiv.) was added. The reaction stirred at RT for 5 h. The solvent was removed *in vacuo*, and the crude product was purified by flash chromatography (MeOH:DCM 1:19). **1-azido-*N*-(2-(2-((6-chlorohexyl) oxy)ethoxy)ethyl)-3,6,9,12,15,18,21,24-octaoxaheptacosan-27-amide ($N_3$-$PEG_8$-CA**, 57 mg, 0.084 mmol, 84% yield) was isolated as a yellow oil.

**TLC (MeOH:DCM, 1:9): $R_f$ =** 0.45. **$^1$H NMR ($CDCl_3$, 400 MHz, 25 °C)**: δ 6.58 (br, 1 H, NH); 3.72 (t, 2 H, $H45_{A,B}$, *J* = 5.98 Hz); 3.69-3.57 (m, 32 H); 3.57-3.50 (m, 6 H, $H52_{A,B}$); 3.48-3.41 (m, 4 H, $H48_{A,B}$ + $H57_{A,B}$); 3.38 (t, 2 H, $H29_{A,B}$, *J* = 5.09 Hz); 2.45 (t, 2 H, $H46_{A,B}$, *J* = 5.98 Hz); 1.77 (q, 2 H, $H53_{A,B}$, *J* = 7.05 Hz); 1.59 (q, 2 H, $H56_{A,B}$, *J* = 7.06 Hz); 1.51-1.31 (m, 4 H, $H54_{A,B}$ + $H55_{A,B}$). **$^{13}$C NMR ($CDCl_3$, 101 MHz, 25 °C)**: δ 171.53 (C47); 71.38 (C57); 70.82; 70.79; 70.76; 70.69; 70.52; 70.43; 70.40; 70.15; 69.95; 67.38 (C45); 50.80 (C29); 45.15 (C52); 39.24 (C48); 37.13 (C46); 32.64 (C53); 29.58 (C56); 26.80 (C54); 25.54 (C55). **HRMS ($ESI^+$):** *m/z* calcd. for $[C_{29}H_{58}N_4O_{11}Cl]^+$: 673.3791, found: 673.3780 ($[M+H]^+$).

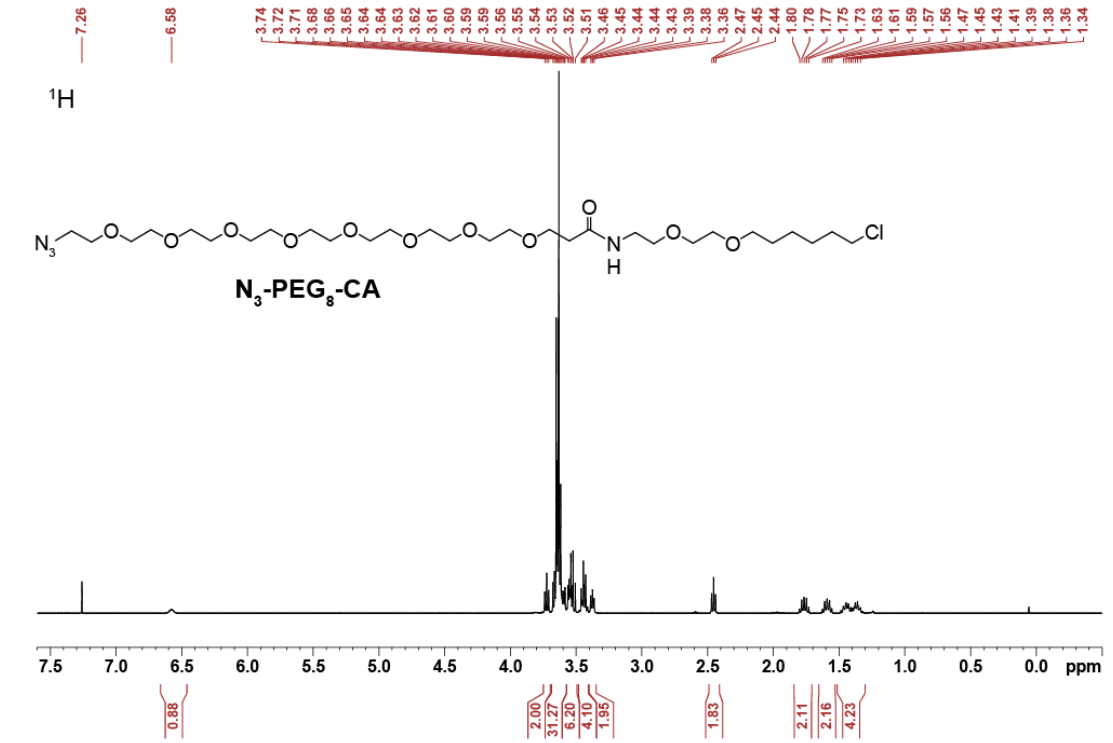
7.26
6.58
3.74 3.72 3.71 3.68 3.66 3.65 3.64 3.64 3.63 3.62 3.61 3.60 3.59 3.59 3.56 3.55 3.54 3.53 3.52 3.51 3.46 3.45 3.44 3.44 3.43 3.39 3.38 3.36 2.47 2.45 2.44 1.80 1.78 1.77 1.75 1.73 1.63 1.61 1.59 1.57 1.56 1.47 1.45 1.43 1.41 1.39 1.38 1.36 1.34
$^1$H
$N_3$-PEG$_8$-CA
7.5 7.0 6.5 6.0 5.5 5.0 4.5 4.0 3.5 3.0 2.5 2.0 1.5 1.0 0.5 0.0 ppm
0.88
2.00 31.27 6.20 4.10 1.95
1.83
2.11 2.16 4.23

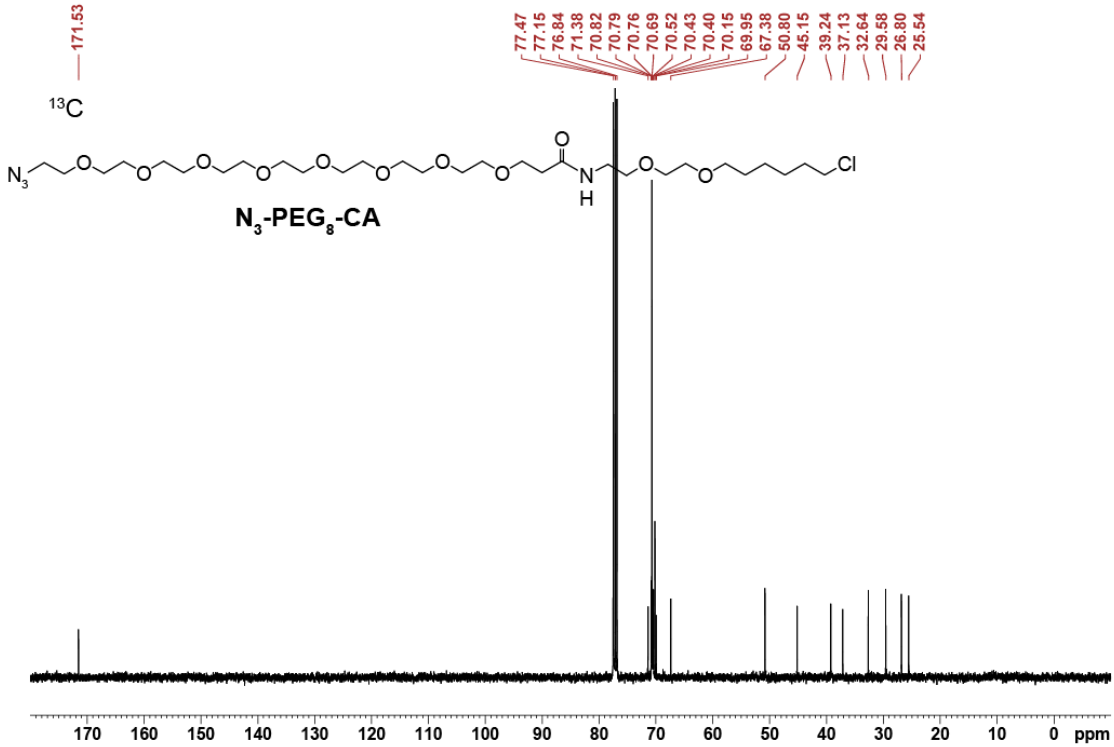
171.53
77.47 77.15 76.84 71.38 70.82 70.79 70.76 70.69 70.52 70.43 70.40 70.15 69.95 67.38 50.80 45.15 39.24 37.13 32.64 29.58 26.80 25.54
$^{13}$C
$N_3$-PEG$_8$-CA
170 160 150 140 130 120 110 100 90 80 70 60 50 40 30 20 10 0 ppm

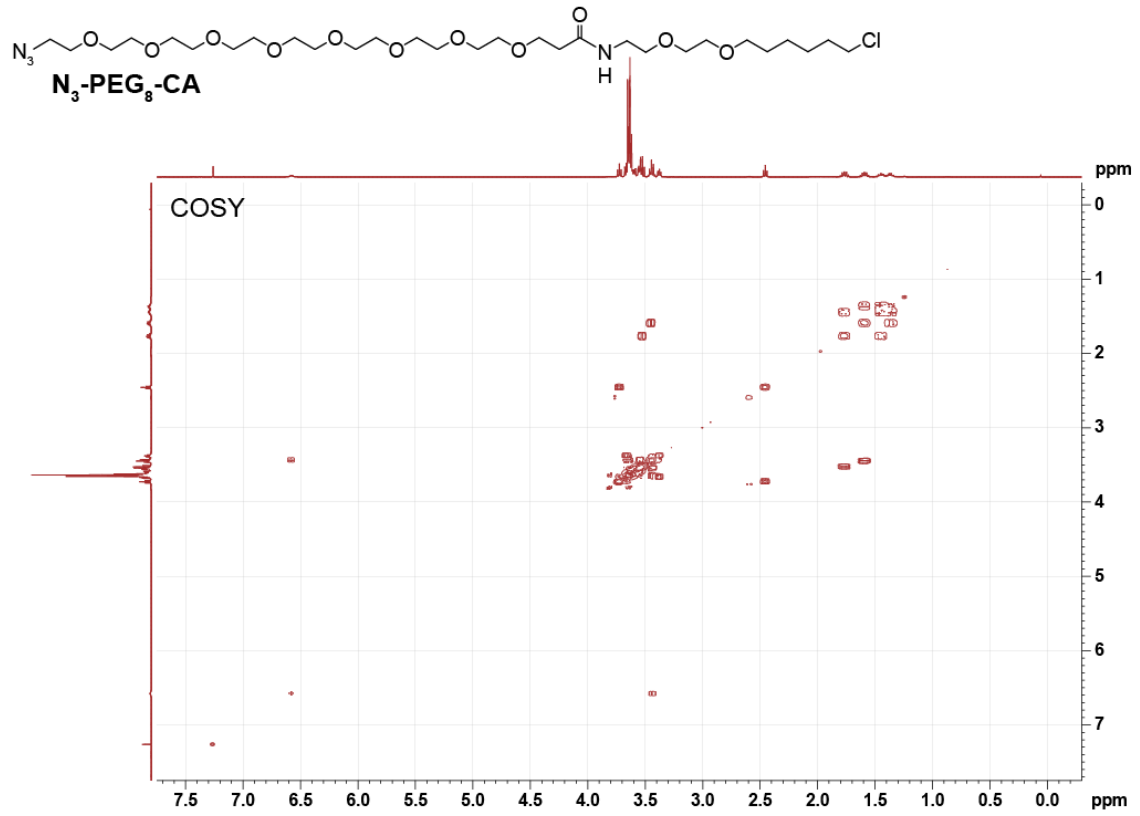
N3-PEG8-CA
COSY
ppm
7.5 7.0 6.5 6.0 5.5 5.0 4.5 4.0 3.5 3.0 2.5 2.0 1.5 1.0 0.5 0.0 ppm

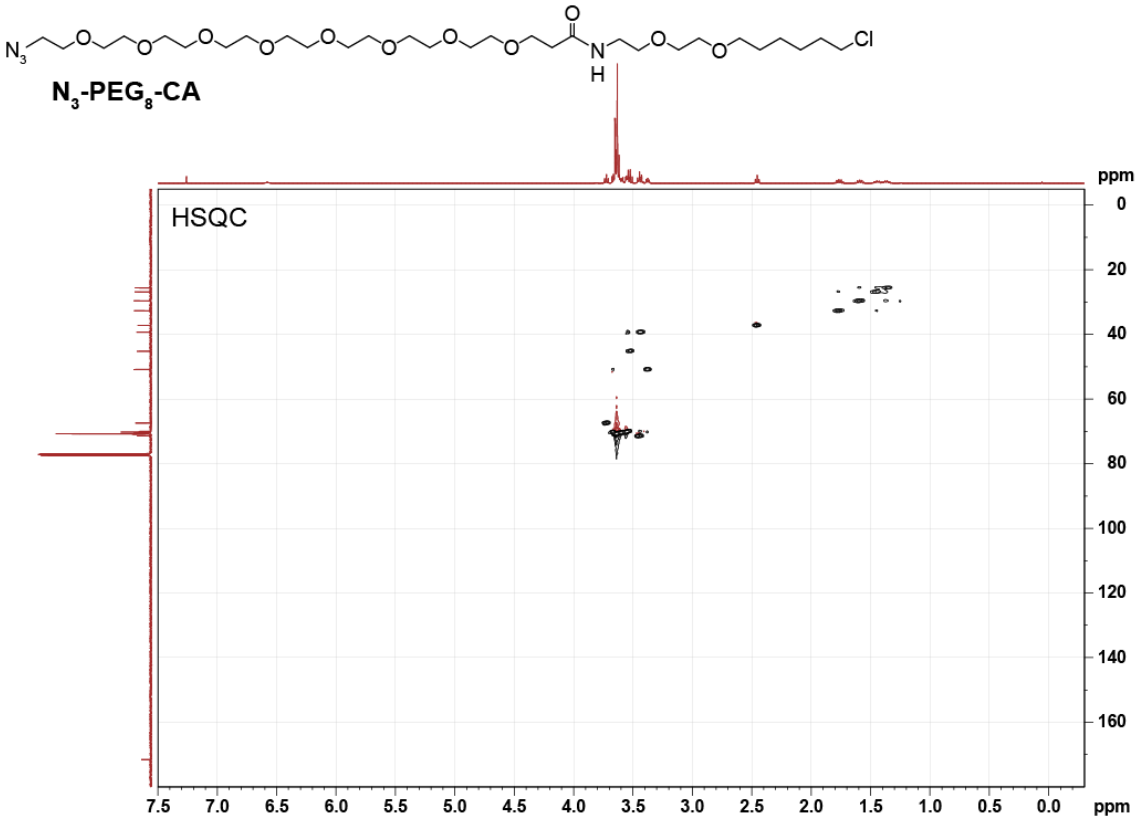
N3-PEG8-CA
HSQC
ppm
7.5 7.0 6.5 6.0 5.5 5.0 4.5 4.0 3.5 3.0 2.5 2.0 1.5 1.0 0.5 0.0 ppm

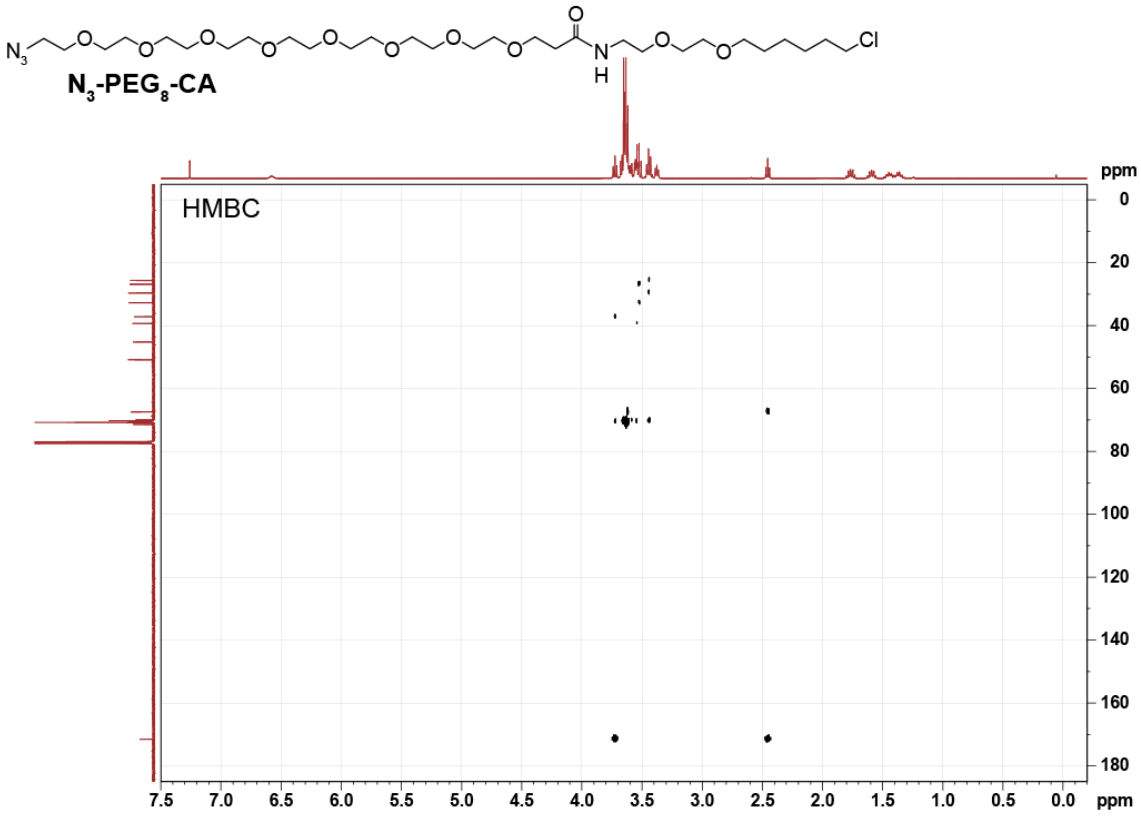
N3-PEG8-CA
HMBC
ppm
0
20
40
60
80
100
120
140
160
180
7.5
7.0
6.5
6.0
5.5
5.0
4.5
4.0
3.5
3.0
2.5
2.0
1.5
1.0
0.5
0.0
ppm

### 3.5.13. Synthesis of 1-(4-((3-((*N*-(2-(*tert*-butoxy)ethyl)palmitamido)methyl)-4-nitrophenoxy) methyl)-1*H*-1,2,3-triazol-1-yl)-*N*-(2-(2-((6-chlorohexyl)oxy)ethoxy)ethyl)-3,6,9,12,15,18,21,24-octaoxaheptacosan-27-amide (13)

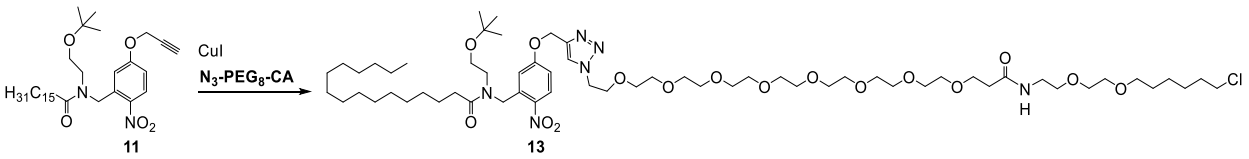


CuI (3.1 mg, 0.012 mmol, 0.70 equiv.) and sodium ascorbate (5.2 mg, 0.026 mmol, 1.4 equiv.) were added to **$N_3$-$PEG_8$-CA** (12 mg, 0.018 mmol, 1.0 equiv.), and placed under an argon atmosphere. Separately, ***N*-(2-(*tert*-butoxy)ethyl)-*N*-(2-nitro-5-(prop-2-yn-1-yloxy)benzyl) palmitamide** (**11**, 14 mg, 0.026 mmol, 1.4 equiv.) was dissolved in anhydrous DMF (0.5 ml), and transferred to **$N_3$-$PEG_8$-CA** mixture. The reaction was stirred overnight at RT was purified via reverse phase flash chromatography (MeCN:$H_2O$ 0:1 → MeCN:$H_2O$ 1:0). **1-(4-((3-((*N*-(2-(*tert*-butoxy)ethyl)palmitamido)methyl)-4-nitrophenoxy)methyl)-1*H*-1,2,3-triazol-1-yl)-*N*-(2-(2-((6-chlorohexyl)oxy)ethoxy)ethyl)-3,6,9,12,15,18,21,24-octaoxaheptacosan-27-amide** (**13**, 15 mg, 0.012 mmol, 67%) was isolated as a yellow oil.

**TLC (MeOH:DCM, 1:19): $R_f$ =** 0.25. **$^1$H NMR ($CDCl_3$, 400 MHz, 25 °C):** δ 8.24 (d, 0.5 H, H3, *J* = 9.1 Hz); 8.11 (d, 0.5 H, H3, *J* = 9.1 Hz); 7.86 (d, 1 H, H9, *J* = 9.5 Hz); 7.06 (dd, 0.5 H, H2, *J* = 9.1, 2.7 Hz); 6.95 (dd, 0.5 H, H2, *J* = 9.1, 2.8 Hz); 6.88 (d, 0.5 H, H6, *J* = 2.7 Hz); 6.82 (d, 0.5 H, H6, *J* = 2.6 Hz); 6.57 (br, 1 H, N<u>H</u>); 5.23 (s, 1.7 H, $H8_{A,B}$); 5.16 (d, 0.3 H, $H8_B$); 5.12 (s, 1 H, $H7_A$); 5.00 (s, 1 H, $H7_B$); 4.55 (q, 2 H, $H10_{A,B}$, *J* = 5.0 Hz); 3.87 (q, 2 H, $H11_{A,B}$, *J* = 4.7 Hz); 3.72 (t, 2 H, $H45_{A,B}$, *J* = 6.0 Hz); 3.68-3.57 (m, 30 H, H30-44); 3.57-3.40 (m, 14 H, H29 + H48-52 +$H57_{A,B}$); 2.57 (t, 1 H, $H13_A$, *J* = 7.6 Hz); 2.45 (t, 2 H, $H46_{A,B}$, *J* = 6.0 Hz); 2.18 (t, 1 H, $H13_B$, *J* = 7.6 Hz); 1.76 (q, 2 H, $H53_{A,B}$, *J* = 7.0 Hz); 1.72-1.65 (m, 1 H, $H14_A$); 1.59 (q, 3 H, $H14_B$ + $H56_{A,B}$, *J* = 7.0 Hz); 1.50-1.17 (28 H, H54-55 + H15-26); 1.14 (s, 9 H, C($C\underline{H}_3$)$_3$); 0.86 (t, 3 H, $H27_{A,B,C}$, *J*

= 6.6 Hz). **$^{13}$C NMR ($CDCl_3$, 101 MHz, 25 °C):** δ 174.62 / 174.21 (C12); 171.44 (C47); 163.14 / 162.56 (C1); 142.64 / 142.31 (C28); 141.64 / 140.98 (C5); 137.56 / 137.40 (C4); 128.87 / 128.12 (C3); 124.68 / 124.65 (C9); 114.17 / 114.14 (C6); 113.23 / 112.71 (C2); 73.50 / 73.24 ($\underline{C}(CH_3)_3$); 71.36 (C57); 70.65; 70.57- 69.94 (C30-44); 69.45 / 69.43 (C11); 69.29; 67.38 (C45); 62.48 / 62.29 (C8); 60.72; 59.87; 51.47 (C7); 50.54 / 50.50 (C10); 48.94; 47.52 (C7); 47.48; 45.14 (C52); 39.22 (C48); 37.13 (C46); 33.24 / 33.16 (C13); 32.63 (C53); 32.02, 29.80-29.46, 22.79 (C15-26, C56); 27.53 / 27.45 ($C(\underline{C}H_3)_3$); 26.79 (C54); 25.53 (C55); 25.41 / 25.38 (C14); 14.23 (C27). **HRMS (ESI$^+$):** *m/z* calcd. for $[C_{61}H_{110}N_6O_{16}\ Cl]^+$: 1217.7667, found: 1217.7649 ($[M+H]^+$).

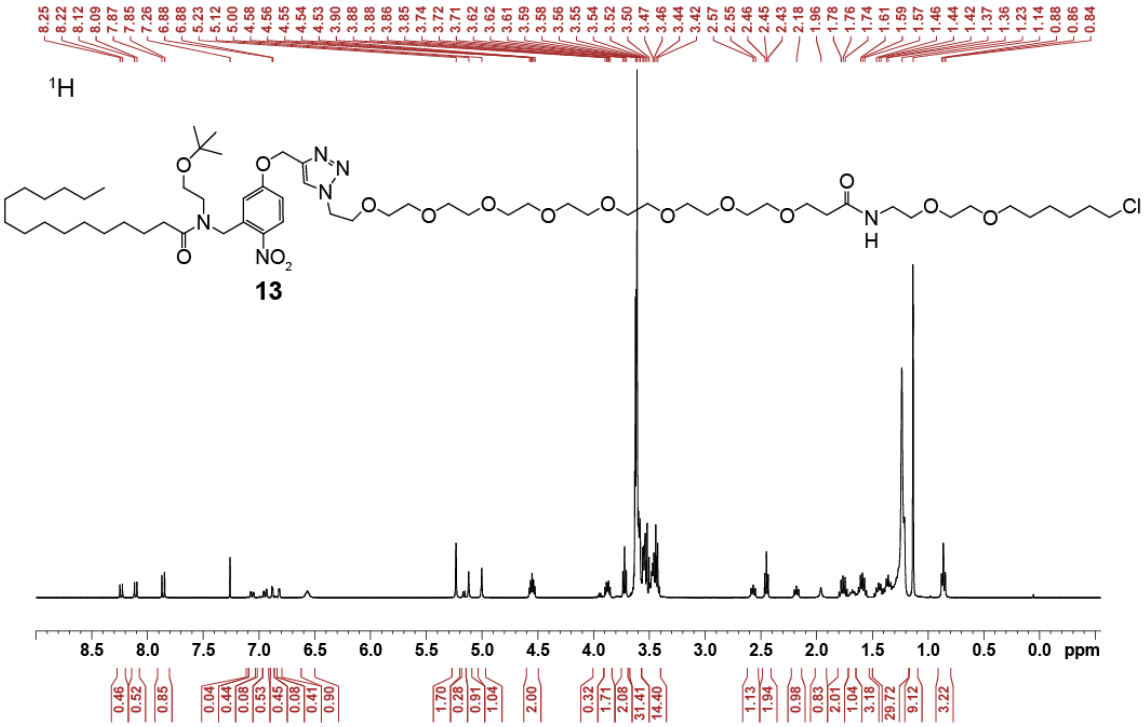
8.25 8.22 8.12 8.09 7.87 7.85 7.26 6.88 6.88 5.23 5.12 5.00 4.58 4.56 4.55 4.54 4.53 3.90 3.88 3.88 3.86 3.85 3.74 3.72 3.71 3.62 3.62 3.61 3.59 3.58 3.56 3.55 3.54 3.52 3.50 3.47 3.46 3.44 3.42 2.57 2.55 2.46 2.45 2.43 2.18 1.96 1.78 1.76 1.74 1.61 1.59 1.57 1.46 1.44 1.42 1.37 1.36 1.23 1.14 0.88 0.86 0.84
$^{1}$H
Cl
13
8.5 8.0 7.5 7.0 6.5 6.0 5.5 5.0 4.5 4.0 3.5 3.0 2.5 2.0 1.5 1.0 0.5 0.0 ppm
0.46 0.52 0.85 0.04 0.44 0.08 0.53 0.45 0.08 0.41 0.90 1.70 0.28 0.91 1.04 2.00 0.32 1.71 2.08 31.41 14.40 1.13 1.94 0.98 0.83 2.01 1.04 3.18 29.72 9.12 3.22

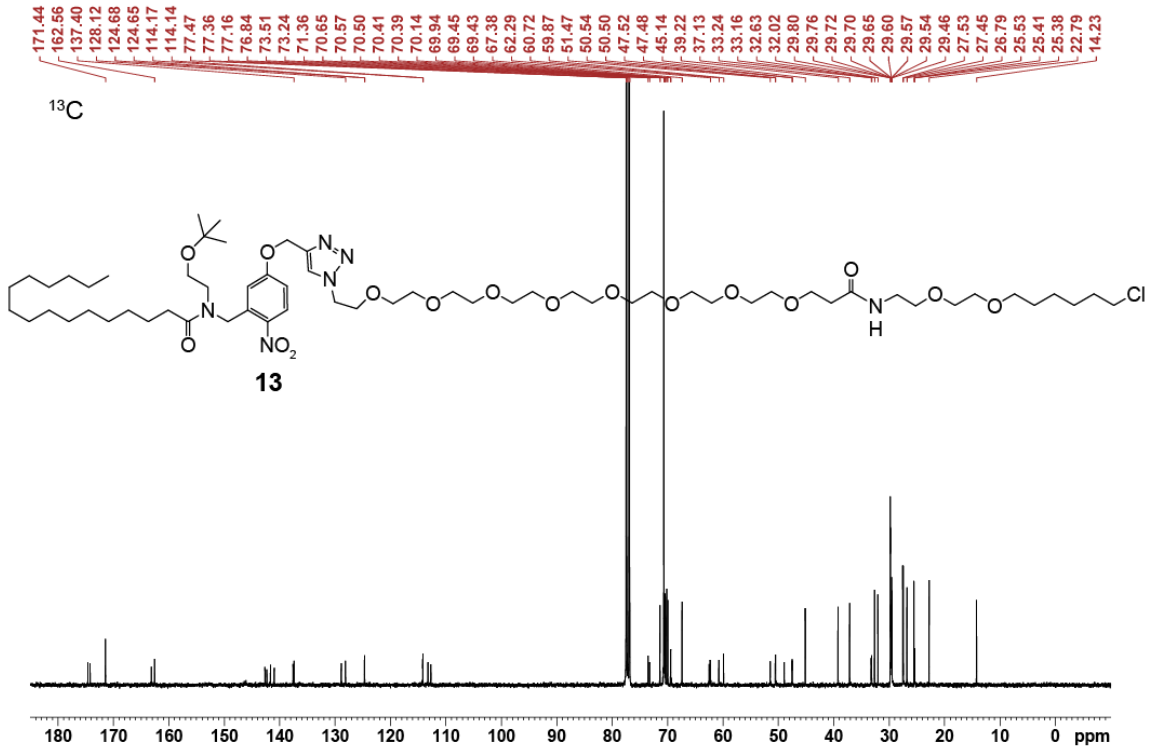
171.44 162.56 137.40 128.12 124.68 124.65 114.17 114.14 77.47 77.36 77.16 76.84 73.51 73.24 71.36 70.65 70.57 70.50 70.41 70.39 70.14 69.94 69.45 69.43 67.38 62.29 60.72 59.87 51.47 50.54 50.50 47.52 47.48 45.14 39.22 37.13 33.24 33.16 32.63 32.02 29.80 29.76 29.72 29.70 29.65 29.60 29.57 29.54 29.46 27.53 27.45 26.79 25.53 25.41 25.38 22.79 14.23
$^{13}$C
Cl
13
180 170 160 150 140 130 120 110 100 90 80 70 60 50 40 30 20 10 0 ppm

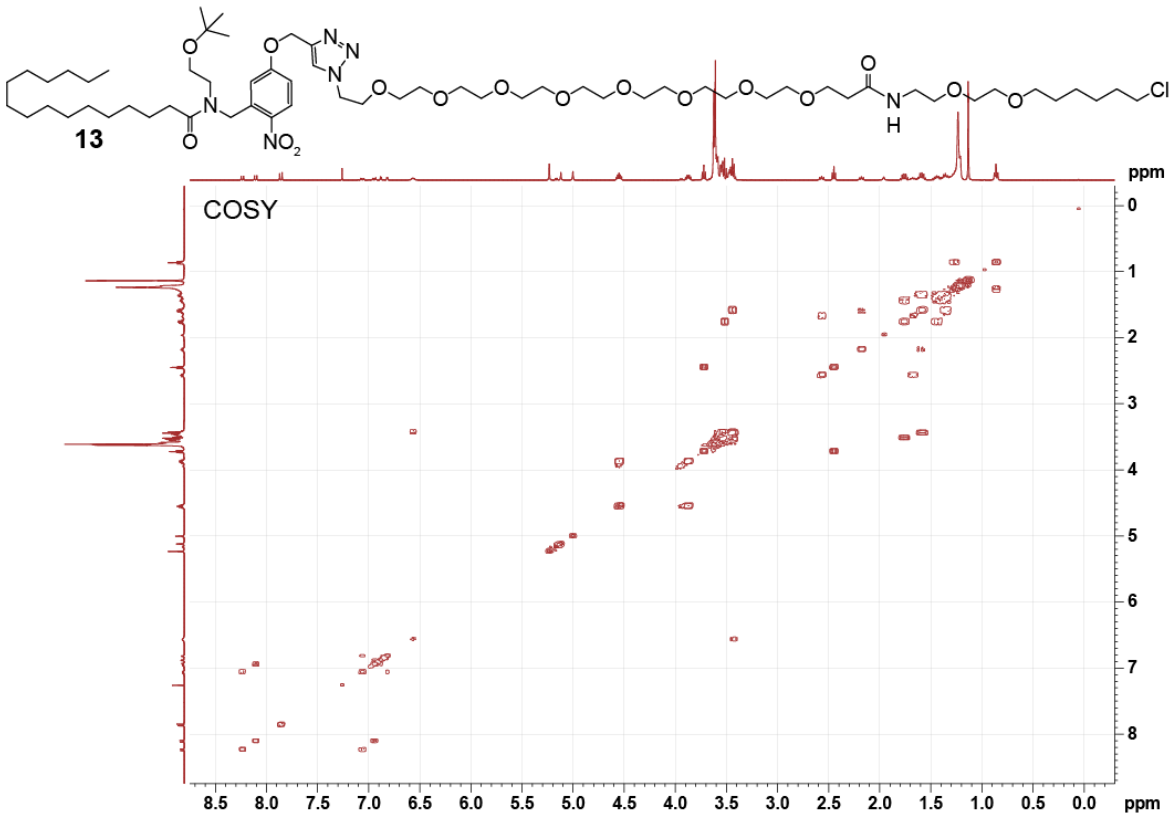
13
COSY
ppm

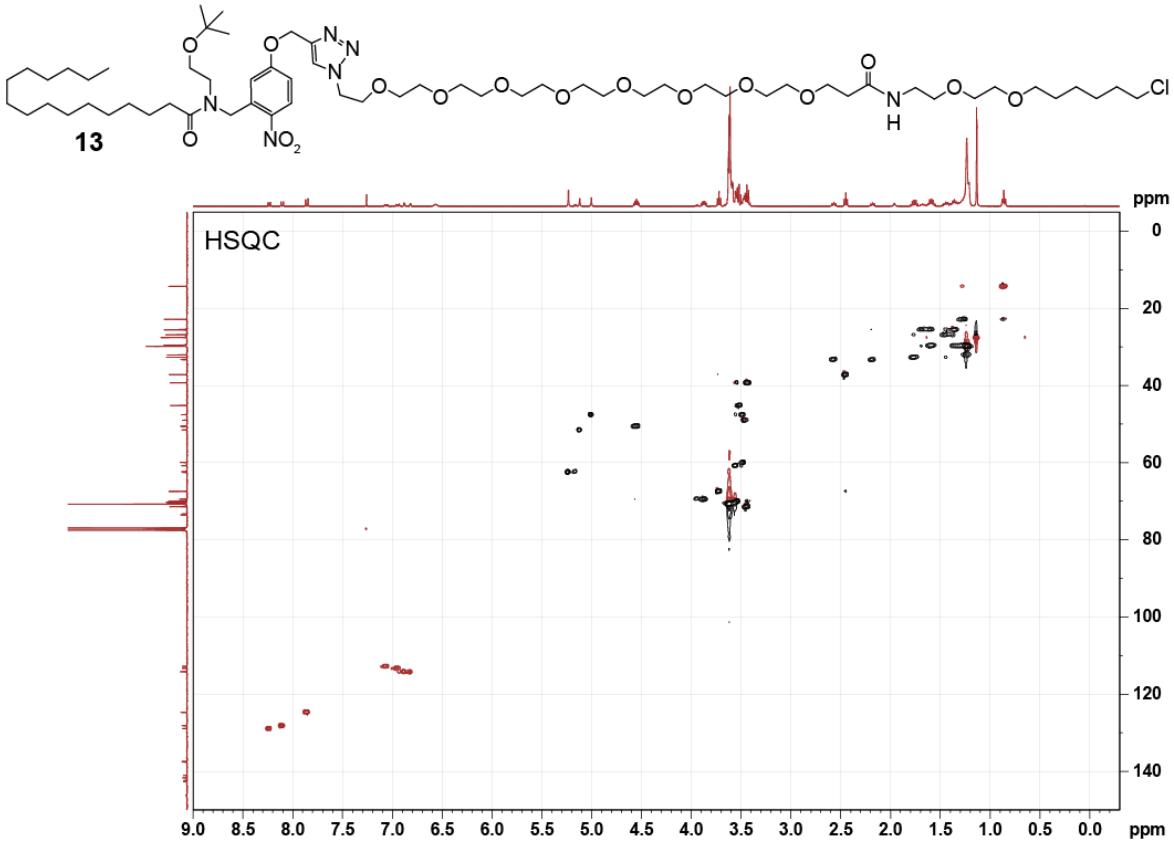
13
HSQC
ppm

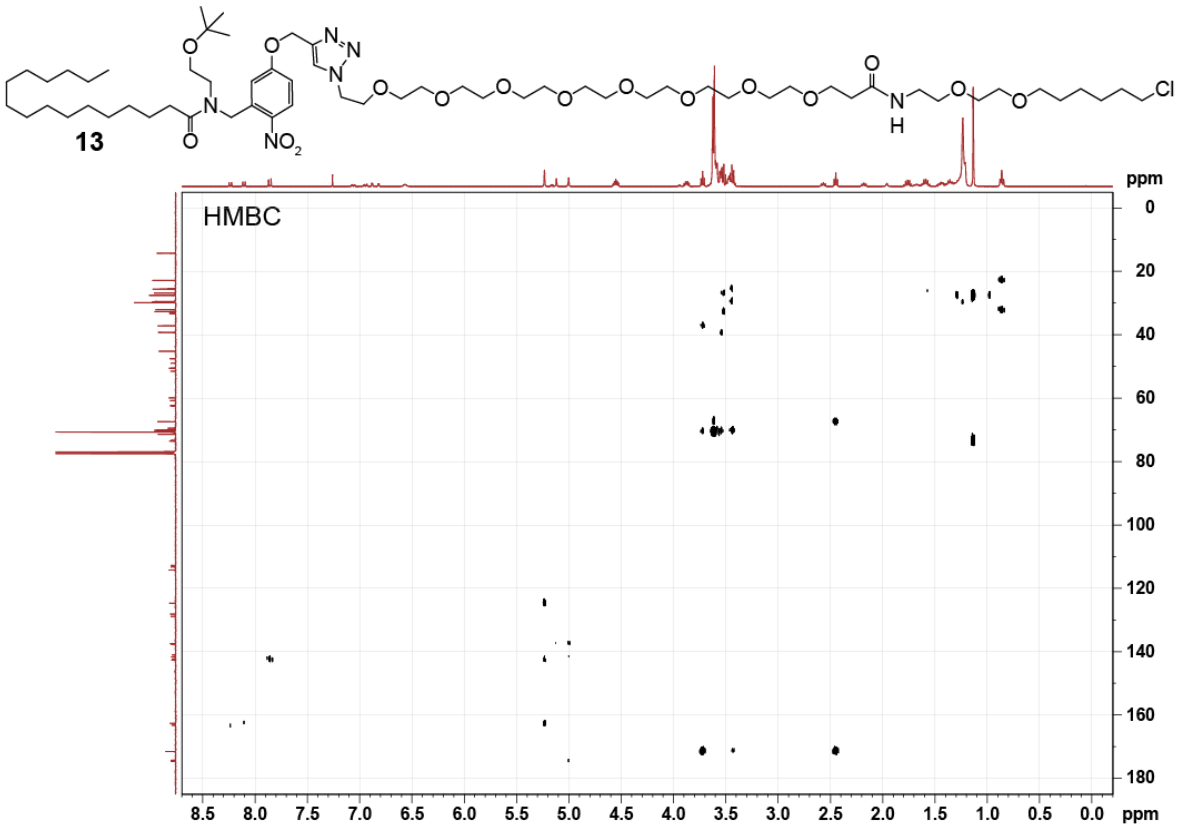
13
HMBC
ppm
8.5 8.0 7.5 7.0 6.5 6.0 5.5 5.0 4.5 4.0 3.5 3.0 2.5 2.0 1.5 1.0 0.5 0.0 ppm
0 20 40 60 80 100 120 140 160 180

### 3.5.14. Synthesis of *N*-(2-(2-((6-chlorohexyl)oxy)ethoxy)ethyl)-1-(4-((3-((*N*-(2-hydroxyethyl) palmitamido)methyl)-4-nitrophenoxy)methyl)-1*H*-1,2,3-triazol-1-yl)-3,6,9,12,15,18,21,24-octaoxaheptacosan-27-amide (hOCT-PEA4)

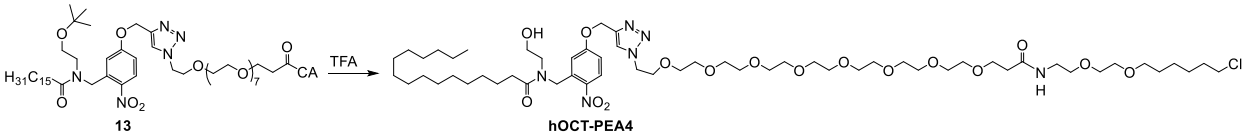


**1-(4-((3-((*N*-(2-(*tert*-butoxy)ethyl)palmitamido)methyl)-4-nitrophenoxy)methyl)-1*H*-1,2,3-triazol-1-yl)-*N*-(2-(2-((6-chlorohexyl)oxy)ethoxy)ethyl)-3,6,9,12,15,18,21,24-octaoxaheptacosan-27-amide** (13, 26 mg, 0.021 mmol, 1.0 equiv.) was placed under an argon atmosphere, and neat TFA (0.5 ml, 6.7 mmol, excess) was added. The reaction was stirred for 45 min at RT, before it was diluted with DCM and the solvent was removed *in vacuo*. The crude product was re-dissolve 2× in DCM and concentrated *in vacuo* to remove residual TFA. The crude product was purified via $SiO_2$ flash chromatography (MeOH:DCM 1:99 → MeOH:DCM 1:20). ***N*-(2-(2-((6-chlorohexyl)oxy)ethoxy)ethyl)-1-(4-((3-((*N*-(2-hydroxyethyl)palmitamido) methyl)-4-nitrophenoxy)methyl)-1*H*-1,2,3-triazol-1-yl)-3,6,9,12,15,18,21,24-octaoxaheptacosan-27-amide** (**hOCT-PEA4**, 13.9 mg, 0.0120 mmol, 56%) was isolated as a yellow oil.

**TLC (MeOH:DCM, 1:10): $R_f$ =** 0.39. **$^1$H NMR ($MeOD_4$ 400 MHz, 25 °C):** δ 8.29 (d, 0.3 H, H3, *J* = 9.1 Hz); 8.21 (s, 0.3 H, H3); 8.19 (s, 1 H, H9); 8.17 (s, 0.4 H, H3); 7.23 (dd, 0.3 H, H2, *J* = 9.1, 2.7 Hz); 7.11 (dd, 0.6 H, H2, *J* = 9.1, 2.7 Hz); 6.99 (d, 0.6 H, H6, *J* = 2.7 Hz); 6.90 (d, 0.3 H, H6, *J* = 2.7 Hz); 5.33 (d, 2 H, $H8_{A,B}$, *J* = 5.3 Hz); 5.15 (s, 0.6 H, $H7_A$); 5.01 (s, 1.2 H, $H7_B$); 4.62 (q, 2 H, $H10_{A,B}$, *J* = 4.6 Hz); 3.95-3.88 (m, 2 H, $H11_{A,B}$); 3.77-3.70 (m, 4 H, $H45_{A,B}$); 3.68-3.53 (m, 38 H, H29-44 + H49-52); 3.50 (t, 2 H, $H57_{A,B}$, *J* = 6.6); 3.38 (t, 2 H, $H48_{A,B}$, *J* = 5.6); 2.68 (t, 1.2 H, $H13_{A,B}$, *J* = 7.57 Hz); 2.47 (t, 2 H, $H46_{A,B}$, *J* = 6.2 Hz); 2.29 (t, 0.8 H, $H13_B$, *J* = 7.4); 1.79 (q, 2 H, $H53_{A,B}$, *J* = 7.0 Hz); 1.74-1.67 (m, 1 H, $H14_A$); 1.62 (q, 3 H, $H14_B$ + $H56_{A,B}$, *J* = 7.0 Hz); 1.55-

1.21 (m, 28 H, H54-55 + H15-26); 0.92 (t, 3 H, $H27_{A,B,C}$, *J* = 6.8 Hz). **$^{13}$C NMR ($MeOD_4$, 101 MHz, 25 °C):** δ 176.99 / 176.90 (C12); 173.98 (C47); 164.31 / 163.93 (C1); 143.80 / 143.59 (C28); 142.81 / 142.40 (C5); 138.00 / 137.94 (C4); 129.78 / 129.05 (C3); 126.65 (C9); 115.01 (C6); 114.84 (C2); 114.60, 114.55 (C2, C6); 72.22 (C57); 71.56; 71.51; 71.47; 71.42; 71.36; 71.30; 71.21; 70.57; 70.30 (C11); 68.28 (C45); 63.12 / 63.01 (C8); 60.94; 60.69; 52.39 (C7); 51.94; 51.53 (C10); 50.63; 45.72 (C52); 40.40 (C48); 37.62 (C46); 34.04 / 33.98 (C13); 33.75 (C53); 33.08, 30.81-30.29, 23.74 (C15-26); 30.57 (C56); 27.74 (C54); 26.50 (C55, C14); 26.24 (C14); 14.46 (C27). **HRMS (ESI$^+$):** *m/z* calcd. for $[C_{57}H_{102}N_6O_{16}\ Cl]^+$: 1161.7041, found: 1161.7032 ($[M+H]^+$).

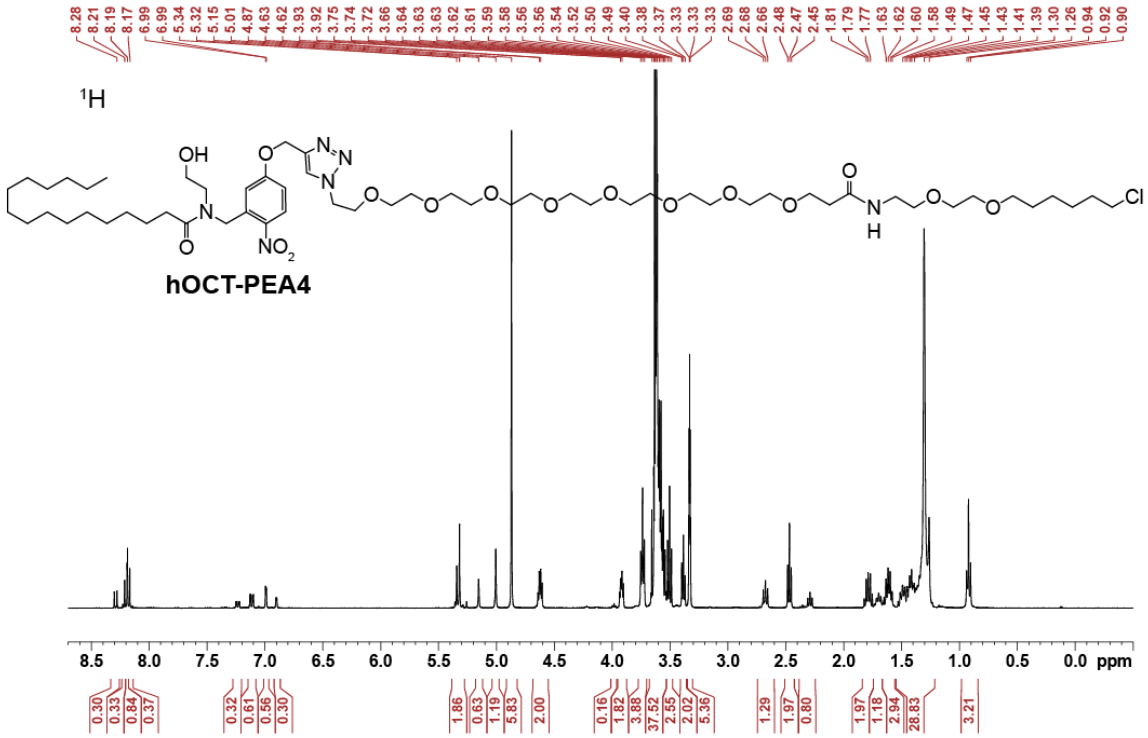
8.28 8.21 8.19 8.17 6.99 6.99 5.34 5.32 5.15 5.01 4.87 4.63 4.62 3.93 3.92 3.75 3.74 3.72 3.66 3.64 3.63 3.63 3.62 3.61 3.59 3.58 3.56 3.56 3.54 3.52 3.50 3.49 3.40 3.38 3.37 3.33 3.33 3.33 2.69 2.68 2.66 2.48 2.47 2.45 1.81 1.79 1.77 1.63 1.62 1.60 1.58 1.49 1.47 1.45 1.43 1.41 1.39 1.30 1.26 0.94 0.92 0.90
1H
OH
O
N
N
N
O
O
O
O
O
O
O
O
O
O
O
N
H
Cl
N
O
O
NO2
hOCT-PEA4
8.5 8.0 7.5 7.0 6.5 6.0 5.5 5.0 4.5 4.0 3.5 3.0 2.5 2.0 1.5 1.0 0.5 0.0 ppm
0.30 0.33 0.84 0.37 0.32 0.61 0.56 0.30 1.86 0.63 1.19 5.83 2.00 0.16 1.82 3.88 37.52 2.55 2.02 5.36 1.29 1.97 0.80 1.97 1.18 2.94 28.83 3.21

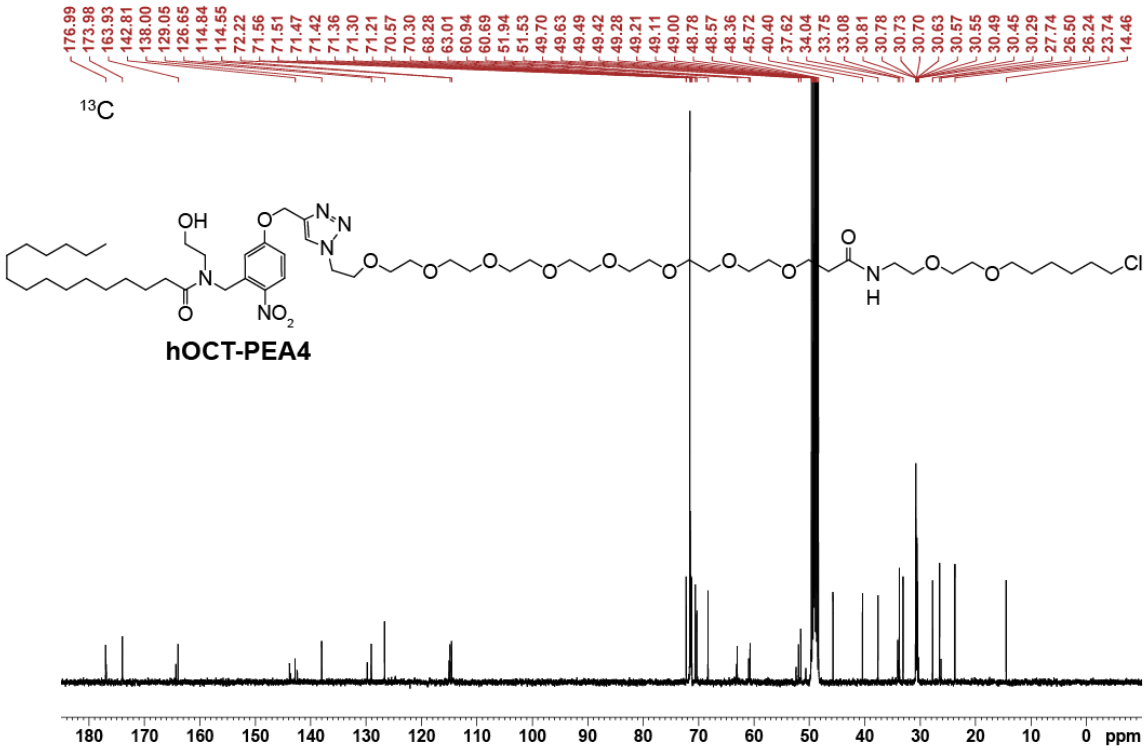
176.99 173.98 163.93 142.81 138.00 129.05 126.65 114.84 114.55 72.22 71.56 71.51 71.47 71.42 71.36 71.30 71.21 70.57 70.30 68.28 63.01 60.94 60.69 51.94 51.53 49.70 49.63 49.49 49.42 49.28 49.21 49.11 49.00 48.78 48.57 48.36 45.72 40.40 37.62 34.04 33.75 33.08 30.81 30.78 30.73 30.70 30.63 30.57 30.55 30.49 30.45 30.29 27.74 26.50 26.24 23.74 14.46
13C
OH
O
N
N
N
O
O
O
O
O
O
O
O
O
O
O
N
H
Cl
N
O
O
NO2
hOCT-PEA4
180 170 160 150 140 130 120 110 100 90 80 70 60 50 40 30 20 10 0 ppm

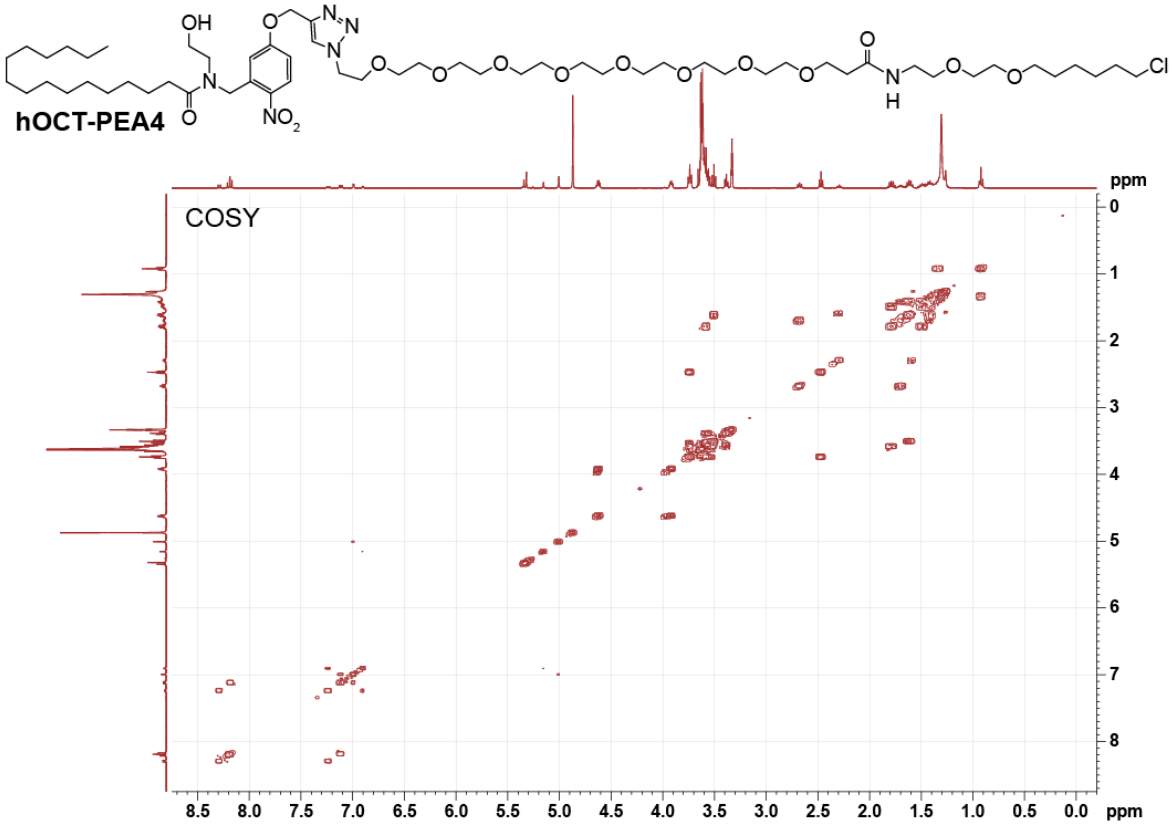
hOCT-PEA4
COSY
ppm

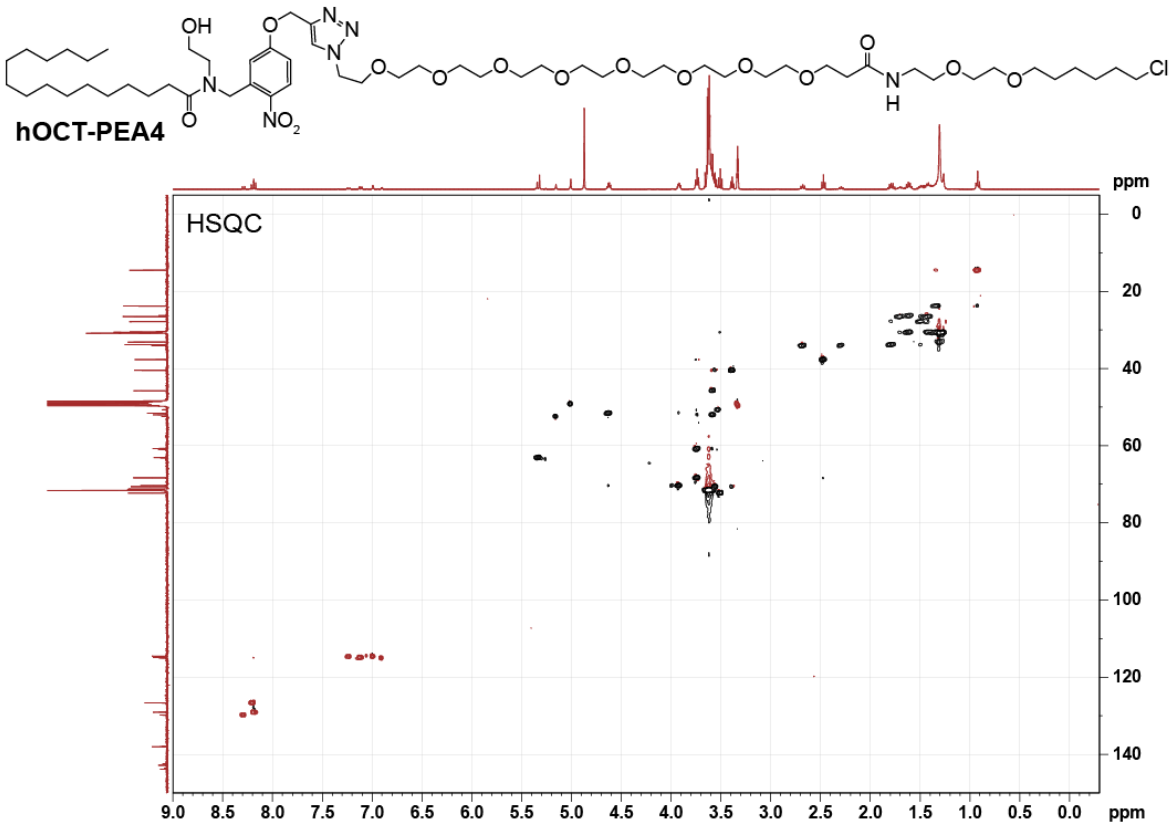
hOCT-PEA4
HSQC
ppm

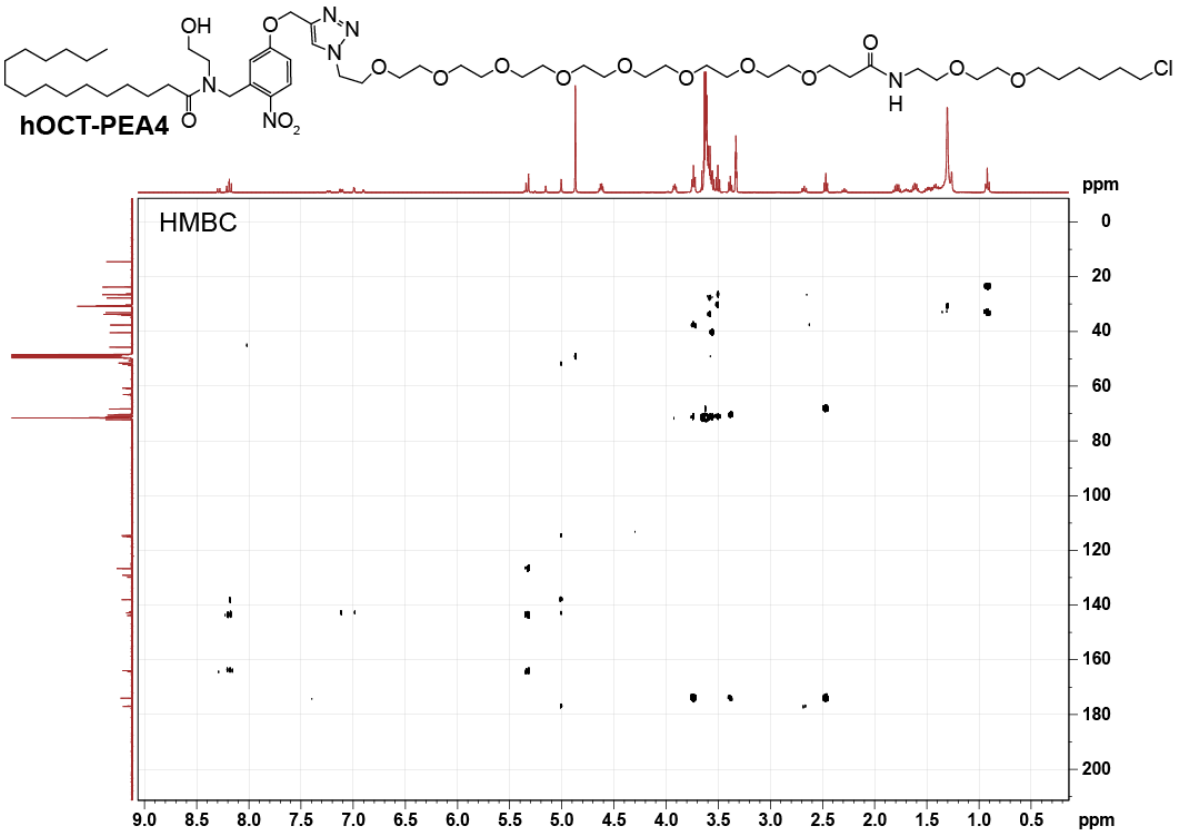
hOCT-PEA4
HMBC
ppm
0
20
40
60
80
100
120
140
160
180
200
9.0
8.5
8.0
7.5
7.0
6.5
6.0
5.5
5.0
4.5
4.0
3.5
3.0
2.5
2.0
1.5
1.0
0.5
ppm

# Chapter 4. Expanding the OCT-ligand platform to other ligands: hOCT-Anandamide

Janelle M. Tobias[1] and James A. Frank[1]

[1] Department of Chemical Physiology & Biochemistry, Oregon Health & Science University, Portland, OR, USA.

Author contribution:

**J.M.T.** and J.A.F. conceived and coordinated the study. **J.M.T.** synthesized and characterized **hOCT-anandamide**, performed experiments in cultured cells, and performed insulin ELISA on human islets. J.A.F. performed islet live imaging, and **J.M.T.** processed and analysed the data.

## 4.1. Introduction

The endocannabinoid system (ECS) regulates metabolism and plays an unresolved role within the pancreas[41]. In 1992, anandamide (AEA) was discovered as the first endogenous cannabinoid (CB) ligand (CB1)[7]. AEA is generated by NAPE-PLD and degraded by fatty acid amide hydrolase (FAAH)[12]. AEA is composed of an ethanolamine head group attached to an arachidonate (20:4n6) lipid chain and activates CB1, CB2 and transient receptor potential vanilloid-1 (TRPV1)[3,12]. CB1 is expressed in the central nervous system and throughout the periphery, including pancreatic islets[13,89]. CB1 is an inhibitory GPCR that is expressed in β-cells[90], and inhibits GSIS[91], presumably through inhibition of adenylyl cyclase activity[92]. INS-1E cells, a model β-cell line, have been reported to express TRPV1, another target of AEA, measured by PCR, and CB1, measured by PCR, Western Blot, and immunofluorescent staining[34]. However, due to conflicting physiological and immunohistochemical studies, the precise localization and function of CB1 in β-cells remain unclear[3]. Although intracellular CB1 signaling has been characterized in other cell types[74,75,93], nothing is known about intracellular CB1 in the pancreas.

There are a few optical tools that have been developed to study CB1. Optical tools are advantageous because they offer a high degree of temporal control, since light can be applied with unmatched speed. *Azo*-THC is a photoswitchable compound with a THC pharmacore that favors CB1 activation over CB2[43]. Caged-anandamide was first used to evaluate the dynamics of endocannabinoid retrograde signaling in rat hippocampus[47]. Caged-2-arachidonoylglycerol activated CB1 in MIN6 cells, a mouse-derived model β-cell line[48]. Together, these tools allow for optical control over cannabinoid signaling pathways with high temporal precision. However, these tools are freely diffusible, and do not allow for endogenous control of CB1 signaling with subcellular precision. A novel approach is needed to elucidate the subcellular role of CB1 on GSIS.

Building on the work presented in **Chapters 2** and **3**, I wanted to build an Optically-Cleavable Targeted (OCT)-ligand capable of targeting CB1. This work presents **hOCT-Anandamide**, which can target CB1, CB2 and TRPV1 (**Figure 4.1**). AEA is an ideal photocaged agonist, as it has already been shown to tolerate photocage modification[47], and it favors CB1 over other CBRs[12]. By linking photocaged AEA to a chloroalkane motif, it can be tethered to genetically encoded HaloTags[56]. These protein tags are fused to trafficking peptides for targeted expression on specific membranes, allowing us to enrich and release **hOCT-AEA** at genetically defined compartments. By combining **hOCT-AEA** with AAV-Halo (**Chapter 3**), a virus which expresses HaloTags on exclusively β-cells in human islets, we were able to achieve cell-targeted photorelease of AEA in intact human islets, and evaluate $Ca^{2+}$ dynamics in real time. Moving forward, **hOCT-AEA** can be used to probe endocannabinoid signaling with improved spatiotemporal control.

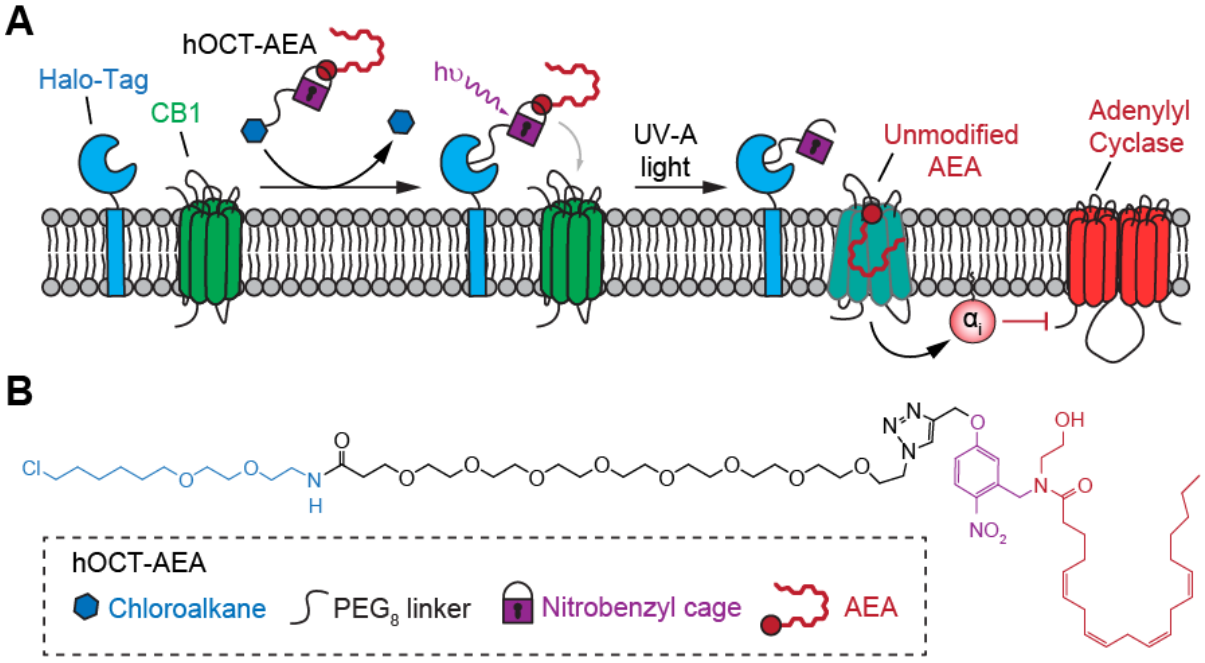


*Figure 4.1. hOCT-Anandamide (AEA) labels HaloTags and activates CB1.*
*(**A**) Schematic depiction of **hOCT-AEA**, which activates CB1 through $G\alpha_i$. (B) Chemical structure of **hOCT-AEA** which contains: a chloroalkane tag, $PEG_8$ linker, nitrobenzyl cage, and AEA ligand.*

## 4.2. Results

### 4.2.1. Design and synthesis of hOCT-AEA

The design of **hOCT-AEA** mimics the design of **hOCT-PEA4**, which was described in **Chapter 3**. The improved labeling efficiency and solubility due to the PEG8 linker were desirable features that were incorporated into the **hOCT-AEA** synthetic scheme (**Figure 4.2**). **hOCT-AEA** has a chloroalkane biorthogonal handle connected via a PEG8 linker to a nitrobenzyl photocage and AEA ligand. First, 5-hydroxy-2-nitrobenzaldehyde was reacted with a 3-bromoprop-1-yne linker under basic conditions to form phenolic ether **9**. Reductive amination with 2-(*t*-butyloxy)-ethanamine formed amine **10**, which was followed by acylation with arachidonyl chloride (AEA-Cl) to yield the tertiary amide **11**. Amide coupling of the $PEG_8$ acid with the **CA** led to **$N_3$-$PEG_8$-CA**, which was clicked onto alkyne **11** to afford triazole **13**. Finally, deprotection of the *t*Bu-ether afforded **hOCT-AEA** in 12% yield over 5 steps.

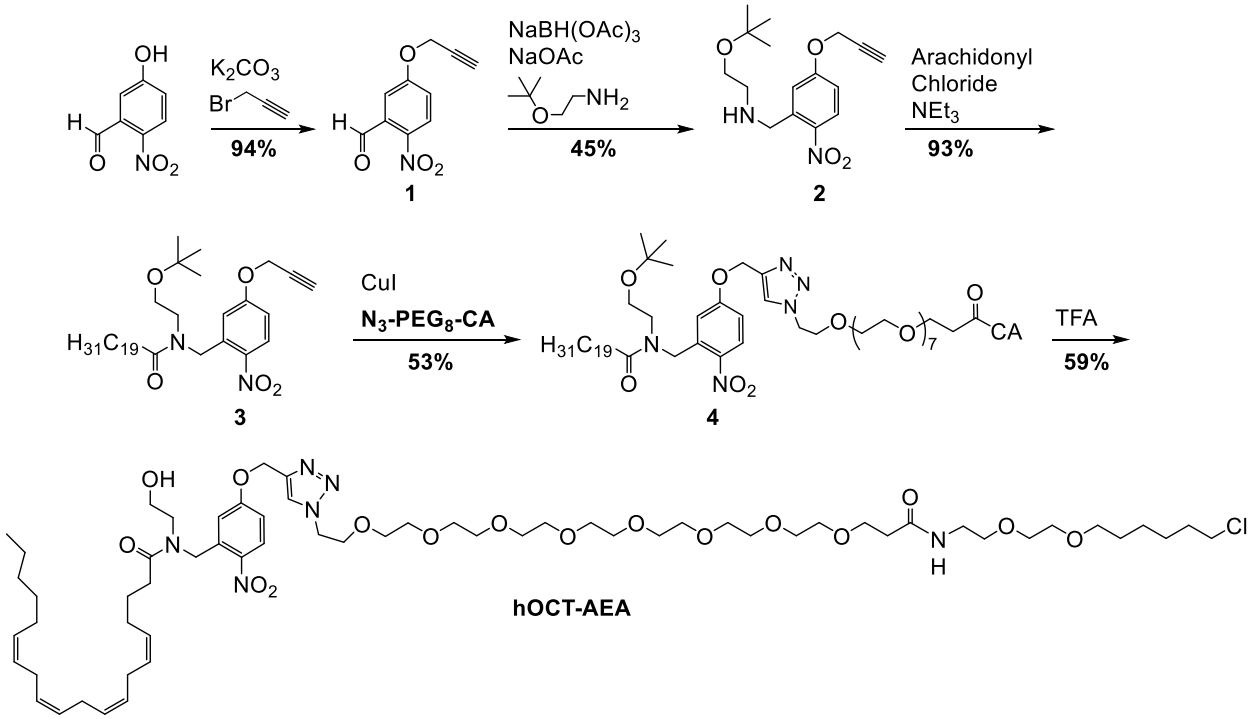


*Figure 4.2. Chemical synthesis of **hOCT-AEA**, which was prepared in 5 steps with 12% yield.*

UV-Vis spectroscopy was used to assess the photophysical properties of uncaging **hOCT-AEA** (**Figure 4.3 A**). Before UV-A exposure, **hOCT-AEA** had an absorbance peak at $\lambda_{max}$ = 306 nm (**Figure 4.3 B**, black). Irradiation with a 365 nm LED over 5 min caused a bathochromic shift to $\lambda_{max}$ = 359 nm, which is consistent with the formation of the nitroso-aldehyde that extends the electron $\pi$-network. The uncaging reaction proceeded with a $\tau$ = 22 s (**Figure 4.3 C**).

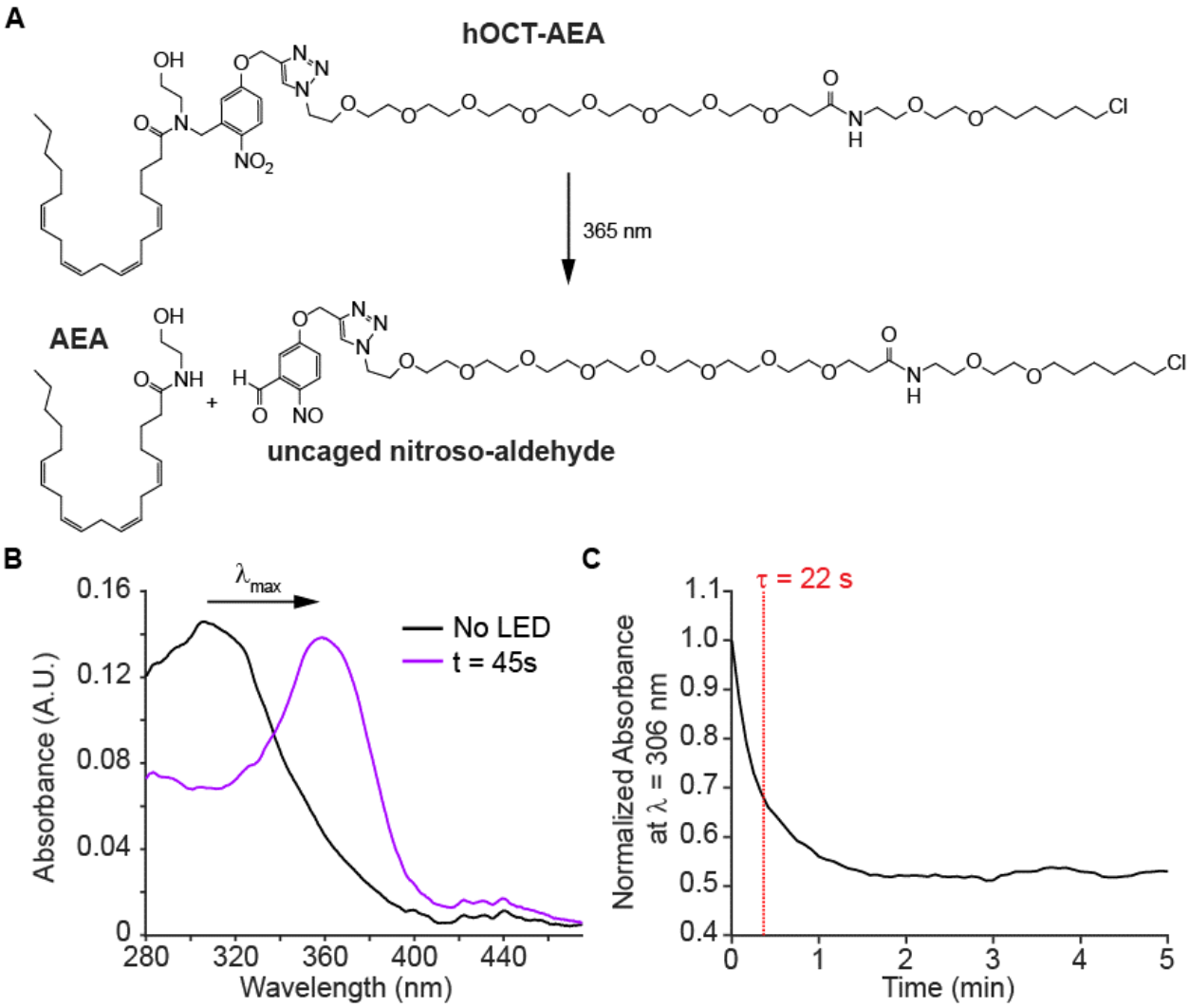


*Figure 4.3. Photophysical properties of uncagingg **hOCT-AEA** with 365 nm. (**A**) Chemical structures showing the uncaging reaction for **hOCT-AEA**. Uncaging **hOCT-AEA** releases AEA and the nitroso-aldehyde. (**B**) UV-Vis absorbance spectra of hOCT-AEA (40 $\mu$M, DMSO) before LED exposure (black) and after 45 s of 365 nm LED exposure (magenta). (**C**)*

*Kinetics of uncaging reaction, measured by monitoring the change in absorbance at $\lambda_{max}$ (306 nm) of the caged species over time with constant 365 nm LED exposure.*

### 4.2.2. INS-1 cells express FAAH

Fatty acid amide hydrolase (FAAH) is an ECS enzyme that degrades AEA. I wanted to confirm whether model β-cells expressed FAAH to ensure the proper machinery was present to metabolize AEA. I evaluated two model β-cell lines, INS-1[66] and MIN6[94] cells using western blot analysis and immunofluorescent staining. For western blot analysis, cell lysates were separated on an SDS-PAGE gel, transferred to a membrane, and stained with Ponceau to visualize total protein content (**Figure 4.4 A**, **left**). The membrane was probed for FAAH, and a band of the correct molecular weight (~63 kDa) was present in INS-1 lysate but not MIN6 lysate (**Figure 4.4 A**, **right**). Similar results were found with immunofluorescent staining, where INS-1 cells showed robust fluorescent signal, meanwhile MIN6 cells under the identical microscope settings showed minimal fluorescence (**Figure 4.4 B**). Staining controls for INS-1 cells, where the primary antibody was co-incubated with a blocking peptide and where the primary antibody was omitted, showed no fluorescent signal (**Figure 4.4 C**). Together, this data show that INS-1 cells express FAAH, while FAAH cannot be detected with this antibody in MIN6 cells. Consequently, INS-1 cells were used as the model system to evaluate **hOCT-AEA**.

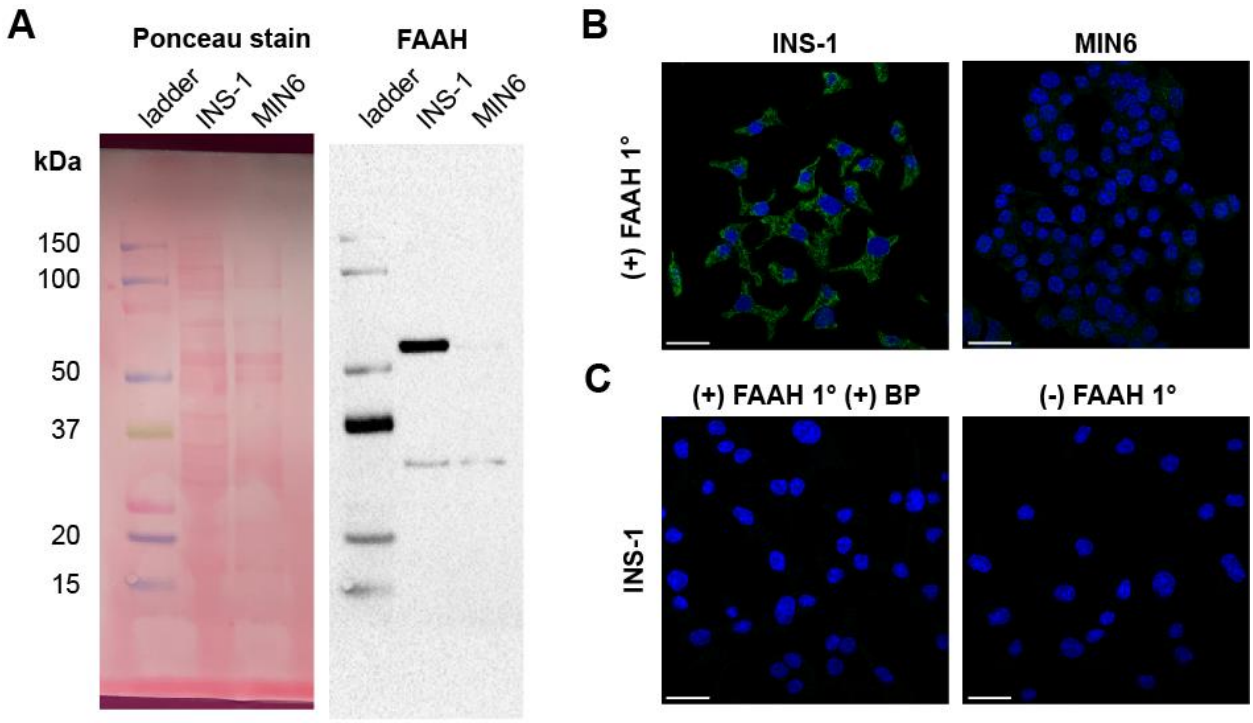


*Figure 4.4. FAAH characterization in model β-cells lines INS-1 and MIN6.*
*(**A**) Western blot analysis of INS-1 and MIN6 cells. The ponceau stain (left) shows total protein content, while the chemiluminescent signal (right) shows a robust band at the molecular weight for FAAH ( ~63 kDa) in INS-1 cells, but not MIN6 cells. 15 μg of cell lysate was loaded in each well. Chemiluminescent exposure was 30 s. (**B**) Immunofluorescent staining showing the merged image of the 2° donkey anti-rabbit Alexa488 (green) and DAPI (1:200k) to mark nuclei. FAAH was detected in INS-1 cells (left), but not MIN6 cells (right). (**C**) Immunofluorescent staining controls in INS-1 cells included co-incubation of FAAH 1° with the blocking peptide (BP, left) or staining with the 2° antibody without primary FAAH antibody (right). Scale bar 20 μm.*

### 4.2.3. Labeling of cell surface HaloTags in INS-1 cells

To verify that **hOCT-AEA** could label Halo-tags expressed on the surface of INS-1 cells, I used the pDisplayHalo-EGFP, which was described in **Chapter 3**. This plasmid co-express a cytosolic EGFP and a surface expressing HaloTag, which allows for data normalization against the EGFP channel. INS-1 cells were transfected with pDisplayHalo-EGFP, labelled with increasing doses of **hOCT-AEA** for 1 h, washed, and then labelled with jFHalo549i dye (**Figure 4.5 A**). **hOCT-**

**AEA** completely labelled the HaloTags at a concentration of 2 μM (**Figure 4.5 B**). Interestingly, this was the same optimal labeling conditions for **hOCT-PEA4**, which has the same linker as **hOCT-AEA**. This data suggests that while the linker influences the labeling kinetics, the acyl chain of the ligand has minimal impact on labeling efficiency.

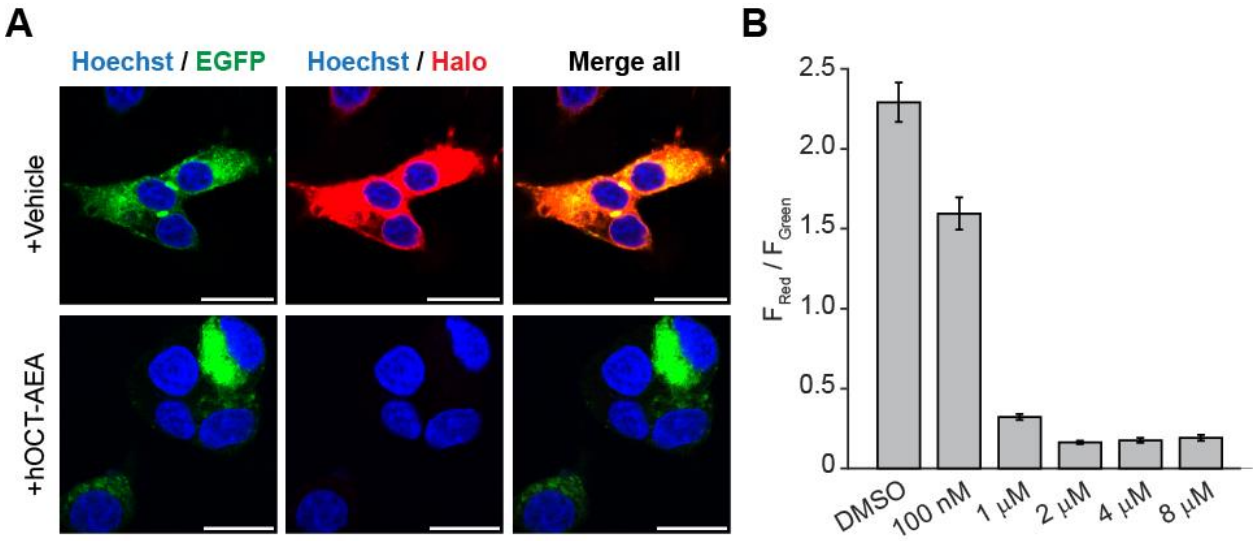


*Figure 4.5. hOCT-AEA labels surface expressing HaloTags in INS-1 cells.*
*(**A**) Representative images of INS-1 cells expressing pDisplayHalo-EGFP, preincubated with vehicle (DMSO, 0.1% v/v, top) or **hOCT-AEA** (2 μM, bottom) for 1 h, washed, and then co-labelled with jfHalo549i dye (500 nM, 15 min) and Hoechst-33342 (10 μM, 15 min). In the vehicle treated well, the Halo fluorescence overlaps with the EGFP channel as expected. In contrast, in the **hOCT-AEA** treated wells, jfHalo549i fluorescence is abolished, indicated that hOCT-AEA occupies most of the HaloTags. Scale bar 15 μm. (**B**) Quantification of competition labeling. Bar graph shows the ratio of the jFHalo549i fluorescence intensity normalized against the EGFP fluorescence.*

### 4.2.4. Plasma membrane uncaging of hOCT-AEA affects $Ca^{2+}$ but not cAMP in INS-1 cells

Since AEA targets CB1, which is $G\alpha_{i/o}$ coupled, I expected that uncaging **hOCT-AEA** would cause a decrease in cAMP. Thus, I performed preliminary experiments using $ePAC^{s\text{-}h18}$, a cAMP FRET sensor[95]. This biosensor uses CFP and YFP fluorescent proteins, which have overlapping

emission spectra with the pDisplayHalo-EGFP plasmid. Consequently, I used pDisplayHalo which lacks the EGFP transfection marker. I transfected INS-1 cells with a 3:1 cDNA ratio of pDisplayHalo:ePAC $^{s\text{-}h187}$ to promote the chances that the ePAC $^{s\text{-}h187}$ positive cells would also express pDisplayHalo. Uncaging **hOCT-AEA** in INS-1 cells in 20 mM glucose buffer had no effect on cAMP (**Figure 4.6 A**, **B**). Notably, cAMP oscillations were not observed at baseline. I also tried stimulating the INS-1 cells with forskolin first, followed by uncaging **hOCT-AEA**. However, uncaging **hOCT-AEA** after forskolin addition did not have a noticeable effect on cAMP (**Figure 4.6 C**, **D**). Further experiments are needed, including vehicle control and rimonabant treatment (CB1 inverse agonist), to draw conclusions on **hOCT-AEA** impact on cAMP in INS-1 cells.

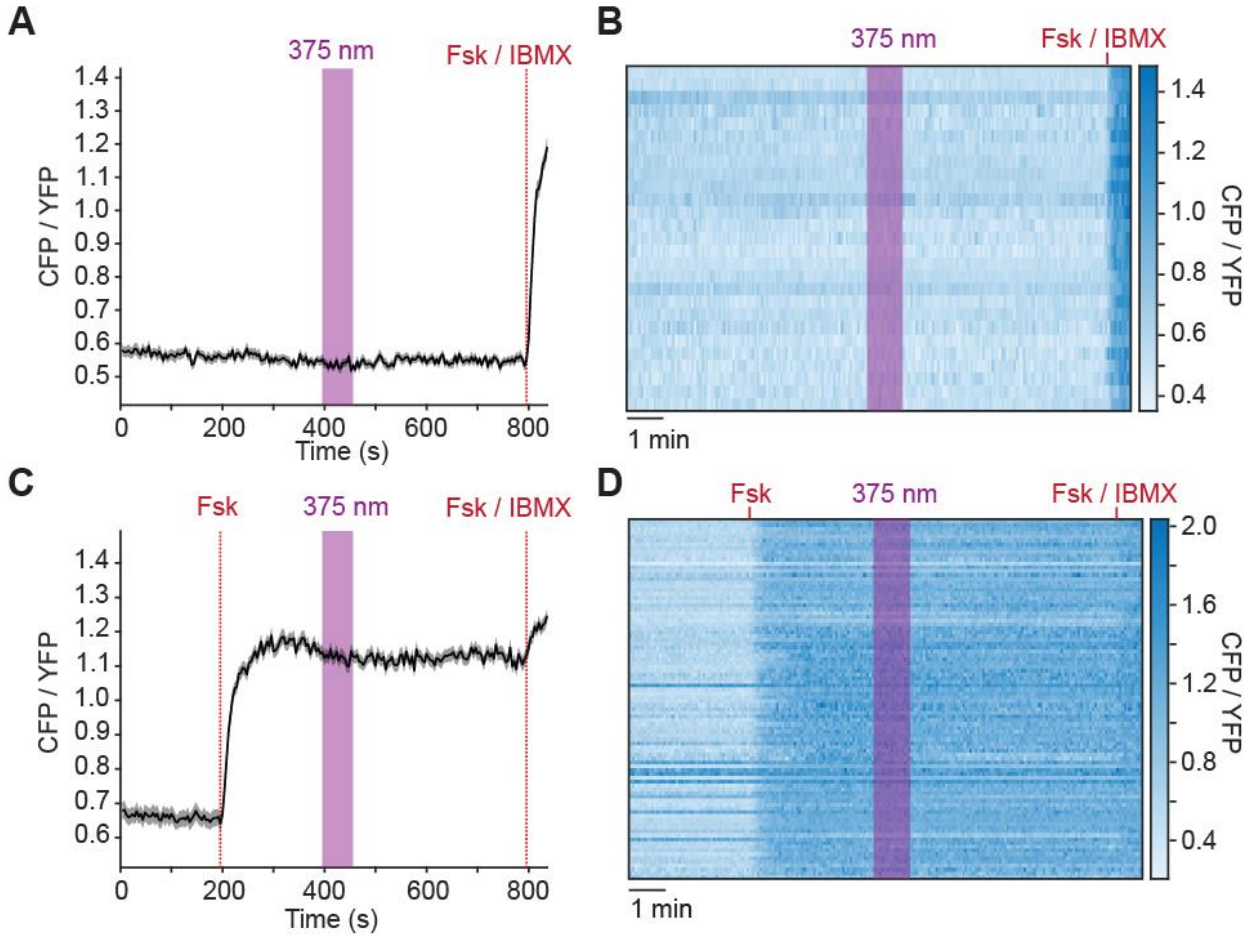


*Figure 4.6. Surface targeted uncaging of **hOCT-AEA** does not affect cAMP in INS-1 cells.*

*(**A**) Average trace and (**B**) heat map showing live fluorescent cAMP imaging using ePAC $^{s\text{-}h187}$. INS-1 cells were preincubated with **hOCT-AEA** (2 $\mu$M, 1 h, N = 27, T = 1) and uncaged with 375 nm stimulation (1 min), which did not affect the $[cAMP]_i$ in INS-1 cells. A mixture of forskolin (fsk, 25 $\mu$M) / IBMX (50 $\mu$M) was added as a positive control. (**C**) Average trace and (**D**) heat map showing live fluorescent cAMP imaging using ePAC $^{s\text{-}h187}$. INS-1 cells were preincubated with **hOCT-AEA** (2 $\mu$M, 1 h, N = 94, T = 3), stimulated with fsk (1 $\mu$M), flashed with UV, then a mixture of fsk (25 $\mu$M) / IBMX (50 $\mu$M) was added as a positive control. Uncaging **hOCT-AEA** did not seem to have a strong effect on $[cAMP]_i$, but more data is needed to be conclusive.*

Next, I wanted to evaluate how uncaging **hOCT-AEA** affected $[Ca^{2+}]_i$. I performed live confocal imaging on INS-1 cells co-transfected with cDNA encoding pDisplayHalo-EGFP and RGECO. The EGFP serves as a transfection marker that allows for cell picking of regions of interest (ROIs) that are both RGECO and EGFP positive. INS-1 cells were preincubated with **hOCT-AEA**, washed, and then left to equilibrate in the microscope environment box before imaging (~15 min). Unexpectedly, uncaging **hOCT-AEA** increased $Ca^{2+}$ oscillations relative to vehicle (**Figure 4.7 A**). While this increase in $Ca^{2+}$ oscillations was modest, it was significant (p value = 0.021, **Figure 4.7 B**).

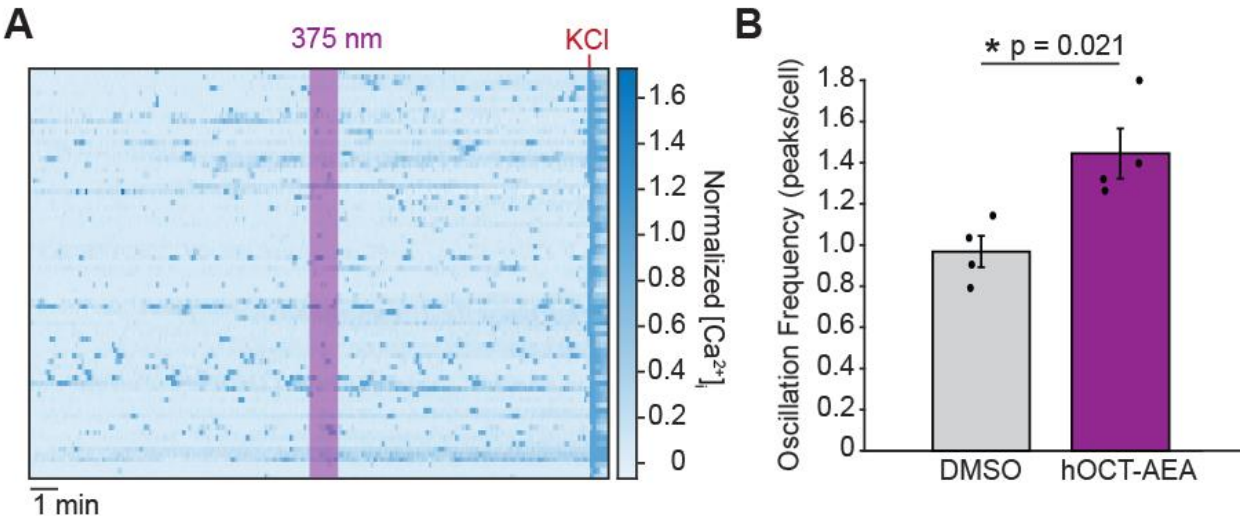


*Figure 4.7. Surface targeted uncaging of **hOCT-AEA** stimulates $Ca^{2+}$ in INS-1 cells.*

*(**A**) Heat map showing RGECO $Ca^{2+}$ traces from INS-1 cells that were preincubated with **hOCT-AEA** (2 μM, 1 h, N = 75, T = 4). Each row represents the normalized $Ca^{2+}$ trace of an individual cell. Data is normalized to the KCl response. (**B**) Bar graph showing the fold change in oscillation frequency in response to vehicle (N = 114, T = 4) or **hOCT-AEA** uncaging (N = 75, T = 4). **hOCT-AEA** significantly increased $Ca^{2+}$ oscillation frequency compared to vehicle, p = 0.021.*

### 4.2.5. AEA stimulates $Ca^{2+}$ and insulin in human islets, preliminary data

Finally, we evaluated how AEA affected intact human islets. Using the AAV-Halo virus described in **Chapter 3.2.5**, we targeted HaloTags to the β-cell surface of human islets and observed $Ca^{2+}$ events using a β-cell specific jRGECO1a (AdV-RIP-jRGECO1a). We preincubated islets with either vehicle (0.1% v/v DMSO) or **hOCT-AEA**, and measured jREGECO1a fluorescence at 11 mM glucose conditions (**Figure 4.8 A**). Similar to the INS-1 data, human islets treated with **hOCT-AEA** had an increased trend in $Ca^{2+}$ oscillations relative to vehicle after UV stimulation, although it was not significant. Of note, data was collected from one islet donor. Further, I wanted to evaluate how AEA treatment affected insulin release. Untransduced islets were treated with vehicle (0.1% v/v DMSO), AEA (10 μM), or Exendin-4 (100 nM) under high glucose (11 mM), and the supernatant was evaluated using a human insulin ELISA. Relative to vehicle, AEA and Exendin-4 increased insulin release trending towards significance in two donors (**Figure 4.8 B**). Insulin release was evaluated in two islet donors. Together, these data suggest that AEA can potentially stimulate $Ca^{2+}$ and insulin release from β-cells in human islets. Further data collection is needed in more islet donors to verify these results.

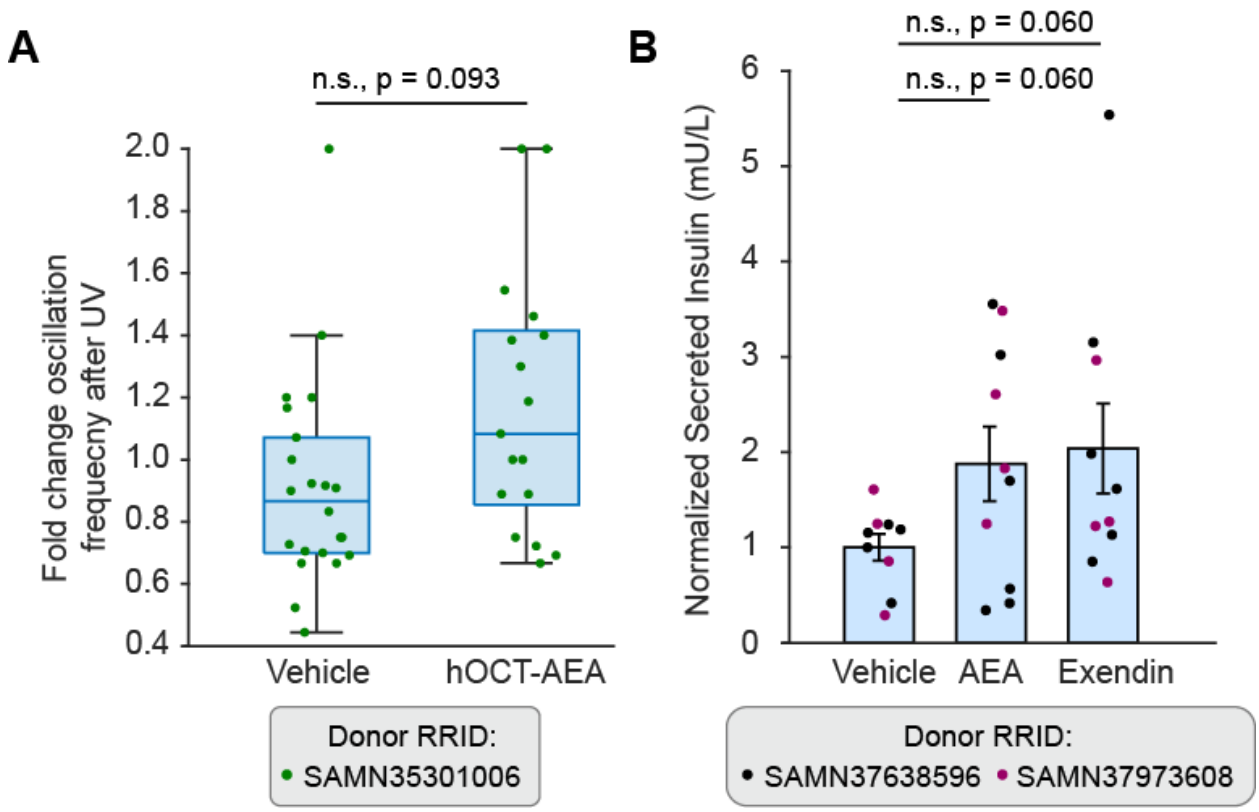


*Figure 4.8. AEA stimulates $Ca^{2+}$ and insulin in human islets.*

(**A**) *Comparison bar graph showing fold change in $Ca^{2+}$ oscillation counts after 375 nm stimulation relative to baseline. Uncaging **hOCT-AEA** (5 $\mu$M, 90 min, N = 17) on cells lead to a higher fold change in $Ca^{2+}$ events relative to vehicle (0.1% v/v DMSO, N = 22) across one donor. (**B**) Comparison bar graph showing the normalized secreted insulin (mU/L) from human islets in response to vehicle (0.1% v/v DMSO), AEA (10 $\mu$M), Exendin-4 (100 nM). Data collected from 2 donors.*

## 4.3. Discussion

This chapter presents a novel tool to place cannabinoid signaling under optical control. Expanding on our OCT-ligand technology, I synthesized **hOCT-AEA** that labels HaloTags and releases the classic endocannabinoid, AEA. Interestingly, **hOCT-AEA** had similar labeling efficiency as **hOCT-PEA4**, which has the same linker but differs in the composition of the lipid chain. This finding demonstrates how our synthetic scheme can be applied to different NAE ligands, while maintaining favorable properties such as labeling efficiency and uncaging $\tau$. I demonstrated that INS-1 cells were a better model $\beta$-cell system to test **hOCT-AEA** over MIN6 cells due to the presence of FAAH. However, due to the species difference between INS-1 (rat) and MIN6 (mouse) cells, FAAH expression should be evaluated via another antibody or another method, such as PCR, to confirm that MIN6 cells do not express FAAH. Uncaging **hOCT-AEA** on the surface did not seem to affect cAMP in INS-1 cells, suggesting that AEA did not activate CB1 in a $G\alpha_i$-coupled pathway. The forskolin addition could have oversaturated the sensor, demonstrating that the assay requires further optimization to test this probe in this cell line. However, characteristic cAMP oscillations in INS1 cells were also not observed, suggesting that the dynamic range of the sensor may not be suitable for INS-1 cells. In contrast, uncaging **hOCT-AEA** modestly stimulated $Ca^{2+}$ in INS-1 cells and islets. Further, AEA treatment led to enhanced insulin secretion in islets. Together, this data suggests that AEA could have a stimulatory role in $\beta$-cells and intact islets but requires further characterization to deduce the mechanism of action.

Future efforts for this project include completing necessary control experiments. For example, performing live imaging in the presence of rimonabant will help determine if the $Ca^{2+}$ stimulation observed from uncaging **hOCT-AEA** is CB1-mediated. Notably, $\beta$-cells also express TRPV1 which is activated by AEA. Given that the observed $Ca^{2+}$ stimulation is subtle and does not match a large $Ca^{2+}$ burst expected from a channel, TRPV1 is not the expected target.

However, treatment with capsazepine[96]—a TRPV1 antagonist—could deduce if TRPV1 is partially mediating the observed effect and should be considered in future studies. Live imaging in cells transfected with the pDisplayHalo$^{D107A}$-EGFP, the mutant plasmid which cannot label the probe, is necessary to deduce contributions of uncaging untethered probe. A current limitation of the presented tool is the dependence on UV-A for uncaging. Red-shifting the photocage will allow **hOCT-AEA** to be uncaged with longer wavelengths of light, and consequently more compatible with *in vivo* work. Red light penetrates deeper into tissue and is less phototoxic, and could be used with a cranial window for long-term imaging in the brain[97].

While I used **hOCT-AEA** to investigate AEA's role in pancreatic β-cells, this technology can be applied to other systems. Most neurological disorders have disrupted endocannabinoid signaling[4]. CB1 is the most highly expressed GPCR in the brain and tends to be located presynaptically in neurons[4]. Targeting **hOCT-AEA** to specific cell populations, or comparing presynaptic vs postsynpatic uncaging in the brain, could be a promising application of this approach. Further, a current collaboration with Tania Miramontes in Kelly Monk's lab (OHSU) showed that **hOCT-AEA** can label HaloTags expressed under the sox10 promoter in zebrafish, demonstrating the first application of OCT-ligand technology in a whole animal (data not shown). Overall, **hOCT-AEA** expands the toolset available to study AEA signaling and offers additional spatiotemporal control which is not possible with current technology. Moving forward, **hOCT-AEA** offers improved cell-targeted photopharmacology that will enable investigation of AEA's role in complex tissue.

## 4.4. Methods

### 4.4.1. General synthetic methods

Unless otherwise noted, all chemicals were purchased from TCI Chemicals, Fisher Scientific, Sigma-Aldrich, or Acros Organics, and were used without further purification. Dry solvents were purchased as “extra dry” or “anhydrous” and used without further purification. Reactions and chromatography were monitored by analytical thin layer chromatography (TLC) on Merck silica gel 60 $F_{254}$ glass plates. The plates were first visualized under 254 nm UV light, followed by staining with $KMnO_4$ solution or cerium (IV) molybdate solution (Hanessian’s stain) and gentle heating with a heat gun. Flash column chromatography was performed using silica gel (ACROS Organics™ 240360300, 0.035-0.070 mm, 60 A) or a Buchi Pure chromatography system.

Nuclear magnetic resonance (NMR) spectra were acquired on a BRUKER 400 MHz instrument. Chemical shifts ($\delta$) are reported in ppm and referenced to residual non-deuterated solvent peaks ($^1H/^{13}C$): $MeOD_4$ (3.31/49.00), and $CDCl_3$ (7.26/77.16). Multiplicities are abbreviated as: s = singlet, d = doublet, t = triplet, q = quartet, br = broad, m = multiplet. Data in $^{13}C$ is reported as E/Z isomer, where assignment of isomers are separated by a slash ( / ), and each peak assignment is separated by a semicolon. Separate atom peaks that are merged under one large peak (*i.e.,* acyl PEA chain, PEG linker) are separated by a comma.

High-resolution (35,000) mass spectrometry data were acquired at Portland State University’s BioAnalytical Mass Spectra Facility. Data were acquired on a vanquish UHPLC/HPLC system coupled to a Q-Exactive MS equipped with an electrospray ionization source operating in the positive mode.

### 4.4.2. UV-Vis spectroscopy

Compounds were diluted to 40 $\mu$M in DMSO and placed in a 1 ml Quartz cuvette (10 mm light path). A deuterium-halogen light source (Ocean Optics, DH-2000) transmitted light through

the sample, which was collected by a Flame UV-Vis-ES spectrophotometer (FLMT05021, Ocean Insight) using OceanView (Version 2.0.7) Software. Uncaging was achieved using 365 nm (Thorlabs M365FP1), 415 nm (Thorlabs M415F3), 470 nm (Thorlabs M470F4) and 565 nm (M565F3) fiber-coupled LEDs guided through a fiber-optic cable (Thorlabs #FP400URT, 400 μm diameter, 0.50 numerical aperture) and optical cannula (400 μm, Thorlabs). LED power was quantified by a power meter (Thorlabs, PM100D) with its photodiode power sensor (Thorlabs, S120VC) positioned directly at the fiber tip. The cannula tip was pointed directly into the top of the sample.

### 4.4.3. Cell Culture media and solutions

**INS-1 media** contains: RPMI 1640 with L-glutamine (Gibco, #11875-093) with 10% FBS, Penicillin-strep (1:100) and (in mM) 10 HEPES (Fisher, #BP310-500), 1 sodium pyruvate (Alfa Aesar, #A11148). INS-1 media was filtered and distributed into 50 ml aliquots. 50 μM 2-mercaptoethanol (BME, Sigma, #M3148) was added fresh to each 50 ml aliquot prior to use.

**INS-1 imaging buffer** contains (in mM): 185 NaCl, 1.2 $CaCl_2$, 1.2 $MgCl_2$, 1.2 $K_2HPO_4$, 20 HEPES. Adjusted to pH 7.4 with NaOH. D-glucose was supplemented at 5, 11 or 20 mM.

**INS-1 permeabilization buffer** contains: Phosphate buffered saline (PBS, Gibco, #70013-032) with 5 vol% donkey serum, and 0.3 vol% triton X-100 (Fisher, #BP151-100).

**INS-1 blocking buffer** contains: Phosphate buffered saline (PBS, Gibco, #70013-032) with 5 vol% donkey serum, and 0.1 vol% triton X-100 (Fisher, #BP151-100).

**Islet culture media** contains: RPMI 1640 with L-glutamine (Gibco, #11875-093) with 15 vol% FBS, Penicillin-strep (1:100)

**Islet imaging buffer** contains (in mM): 119 NaCl, 4.7 KCl, 1.0 $CaCl_2$, 1.5 $MgSO_4$, 1.2 $K_2HPO_4$, 10 HEPES. Adjusted to pH 7.35 with NaOH. Glucose was supplemented at 2, 11 or 20 mM.

**Islet blocking buffer** contains 0.3 vol% triton X-100 (Fisher, #BP151-100), 0.1 vol% BSA, 2 vol% donkey serum, phosphate buffer saline (PBS, Gibco, #70013-032)

**MIN6 media** contains: RPMI 1640 with L-glutamine (Gibco, #11875-093) with 15 vol% FBS, Penicillin-strep (1:100) and (in mm) 10 HEPES (Fisher, #BP310-500), 1 sodium pyruvate (Alfa Aesar, #A11148). MIN6 media was filtered and distributed into 50 ml aliquots. 70 μM BME was added fresh to each 50 ml aliquot prior to use.

**HEK culture (D10) media** contains high glucose DMEM (Gibco, #11965-092), 10 vol% FBS (HyClone's USDA tested, #SH30910), 0.5 vol% Penicillin-strep (Gibco, #15070). Sterile filtered and aliquoted.

**Phosphate buffer** contains (in mM): 320 $Na_2HPO_4$ (Fisher, #BP332-500), 80 $Na(PO_4H_2)•H_2O$ (Fisher, #S369-1). Adjusted pH to 7.4 with NaOH.

**Ponceau stain**: 5% glacid acetic acid, 0.2% ponceau stain in $dH_20$

**TBST**: 0.1% Tween-20, in TBS (10 mM Tris-HCl, pH 7.5, 150 mM NaCl)

**4% PFA:** paraformaldehyde (2 g, Sigma-Aldrich, #158127), 0.2 M phosphate buffer (25 ml), deionized $H_2O$ (25 ml). Adjusted pH to 7.4. Kept on ice until use.

### 4.4.4. Cell Culture

INS-1 832/13 cells[66] were grown in INS-1 media and incubated at 37 °C and 5% $CO_2$. Cells were used between passages 65-80. For live-cell $Ca^{2+}$ imaging, INS-1 cells were plated at a density of 150,000 cells per well on 8-well glass bottom chambered coverslips (Ibidi, #0827-90). 18-24 h later, cells were starved in Opti-MEM™ (250 μl) for 2 h before adding the transfection mixture containing (20 μl per well): 1 μl Lipofectamine-2000 (Fisher Scientific, #11668019), 75 ng R-GECO + 225 ng pDisplayHalo-EGFP, or 75 ng ePAC $^{s\text{-}h187}$ + 225 ng pDisplayHalo-EGFP in Opti-MEM™. The cells were then incubated at 37 °C and 5% $CO_2$ for 18-24 h before

exchanging the transfection mixture with INS-1 media. Microscopy experiments were performed 60-72 h post-transfection.

MIN6[98] cells were grown in MIN6 media and incubated at 37 °C and 5% $CO_2$. Cells were used between passages 40-55.

Human pancreatic islets from nondiabetic donors were received from the Integrated Islet Distribution Program (IIDP) funded by the National Institute of Diabetes and Digestive and Kidney Disease (NIDDK). Islets were cultured in islet culture media in non-surface treated 24-well suspension plates (VWR® #10861-558), or non-surface treated 10 cm culture dishes (Falcon® #351029) at 37 °C and 5% $CO_2$ for up to two weeks after receiving the shipment. Islets were transduced by mixing AAV-Halo only in 200 μl islet culture media in a 15 ml conical centrifuge tube set at ~10° angle for 1 h at 4 °C on an orbital shaker. They were then transferred to 24-well suspension plates or 10 cm culture dishes and cultured for 4 days at 37 °C and 5% $CO_2$ before experiments. For jRGECO1a AdV transductions, the islets were placed in a 24-well plate in 2 ml islet media, then 1 μl concentrated jRGECO1a solution was added directly to the media of the wells and cultured for 4 days before experiments.

### 4.4.5. INS-1 Competition Labeling Assay

For the **hOCT-AEA** competition labeling assay, a transfection mixture containing (50 μl per well) 1 μl Lipofectamine-2000 and 150 ng pDisplay-Halo-EGFP in Optim-MEM™ was added to acid-etched glass coverslips (12 mm, #1.5) in a 24-well plate. INS-1 cells were then plated at a density of 150,000 cells per well on top of the transfection mixture, and Opti-MEM™ was added to a final volume of 0.5 ml. The cells were then incubated at 37 °C and 5% $CO_2$ for 18-24 h before exchanging the media with fresh INS-1 media. 60-72 h post transfection, the cells were labeled with vehicle or **hOCT-AEA** (100 nM – 8 μM) in INS-1 media (without BME) for 1 h. The cells were washed once with INS-1 media (without BME), then labelled with a dye mixture

containing jFHalo549i (500 nM) and Hoechst-33342 (10 μM) for 10 min. The coverslips were washed with cold PBS, fixed in 4% PFA for 5 min at RT, and washed 3× in PBS. The coverslips were mounted on a microscope slide (VWR® Superfrost® Plus Micro Slide, 75×25×1 mm, #48311-703) with mounting solution (Fluoromount™) and sealed with nail polish. Imaging parameters are described below in the "Fixed cell microscopy" section.

Two images per coverslip were acquired with a 20× objective at 1024×1024 pixel resolution for quantification, and one representative image was acquired with a 63× oil objective at 2048×2048 pixel resolution. For quantification, intensity from regions-of-interest drawn using the Fiji software[76] around each EGFP+ cell across 4 images from two biological replicates, and the intensities from the green and red channels were exported to be analyzed with MATLAB scripts written in-house.

#### 4.4.6. rAAV production and purification

We produced and purified the rAAV's using the *Easy AAV production* as previously described[83]. After cloning in our pDisplay-PT's into their AAV vector and verifying insert size from restriction digest and sequencing, we grew and maintained HEK293 cells for two passages before plating them in 10-cm culture dishes in HEK culture media to achieve 90% confluency the following day. For each plate, the media was replaced with 6.5 ml modified HEK culture media featuring DMEM + L-glutamine, 2% FBS, and no antibiotics. 6 μg of each AAV plasmid (AAV-INSx2-pDisplay-HaloTag-3MRE's, pAd5 Adeno Helper, and pAAV-KP1 Rep-Cap[86]) were mixed in a 50 ml conical tube with 54 μl of 1mg/ml polyethylenemine (PEI, Polysciences MW 2500). 3.5 ml of OptiMEM was added before vigorous mixing with a benchtop vortex mixer, followed by 20 min incubation at RT and addition to the HEK cells. The plates were cultured for 7 days at 37° C and 5% $CO_2$ prior to AAV harvest and purification. The AAV-containing culture media was collected from the plates and placed into a 250 ml conical tube, 2× centrifuged at 1800g for 30 min and

then placed into a new conical tube. The filtrate was then passed through a 0.25 μm PES filter into a new 250 ml conical tube before 1 μl of benzonase was added. The tube was gently inverted 10× to mix the solutions. The conical tube was then incubated at 37° C and 5% $CO_2$ for 30 min, followed by centrifugation at 1800g for 30 min. The solution was again filtered through a 0.25 μm PES filter into a new 250 ml conical tube. The filtrate was then mixed with 5× PEG8000 / NaCl to achieve 1× concentration and inverted 50 times. The mixture was stored at 4 °C overnight to precipitate the viral particles. The mixture was again centrifuged at 5000g at 4° C for 1 h before the supernatant was carefully removed. The viral pellet was resuspended in 500 μl PBS and placed on an orbital shaker overnight at 4° C. The virus / PBS mixture was collected into 1.5 ml tubes and centrifuged at 5000 rpm for 4 min at RT. The viral lysate was then collected and transferred into a new 1.5 ml tube, then aliquoted into 0.5 ml tubes. The viral aliquots were quickly frozen on dry ice, and stored in -80° C for future use.

### 4.4.7. Immunofluorescence staining in cultured β-cells

INS-1 or MIN6 cells were plated on acid-etched glass coverslips (12 mm, #1.5) at a density of 100,000 cells per well in a 24-well plate (Fisherbrand, #FB012929). The coverslips were washed with cold PBS, fixed in ice-cold 4% PFA for 5 min at RT and washed 2× with PBS (5 min). The fixed cells were then incubated in the INS-1 permeabilization buffer for 1 h. The cells were then incubated in 1° FAAH antibody (1:500, Cayman 10010183, Batch 0568775-1) with or without rabbit FAAH blocking peptide (1:5 primary : blocking peptide, Cayman 301600, lot #0500350-1) diluted in INS-1 blocking buffer and shook overnight (12-14 h, 4 °C) in the dark. The coverslips were then washed 3× with PBS (5 min, RT), then incubated with 2° donkey anti-rabbit Alexa Fluor™488 (1:2000) diluted in INS-1 blocking buffer for 1 h in the dark shaking at RT. The coverslips were washed 3× with PBS (5 min), stained for DAPI (1:200k, Invitrogen D1306, 5 min) and then washed 2× with deionized $H_2O$ (5 min). The coverslips were mounted

on a microscope slide (VWR® Superfrost® Plus Micro Slide, 75×25×1 mm, #48311-703) with mounting solution (Fluoromount™) and sealed using nail polish. The slides were kept in the dark until imaging within one week.

### 4.4.8. Live-cell confocal microscopy

Live cell and islet imaging was performed on an Olympus Fluoview 1200 laser scanning confocal microscope at 37 °C and 5% $CO_2$. Videos were acquired with a 20× objective, 512×512-pixel resolution, and scan rate of 4 s per frame. R-GECO and jRGECO1a excitation was performed with a 559 nm laser at low laser power (<6%) and emission was collected at 570-670 nm. EGFP excitation was performed with a 488 nm laser at low laser power (<5%) and emission was collected at 500-545 nm. CFP / YFP excitation was performed with 405 nm laser at low laser power (<5%) and emission was collected at 450-490 nm (CYP) and 500-550 nm (YFP). Photo-activation was performed with a 375 nm laser (PicoQuant, PDL 800-D, 100% laser power) triggered using the quench function in the Olympus software.

For $Ca^{2+}$ imaging experiments, regions-of-interest were manually drawn around oscillating cells that were EGFP+ (INS-1) or entire islets using the Fiji software, and the resulting data were analyzed with MATLAB scripts written in-house.

For $Ca^{2+}$ imaging experiments in human islets, AdV-RIP-jRGECO1a-expressing islets were transferred to 8-well Ibidi glass bottom chambered coverslips (Ibidi, #0827-90) containing 300 μL of islet imaging buffer. 10-15 islets were added to each chamber, and the chamber was gently swirled to cluster the islets in the center of the chamber. The islets were placed on the microscope and allowed to equilibrate at 37 °C and 5% $CO_2$ for at least 25 min before imaging.

### 4.4.9. Fixed cell microscopy

Fixed samples were imaged on a Zeiss LSM880 confocal laser scanning microscope with Airyscan with a 40× oil objective or a 63× oil objective at 2048×2048 pixel resolution. Hoechst-33342 and DAPI excitation were performed with a 405 nm laser at low laser power (<1%). Green fluorophores were excited with a 488 nm laser at low laser power (<2%). Red fluorophores were excited with a 550 nm laser at low laser power (<10%).

### 4.4.10. Western Blot

MIN6 and INS-1 cells were seeded in a 6 cm dish and were grown until 80% confluent. Cells were washed with cold PBS, then aspirated before freezing in -80 °C until ready to use. Cells were scraped off of the plate in cold PBS, spun for 5 min at 1000 rpm, and the PBS was aspirated. The pellet was resuspended in RIPA buffer spiked with protease inhibitor (Thermo Scientific™ Pierce™ protease inhibitor tablets, EDTA-free, Fisher, PIA32965) and was spun down for 10 min at 14,000 x g at 4 °C. Lysates were quantified using a BCA assay, and 15 μg of lysate was diluted in sample buffer (Nu PAGE LDS sample buffer), boiled for 5 min at 95 °C, and then loaded onto a 4-12% precast acrylamide gel. Lysates were separated by SDS-PAGE (130V, 75 min), and transferred to a nitrocellulose membrane (100V, 1 h, RT). The membrane was stained with Ponceau stain, washed, and then blocked in 5% BSA in TBST (30 min, RT). The membrane was washed 3x, and then incubated at 4 °C overnight with primary rabbit FAAH antibody (1:1000, Cayman 10010183, Batch 0568775-1). Membrane was washed 3x, probed with donkey anti-rabbit HRP-conjugated secondary antibody (1:10,000) in 5% BSA in TBST (1 h, RT), and washed 3x. The membrane was developed in Super Signal West Pico PLUS chemiluminescent substrate and imaged on a Bio-Rad MP imager.

### 4.4.11. Insulin ELISA assay

Each islet treatment was performed in triplicate or quadruplet per drug stimulation. For one treatment, 20 islets were handpicked and transferred to a 1.5 ml tube. The islets were centrifuged at 310 rcf for 4 min and the media was aspirated. The islets were preconditioned in INS-1 imaging buffer spiked with 5 mM glucose for 1 h at 37 °C and 5% $CO_2$. The islets were again spun at 310 rcf for 4 min, and the buffer was aspirated. The islets were then treated with INS-1 imaging buffer spiked with 11 mM glucose + drug (vehicle, 10 μM AEA, 100 nM Exendin-4) for 30 min at 37 °C and 5% $CO_2$. The stimulated islets were centrifuged at 310 rcf for 4 min, then the supernatant was collect and evaluated via a human insulin ELISA assay (Mercodia 10-1113-01) per manufacturer instructions. Absorbance values at 450 nm were recorded using a CLARIOstarPLUS plate reader (BMG Labtech, 0430), and the data was processed using myAssays.com and MATLAB. Data was normalized against the mean of the vehicle treatment per trial.

### 4.4.12. Data analysis and code availability

Unless otherwise described, all data are presented as mean ± S.E.M, which was calculated as:

$$\mathrm{S.E.M.} = \frac{\text{standard deviation}}{\sqrt{\mathrm{N}}}$$

For imaging experiments, N is the total number of cells (technical replicates), and T is the number of independent experiments (biological replicates). $Ca^{2+}$ oscillations were calculated in MATLAB using the 'findpeaks' function with and y threshold of 0.5 for RGECO (INS-1 data), a y threshold of 0.2 for jRGECO1a (islet data). For RGECO and jRGECO1a data, the total number of oscillations across the field of view was counted from the beginning of the video to UV-A irradiation. Separately, the total number of oscillations were counted over an equivalent time post-stimulation. The sum of the peaks was normalized against the number of cells per

video (to quantify “oscillations per cell” for each trial and condition), and then the mean fold change for post/pre-stimulation was calculated alongside the S.E.M.

Statistical significance was assessed using MATLAB (Mathworks). For the comparison between two groups in oscillation frequency or ELISA analysis, a Welch’s two-sample t-test was used, with significance threshold placed at *P<0.05, **P<0.01, ns = P>0.05.

## 4.5. Detailed synthetic methods

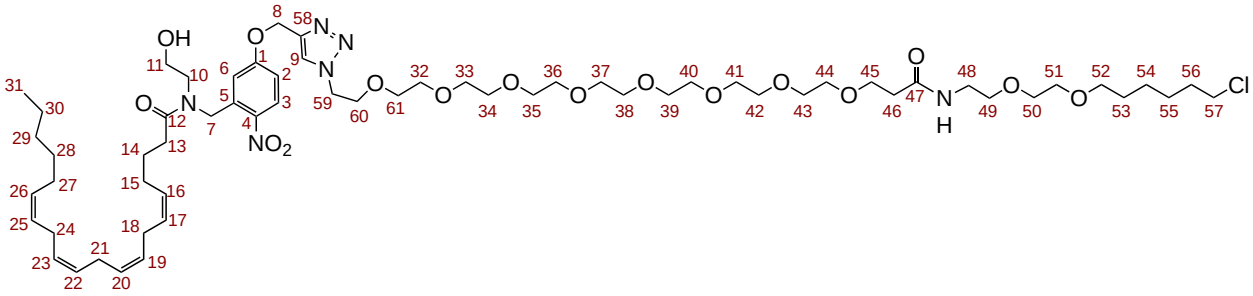

*Figure 4.9. Numbering system utilized in the NMR assignments for **hOCT-AEA**.*

### 4.5.1. Synthesis of (5Z,8Z,11Z,14Z)-*N*-(2-(tert-butoxy)ethyl)-*N*-(2-nitro-5-(prop-2-yn-1-yloxy)benzyl)icosa-5,8,11,14-tetraenamide (3).

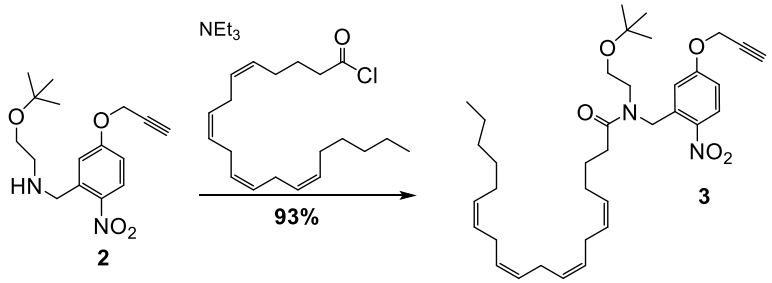


**2-(*tert*-butoxy)-*N*-(2-nitro-5-(prop-2-yn-1-yloxy)benzyl)ethan-1-amine (2)** was prepared as described in section **3.5.7**.

Arachidonic acid (75 mg, 0.25 mmol, 2.4 equiv.) was placed under an argon atmosphere and dissolved in anhydrous DCE (2.5 ml), then oxalyl chloride (27 μl, 0.31 mmol) and a drop of anhydrous DMF were added to initiate the reaction. The reaction was stirred for 1 h at room temperature, then concentrated *in vacuo*. The crude reaction was re-dissolved and concentrated *in vacuo* in DCM 2× and then in toluene 2×. The crude arachidonoyl chloride was placed under an argon atmosphere and dissolved in anhydrous DCE (2 ml).

Separately, compound **2** (32 mg, 0.11 mmol, 1.0 equiv.) was placed under an argon atmosphere, dissolved in anhydrous DCE (5 ml), and then the arachidonoyl chloride was transferred to the amine reaction. $NEt_3$ (30 μl, 0.22 mmol, 2.0 equiv.) was added dropwise. After 30 min the reaction was diluted in DCM (5 ml), transferred to a separatory funnel, and was quenched with saturated $NaHCO_3$ (10 mL). The organic layer was washed 2× with saturated $NaHCO_3$ and wash once with brine. The organic phase was separated, dried over anhydrous $MgSO_4$, and then filtered. The solvent was removed in vacuo, and the crude product was purified by $SiO_2$ flash chromatography (EtOAc:Hexane 1:19 → EtOAc:Hexane 1:4). **(5Z,8Z,11Z,14Z)-*N*-(2-(tert-butoxy)ethyl)-*N*-(2-nitro-5-(prop-2-yn-1-yloxy)benzyl)icosa-5,8,11,14-tetraenamide** (**3**, 58 mg, 0.98 mmol, 93%) was isolated as a yellow oil.

**TLC (EtOAc:Hexane, 1:4 ): $R_f$ =** 0.22. **$^1$H NMR ($CDCl_3$, 400 MHz, 25 °C):** δ 8.25 (d, 0.5 H, H3, *J* = 9.1 Hz); 8.14 (d, 0.5 H, H3, *J* = 9.1 Hz); 6.99 (dd, 0.5 H, H2, *J* = 9.1, 2.8 Hz); 6.92 (dd, 0.5 H, H2, *J* = 9.1, 2.8 Hz); 6.87-6.82 (m, 1 H, H6); 5.48-5.22 (m, 8 H, H16, H17, H19, H20, H22, H23, H25, H26); 5.14 (s, 1 H, $H7_A$); 5.03 (s, 1 H, $H7_B$); 4.76 (d, 1 H, $H8_A$, *J* = 2.4 Hz); 4.73 (d, 1 H, $H8_B$, *J* = 2.4 Hz); 3.61-3.45 (m, 4 H, $H10_{A,B}$, $11_{A,B}$); 2.91-2.70 (m, 6 H, $H18_{A,B}$, $H21_{A,B}$, $H24_{A,B}$); 2.62-2.53 (m, 2 H, $H13_A$, H9); 2.27-2.12 (m, 2 H, $H13_B$, $H15_A$); 2.12-1.96 (m, 3 H, $H15_B$, $H27_{A,B}$); 1.85-1.64 (m, 2 H, $H14_{A,B}$); 1.42-1.22 (m, 6 H, H28-30); 1.15 (d, 9 H, $C(C\underline{H}_3)_3$, *J* = 4.3 Hz); 0.95-0.80 (m, 3 H, $H31_{A,B,C}$). **$^{13}$C NMR ($CDCl_3$, 101 MHz, 25 °C):** δ 177.71; 174.33 / 173.98 (C12); 162.16 / 161.69 (C1); 142.01 / 141.33 (C4); 137.56 / 137.27 (C5); 130.64; 130.62; 129.53 (C26); 129.24; 129.10 (C3); 128.96, 128.90, 128.79, 128.73, 128.70, 128.69, 128.39, 128.36, 128.33, 128.28, 128.26, 128.22, 128.08, 127.99, 127.97, 127.66 (C3, C16, C17, C19, C20, C22, C23, C25, C26); 114.57 / 113.85 (C6); 113.44 / 112.92 (C2); 77.48; 77.43; 77.16; 77.11 (C9); 77.07; 76.84; 76.75; 73.60 / 73.31 ($\underline{C}(CH_3)_3$); 60.75 / 59.77 (C11); 56.40 / 56.25 (C8); 51.49 (C7); 49.11 (C10); 47.59 (C7, C10); 33.28 / 32.67 / 32.55 (C13); 31.64 (C29); 29.45 (C28); 27.54 / 27.46 ($C(\underline{C}H_3)_3$); 27.34 (C27); 27.07 / 26.79 (C15); 26.61; 25.77, 25.75, 25.73 (C18, C21, C24); 25.31 / 25.17 (C14); 24.69; 22.70 (C30); 14.19 (C31). **HRMS (ESI$^+$):** *m/z* calcd. for $[C_{36}H_{52}N_2O_5]^+$: 593.3954, found: 593.3923 ($[M+H]^+$).

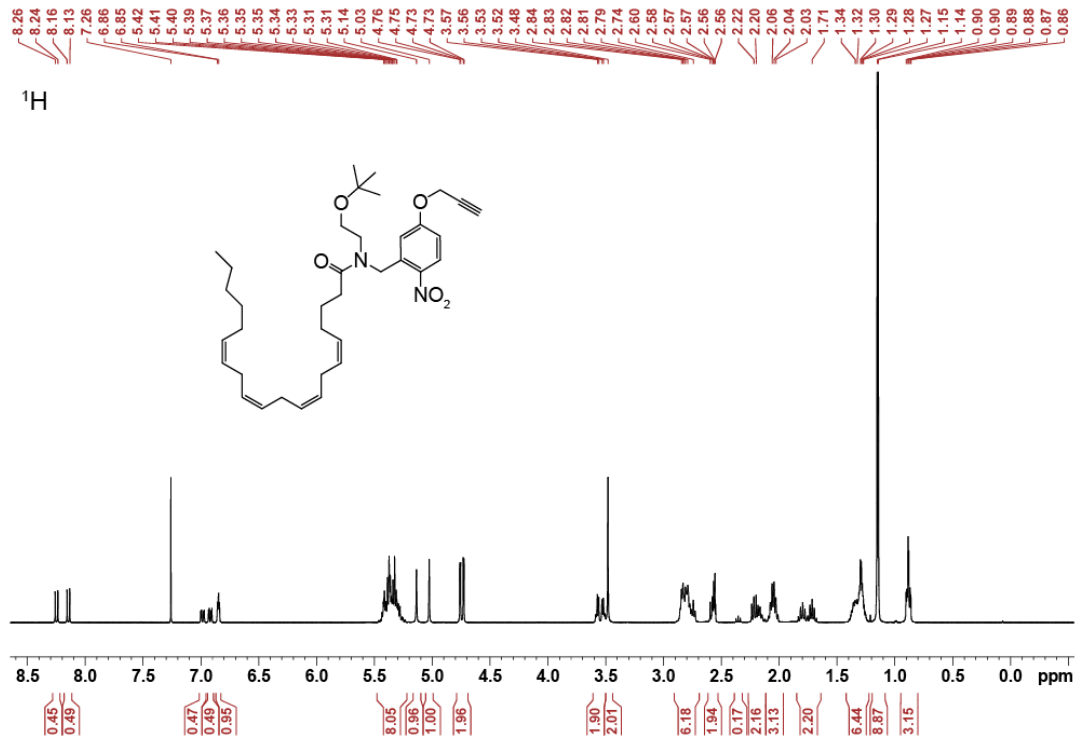
8.26
8.24
8.16
8.13
7.26
6.86
6.85
5.42
5.41
5.40
5.39
5.37
5.36
5.35
5.35
5.34
5.33
5.31
5.31
5.14
5.03
4.76
4.75
4.73
4.73
3.57
3.56
3.53
3.52
3.48
2.84
2.83
2.82
2.81
2.79
2.74
2.60
2.58
2.57
2.57
2.56
2.56
2.22
2.20
2.06
2.04
2.03
1.71
1.34
1.32
1.30
1.29
1.28
1.27
1.15
1.14
0.90
0.90
0.89
0.88
0.87
0.86
1H
O
O
O
N
NO2
8.5
8.0
7.5
7.0
6.5
6.0
5.5
5.0
4.5
4.0
3.5
3.0
2.5
2.0
1.5
1.0
0.5
0.0
ppm
0.45
0.49
0.47
0.49
0.95
8.05
0.96
1.00
1.96
1.90
2.01
6.18
1.94
0.17
2.16
3.13
2.20
6.44
8.87
3.15

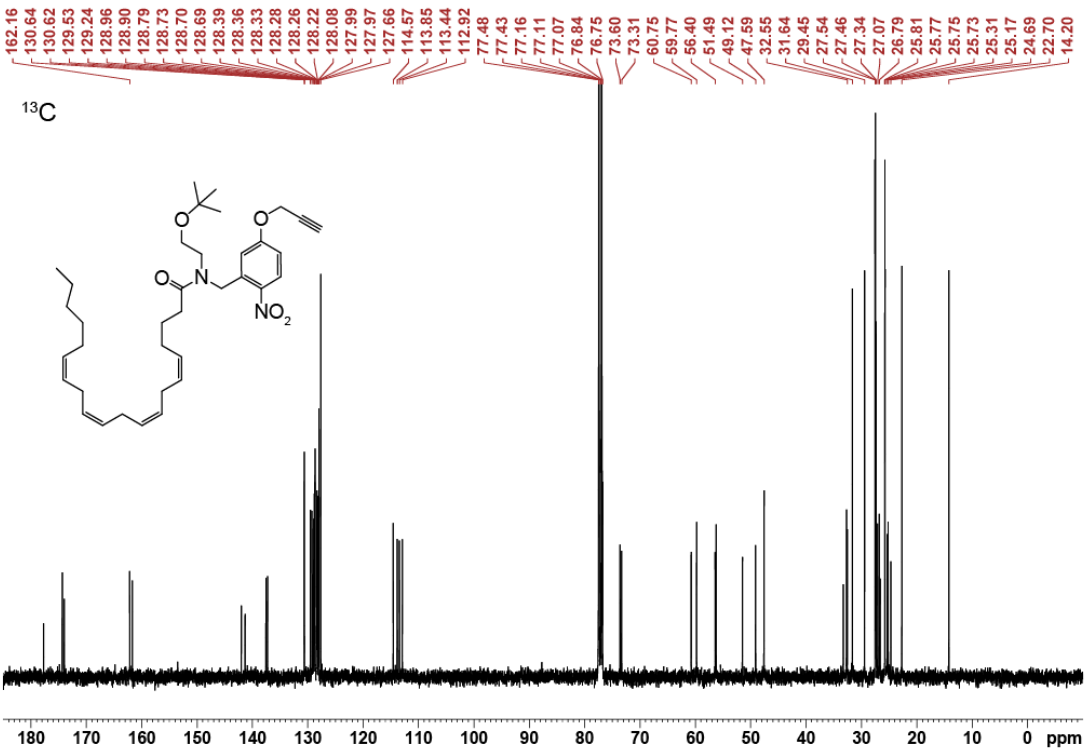
162.16
130.64
130.62
129.53
129.24
128.96
128.90
128.79
128.73
128.70
128.69
128.39
128.36
128.33
128.28
128.26
128.22
128.08
127.99
127.97
127.66
114.57
113.85
113.44
112.92
77.48
77.43
77.16
77.11
77.07
76.84
76.75
73.60
73.31
60.75
59.77
56.40
51.49
49.12
47.59
32.55
31.64
29.45
27.54
27.46
27.34
27.07
26.79
25.81
25.77
25.75
25.73
25.31
25.17
24.69
22.70
14.20
13C
O
O
O
N
NO2
180
170
160
150
140
130
120
110
100
90
80
70
60
50
40
30
20
10
0
ppm

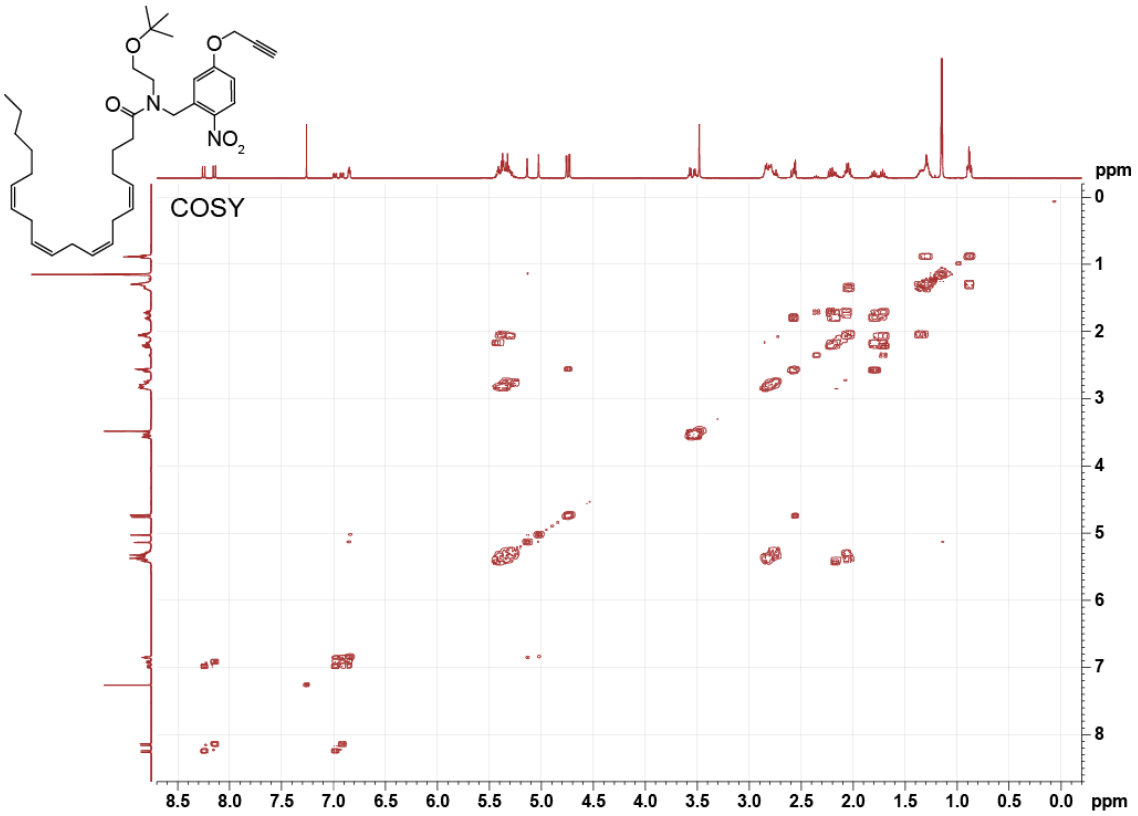
COSY
ppm
8.5 8.0 7.5 7.0 6.5 6.0 5.5 5.0 4.5 4.0 3.5 3.0 2.5 2.0 1.5 1.0 0.5 0.0 ppm
0 1 2 3 4 5 6 7 8

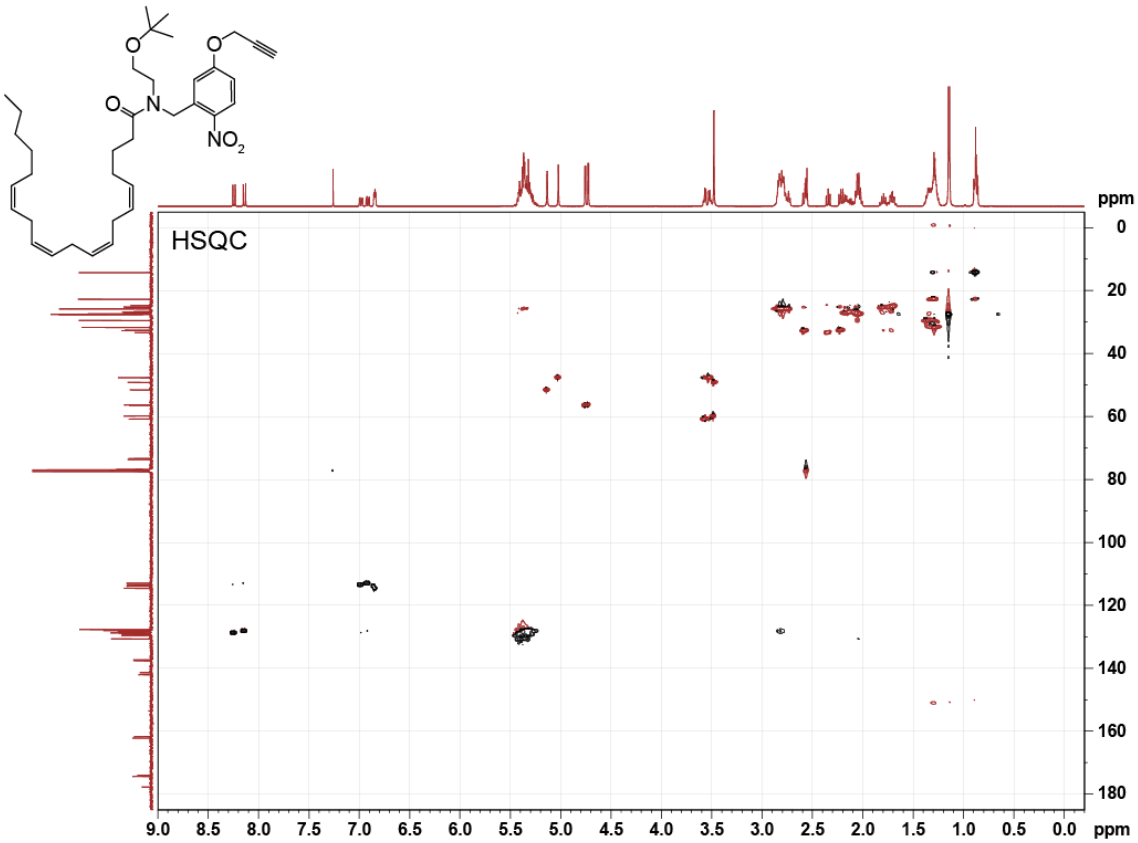
HSQC
ppm
9.0 8.5 8.0 7.5 7.0 6.5 6.0 5.5 5.0 4.5 4.0 3.5 3.0 2.5 2.0 1.5 1.0 0.5 0.0 ppm
0 20 40 60 80 100 120 140 160 180

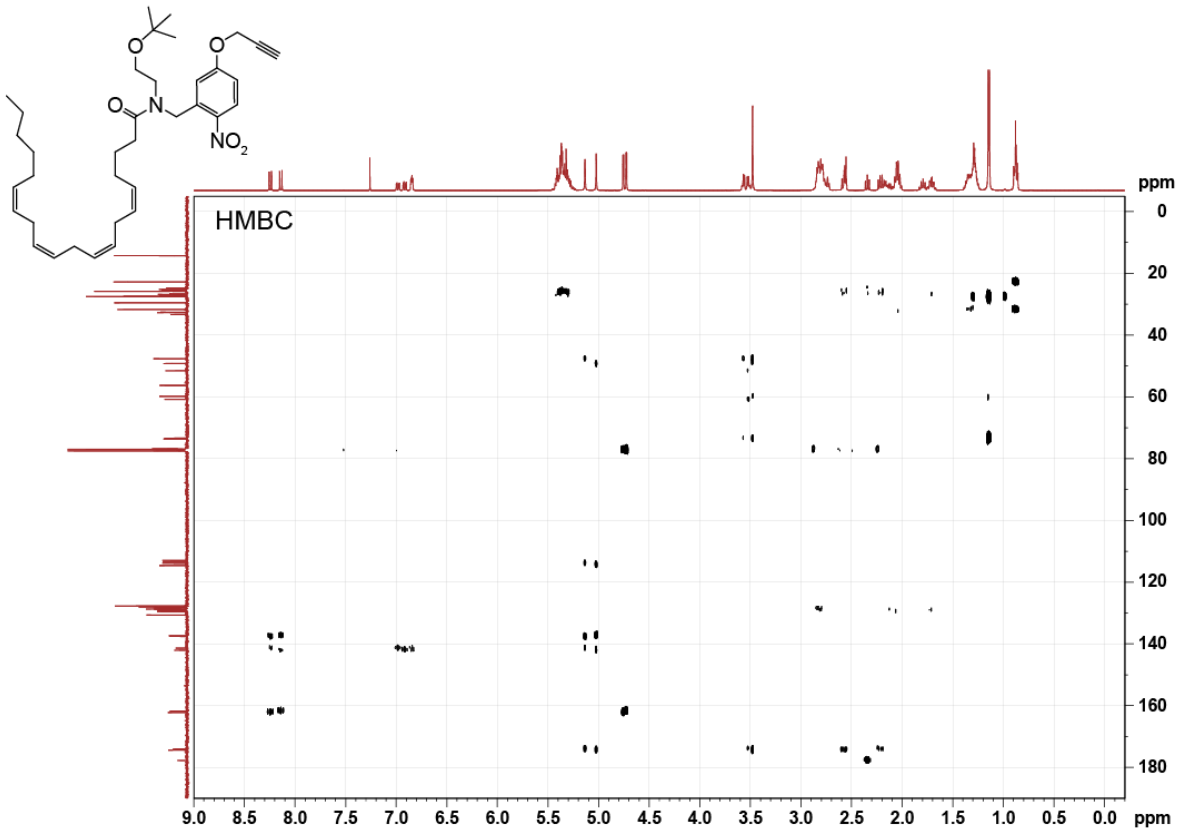
HMBC
ppm
0
20
40
60
80
100
120
140
160
180
9.0
8.5
8.0
7.5
7.0
6.5
6.0
5.5
5.0
4.5
4.0
3.5
3.0
2.5
2.0
1.5
1.0
0.5
0.0
ppm

### 4.5.2. Synthesis of 1-(4-((3-(((5*Z*,8*Z*,11*Z*,14*Z*)-*N*-(2-(*tert*-butoxy)ethyl)icosa-5,8,11,14-tetraenamido)methyl)-4-nitrophenoxy)methyl)-1*H*-1,2,3-triazol-1-yl)-*N*-(2-(2-((6-chlorohexyl)oxy)ethoxy)ethyl)-3,6,9,12,15,18,21,24-octaoxaheptacosan-27-amide. (4)

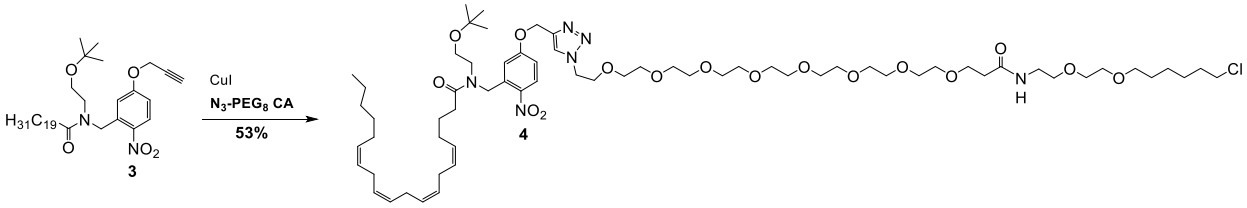


CuI (5.8 mg, 0.023 mmol, 0.4 equiv.) and sodium ascorbate (12 mg, 0.059 mmol, 1.1 equiv.) were added to **(5Z,8Z,11Z,14Z)-*N*-(2-(tert-butoxy)ethyl)-*N*-(2-nitro-5-(prop-2-yn-1-yloxy)benzyl)icosa-5,8,11,14-tetraenamide** (**3**, 32 mg, 0.055 mmol, 1.0 equiv.) and placed under an argon atmosphere. Separately, **$N_3$-$PEG_8$-CA** (25 mg, 0.058 mmol, 1.1 equiv.) was dissolved in anhydrous DMF (2.0 ml), transferred to reaction mixture, and the combined reaction was spun overnight at room temperature The crude product was purified via reverse phase flash chromatography (MeOH:$H_2O$ 0:1 → MeOH:$H_2O$ 1:0), dissolved MeOH:DCM (1:99), loaded onto a $SiO_2$ column (5.1 g) and purified by flash chromatography (MeOH:DCM 1:99 → MeOH:DCM 1:19). **1-(4-((3-(((5*Z*,8*Z*,11*Z*,14*Z*)-*N*-(2-(*tert*-butoxy)ethyl)icosa-5,8,11,14-tetraenamido) methyl)-4-nitrophenoxy)methyl)-1*H*-1,2,3-triazol-1-yl)-*N*-(2-(2-((6-chlorohexyl)oxy) ethoxy)ethyl)-3,6,9,12,15,18,21,24-octaoxaheptacosan-27-amide** (**4**, 36 mg, 0.029 mmol, 53%) was isolated as a yellow oil.

**TLC (MeOH:DCM 1:19): $R_f$ =** 0.15. **$^1$H NMR ($CDCl_3$, 400 MHz, 25 °C):** δ 8.29 (d, 0.3 H, H3, *J* = 9.1 Hz); 8.20 (d, 0.7 H, H3, *J* = 3.2 Hz); 8.18 (d, 1.0 H, H9, *J* = 3.0 Hz); 7.25 (dd, 0.3 H, H2, *J* = 9.1, 2.7 Hz); 7.14 (dd, 0.7 H, H2, *J* = 9.1, 2.8 Hz); 6.97 (d, 0.7 H, H6, *J* = 2.7 Hz); 6.87 (d, 0.3 H, H6, *J* = 2.7 Hz); 5.51-5.21 (m, 10 H, $H8_{A,B}$, H16, H17, H19, H20, H22, H23, H25, H26); 5.17 (s, 0.7 H, $H7_A$); 5.00 (s, 1.3 H, $H7_{A,B}$); 4.67-4.57 (m, 2 H, $H10_{A,B}$); 3.95-3.87 (m, 2 H, $H11_{A,B}$); 3.74 (t, 2 H, $H45_{A,B}$, *J* = 6.2 Hz); 3.69-3.53 (m, 20 H, H32-44, H49-52, H59-61); 3.51 (t, 2 H, $H57_{A,B}$, *J* =

6.2 Hz); 3.39 (t, 2 H, $H48_{A,B}$, *J* = 5.6 Hz); 2.92-2.74 (m, 7 H, $H18_{A,B}$, $H21_{A,B}$, $H24_{A,B}$, $H13_{A}$); 2.47 (t, 2 H, $H46_{A,B}$, *J* = 6.2 Hz); 2.32-2.16 (m, 2 H, $H13_{B}$, $H15_{A}$); 2.14-2.02 (m, 3 H, $H15_{B}$, $H27_{A,B}$); 1.84-1.56 (m, 6 H, $H14_{A,B}$, $H53_{A,B}$, $H56_{A,B}$); 1.55-1.25 (m, 10 H, $H54_{A,B}$, $H55_{A,B}$, H28-30); 1.18 (s, 9 H, $C(C\underline{H}_3)_3$); 0.98-0.85 (m, 3 H, $H31_{A,B,C}$). **$^{13}$C NMR ($CDCl_3$, 101 MHz, 25 °C):** δ 176.83 / 176.38 (C12); 173.97 (C47); 164.30 / 163.89 (C1); 143.76 (C58); 142.83 (C5); 137.98 (C4); 131.23; 130.46; 130.10; 129.98; 129.81; 129.75; 129.48; 129.43; 129.29; 129.12; 129.08; 129.04; 128.94; 128.90; 128.78; 126.67 (C9); 115.34 / 115.2 (C6); 114.29 / 114.21 (C2); 74.46 / 74.33 ($\underline{C}(CH_3)_3$); 72.22 (C57); 71.56; 71.51; 71.47; 71.42; 71.36; 71.30; 71.21; 70.56; 70.32 (C11); 68.27 (C45); 63.12 / 63.00 (C8); 61.39; 60.98; 52.58 (C7); 51.52 (C10); 50.45; 49.63; 49.49; 49.42; 49.28; 49.21; 48.99; 48.78; 48.57; 48.36; 45.72; 40.39 (C48); 37.62 (C46); 33.75 (C53); 33.59 / 33.37 (C13); 32.66 (C29); 30.55 (C56); 30.47 (C28); 28.20 (C27); 27.94 (C15); 27.75 ($C(\underline{C}H_3)_3$, C54); 27.58, 26.64, 26.60 (C18, C21, C24); 26.49 (C55); 26.31 / 26.26 (C14); 23.64 (C30); 14.47 (C31). **HRMS (ESI$^+$):** *m/z* calcd. for $[C_{65}H_{109}N_6O_{16}Cl]^+$: 1265.7667, found: 1265.7629 ($[M+H]^+$).

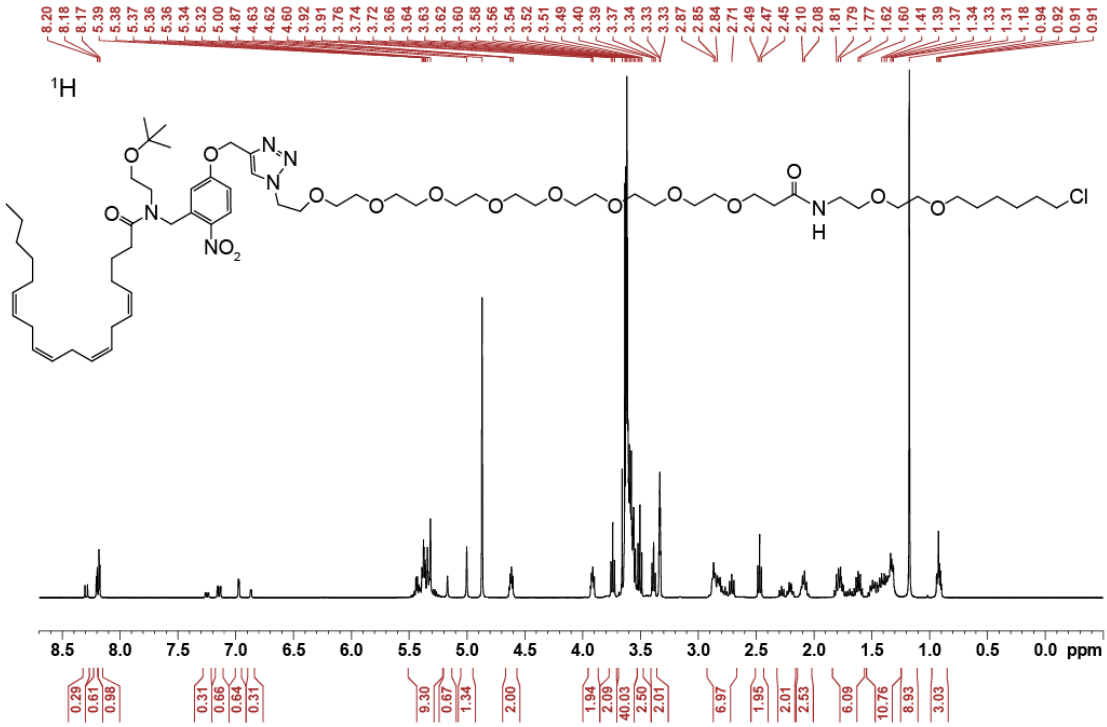
8.20 8.18 8.17 5.39 5.38 5.37 5.36 5.36 5.34 5.32 5.00 4.87 4.63 4.62 4.60 3.92 3.91 3.76 3.74 3.72 3.66 3.64 3.63 3.62 3.60 3.58 3.56 3.54 3.52 3.51 3.49 3.40 3.39 3.37 3.34 3.33 3.33 2.87 2.85 2.84 2.71 2.49 2.47 2.45 2.10 2.08 1.81 1.79 1.77 1.62 1.60 1.41 1.39 1.37 1.34 1.33 1.31 1.18 0.94 0.92 0.91 0.91
1H
NO2
Cl
8.5 8.0 7.5 7.0 6.5 6.0 5.5 5.0 4.5 4.0 3.5 3.0 2.5 2.0 1.5 1.0 0.5 0.0 ppm
0.29 0.61 0.98 0.31 0.66 0.64 0.31 9.30 0.67 1.34 2.00 1.94 2.09 40.03 2.50 2.01 6.97 1.95 2.01 2.53 6.09 10.76 8.93 3.03

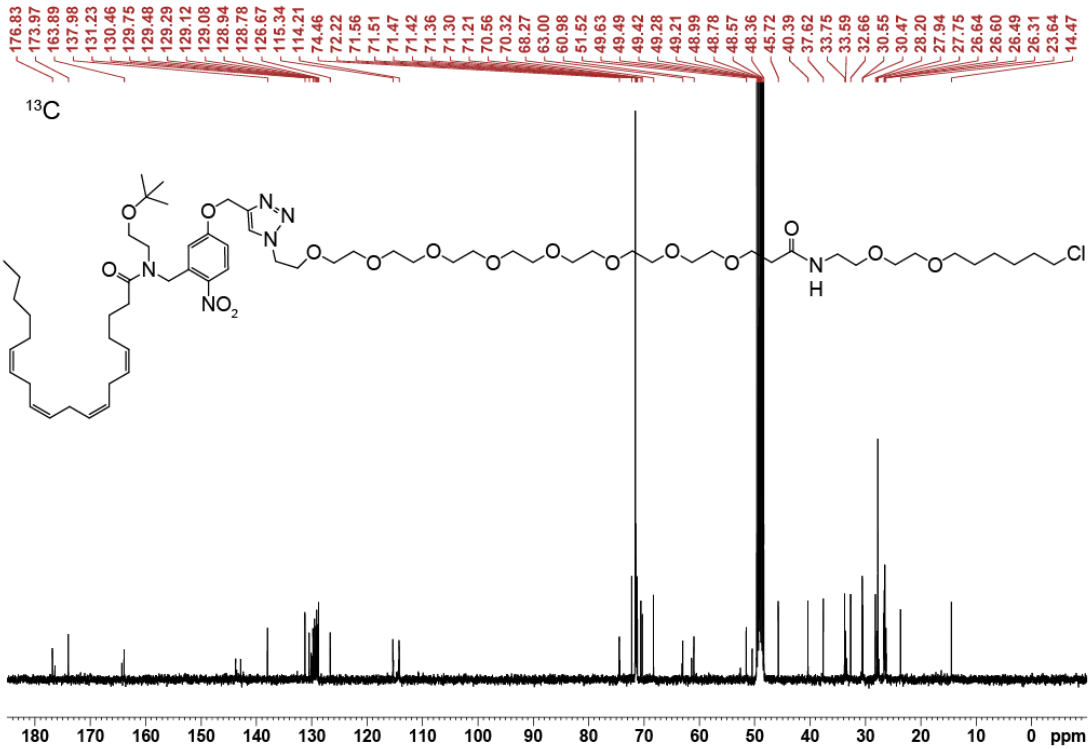
176.83 173.97 163.89 137.98 131.23 130.46 129.75 129.48 129.29 129.12 129.08 128.94 128.78 126.67 115.34 114.21 74.46 72.22 71.56 71.51 71.47 71.42 71.36 71.30 71.21 70.56 70.32 68.27 63.00 60.98 51.52 49.63 49.49 49.42 49.28 49.21 48.99 48.78 48.57 48.36 45.72 40.39 37.62 33.75 33.59 32.66 30.55 30.47 28.20 27.94 27.75 26.64 26.60 26.49 26.31 23.64 14.47
13C
NO2
Cl
180 170 160 150 140 130 120 110 100 90 80 70 60 50 40 30 20 10 0 ppm

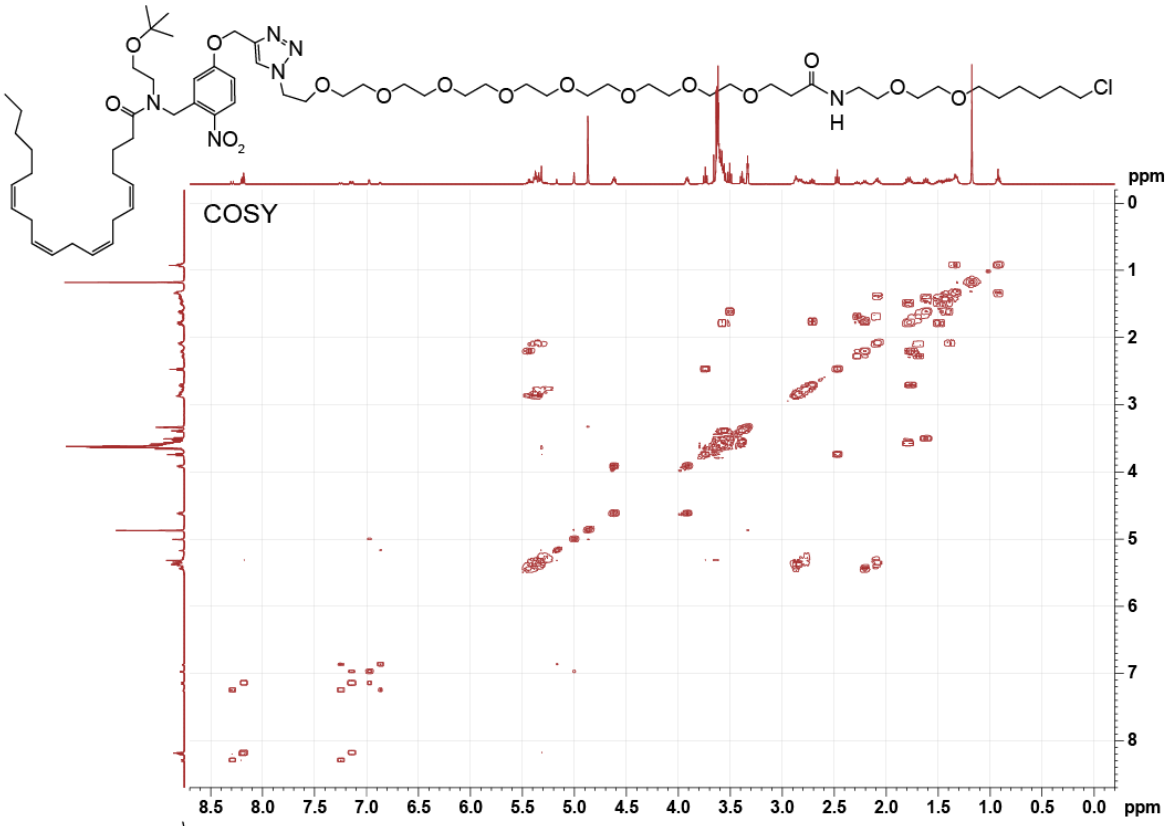
COSY
ppm
8.5 8.0 7.5 7.0 6.5 6.0 5.5 5.0 4.5 4.0 3.5 3.0 2.5 2.0 1.5 1.0 0.5 0.0 ppm
0 1 2 3 4 5 6 7 8

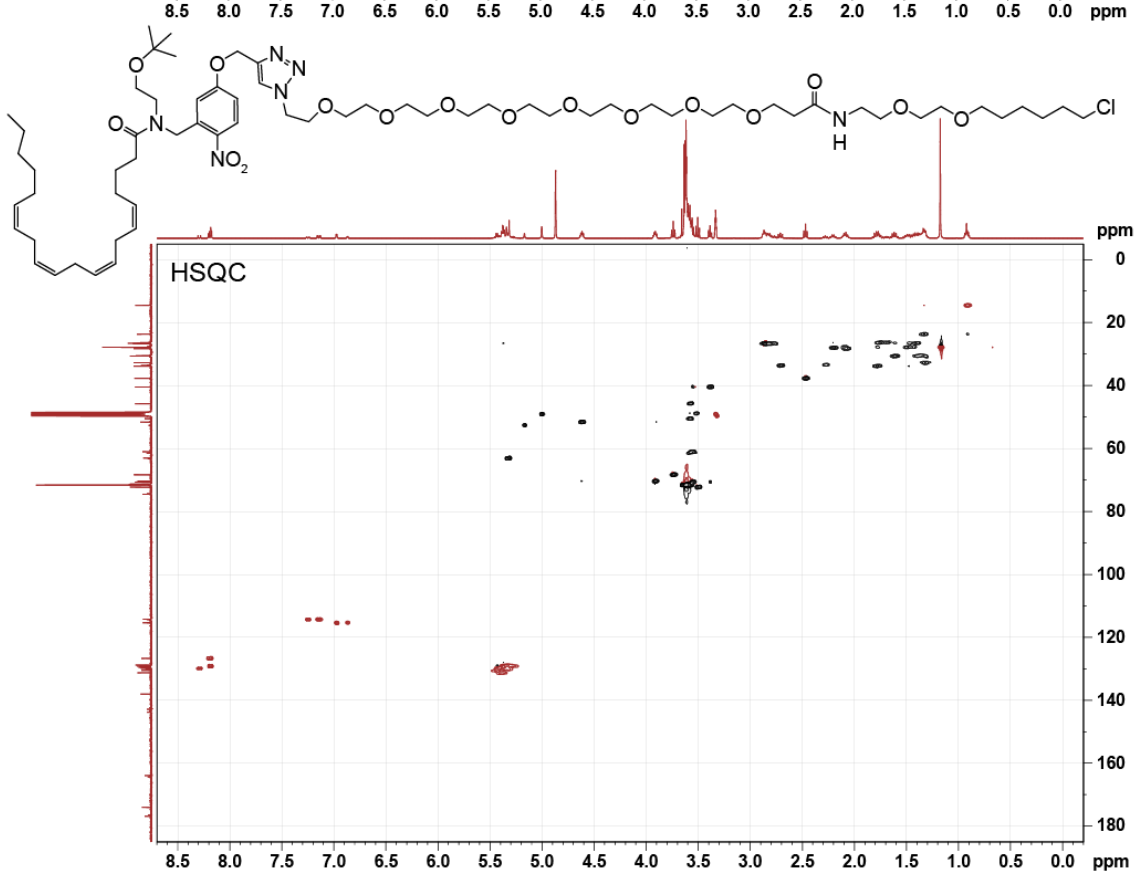
HSQC
ppm
8.5 8.0 7.5 7.0 6.5 6.0 5.5 5.0 4.5 4.0 3.5 3.0 2.5 2.0 1.5 1.0 0.5 0.0 ppm
0 20 40 60 80 100 120 140 160 180

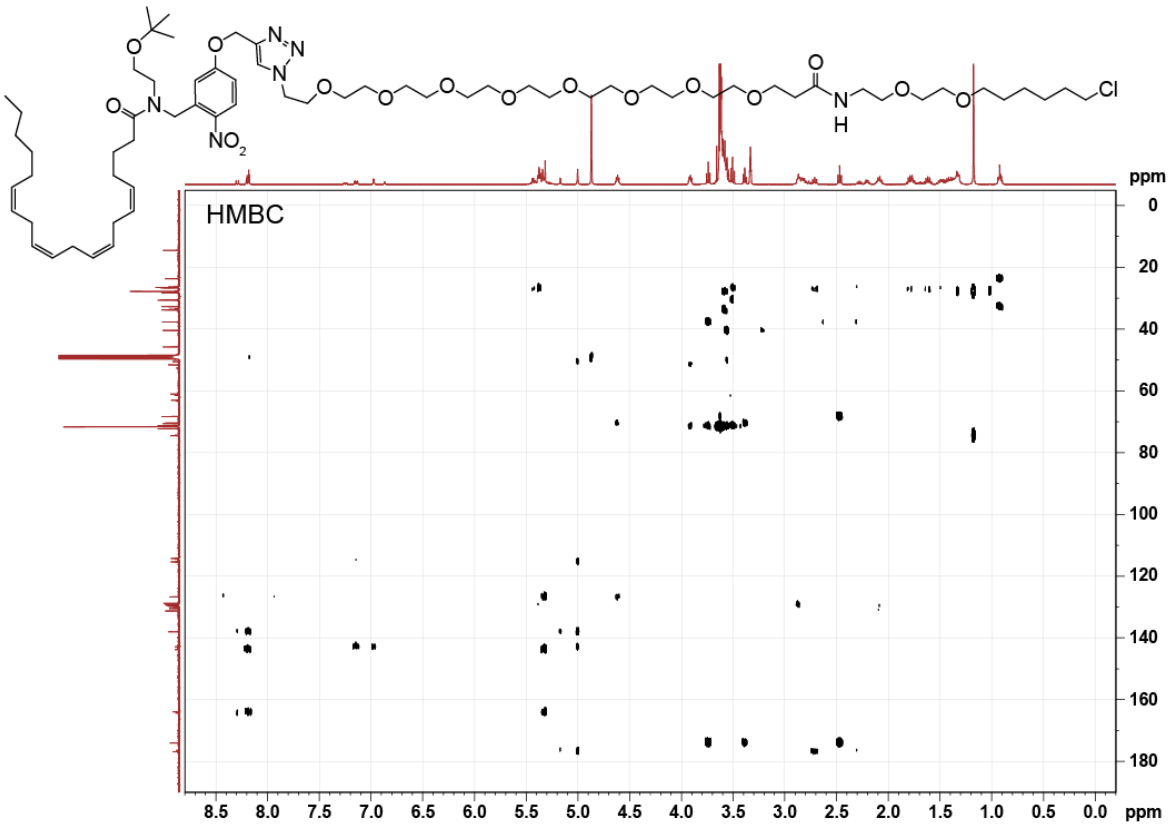
HMBC
ppm
0
20
40
60
80
100
120
140
160
180
8.5
8.0
7.5
7.0
6.5
6.0
5.5
5.0
4.5
4.0
3.5
3.0
2.5
2.0
1.5
1.0
0.5
0.0
ppm

### 4.5.3. Synthesis of *N*-(2-(2-((6-chlorohexyl)oxy)ethoxy)ethyl)-1-(4-((3-(((5*Z*,8*Z*,11*Z*,14*Z*)-*N*-(2-hydroxyethyl)icosa-5,8,11,14-tetraenamido)methyl)-4-nitrophenoxy)methyl)-1*H*-1,2,3-triazol-1-yl)-3,6,9,12,15,18,21,24-octaoxaheptacosan-27-amide (hOCT-AEA).

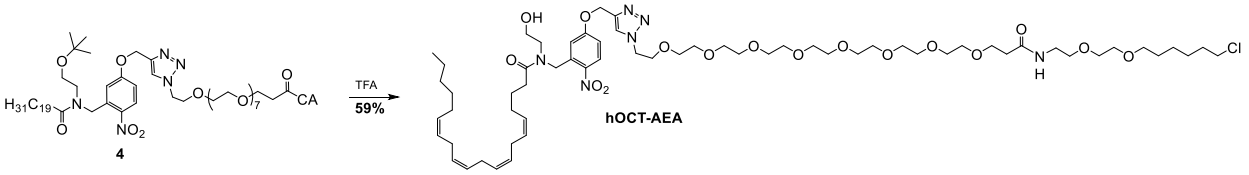


**4**

**1-(4-((3-(((5*Z*,8*Z*,11*Z*,14*Z*)-*N*-(2-(*tert*-butoxy)ethyl)icosa-5,8,11,14-tetraenamido)methyl)-4-nitrophenoxy)methyl)-1*H*-1,2,3-triazol-1-yl)-*N*-(2-(2-((6-chlorohexyl)oxy)ethoxy)ethyl)-3,6,9,12,15,18,21,24-octaoxaheptacosan-27-amide** (**4**, 82 mg, 0.065 mmol, 1.0 equiv.) was put under an argon atmosphere, and neat TFA (2.6 ml, 35 mmol, excess) was added. The reaction was stirred for 1 h at room temperature, before it was diluted with DCM (10 ml) and the solvent was removed *in vacuo*. The crude product was re-dissolve 2× in DCM and concentrated *in vacuo* to remove residual TFA. The crude product was purified via $SiO_2$ flash chromatography (MeOH:DCM 0:1 → MeOH:DCM 1:9). ***N*-(2-(2-((6-chlorohexyl)oxy)ethoxy) ethyl)-1-(4-((3-(((5*Z*,8*Z*,11*Z*,14*Z*)-*N*-(2-hydroxyethyl)icosa-5,8,11,14-tetraenamido)methyl)-4-nitrophenoxy)methyl)-1*H*-1,2,3-triazol-1-yl)-3,6,9,12,15,18,21,24-octaoxaheptacosan-27-amide** (**hOCT-AEA**, 47 mg, 0.039 mmol, 59%) was isolated as a yellow oil.

**TLC (MeOH:DCM 1:19): $R_f$ =** 0.20. **$^1$H NMR ($CDCl_3$, 400 MHz, 25 °C):** δ 8.29 (d, 0.3 H, H3, *J* = 9.1 Hz); 8.24-8.14 (m, 1.7 H, H3, H9); 7.24 (dd, 0.4 H, H2, *J* = 9.1, 2.7 Hz); 7.12 (dd, 0.6 H, H2, *J* = 9.1, 2.7 Hz); 7.00 (d, 0.6 H, H6, *J* = 2.7 Hz); 6.90 (d, 0.4 H, H6, *J* = 2.6 Hz); 5.51-5.20 (m, 10 H, $H8_{A,B}$, H16, H17, H19, H20, H22, H23, H25, H26); 5.14 (s, 0.8 H, $H7_A$); 5.01 (s, 1.2 H, $H7_{A,B}$); 4.67-4.57 (m, 2 H, $H10_{A,B}$); 3.96-3.86 (m, 2 H, $H11_{A,B}$); 3.78-3.48 (m, 44 H, H32-45, H49-52, H57, H59-61); 3.42-3.36 (m, 2 H, $H48_{A,B}$), 2.92-2.60 (m, 7 H, $H18_{A,B}$, $H21_{A,B}$, $H24_{A,B}$, $H13_A$), 2.47 (t, 2 H, $H46_{A,B}$, *J* = 6.2 Hz), 2.33-2.16 (m, 2 H, $H13_B$, $H15_A$), 2.14-2.02 (m, 3 H, $H15_B$,

$H27_{A,B}$), 1.87-1.56 (m, 6 H, $H14_{A,B}$, $H53_{A,B}$, $H56_{A,B}$), 1.56-1.25 (m, 10 H, $H54_{A,B}$, $H55_{A,B}$, H28-30), 0.99-0.84 (m, 3 H, $H31_{A,B,C}$). **$^{13}$C NMR ($CDCl_3$, 101 MHz, 25 °C):** δ 176.66 (C12); 173.98 (C47); 164.36 / 163.94 (C1); 143.81 / 143.58 (C58); 142.80 / 142.35 (C5); 137.99 / 137.96 (C4); 131.22, 130.42, 130.14,129.93, 129.83, 129.76, 129.48, 129.43, 129.30, 129.13, 129.09, 129.07, 129.04, 128.95, 128.90, 128.78 (C3, C16, C17, C19, C20, C22, C23, C25, C26); 126.65 (C9); 115.01 / 114.65 (C6); 114.80 / 114.56 (C2); 72.22 (C57); 71.57, 71.51, 71.47, 71.42, 71.36, 71.30, 71.21, 60.94, 60.68, 51.90, 50.68, 45.73 (C32-44, C49-52, C59-61); 70.57 / 70.31 (C11); 68.28 (C45); 63.13 / 63.03 (C8); 57.68; 52.44 (C7); 51.54 (C7); 40.40 (C48); 37.63 (C46); 33.75 (C53); 33.50 / 33.39 (C13); 32.66 (C29); 30.55 (C56); 30.47 (C28); 28.20 (C27); 27.89 / 27.58 (C15); 27.75 (C54); 26.62 (C55); 26.58, 26.54, 26.50 (C18, C21, C24); 26.39 / 26.09 (C14); 23.64 (C30); 14.47 (31). **HRMS (ESI$^+$):** *m/z* calcd. for $[C_{61}H_{101}N_6O_{16}Cl]^+$: 1209.7041, found: 1209.7003 ($[M+H]^+$).

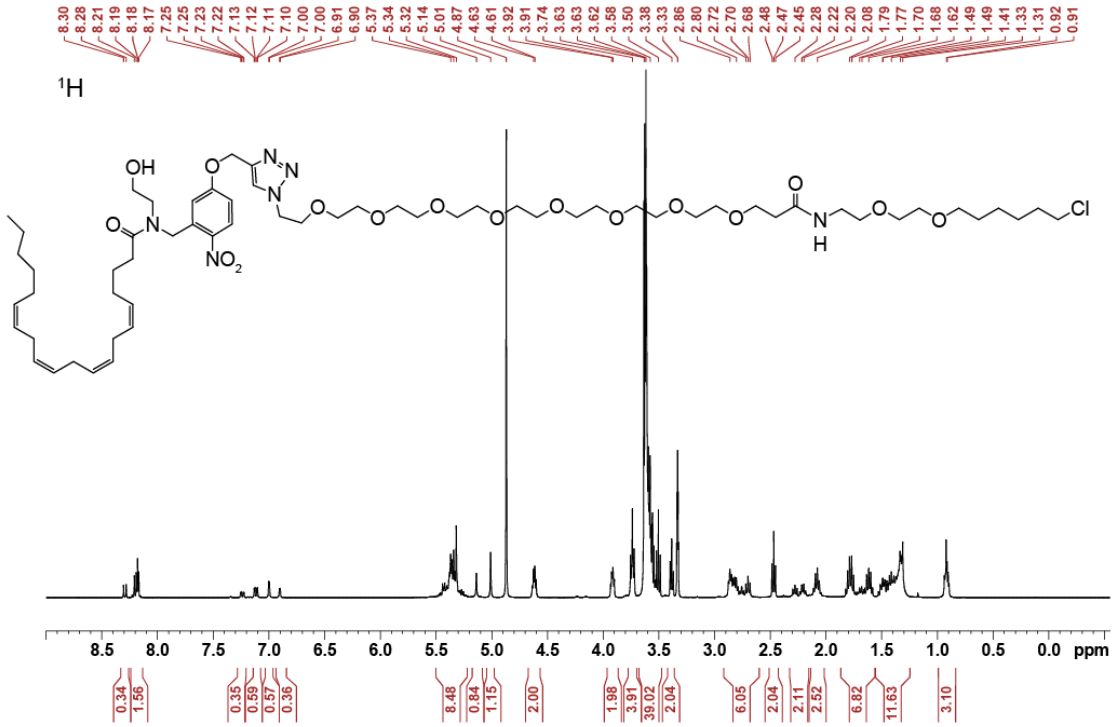
8.30
8.28
8.21
8.19
8.18
8.17
7.25
7.25
7.23
7.22
7.13
7.12
7.11
7.10
7.00
7.00
6.91
6.90
5.37
5.34
5.32
5.14
5.01
4.87
4.63
4.61
3.92
3.91
3.74
3.63
3.63
3.62
3.58
3.50
3.38
3.33
2.86
2.80
2.72
2.70
2.68
2.48
2.47
2.45
2.28
2.22
2.20
2.08
1.79
1.77
1.70
1.68
1.62
1.49
1.49
1.41
1.33
1.31
0.92
0.91
1H
OH
O
N
N
N
O
O
O
O
O
O
O
O
O
O
O
O
N
H
Cl
NO2
8.5
8.0
7.5
7.0
6.5
6.0
5.5
5.0
4.5
4.0
3.5
3.0
2.5
2.0
1.5
1.0
0.5
0.0
ppm
0.34
1.56
0.35
0.59
0.57
0.36
8.48
0.84
1.15
2.00
1.98
3.91
39.02
2.04
6.05
2.04
2.11
2.52
6.82
11.63
3.10

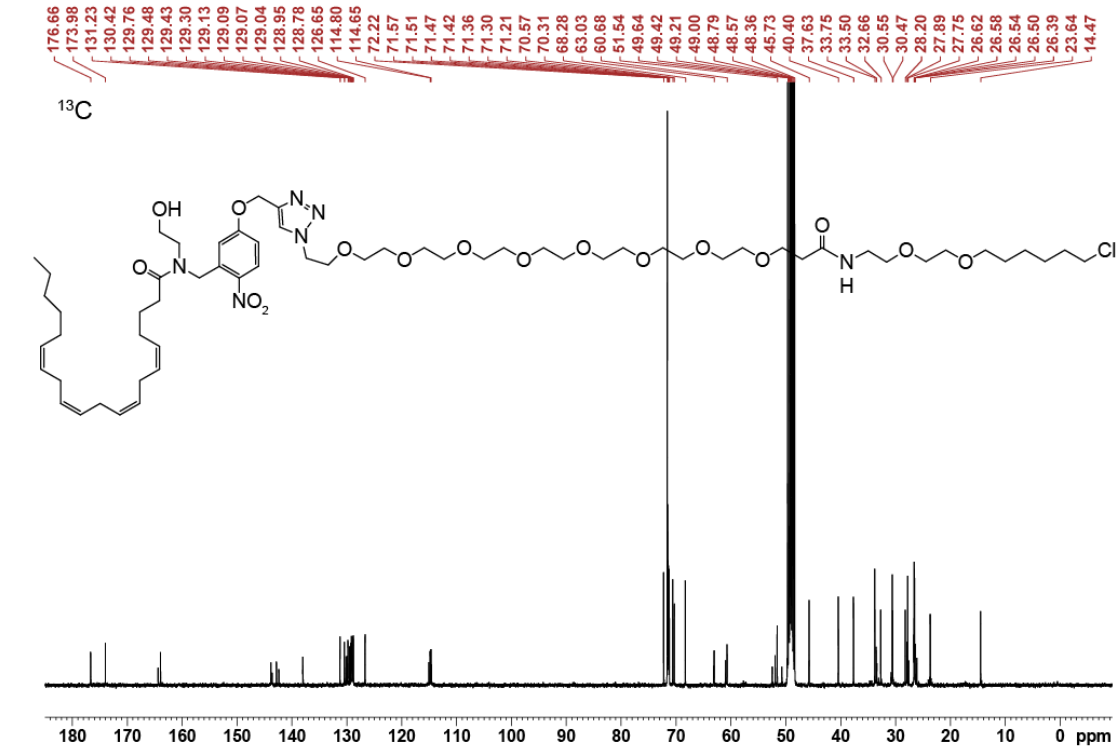
176.66
173.98
131.23
130.42
129.76
129.48
129.43
129.30
129.13
129.09
129.07
129.04
128.95
128.78
126.65
114.80
114.65
72.22
71.57
71.51
71.47
71.42
71.36
71.30
71.21
70.57
70.31
68.28
63.03
60.68
51.54
49.64
49.42
49.21
49.00
48.79
48.57
48.36
45.73
40.40
37.63
33.75
33.50
32.66
30.55
30.47
28.20
27.89
27.75
26.62
26.58
26.54
26.50
26.39
23.64
14.47
13C
OH
O
N
N
N
O
O
O
O
O
O
O
O
O
O
O
O
N
H
Cl
NO2
180
170
160
150
140
130
120
110
100
90
80
70
60
50
40
30
20
10
0
ppm

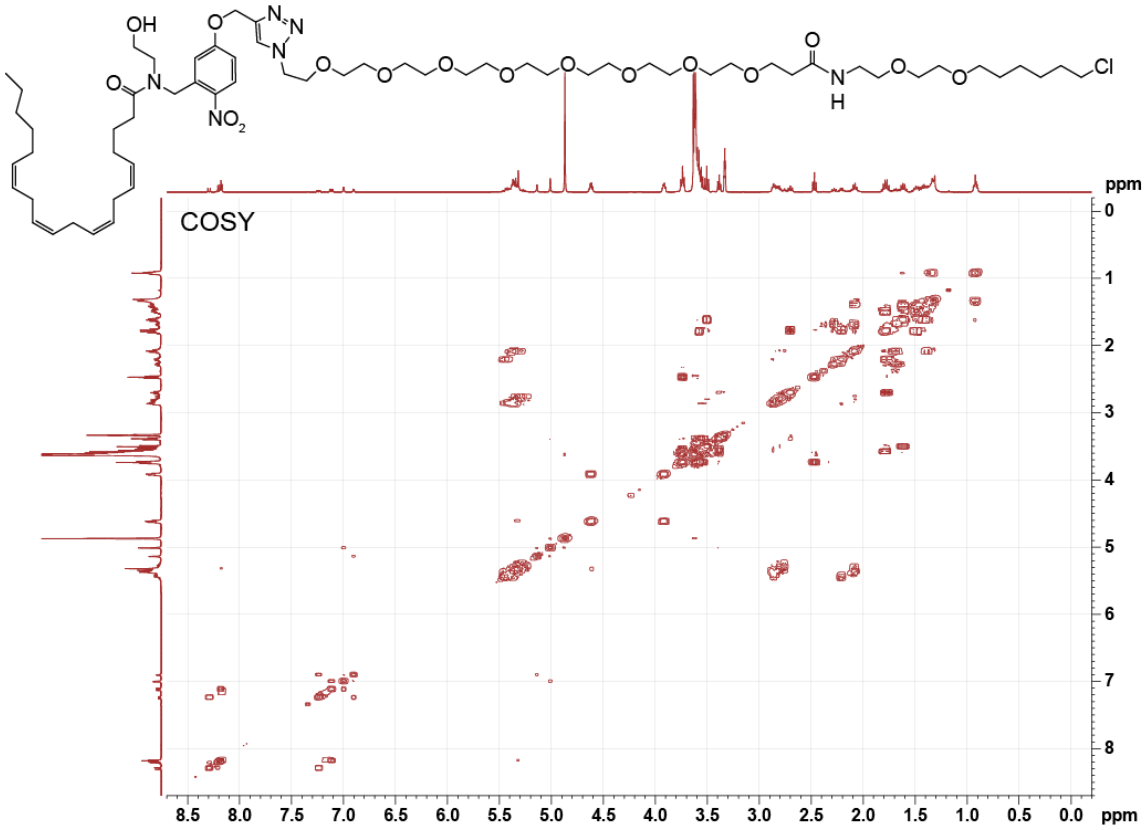
OH
O
N
O
NO2
N
N
O
O
O
O
O
O
O
O
O
O
N
H
Cl
COSY
ppm
0
1
2
3
4
5
6
7
8
8.5
8.0
7.5
7.0
6.5
6.0
5.5
5.0
4.5
4.0
3.5
3.0
2.5
2.0
1.5
1.0
0.5
0.0
ppm

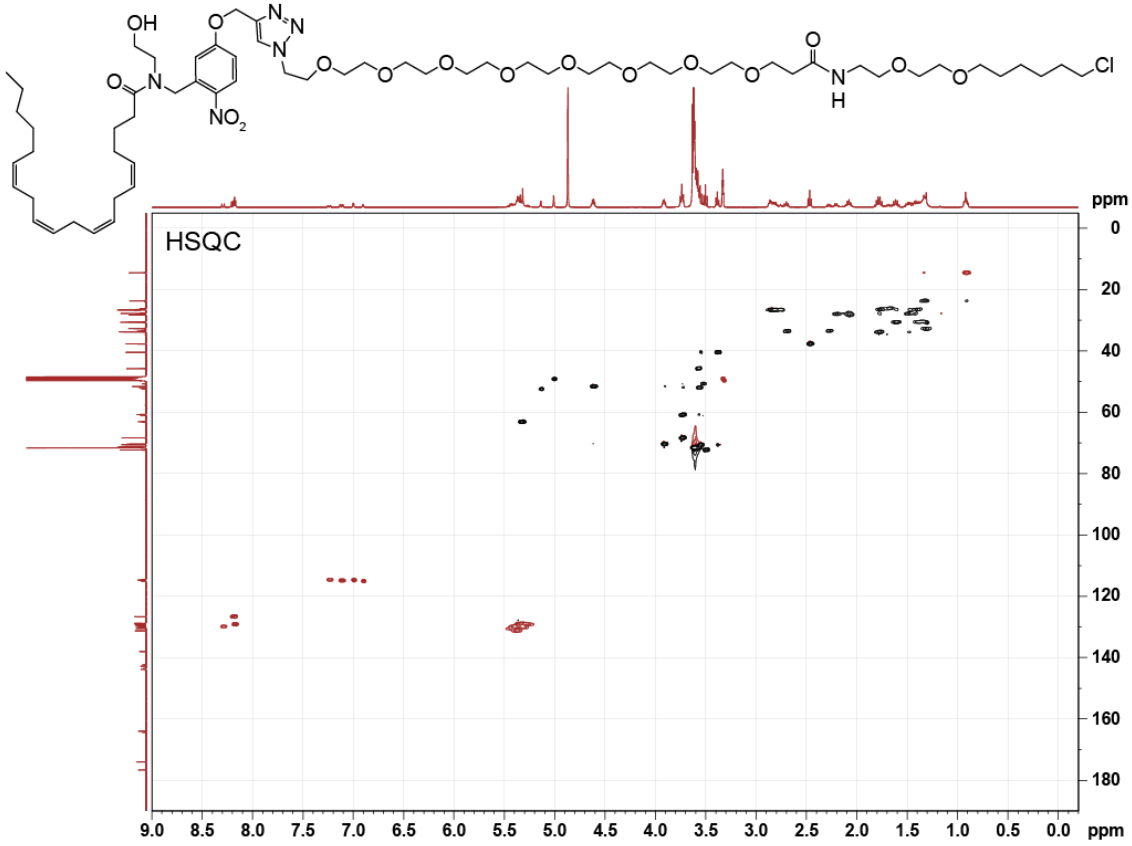
OH
O
N
O
NO2
N
N
O
O
O
O
O
O
O
O
O
O
N
H
Cl
HSQC
ppm
0
20
40
60
80
100
120
140
160
180
9.0
8.5
8.0
7.5
7.0
6.5
6.0
5.5
5.0
4.5
4.0
3.5
3.0
2.5
2.0
1.5
1.0
0.5
0.0
ppm

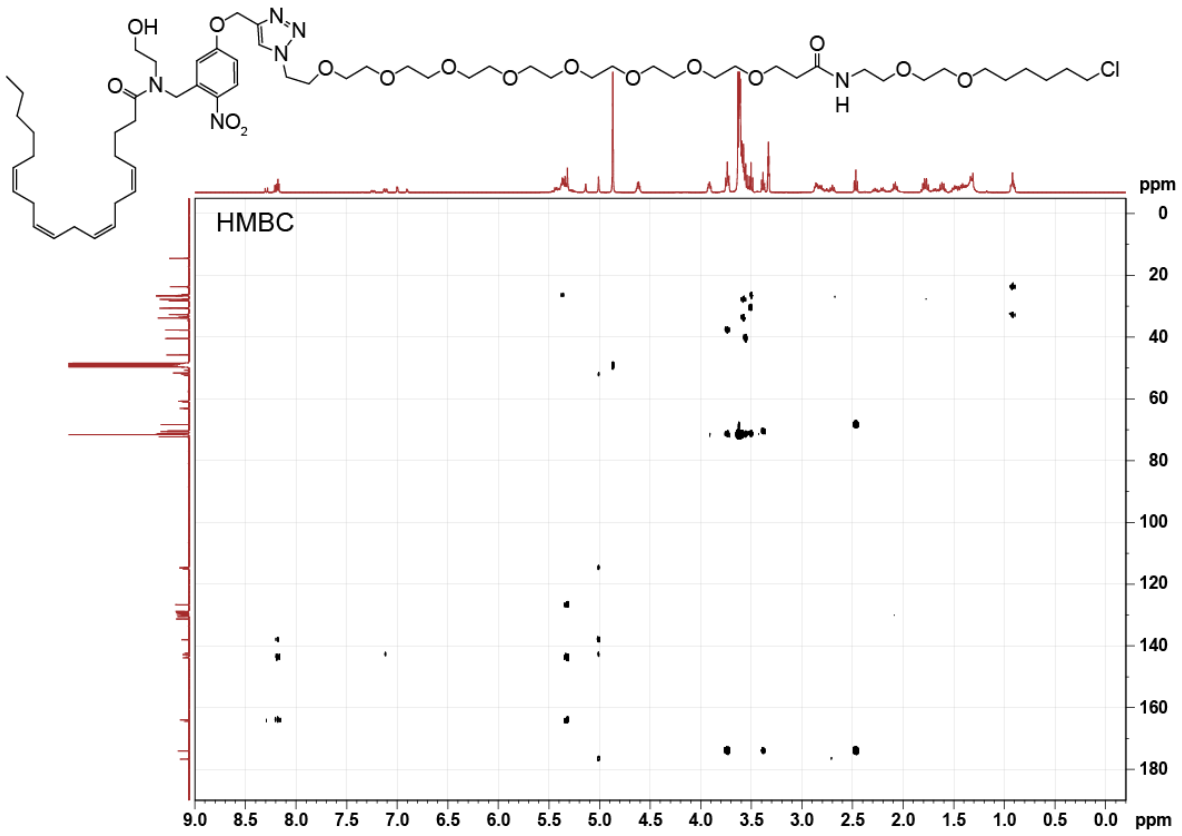
OH
O
N
O
NO2
N
N
N
O
O
O
O
O
O
O
O
O
O
O
O
N
H
Cl
HMBC
ppm
0
20
40
60
80
100
120
140
160
180
9.0
8.5
8.0
7.5
7.0
6.5
6.0
5.5
5.0
4.5
4.0
3.5
3.0
2.5
2.0
1.5
1.0
0.5
0.0
ppm

# Chapter 5. Outlook

As more states legalize marijuana, its use will also increase as it becomes more accessible[1]. While cannabis has been therapeutically beneficial in a variety of diseases, including epilepsy, multiple sclerosis and Tourette syndrome[4], the basic biology underlying the endocannabinoid system (ECS) is unclear. The ECS is ubiquitously expressed throughout the body and performs a variety of functions, including metabolic regulation. Many cannabinoid-sensitive receptors are GPCRs, which are a highly druggable class of proteins. The ECS has already been the target of drugs in clinical trials[29,73], but until we understand the basic biology, these drugs will continue to fail. In order to make informed drug discovery efforts, it is necessary to build new tools that will allow us to better understand the ECS signaling network.

This thesis presents the Optically-cleavable targeted (OCT)-ligand approach, a chemigenetic method to help unravel the ECS signaling network activated by *N*-acylethanolamines (NAE), a family of endocannabinoid ligands. OCT-ligands combine the temporal advantage of photocaged ligands with the spatial targeting of genetically-encoded self-labeling proteins, such as SNAP-tags and HaloTags. This toolset is necessary for dissecting NAE biology because their lipophilicity affects their kinetics, while the expression of multiple cannabinoid receptors across tissue complicates their role in a given cell type. Thus, having a tool like OCT-ligands that can manipulate signaling activation in time and space is critical to address this problem.

OCT-ligands have four key components: a ligand of interest, photocage, linker, and bioorthogonal handle. However, moving forward each of these features can be modified to adjust the pharmacology, photophysical properties, cell permeability and genetic targeting of new derivatives, respectively. From a tool building perspective, NAEs are an attractive pharmacore, because subtle changes in the lipid composition impacts the pharmacology of the ligand. For example, by adjusting the acyl chain length or saturation, stimulatory or inhibitory

coupled GPCRs can be targeted. Nevertheless, ligands beyond NAEs are amendable to this approach, and future efforts should include developing OCT-ligands for other signaling molecules, such as other lipid classes, small peptides and neurotransmitters.

A current limitation of the presented OCT-ligands is that they cannot be visualized in cells. While our competition labeling and mutant SNAP-tag / HaloTag experiments confirms that our tools are properly labeling the respective self-labeling protein, we cannot visualize whether the probe is accumulating in cells. A related limitation is the dependence of the probe's action on the SLP expression. Chapters 2 and 3 describe an OCT-PEA that targets SNAP-tags or HaloTags, respectively. In both cases, PEA is the ligand of interest that is released, however the effect on $Ca^{2+}$ oscillations differs between the **OCT-PEA** (SNAP targeting) and **hOCT-PEA4** (HaloTag targeting). While both probes stimulate $Ca^{2+}$ in INS-1 cells, **OCT-PEA** had a stronger effect relative to **hOCT-PEA4**, which could be due to differences in SLP expression. When evaluating **hOCT-PEA4**, I used a plasmid that coexpressed a surface targeting HaloTag and a cytosolically expressed EGFP, separated by a T2A linker. This plasmid (pDisplayHalo-EGFP) is a larger construct relative to the pDisplay™-SNAP that was used to evaluate **OCT-PEA** and could account for difference in protein expression that impacted the effect observed from uncaging. To test this hypothesis, flow cytometry could be used. INS-1 cells would be transfected with an SLP-EGFP construct, treated with a vehicle or probe followed by a fluorescent SLP dye, then fluorescence would be quantified via flow cytometry. The EGFP fluorescence would be a readout for protein expression, whereas the SLP dye fluorescence would quantify the probe labeling efficiency.

The OCT-ligands presented here have a nitrobenzyl photocage. However, new OCT-ligands could include a coumarin photocage, which would allow for live visualization of the probe using microscopy. Another strategy for probe visualization includes incorporating a silicon rhodamine linker into the design. Rhodamine-based HaloTag fluorophores have been shown to

have increased fluorescence upon HaloTag binding[79], and since silicon rhodamines have a red-shifted excitation / emission spectrum, they would be compatible with the nitrobenzyl photocage.

More broadly, this thesis outlines the process for chemical biology tool development, from proof-of-concept studies (**Chapter 2**), to evolution of technology to more complex systems (**Chapter 3**), and finally to expansion of the technology to investigate other ligands (**Chapter 4**, **Appendix 6.2**). OCT-ligands expand the chemigenetic toolset, and allow for cell-targeted, photopharmacology in human tissue.

# Chapter 6. Appendix

## 6.1. Abbreviations

2-AG – 2-arachidonoylglycerol

AEA – anandamide

BG-$NH_2$ – 6-((4-(aminomethyl)benzyl)oxy)-*9H*-purin-2-amine

BG – benzylguanine

BME – 2-mercaptoethanol

BSA – bovine serum albumin

CA – 2-(2-((6-chlorohexyl)oxy)ethoxy)ethan-1-amine *I* chloroalkane

CB1 – cannabinoid receptor 1

CBD – cannabidiol

DART – drugs acutely restricted by tethering

DCE – 1,2-dichloroethane

DCM – dichloromethane

DIPEA – *N,N*-diisopropylethylamine

DMF – *N,N*-dimethylformamide

ECS – endocannabinoid system

EDC·HCl – 1-(3-dimethylaminopropyl)-3-ethylcarbodiimide hydrochloride

FAAH – fatty acid amide hydrolase

GPCR – G protein-coupled receptor

GSIS – glucose-stimulated insulin secretion

HOBt – 1-hydroxybenzotriazole

KD – kockdown

KO – knockout

MTT – 3-(4,5-dimethylthiazol-2-yl)-2,5-diphenyltetrazolium bromide

NAE – *N*-acylethanolamines

NMR – nuclear magnetic resonance

PBS – phosphate buffered saline

PEA – palmitoylethanolamide

PFA – paraformaldehyde

PLC – phospholipase C

PORTL – photoswitchable orthogonal remotely tethered ligand

RT – room temperature, ~ 25 °C

SLP – self-labeling protein

TFA – trifluoroacetic acid

THC – $\Delta^9$-tetrahydrocannabinol

TLC – thin layer chromatography

TRPV1 – transient receptor potential vanilloid-1

## 6.2. Synthesis of OCT-stearoylethanolamine (SEA)

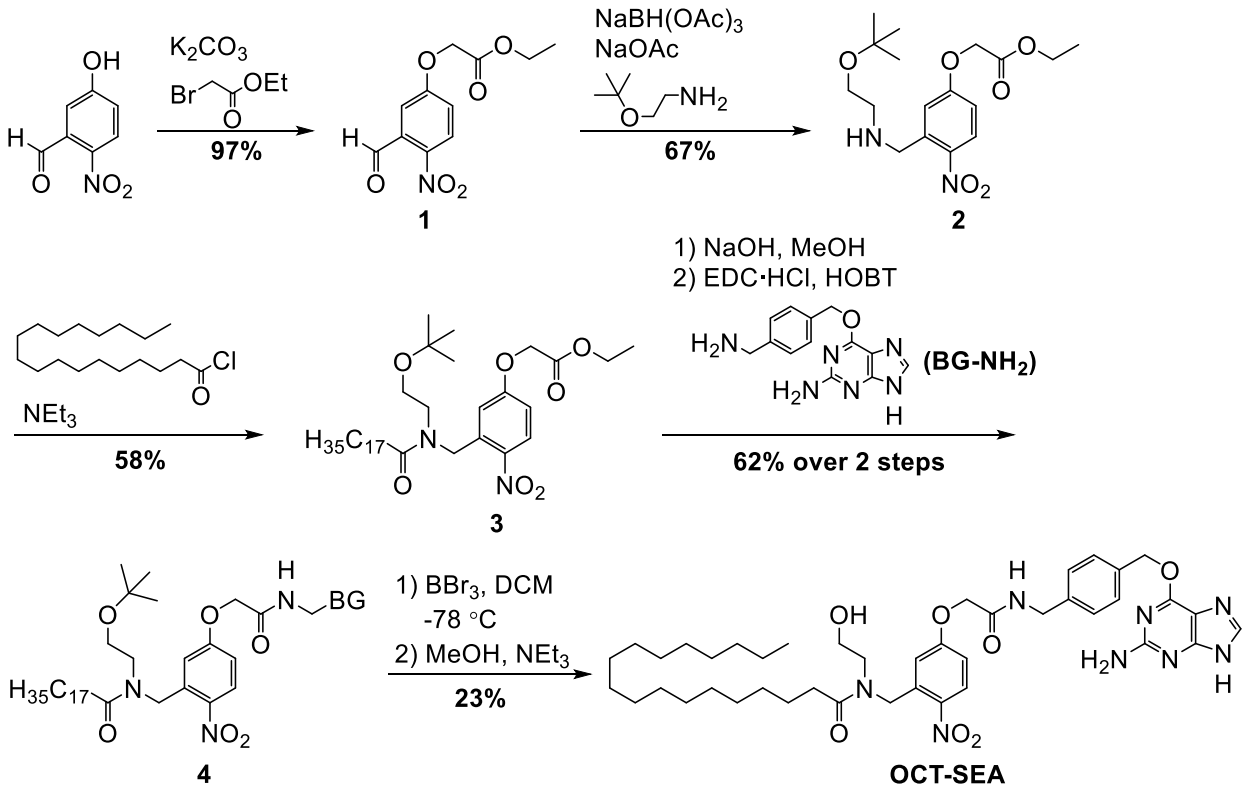


*Figure 6.1. Chemical synthesis of **OCT-SEA**, which was prepared in 6 steps with 5% yield.*

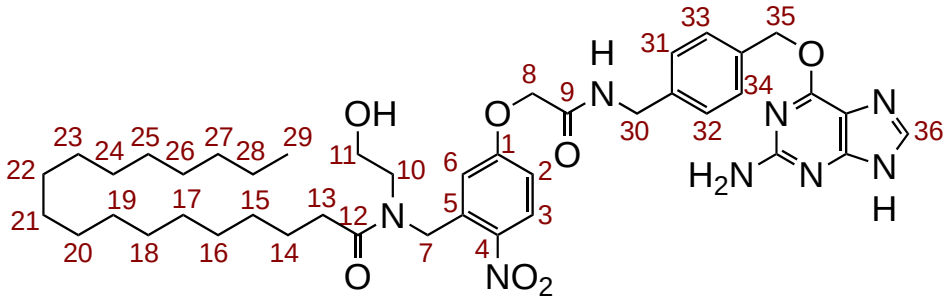

*Figure 6.2. Numbering system utilized in the NMR assignments for **OCT-SEA**.*

### 6.2.1. Synthesis of ethyl 2-(3-((*N*-(2-(*tert*-butoxy)ethyl)stearamido)methyl)-4-nitrophenoxy)acetate (3).

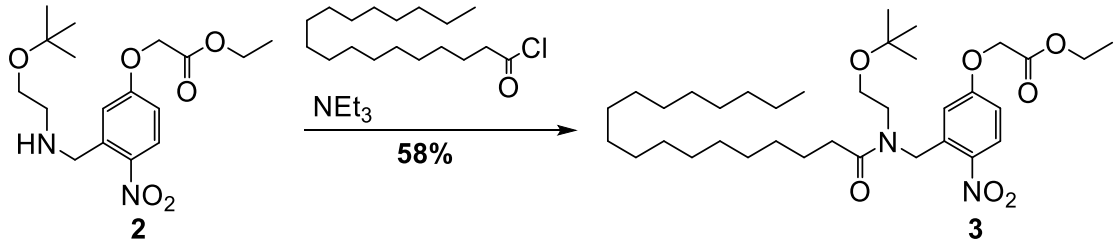


**(2-*tert*-butoxyethyl)-(5-ethoxycarbonylmethoxy-2-nitrobenzyl)amine (2)** was prepared as decribed in section **2.5.2**.

Stearic acid (0.3261 g, 1.15 mmol, 3.4 equiv.) was placed under an argon atmosphere and dissolved in anhydrous DCM (13 ml), then oxalyl chloride (0.13 ml, 1.5 mmol) and a drop of anhydrous DMF were added to initiate the reaction. The reaction was stirred for 1 h at RT, then concentrated *in vacuo*. The crude reaction was re-dissolved and concentrated *in vacuo* in DCM 2×. The crude stearoyl chloride was placed under an argon atmosphere and dissolved in anhydrous DCM (8 ml).

Separately, compound **2** (0.12 g, 0.34 mmol, 1.0 equiv.) was placed under an argon atmosphere, dissolved in anhydrous DCM (11 ml), and then the stearoyl chloride was transferred to the amine reaction. $NEt_3$ (0.1 ml, 0.72 mmol, 2.1 equiv.) was added dropwise. After 2 h the reaction was diluted in DCM (10 ml) and was quenched with saturated $NaHCO_3$. The organic layer was washed 2× with saturated $NaHCO_3$ and wash once with brine. The organic phase was separated, dried over anhydrous $MgSO_4$, and then filtered. The solvent was removed *in vacuo*, redissolved in DCM and $SiO_2$ gel (2.07 g) was added to the crude mixture. The solvent was removed *in vacuo* and the product-containing gel was loaded onto a $SiO_2$ column (40.09 g) and purified by $SiO_2$ flash chromatography (EtOAc:Hexane 1:19 → EtOAc:Hexane 1:4). **Ethyl 2-(3-((*N*-(2-(*tert*-butoxy)ethyl)stearamido)methyl)-4-nitrophenoxy)acetate** (**3**, 0.1215 g, 0.196 mmol, 58%) was isolated as a yellow oil.

**TLC (EtOAc:Hexane 1:2): $R_f$ =** 0.59. **$^1$H NMR ($CDCl_3$, 400 MHz, 25 °C):** δ 8.23 (d, 0.5 H, H3, *J* = 8.8 Hz); 8.12 (d, 0.5 H, H3, *J* = 9.8 Hz); 6.86 (dd, 0.5 H, H2, *J* = 9.3, 2.6 Hz); 6.82-6.74 (m, 1.5 H, H2, H6); 5.14 (s, 1 H, $H7_A$); 5.01 (s, 1 H, $H7_B$); 4.65 (d, 2 H, $H8_{A,B}$); 4.32-4.21 (m, 2 H, $OC\underline{H_2}CH_3$); 3.61-3.42 (m, 4 H, $H10_{A,B}$, $H11_{A,B}$); 2.54 (t, 1 H, $H13_A$); 2.19 (t, 1 H, $H13_B$); 1.76-1.53 (m, 2 H, $H14_{A,B}$); 1.43-1.19 (m, 31 H, H15-28, $OCH_2C\underline{H_3}$); 1.15 (d, 9 H, $C(C\underline{H_3})$, *J* = 4.56 Hz); 0.87 (t, 3 H, $H29_{A,B,C,}$ *J* = 6.8 Hz). **$^{13}$C NMR ($CDCl_3$, 101 MHz, 25 °C):** δ 174.43 / 174.05 (C12); 167.75 / 167.47 (C9); 162.35 / 161.84 (C1); 142.05 / 141.32 (C4); 137.67 / 137.38 (C5); 128.61 / 127.96 (C3); 114.42 / 113.53 (C6); 112.82 / 112.40 (C2); 73.45 / 73.15 ($\underline{C}(CH_3)$); 65.44 / 65.33 (C8); 61.87 / 61.73 ($O\underline{C}H_2CH_3$); 60.62 / 59.71 (C11); 51.34 (C7); 48.96 (C10); 47.37, 47.33 (C7, C10); 33.12 / 33.09 (C13); 31.91, 29.69, 29.65, 29.56, 29.52, 29.48, 29.43, 29.35, 22.68 (C15-28); 27.39 / 27.31 ($C(\underline{C}H_3)$); 25.34 / 25.24 (C14); 14.13, 14.11 (C29, $OCH_2\underline{C}H_3$).

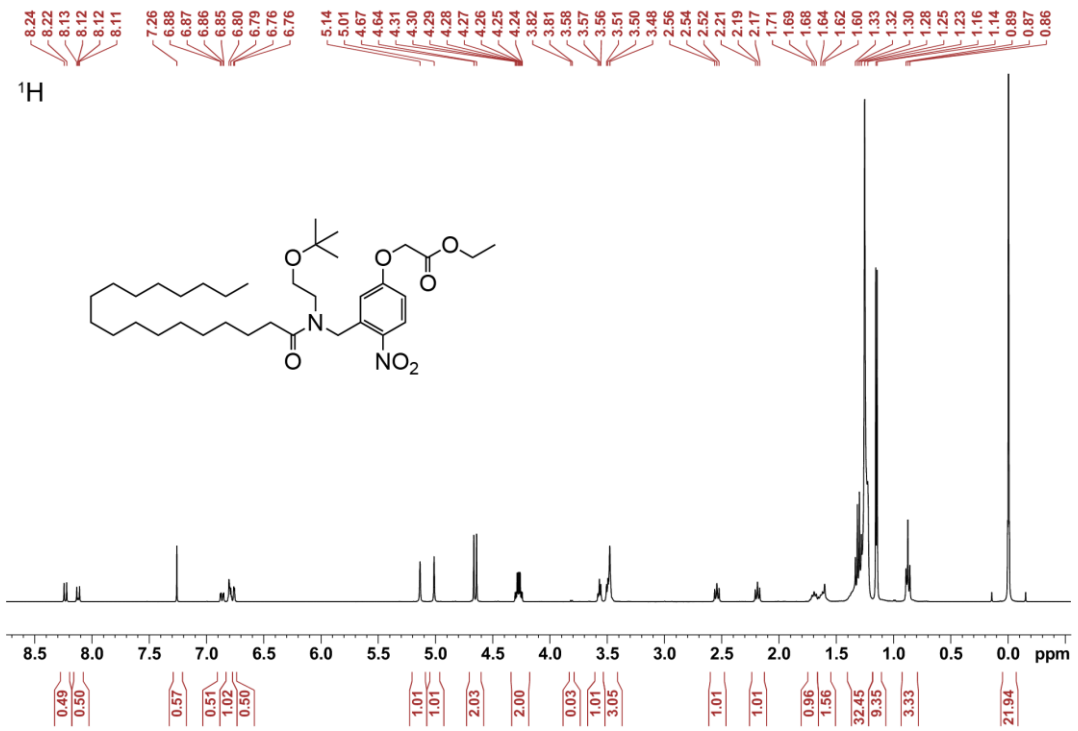
8.24
8.22
8.13
8.12
8.12
8.11
7.26
6.88
6.87
6.86
6.85
6.80
6.79
6.76
6.76
5.14
5.01
4.67
4.64
4.31
4.30
4.29
4.28
4.27
4.26
4.25
4.24
3.82
3.81
3.58
3.57
3.56
3.51
3.50
3.48
2.56
2.54
2.52
2.21
2.19
2.17
1.71
1.69
1.68
1.64
1.62
1.60
1.33
1.32
1.30
1.28
1.25
1.23
1.16
1.14
0.89
0.87
0.86
1H
O
O
O
O
N
O
NO2
8.5
8.0
7.5
7.0
6.5
6.0
5.5
5.0
4.5
4.0
3.5
3.0
2.5
2.0
1.5
1.0
0.5
0.0
ppm
0.49
0.50
0.57
0.51
1.02
0.50
1.01
1.01
2.03
2.00
0.03
1.01
3.05
1.01
1.01
0.96
1.56
32.45
9.35
3.33
21.94

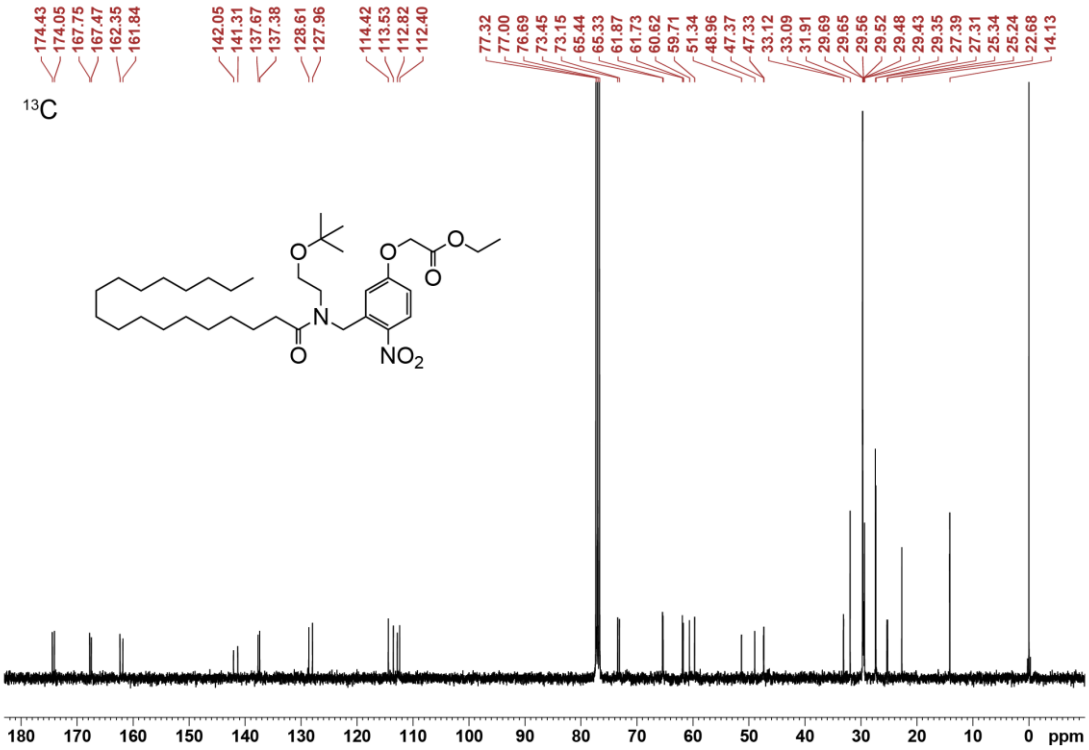
174.43
174.05
167.75
167.47
162.35
161.84
142.05
141.31
137.67
137.38
128.61
127.96
114.42
113.53
112.82
112.40
77.32
77.00
76.69
73.45
73.15
65.44
65.33
61.87
61.73
60.62
59.71
51.34
48.96
47.37
47.33
33.12
33.09
31.91
29.69
29.65
29.56
29.52
29.48
29.43
29.35
27.39
27.31
25.34
25.24
22.68
14.13
13C
O
O
O
O
N
O
NO2
180
170
160
150
140
130
120
110
100
90
80
70
60
50
40
30
20
10
0
ppm

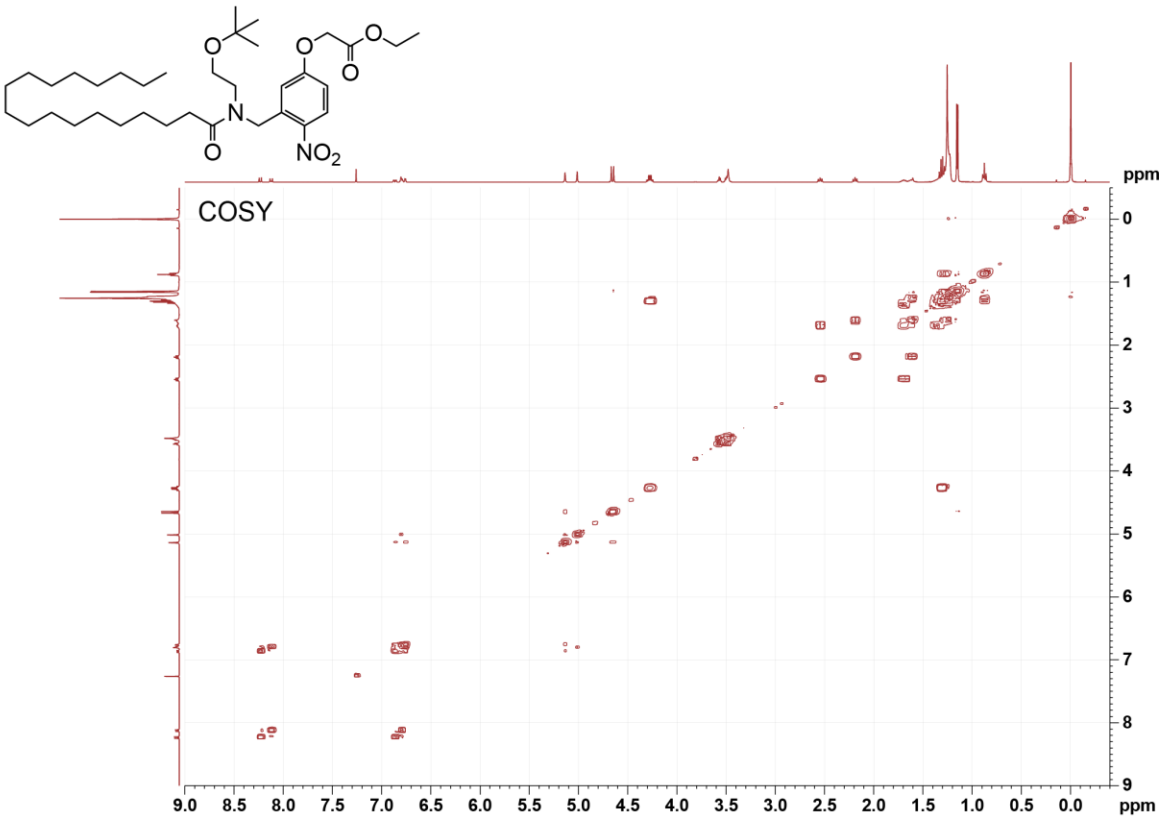
COSY
ppm
9.0 8.5 8.0 7.5 7.0 6.5 6.0 5.5 5.0 4.5 4.0 3.5 3.0 2.5 2.0 1.5 1.0 0.5 0.0 ppm
0 1 2 3 4 5 6 7 8 9

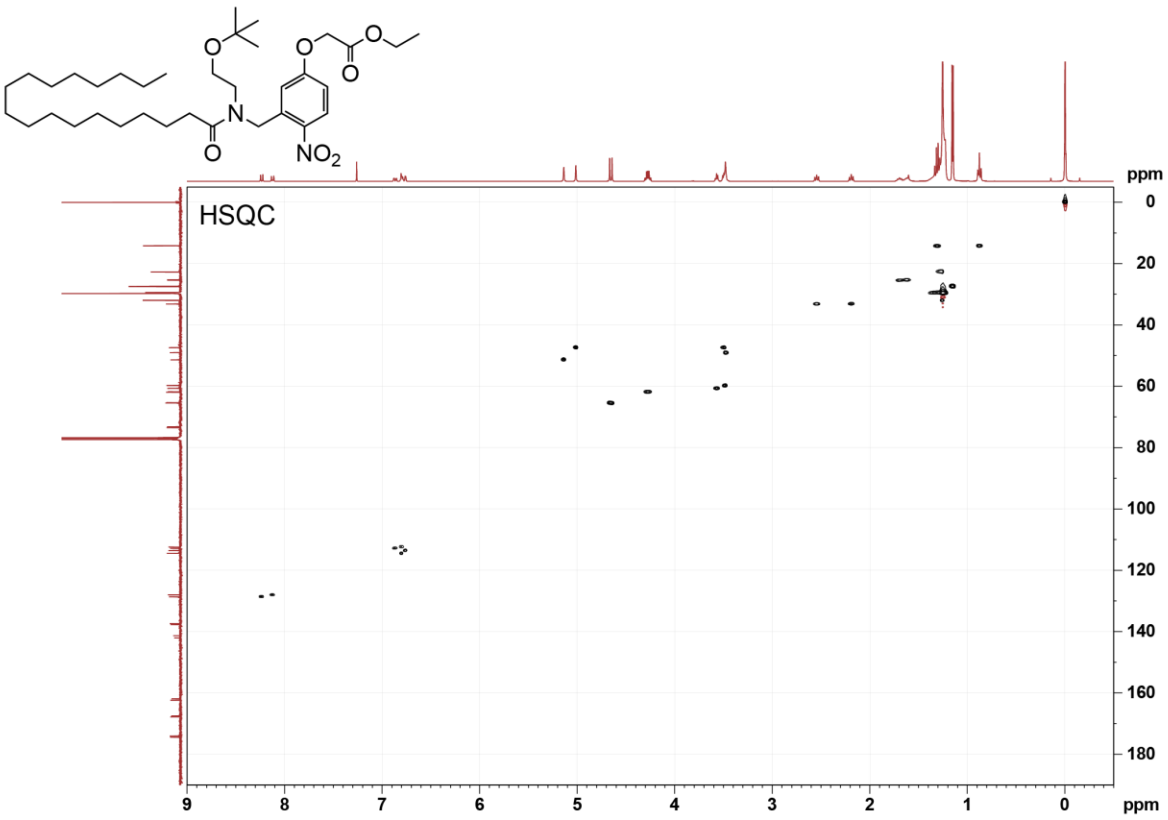
HSQC
ppm
9 8 7 6 5 4 3 2 1 0 ppm
0 20 40 60 80 100 120 140 160 180

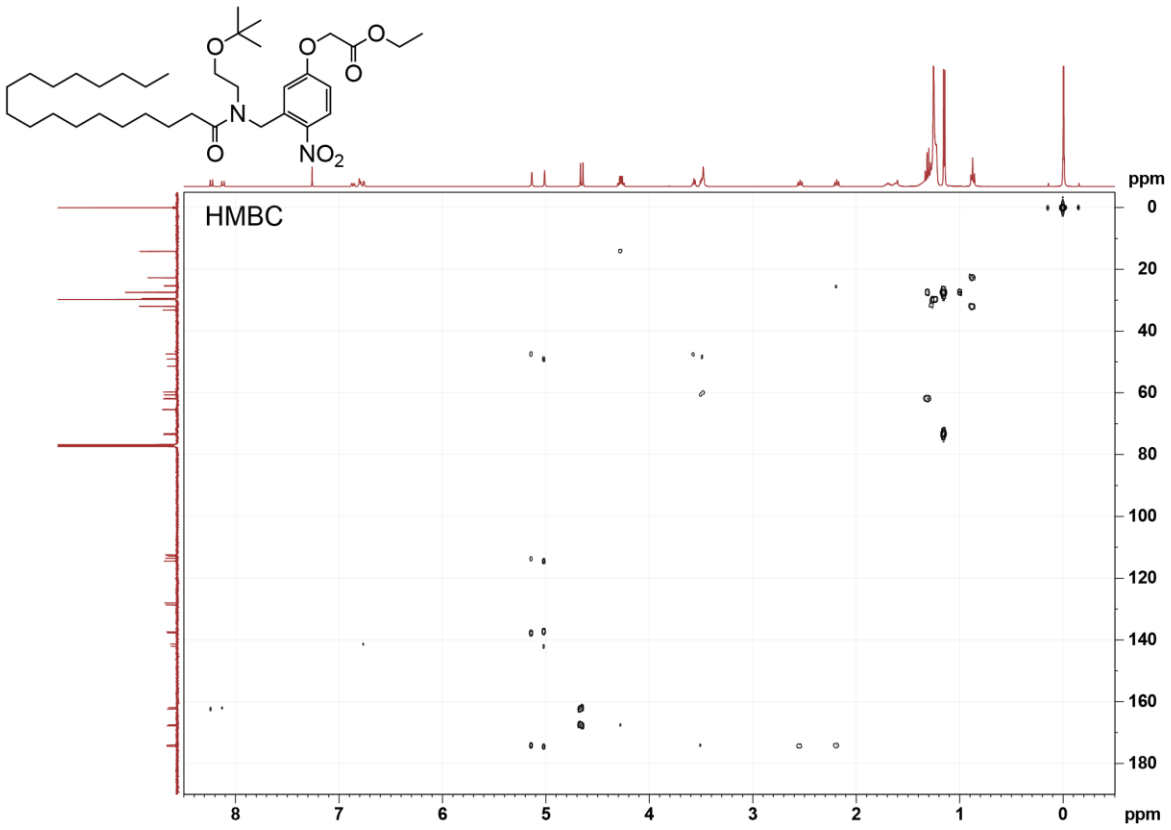
HMBC
ppm
0
20
40
60
80
100
120
140
160
180
8
7
6
5
4
3
2
1
0
ppm

### 6.2.2. Synthesis of *N*-(5-(2-((4-(((2-amino-9*H*-purin-6-yl)oxy)methyl)benzyl)amino)-2-oxoethoxy)-2-nitrobenzyl)-*N*-(2-(*tert*-butoxy)ethyl)stearamide (4).

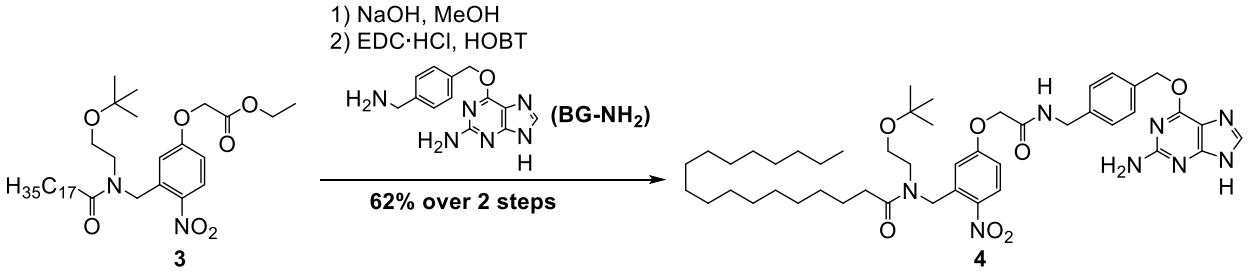


**6-((4-(aminomethyl)benzyl)oxy)-9*H*-purin-2-amine (BG-$NH_2$)** was prepared using a procedure described in Keppler *et al.*[55]

**Ethyl 2-(3-((*N*-(2-(*tert*-butoxy)ethyl)stearamido)methyl)-4-nitrophenoxy)acetate** (**3**, 0.1096 g, 0.177 mmol, 1.0 equiv.) was dissolved in MeOH (1.5 ml), and then aqueous NaOH (1 M, 0.35 ml, 0.35 mmol, 2.0 equiv.) was added dropwise. The reaction continued for 2.5 h before the reaction was diluted in MeOH (1.5 ml), put on an ice bath and then aqueous HCl (1 M, 0.25 ml, 0.25 mmol, 1.4 equiv.) was added until the mixture was at pH = 7.0. The reaction was diluted in EtOAc (5 ml), and the organic layer was 2× extracted with $H_2O$ and 2× with ether. The organic layer was washed once with saturated brine and dried over anhydrous $MgSO_4$. The crude mixture was filtered, and the solvent was removed *in vacuo*. The crude **2-(3-((*N*-(2-(*tert*-butoxy)ethyl)stearamido)methyl)-4-nitrophenoxy)acetic acid** (0.0834 g, 0.141 mmol) was used directly in the next reaction without further purification.

1-Hydroxybenzotriazole monohydrate (HOBt, 25 mg, 0.19 mmol, 1.3 equiv.) was added to the crude **2-(3-((*N*-(2-(*tert*-butoxy)ethyl)stearamido)methyl)-4-nitrophenoxy)acetic acid** (0.0834 g, 0.141 mmol, 1.0 equiv). The mixture was placed under an argon atmosphere and dissolved in anhydrous DMF (7 ml). 1-(3-dimethylaminopropyl)-3-ethylcarbodiimide hydrochloride (EDC·HCl, 32 mg, 0.17 mmol, 1.2 equiv.) was added to the reaction in one portion. Separately, BG-amine (46 mg, 0.17 mmol, 1.2 equiv) was placed under an argon atmosphere and dissolved in anhydrous DMF (2 ml). The BG-amine was transferred via cannula

to the reaction mixture, and the reaction stirred overnight. The reaction was diluted in EtOAc (20 ml), and the organic phase was washed with saturated $NaHCO_3$ (2× 20 ml), HCl (0.1 M, 3× 15 ml), $H_2O$ (2× 20 ml), and once with brine (20 ml). $SiO_2$ gel was added to the crude product and the solvent removed *in vacuo*, then the product-containing $SiO_2$ gel was loaded onto a $SiO_2$ column and purified by flash column chromatography (MeOH:DCM 1:99 → MeOH:DCM 7:93). ***N*-(5-(2-((4-(((2-amino-9*H*-purin-6-yl)oxy)methyl)benzyl)amino)-2-oxoethoxy)-2-nitrobenzyl)-*N*-(2-(*tert*-butoxy)ethyl)stearamide** (**4**, 92 mg, 0.11 mol, 62%) was isolated as a yellow oil.

**TLC (MeOH:DCM 7:93): $R_f$ =** 0.35. **$^1$H NMR ($CDCl_3$, 400 MHz, 25 °C):** δ 8.18 (d, 0.3 H, H3, *J* = 9.2 Hz); 8.08 (d, 0.7 H, H3, *J* = 7.9 Hz); 7.78 (s, 1 H, H36); 7.40 (d, 2 H, H31, H32, *J* = 7.2 Hz); 7.21 (d, 2 H, H33, H34, *J* = 8.6 Hz); 7.02 (d, 0.3 H, H2, *J* = 8.6 Hz); 6.96 (d, 0.7 H, H2, *J* = 8.6 Hz); 6.81 (s, 0.3 H, H6); 6.77 (s, 0.7 H, H6); 5.47 (s, 2 H, $H35_{A,B}$); 5.10 (s, 0.6 H, $H7_A$); 4.91 (s, 1.3 H, $H7_{A,B}$); 4.64 (s, 0.7 H, $H8_A$); 4.61 (s, 1.4 H, $H8_{A,B}$); 4.40 (s, 2 H, $H30_{A,B}$); 2.56 (t, 1 H, $H13_A$, *J* = 7.5 Hz); 2.20 (t, 1 H, $H13_B$, *J* = 7.5 Hz); 1.67-1.44 (m, 2 H, $H14_{A,B}$); 1.37-1.12 (m, 28 H, H15-28); 1.10 (s, 9 H, C($C\underline{H}_3$)); 0.84 (t, 3 H, $H29_{A,B,C}$, *J* = 6.4 Hz).

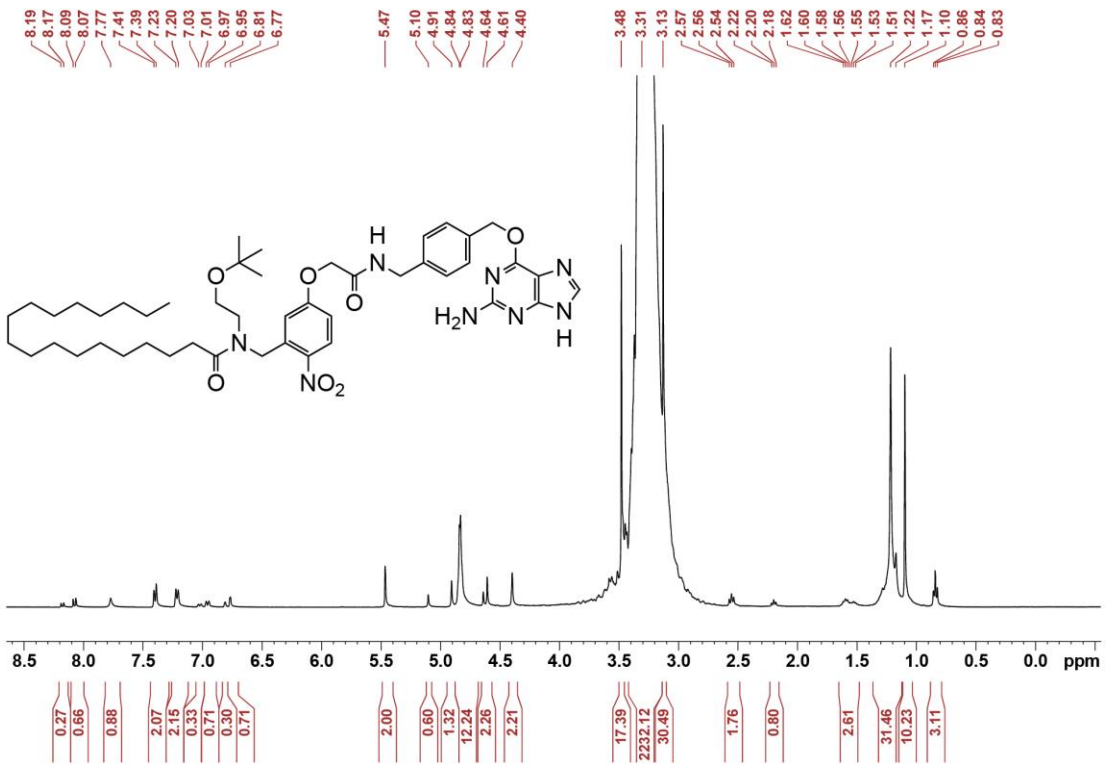
8.19
8.17
8.09
8.07
7.77
7.41
7.39
7.23
7.20
7.03
7.01
6.97
6.95
6.81
6.77
5.47
5.10
4.91
4.84
4.83
4.64
4.61
4.40
3.48
3.31
3.13
2.57
2.56
2.54
2.22
2.20
2.18
1.62
1.60
1.58
1.56
1.55
1.53
1.51
1.22
1.17
1.10
0.86
0.84
0.83
H
N
O
O
O
N
O
N
N
N
H
$H_2N$
O
N
O
$NO_2$
8.5
8.0
7.5
7.0
6.5
6.0
5.5
5.0
4.5
4.0
3.5
3.0
2.5
2.0
1.5
1.0
0.5
0.0
ppm
0.27
0.66
0.88
2.07
2.15
0.33
0.71
0.30
0.71
2.00
0.60
1.32
12.24
2.26
2.21
17.39
2232.12
30.49
1.76
0.80
2.61
31.46
10.23
3.11

### 6.2.3. Synthesis of *N*-(5-(2-((4-(((2-amino-9*H*-purin-6-yl)oxy)methyl)benzyl)amino)-2-oxoethoxy)-2-nitrobenzyl)-*N*-(2-hydroxyethyl)stearamide (OCT-SEA).

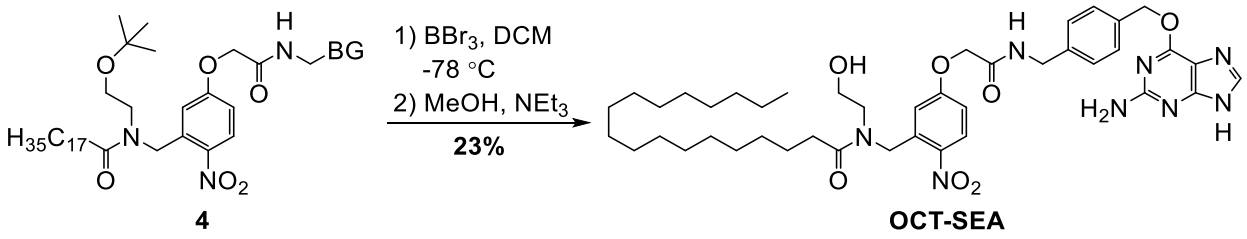


***N*-(5-(2-((4-(((2-amino-9*H*-purin-6-yl)oxy)methyl)benzyl)amino)-2-oxoethoxy)-2-nitrobenzyl)-*N*-(2-(*tert*-butoxy)ethyl)stearamide** (**4**, 8.1 mg, 9.6 μmol, 1.0 equiv.) was placed under an Ar atmosphere, dissolved in anhydrous $CH_2Cl_2$ (0.5 ml), and then cooled in a dry ice / acetone bath. $BBr_3$ (1.0 M in $CH_2Cl_2$, 0.38 ml, 38 μmol, 4.0 equiv.) was added and the reaction continued for 1 h before an additional portion of $BBr_3$ (9 μl, 9 μmol, 0.9 equiv.) was added. The reaction continued for an additional 1 h, was then quenched with 4:1 MeOH:$Et_2O$ (0.25 ml), and stirred vigorously for 5 min. The reaction mixture was neutralized with $NEt_3$ (0.020 ml, 0.14 mmol) and diluted in DCM (3 ml). The reaction mixture was washed 2× with $H_2O$ (5 ml) and once with saturated brine (5 ml). The organic phase was concentrated *in vacuo* and purified *via* flash column chromatography (5.02 g silica, MeOH:DCM 3:97 → MeOH:DCM 3:47). ***N*-(5-(2-((4-(((2-amino-9*H*-purin-6-yl)oxy)methyl)benzyl)amino)-2-oxoethoxy)-2-nitrobenzyl)-*N*-(2-hydroxyethyl)stearamide** (**OCT-SEA**, 1.7 mg, 2.2 μmol, 23%) was isolated as a yellow oil.

**$^1$H NMR ($CDCl_3$, 400 MHz, 25 °C):** δ 8.20 (d, 0.3 H, H3, *J* = 9.6 Hz); 8.10 (d, 0.6 H, H3, *J* = 8.0 Hz); 7.77 (s, 1 H, H36); 7.45-7.34 (m, 2 H, H31, H32); 7.28-7.16 (m, 2 H, H33, H34); 7.08-7.02 (m, 0.3 H, H2); 7.02-6.96 (m, 0.6 H, H2); 6.83 (dd, 1 H, H6, *J* = 13.3, 2.6 Hz); 5.49 (s, 2 H, $H35_{A,B}$); 5.07 (s, 0.5 H, $H7_A$); 4.90 (s, 1.2 H, $H7_{A,B}$); 4.67 (s, 1 H, $H8_A$); 4.63 (s, 1 H, $H8_B$); 4.40 (s, 2 H, $H30_{A,B}$); 2.55 (t, $H13_A$, *J* = 7.4 Hz); 2.21 (t, $H13_B$, *J* = 7.4 Hz); 1.67-1.47 (m, $H14_{A,B}$); 1.35-1.08 (m, H15-28); 0.85 (t, 3 H, $H29_{A,B,C}$, *J* = 6.4 Hz).

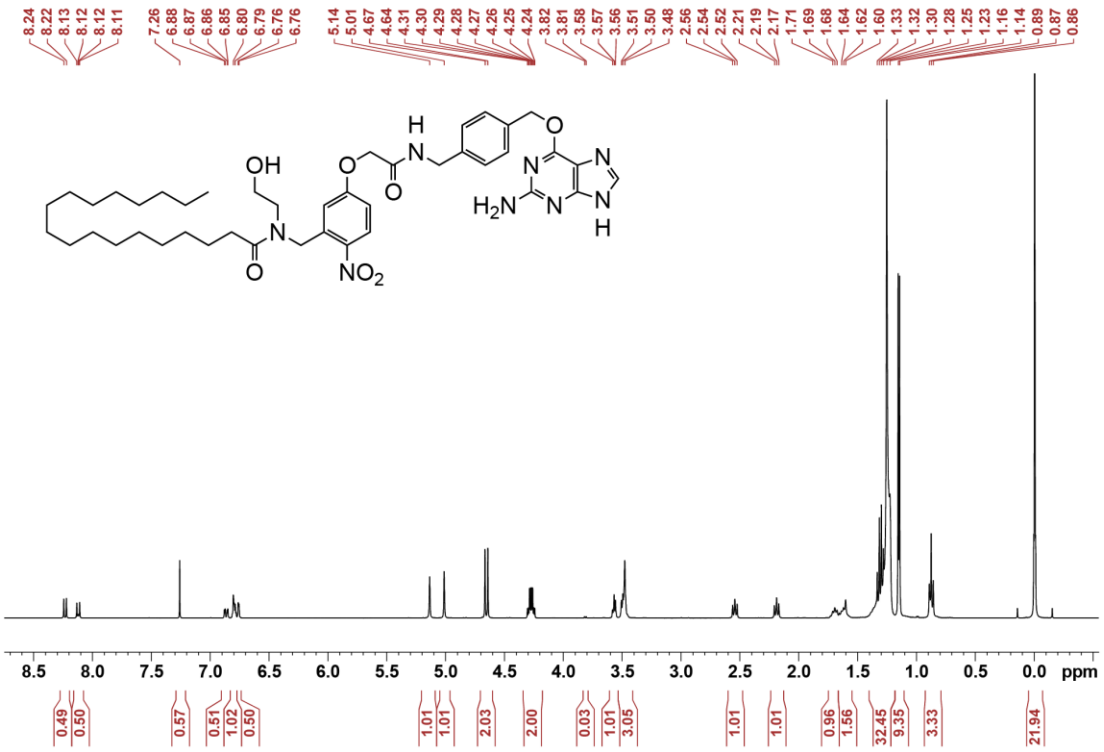
8.24
8.22
8.13
8.12
8.12
8.11
7.26
6.88
6.87
6.86
6.85
6.80
6.79
6.76
6.76
5.14
5.01
4.67
4.64
4.31
4.30
4.29
4.28
4.27
4.26
4.25
4.24
3.82
3.81
3.58
3.57
3.56
3.51
3.50
3.48
2.56
2.54
2.52
2.21
2.19
2.17
1.71
1.69
1.68
1.64
1.62
1.60
1.33
1.32
1.30
1.28
1.25
1.23
1.16
1.14
0.89
0.87
0.86
OH
O
N
O
H
N
O
N
N
H2N
N
N
H
O
NO2
8.5
8.0
7.5
7.0
6.5
6.0
5.5
5.0
4.5
4.0
3.5
3.0
2.5
2.0
1.5
1.0
0.5
0.0
ppm
0.49
0.50
0.57
0.51
1.02
0.50
1.01
1.01
2.03
2.00
0.03
1.01
3.05
1.01
1.01
0.96
1.56
32.45
9.35
3.33
21.94

# References


1. Martins, S. S., Levy, N. S., Bruzelius, E. & Segura, L. E. Cannabis legalization in the US. Where do we go from here? *Trends Psychiatry Psychother* **44**, e20220001 (2022).
2. Pertwee, R. G. Pharmacology of cannabinoid CB1 and CB2 receptors. *Pharmacol. Ther.* **74**, 129–180 (1997).
3. Silvestri, C. & Di Marzo, V. The endocannabinoid system in energy homeostasis and the etiopathology of metabolic disorders. *Cell Metab.* **17**, 475–490 (2013).
4. Cristino, L., Bisogno, T. & Di Marzo, V. Cannabinoids and the expanded endocannabinoid system in neurological disorders. *Nat. Rev. Neurol.* **16**, 9–29 (2020).
5. Sud, M. *et al.* LMSD: LIPID MAPS structure database. *Nucleic Acids Res.* **35**, D527–D532 (2007).
6. Sheskin, T., Hanuš, L., Slager, J., Vogel, Z. & Mechoulam, R. Structural requirements for binding of anandamide-type compounds to the brain cannabinoid receptor. *J. Med. Chem.* **40**, 659–667 (1997).
7. Devane, W. A. *et al.* Isolation and Structure of a Brain Constituent That Binds to the Cannabinoid Receptor. *Science.* **258**, 1946–1949 (1992).
8. Overton, H. A. *et al.* Deorphanization of a G protein-coupled receptor for oleoylethanolamide and its use in the discovery of small-molecule hypophagic agents. *Cell Metab.* **3**, 167–175 (2006).
9. Rankin, L. & Fowler, C. J. The Basal Pharmacology of Palmitoylethanolamide. *Int. J. Mol. Sci.* **21**, 7942 (2020).
10. Syed, S. K. *et al.* Regulation of GPR119 receptor activity with endocannabinoid-like lipids. *Am. J. Physiol. - Endocrinol. Metab.* **303**, 1469–1478 (2012).
11. Laleh, P., Yaser, K. & Alireza, O. Oleoylethanolamide: A novel pharmaceutical agent in the management of obesity-an updated review. *J. Cell. Physiol.* **234**, 7893–7902 (2019).

12. Maccarrone, M. & Finazzi-Agró, A. The endocannabinoid system, anandamide and the regulation of mammalian cell apoptosis. *Cell Death and Differentiation* **10**, 946–955 (2003).
13. Reggio, P. H. Endocannabinoid binding to the cannabinoid receptors: what is known and what remains unknown. *Curr. Med. Chem.* **17**, 1468–86 (2010).
14. Kuipers, E. N. *et al.* High fat diet increases circulating endocannabinoids accompanied by increased synthesis enzymes in adipose tissue. *Front. Physiol.* **9**, 1913 (2019).
15. Joosten, M. M., Balvers, M. G. J., Verhoeckx, K. C. M., Hendriks, H. F. J. & Witkamp, R. F. Plasma anandamide and other N-acylethanolamines are correlated with their corresponding free fatty acid levels under both fasting and non-fasting conditions in women. *Nutr. Metab.* **7**, 49 (2010).
16. Fanelli, F. *et al.* Profiling plasma N-Acylethanolamine levels and their ratios as a biomarker of obesity and dysmetabolism. *Mol. Metab.* **14**, 82–94 (2018).
17. Sipe, J. C., Waalen, J., Gerber, A. & Beutler, E. Overweight and obesity associated with a missense polymorphism in fatty acid amide hydrolase (FAAH). *Int. J. Obes.* **29**, 755–759 (2005).
18. De Moraes Martins, C. J. *et al.* Circulating endocannabinoids and the polymorphism 385C>A in fatty acid amide hydrolase (FAAH) gene may identify the obesity phenotype related to cardiometabolic risk: A study conducted in a Brazilian population of complex interethnic admixture. *PLoS One* **10**, e0142728 (2015).
19. Centers for Disease Control and Prevention. National Diabetes Statistics Report. 1–12 (2023).
20. Rutter, G. A. & Hodson, D. J. Minireview: Intraislet regulation of insulin secretion in humans. *Molecular Endocrinology* **27**, 1984–1995 (2013).
21. Veilleux, A., Di Marzo, V. & Silvestri, C. The Expanded Endocannabinoid

System/Endocannabinoidome as a Potential Target for Treating Diabetes Mellitus. *Curr. Diab. Rep.* **19**, 117 (2019).

22. Nogueiras, R., Rohner-Jeanrenaud, F., Woods, S. C. & Tschöp, M. H. The Endocannabinoid System and the Control of Glucose Homeostasis. *J. Neuroendocrinol.* **20**, 147–151 (2008).
23. Laychock, S. G., Hoffman, J. M., Meisel, E. & Bilgin, S. Pancreatic islet arachidonic acid turnover and metabolism and insulin release in response to delta-9-tetrahydrocannabinol. *Biochem. Pharmacol.* **35**, 2003–2008 (1986).
24. Danielsson, A. K. *et al.* Cannabis Use as Risk or Protection for Type 2 Diabetes: A Longitudinal Study of 18 000 Swedish Men and Women. *J. Diabetes Res.* **2016**, 6278709 (2016).
25. Alshaarawy, O. & Anthony, J. C. Brief Report: Cannabis Smoking and Diabetes Mellitus: Results from Meta-analysis with Eight Independent Replication Samples. *Epidemiology* **26**, 597–600 (2015).
26. Imtiaz, S. & Rehm, J. The relationship between cannabis use and diabetes: Results from the National Epidemiologic Survey on Alcohol and Related Conditions III. *Drug Alcohol Rev.* **37**, 897–902 (2018).
27. Barré, T. *et al.* Cannabis use is associated with a lower risk of diabetes in chronic hepatitis C-infected patients (ANRS CO22 Hepather cohort). *J. Viral Hepat.* **27**, 1473–1483 (2020).
28. Qi, M. *et al.* Chronic marijuana usage by human pancreas donors is associated with impaired islet function. *PLoS One* **16**, e0258434 (2021).
29. Sam, A. H., Salem, V. & Ghatei, M. A. Rimonabant: From RIO to Ban. *J. Obes.* **2011**, 432607 (2011).
30. Rosenstock, J., Hollander, P., Chevalier, S. & Iranmanesh, A. SERENADE: The study

evaluating rimonabant efficacy in drug-naive diabetic patients: Effects of monotherapy with rimonabant, the first selective CB 1 receptor antagonist, on glycemic control, body weight, and lipid profile in drug-naive type 2 diabetes. *Diabetes Care* **31**, 2169–2176 (2008).

31. Islam, M. S. Stimulus-Secretion Coupling in Beta-Cells: From Basic to Bedside. *Adv. Exp. Med.* **1131**, 943–963 (2020).
32. Romero-Zerbo, S. Y. *et al.* A role for the putative cannabinoid receptor GPR55 in the islets of Langerhans. *J. Endocrinol.* **211**, 177–185 (2011).
33. Laguerre, A., Keutler, K., Hauke, S. & Schultz, C. Regulation of Calcium Oscillations in β-Cells by Co-activated Cannabinoid Receptors. *Cell Chem. Biol.* **28**, 88–96 (2021).
34. Malenczyk, K. *et al.* CB1 cannabinoid receptors couple to focal adhesion kinase to control insulin release. *J. Biol. Chem.* **288**, 32685–32699 (2013).
35. Zhou, Y. T. *et al.* Role of peroxisome proliferator-activated receptor α in disease of pancreatic β cells. *Proc. Natl. Acad. Sci. U. S. A.* **95**, 8898–8903 (1998).
36. Drzazga, A. *et al.* Lysophosphatidylcholine and its phosphorothioate analogues potentiate insulin secretion via GPR40 (FFAR1), GPR55 and GPR119 receptors in a different manner. *Mol. Cell. Endocrinol.* **472**, 117–125 (2018).
37. McKillop, A. M., Moran, B. M., Abdel-Wahab, Y. H. A. & Flatt, P. R. Evaluation of the insulin releasing and antihyperglycaemic activities of GPR55 lipid agonists using clonal beta-cells, isolated pancreatic islets and mice. *Br. J. Pharmacol.* **170**, 978–990 (2013).
38. McCloskey, A. G. *et al.* CRISPR/Cas9 gene editing demonstrates metabolic importance of GPR55 in the modulation of GIP release and pancreatic beta cell function. *Peptides* **125**, 170251 (2020).
39. Lauckner, J. E. *et al.* GPR55 is a cannabinoid receptor that increases intracellular calcium and inhibits M current. *Proc. Natl. Acad. Sci. U. S. A.* **105**, 2699–2704 (2008).

40. Segerstolpe, Å. *et al.* Single-Cell Transcriptome Profiling of Human Pancreatic Islets in Health and Type 2 Diabetes. *Cell Metab.* **24**, 593–607 (2016).

41. Aseer, K. R. & Egan, J. M. An Autonomous Cannabinoid System in Islets of Langerhans. *Front. Endocrinol. (Lausanne).* **12**, 699661 (2021).

42. Broichhagen, J., Frank, J. A. & Trauner, D. A Roadmap to Success in Photopharmacology. *Acc. Chem. Res.* **48**, 1947–1960 (2015).

43. Westphal, M. V. *et al.* Synthesis of Photoswitchable Delta9-Tetrahydrocannabinol Derivatives Enables Optical Control of Cannabinoid Receptor 1 Signaling. *J. Am. Chem. Soc.* **139**, 18206–18212 (2017).

44. Dolles, D. *et al.* The First Photochromic Affinity Switch for the Human Cannabinoid Receptor 2. *Adv. Ther.* **1**, 1700032 (2018).

45. Sarott, R. C. *et al.* Optical Control of Cannabinoid Receptor 2-Mediated Ca2+Release Enabled by Synthesis of Photoswitchable Probes. *J. Am. Chem. Soc.* **143**, 736–743 (2021).

46. Weinstain, R., Slanina, T., Kand, D. & Klán, P. Visible-to-NIR-Light Activated Release: From Small Molecules to Nanomaterials. *Chem. Rev.* **120**, 13135–13272 (2020).

47. Heinbockel, T. *et al.* Endocannabinoid Signaling Dynamics Probed with Optical Tools. *J. Neurosci.* **25**, 9449–9459 (2005).

48. Laguerre, A., Hauke, S., Qiu, J., Kelly, M. J. & Schultz, C. Photorelease of 2-Arachidonoylglycerol in Live Cells. *J. Am. Chem. Soc.* **141**, 16544–16547 (2019).

49. Ma, J. *et al.* Thiocoumarin Caged Nucleotides: Synthetic Access and Their Photophysical Properties. *Molecules* **25**, 9–11 (2020).

50. Konrad, D. B., Frank, J. A. & Trauner, D. Synthesis of Redshifted Azobenzene Photoswitches by Late-Stage Functionalization. *Chem. – A Eur. J.* **22**, 4364–4368 (2016).

51. Aujard, I. *et al.* o-Nitrobenzyl Photolabile Protecting Groups with Red-Shifted Absorption:

Syntheses and Uncaging Cross-Sections for One- and Two-Photon Excitation. *Chem. - A Eur. J.* **12**, 6865–6879 (2006).

52. Nadler, A. *et al.* Exclusive photorelease of signaling lipids at the plasma membrane. *Nat. Commun.* **6**, 10056 (2015).

53. Wagner, N., Stephan, M., Höglinger, D. & Nadler, A. A Click Cage: Organelle-Specific Uncaging of Lipid Messengers. *Angew. Chemie - Int. Ed.* **57**, 13339–13343 (2018).

54. Urban, D. J. & Roth, B. L. DREADDs (designer receptors exclusively activated by designer drugs): Chemogenetic Tools with Therapeutic Utility. *Annu. Rev. Pharmacol. Toxicol.* **55**, 399–417 (2015).

55. Keppler, A. *et al.* A general method for the covalent labeling of fusion proteins with small molecules in vivo. *Nat. Biotechnol.* **21**, 86–89 (2003).

56. Los, G. V *et al.* HaloTag: A Novel Protein Labeling Technology for Cell Imaging and Protein Analysis. *ACS Chem. Biol.* **3**, 373–382 (2008).

57. Broichhagen, J. *et al.* Orthogonal optical control of a G protein-coupled receptor with a SNAP-tethered photochromic ligand. *ACS Cent. Sci.* **1**, 383–393 (2015).

58. Shields, B. C. *et al.* Deconstructing behavioral neuropharmacology with cellular specificity. *Science (80-. ).* **356**, eaaj2161 (2017).

59. Tobias, J. M., Rajic, G., Viray, A. E. G., Icka-Araki, D. & Frank, J. A. Genetically-targeted photorelease of endocannabinoids enables optical control of GPR55 in pancreatic β-cells. *Chem. Sci.* **12**, 13506–13512 (2021).

60. Donvito, G., Bettoni, I., Comelli, F., Colombo, A. & Costa, B. Palmitoylethanolamide Relieves Pain and Preserves Pancreatic Islet Cells in a Murine Model of Diabetes. *CNS Neurol. Disord. - Drug Targets* **14**, 452–462 (2015).

61. Petrosino, S. & Di Marzo, V. The pharmacology of palmitoylethanolamide and first data on the therapeutic efficacy of some of its new formulations. *British Journal of*

*Pharmacology* **174**, 1349–1365 (2017).

62. Kuehl, F. A. J., Jacob, T. A., Ganley, O. H., Ormond, R. E. & Meisinger, M. A. P. The Identification of N-(2-Hydroxyethyl)-Palmitamide as a naturally occurring anti-inflammatory agent. *J. Am. Chem. Soc.* **79**, 5577–5578 (1957).

63. Ryberg, E. *et al.* The orphan receptor GPR55 is a novel cannabinoid receptor. *Br. J. Pharmacol.* **152**, 1092–1101 (2007).

64. Liu, B. *et al.* GPR55-dependent stimulation of insulin secretion from isolated mouse and human islets of Langerhans. *Diabetes, Obes. Metab.* **18**, 1263–1273 (2016).

65. Asfari, M. *et al.* Establishment of 2-Mercaptoethanol-Dependent Differentiated Insulin-Secreting Cell Lines. *Endocrinology* **130**, 167–178 (1992).

66. Hohmeier, H. E. *et al.* Isolation of INS-1-derived cell lines with robust ATP-sensitive K+ channel-dependent and -independent glucose-stimulated insulin secretion. *Diabetes* **49**, 424–430 (2000).

67. Cho, Y. J. *et al.* Ginseng gintonin contains ligands for GPR40 and GPR55. *Molecules* **25**, 1102 (2020).

68. Zhao, Y. *et al.* An expanded palette of genetically encoded Ca2+ indicators. *Science* **333**, 1888–1891 (2011).

69. Kargl, J. *et al.* A selective antagonist reveals a potential role of G protein-coupled receptor 55 in platelet and endothelial cell function. *J. Pharmacol. Exp. Ther.* **346**, 54–66 (2013).

70. Bleasdale, J. E. *et al.* Selective inhibition of receptor-coupled phospholipase C-dependent processes in human platelets and polymorphonuclear neutrophils. *J. Pharmacol. Exp. Ther.* **255**, 756–768 (1990).

71. Nestmann, E. R. Safety of micronized palmitoylethanolamide (microPEA): lack of toxicity and genotoxic potential. *Food Sci. Nutr.* **5**, 292–309 (2017).

72. Donthamsetti, P. C. *et al.* Genetically Targeted Optical Control of an Endogenous G Protein-Coupled Receptor. *J. Am. Chem. Soc.* **141**, 11522–11530 (2019).

73. Di Marzo, V. The endocannabinoid system: Its general strategy of action, tools for its pharmacological manipulation and potential therapeutic exploitation. *Pharmacol. Res.* **60**, 77–84 (2009).

74. Mendizabal-Zubiaga, J. *et al.* Cannabinoid CB 1 receptors are localized in striated muscle mitochondria and regulate mitochondrial respiration. *Front. Physiol.* **7**, 476 (2016).

75. Bénard, G. *et al.* Mitochondrial CB 1 receptors regulate neuronal energy metabolism. *Nature Neuroscience* **15**, 558–564 (2012).

76. Schindelin, J. *et al.* Fiji: An open-source platform for biological-image analysis. *Nat. Methods* **9**, 676–682 (2012).

77. Tao, Y. X. & Liang, X. F. G protein-coupled receptors as regulators of glucose homeostasis and therapeutic targets for diabetes mellitus. *Prog. Mol. Biol. Transl. Sci.* **121**, 1–21 (2014).

78. Wilhelm, J. *et al.* Kinetic and Structural Characterization of the Self-Labeling Protein Tags HaloTag7, SNAP-tag, and CLIP-tag. *Biochemistry* **60**, 2560–2575 (2021).

79. Frei, M. S. *et al.* Engineered HaloTag variants for fluorescence lifetime multiplexing. *Nat. Methods* **19**, 65-70 (2021).

80. Magotti, P. *et al.* Structure of Human N-Acylphosphatidylethanolamine-Hydrolyzing Phospholipase D: Regulation of Fatty Acid Ethanolamide Biosynthesis by Bile Acids. *Structure* **23**, 598–604 (2015).

81. Tsuboi, K., Takezaki, N. & Ueda, N. The N-acylethanolamine-hydrolyzing acid amidase (NAAA). *Chem. Biodivers.* **4**, 1914–1925 (2007).

82. Fang, Z. *et al.* The Influence of Peptide Context on Signaling and Trafficking of Glucagon-like Peptide-1 Receptor Biased Agonists. *ACS Pharmacol. Transl. Sci.* **3**, 345-360 (2020).

83. Chai, S. *et al.* Development of a Beta Cell-Specific Expression Control Element for Recombinant Adeno-Associated Virus. *Hum. Gene Ther.* **33**, 789–800 (2022).

84. Okamoto, Y., Morishita, J., Tsuboi, K., Tonai, T. & Ueda, N. Molecular Characterization of a Phospholipase D Generating Anandamide and Its Congeners*. *J. of Biol. Chem.* **279**, 5298-5305 (2004).

85. Nakayama-Iwatsuki, K., Hirabayashi, M. & Hochi, S. Fabrication of functional rat pseudo-islets after cryopreservation of pancreatic islets or dispersed islet cells. *J. Tissue Eng. Regen. Med.* **15**, 686–696 (2021).

86. Pekrun, K. *et al.* Using a barcoded AAV capsid library to select for clincially relevant gene therapy vectors. *JCI insight* **4**, e131610 (2019).

87. Liu, Q. *et al.* Take Immune Cells Back on Track: Glycopolymer-Engineered Tumor Cells for Triggering Immune Response. *ACS Macro Lett.* **8**, 337–344 (2019).

88. Li, L., Deng, X. X., Li, Z. L., Du, F. S. & Li, Z. C. Multifunctional photodegradable polymers for reactive micropatterns. *Macromolecules* **47**, 4660–4667 (2014).

89. Jourdan, T., Godlewski, G. & Kunos, G. Endocannabinoid regulation of β-cell functions: implications for glycaemic control and diabetes. *Diabetes, Obes. Metab.* **18**, 549–557 (2016).

90. González-Mariscal, I. & Egan, J. M. Endocannabinoids in the Islets of Langerhans: the ugly, the bad, and the good facts. *Am. J. Physiol. Metab.* **315**, E174–E179 (2018).

91. Nakata, M. & Yada, T. Cannabinoids inhibit insulin secretion and cytosolic $Ca^{2+}$ oscillation in islet β-cells via CB1 receptors. *Regul. Pept.* **145**, 49–53 (2008).

92. Frank, J. A. *et al.* Optical tools for understanding the complexity of β-cell signaling and insulin release. *Nat. Rev. Endocrinol.* **14**, 721–737 (2018).

93. Ma, L. *et al.* Mitochondrial CB1 receptor is involved in ACEA-induced protective effects on neurons and mitochondrial functions. *Sci. Rep.* **5**, 12440 (2015).

94. McClenaghan, N. H. & Flatt, P. R. Engineering cultured insulin-secreting pancreatic B-cell lines. *J. Mol. Med.* **77**, 235–243 (1999).

95. Van der Krogt, G. N. M., Ogink, J., Ponsioen, B. & Jalink, K. A comparison of donor-acceptor pairs for genetically encoded FRET sensors: Application to the Epac cAMP sensor as an example. *PLoS One* **3**, e1916 (2008).

96. Bevan, S. *et al.* Capsazepine: a competitive antagonist of the sensory neurone excitant capsaicin. *Br. J. Pharmacol.* **107**, 544–552 (1992).

97. Cramer, S. W. *et al.* Through the looking glass: a review of cranial window technology for optical access to the brain. *J. Neurosci. Methods* **354**, 109100 (2021).

98. Ishihara, H. *et al. Pancreatic beta cell line MIN6 exhibits characteristics of glucose metabolism and glucose-stimulated insulin secretion similar to those of normal islets*. *Diabetologia* **36**, 1139-1145 (1993).